Environmental Science and Engineering

Gordon Huang *Editor*

Proceedings of 2022 7th International Conference on Environmental Engineering and Sustainable Development (CEESD 2022)

Springer

Environmental Science and Engineering

The ultimate goal of this series is to contribute to the protection of our environment, which calls for both profound research and the ongoing development of solutions and measurements by experts in the field. Accordingly, the series promotes not only a deeper understanding of environmental processes and the evaluation of management strategies, but also design and technology aimed at improving environmental quality. Books focusing on the former are published in the subseries Environmental Science, those focusing on the latter in the subseries Environmental Engineering.

Gordon Huang
Editor

Proceedings of 2022 7th International Conference on Environmental Engineering and Sustainable Development (CEESD 2022)

CEESD2022

Springer

Editor
Gordon Huang
Faculty of Engineering and Applied Science
University of Regina
Regina, SK, Canada

ISSN 1863-5520 ISSN 1863-5539 (electronic)
Environmental Science and Engineering
ISBN 978-3-031-28192-1 ISBN 978-3-031-28193-8 (eBook)
https://doi.org/10.1007/978-3-031-28193-8

This Springer imprint is published by the registered company Springer Nature Switzerland AG
The registered company address is: Gewerbestrasse 11, 6330 Cham, Switzerland

Organization

Conference Chairs

Gordon Huang, International Society for Environmental Information Sciences
Xiaosheng Qin, Nanyang Technological University, Singapore
Yongping Li, Beijing Normal University, China

Program Committee

Huining Xiao, University of New Brunswisk, Canada
Laurent Ho, Dublin City University, Ireland
Steffen Rao, Carleton University, Canada

Scientific Committee

Solomon W. Leung, Idaho State University, USA
Eugen Rusu, Galati University 'Dunarea de Jos', Romania

Publicity Chair

Malka N. Halgamuge, The University of Melbourne, Australia

Technical Program Committee

Amela Ajanovic, Vienna University of Technology, Austria
Abdeltif Amrane, University of Rennes 1, France
Sabri Berhail, Abdelhafid Boussouf University, Algeria
Yehia M. S. ElShazly, Alexandria University, Egypt
Soufiane Haddout, Ibn Tofail University, Morocco
Mohammad Arif Kamal, Aligarh Muslim University, India
Salvatore Monteleone, Niccolò Cusano University, Italy
Kapil Pareek, Malaviya National Institute of Technology Jaipur, India
Roslynna Rosli, Universiti Teknologi Brunei, Brunei Darussalam
Monica Siroux, INSA Strasbourg—ICUBE Strasbourg University, France
Che Hang Seng, University of Malaya, Malaysia
Wai Yuen Szeto, The University of Hong Kong, Hong Kong, S.A.R, China
Kaimin Shih, The University of Hongkong, Hong Kong, S.A.R, China
Mysore Satish, Dalhousie University, Canada
Chih-Huang Weng, I-Shou University, Taiwan, ROC

Additional Reviewers

Wai Yuen Szeto
Sabri Berhail
Yanfeng Li
Soufiane Haddout
Che Hang Seng
Amela Ajanovic
Kaimin Shih
Haiyan Fu
Eric Strauss
Roslynna Rosli
Kapil Pareek
Salvatore Monteleone

Preface

The 2022 7th International Conference on Environmental Engineering and Sustainable Development (CEESD 2022) was organized by the Asia Pacific Institute of Science and Engineering (APISE), sponsored by the International Society for Environmental Information Sciences (ISEIS), the United Nations Development Programme (UNDP), the Water Governance Programme and South-South Cooperation Center for Sustainable Development, China. The conference was planned to be held as a hybrid event in Nanjing, China, from October 28 to 30, 2022. Due to recent pandemic, it was finally held as an online conference via Tencent Meeting Software on October 29, 2022. The online conference was a great success. The participants were from a number of countries (Canada, India, Korea, Germany, the USA, China, etc.) with diverse backgrounds, forming a coherent environment for facilitating tremendous learning, sharing and collaborating opportunities.

CEESD 2022 is targeted on providing opportunities to bring together the related researchers to share their most recent research achievements in these fields, and thus promote more advanced research.

On behalf of the conference organizing committee, I would like to express my great appreciation to the three keynote speakers (40 min. each, including Q&A) (Prof. Solomon W. Leung from Idaho State University, Prof. Yang Liu from the University of Alberta and Prof. Chiyuan Miao from Beijing Normal University) for sharing their most recent research achievements and their insights on future challenges. In addition, the conference included two oral sessions and a poster one. In the oral sessions, each presentation was allotted 12 min. At the end of each session, the participants were engaged in discussions for future collaborations. A group photo was taken at the conference. Together, the presentations represent a set of high-quality contributions to the literature on agile research and experience for addressing a wide range of contemporary topics.

These proceedings contain full research papers. Through peer reviews undertaken by conference committee members and international experts, 21 outstanding papers (out of 56 submissions) are included in this book. Each paper was reviewed by two to three reviewers. As conference proceedings, this book contains three chapters, including (1) Emerging Technologies in Environmental Science and Engineering,

(2) Environmental Management for Sustainable Development and (3) Energy, Water and Environment.

I hope that readers of the proceedings will find that the presented papers are valuable references for supporting their research and development in the fields of energy and environmental research. Thank you very much, and we look forward to seeing you at CEESD 2023.

Regina, Canada
October 2022

Gordon Huang
Yongping Li

About This Book

This book provides audiences with the research ideas and research achievements of authors who attended CEESD 2022. Although all countries in the world are vigorously promoting environmental governance and improving people's living environment, environmental pollution is still serious, and environmental protection requires more advanced concepts and technologies. This conference attracted many scientific researchers in the environmental field to actively discuss and share their scientific research results and ideas, which will provide an important reference value for others.

Contents

Part I
Emerging Technologies in Environmental Science and Engineering

Chapter 1
Enhanced Electrocatalytic CO_2 Reduction Over 2D Conjugated Cu MOF via Doping with Carbon Nanotubes

Yijun Li and Pengfei Li

Abstract 2D conjugated metal–organic frameworks (2D *c*-MOFs) are regarded as a kind of promising functional material due to their highly crystalline porous structure and excellent planar π-conjugation, which have found application in many areas. 2D *c*-MOFs consist of transition metals and planar fused aromatic rings. Due to the limited choice of metal elements and organic ligands, there is only a few 2D *c*-MOFs have been reported, which poses a great challenge to fully release its potential in electrocatalysis and other aspects. On the other hand, defects have proved to be an important role in the development of metal–organic frameworks. To the best of our knowledge, a deliberate introduction of defects in 2D *c*-MOFs has not been reported. Herein, we first realized the introduction of defects to 2D conjugated MOFs with a nonstoichiometric reaction condition. With a series of characterizations, defective sites within the structure of defective CAT-Cu (*d*-CAT-Cu) were finally confirmed. In the last part, we doped carbon nanotubes (CNT) in *d*-CAT-Cu to enhance the material's conductivity and increase the current density of the electrolysis. Meanwhile, the Faradaic efficiency of different products was tuned. Finally, the introduced defects in 2D *c*-MOFs have a significant influence on the performance of the electrocatalytic carbon dioxide reduction. This work provides a new path for the development of 2D *c*-MOFs.

Keywords 2D conjugated MOFs · Defects · Electrocatalysis · CO_2RR

1.1 Introduction

Defects have gradually been considered as an important strategy to finely modify the physicochemical property of metal–organic frameworks (MOFs) (Cheetham et al. 2016; Dissegna et al. 2018; Fang et al. 2015). There are two types defects in MOFs,

Y. Li · P. Li (✉)
Advanced Research Institute of Multidisciplinary Science, Beijing Institute of Technology, Beijing 100081, China
e-mail: lipengfei@bit.edu.cn

G. Huang (ed.), *Proceedings of 2022 7th International Conference on Environmental Engineering and Sustainable Development (CEESD 2022)*, Environmental Science and Engineering, https://doi.org/10.1007/978-3-031-28193-8_1

which are linker defects or cluster defects. The introduction of these defects to MOFs can not only change the pore structure but also alter the basic physicochemical property such as acidity/basicity and conductivity. These defective MOFs have found important applications in adsorption/separation (Wang et al. 2020), catalysis (Wang and Woll 2018), energy conversion/storage (Kayal and Chakraborty 2022) and many others (Peterson Gregory et al. 2017). 2D conjugated MOFs (2D *c*-MOFs) are a subclass of MOFs, which are constructed with 2D extended metal–organic coordinated planes (Wang et al. 2021). 2D *c*-MOFs have a well-defined 2D structure, excellent conductivity and high porosity, which have received tremendous attention in many applications in recent years (Park et al. 2018; Zhong et al. 2022). However, compared with the 3D MOFs, the number of reported 2D *c*-MOFs is quite small. The majority limitation would be the difficulty in the design and synthesis of highly conjugated and highly substituted fused aromatic rings. Currently, the 2D *c*-MOFs are mainly constructed with triphenylene, porphyrin and phthalocyanine. Even though a few other ligands have been reported in recent years, the functionalization of 2D *c*-MOFs is still a challenge. The introduction of defects could be a good choice for the modification of 2D *c*-MOFs, which has not been explored.

The electrochemical reduction of CO_2 (CO_2RR) is an attractive path to alleviate the excess amount CO_2 that is emitted into the atmosphere (Kibria et al. 2019; Wang et al. 2019; Wu et al. 2017). Over years, several metals, metal oxides, and metal complexes have been found to be excellent electrocatalysis in CO_2RR to convert CO_2 to high added-value chemical products, for instance, methane (Liu et al. 2021), ethylene (Zeng et al. 2021), ethanol and others. 2D *c*-MOFs as a porous conductive material, have been vigorously explored in the CO_2RR. However, the conductivity of 2D *c*-MOFs is varied in a large range from ~10^{-8} to ~10^{-1} S/cm (Day et al. 2019; Yi et al. 2020), which depends not only on the intrinsic framework connectivity but also on the crystallinity and morphology of the resultant 2D *c*-MOFs. The low conductivity of 2D *c*-MOFs posed a huge obstacle to the full utilization of their intrinsic catalytic activities. The formation of composites has been determined as an effective strategy in the improvement of materials performance. Carbon nanotubes (CNTs) are allotropes of carbon, which have excellent chemical robustness and high electrical conductivity. CNTs have been doped into different types of materials to increase their electrochemical performance (Abdi et al. 2017; Yang et al. 2018). To the best of our knowledge, the doping of CNTs to defective 2D *c*-MOFs has not been reported.

Herein we proposed the functionalized of 2D *c*-MOFs with the creation of defects and further boosting the electrochemical CO_2RR performance of 2D *c*-MOFs with the formation of composites with CNTs.

1.2 Synthesis and Characterization of *d*-CAT-Cu

CAT-Cu is first reported by the Yaghi's group (Hmadeh et al. 2012), which attracted great attention in recent years. We choose CAT-Cu as an example to demonstrate

the creation of defects in 2D *c*-MOFs. Generally, the 2D *c*-MOFs are synthesized with stoichiometrically metal ions and ligands, which realize an ideal framework. To generate defects, we synthesized *d*-CAT-Cu with a deviation from the standard equivalent of Cu^{2+} and hexahydroxyltriphenylene (HHTP). Here, *d*-CAT-Cu is prepared with a mole ratio of $Cu(NO_3)_2{\cdot}2.5H_2O$ to HHTP for 1:1.33. After optimization, a mixed solvent containing H_2O/methanol/*N*, *N*'-dimethylformamide (DMF) in a volume ratio of 10:1:1 was chosen as the solvent to prepare *d*-CAT-Cu at 85 °C for 48 h (Fig. 1.1a). Dark blue powder of *d*-CAT-Cu was collected after washing by DMF, H_2O and methanol, successively. The result of *d*-CAT-Cu was first characterized with powder X-ray diffraction (PXRD). The experimental PXRD of *d*-CAT-Cu shows a series of diffraction peaks at 4.7 °, 8.2 °, 9.4 °, 12.5 °, and 16.4 °. Compared with previously reported PXRD for CAT-Cu, *d*-CAT-Cu is in an AA stacked model with hexagonal distributed pores (Fig. 1.1b). We used the Fourier transform infrared spectroscopy (FT-IR) to detect hydroxyl groups to verify the existence of defects in *d*-CAT-Cu. The FT-IR of *d*-CAT-Cu exhibits uncoordinated phenolic hydroxyl belonging to HHTP at around 3200 cm^{-1} which preliminarily confirmed the existence of defects in *d*-CAT-Cu (Fig. 1.1c).

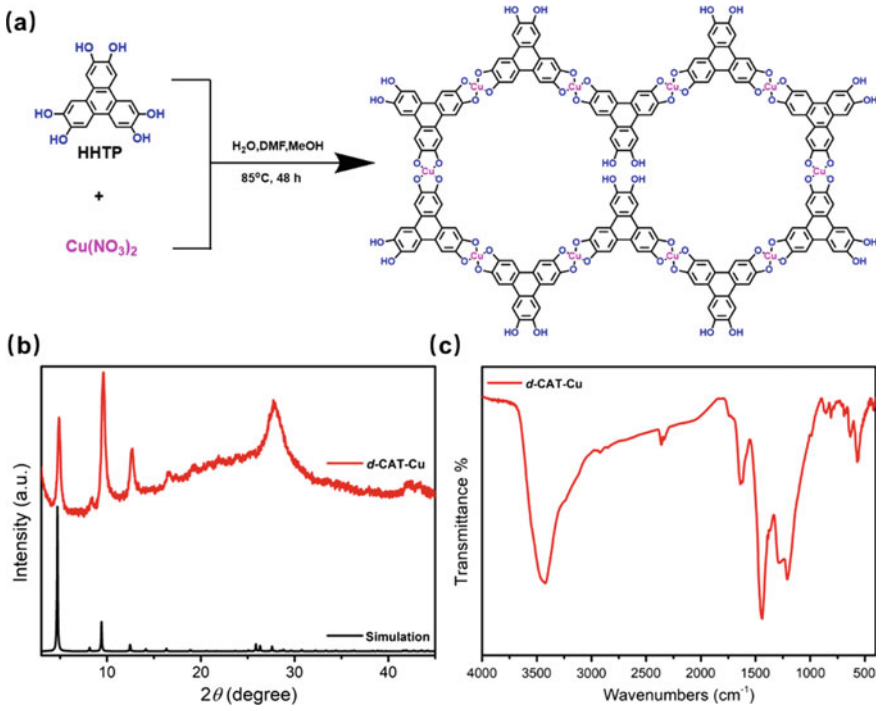

Fig. 1.1 **a** The synthesis and structure of *d*-CAT-Cu under solvothermal conditions with a representative defect shown in the middle of the structure. **b** The experimental and simulated PXRD patterns of *d*-CAT-Cu. **c** FT-IR spectrum of *d*-CAT-Cu

Furthermore, the X-ray photoelectron spectroscopy (XPS) survey of *d*-CAT-Cu also verified its chemical structure with all the elements, such as C, O, and Cu existing in the XPS spectrum (Fig. 1.2a). In the Cu 2p XPS spectrum, Cu^{2+} $2p_{3/2}$ and Cu^{2+} $2p_{1/2}$ signals were observed at 933.4 and 953.5 eV, respectively (Fig. 1.2b). The N_2 isotherm of *d*-CAT-Cu at 77 K shows a Brunauer–Emmett–Teller (BET) surface area of 280 m^2/g (Fig. 1.2c), which is much higher than some of the previous reported (Yi et al. 2020). N_2 adsorption at 77 K was also used to investigate the defective porous structure of *d*-CAT-Cu, which exhibited a large number of mesopores around 4 nm (Fig. 1.2d). The existence of these large mesopores could be direct evidence for the introduction of defects. To sum up, we eventually confirm the successful synthesis of *d*-CAT-Cu. Based on the structure of *d*-CAT-Cu, a large amount of hydroxy functional groups has been introduced in the frameworks, which would have a significant influence on their catalytic behavior.

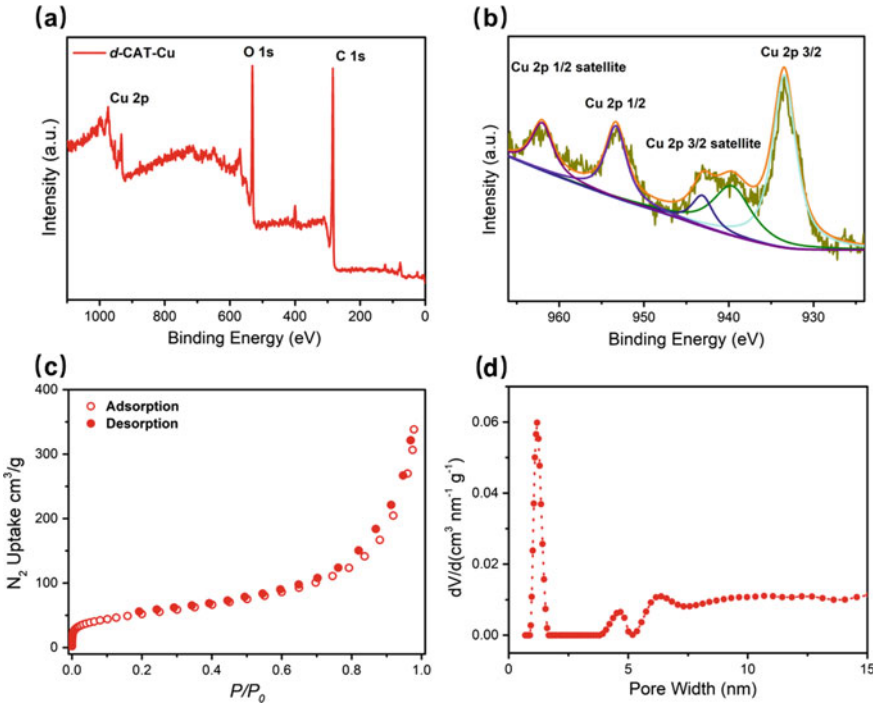

Fig. 1.2 **a** XPS survey spectrum of *d*-CAT-Cu. **b** The high-resolution Cu 2p XPS spectrum of *d*-CAT-Cu. **c** N_2 adsorption isotherm of *d*-CAT-Cu at 77 K. **d** Pore width distribution of *d*-CAT-Cu shows the existence of defects around 4 nm

1.3 Experiment of CO_2 Reduction Reaction (CO_2RR)

1.3.1 Preparation of Catalyst

The working electrode was prepared with 5 mg of catalyst and 40 μL 5 wt% Nafion. The above materials were dispersed well in 0.5 mL isopropanol and sonicated for 5 min, then 1 mg CNT was added into it and sonicated for 30 min to obtain *d*-CAT-Cu-CNT. After that, 10 μL of the resulting ink was dropped onto the surface of a glass carbon electrode (GCE) with a disk diameter of 5 mm to form the working electrode.

1.3.2 Electrocatalytic CO_2RR

The electrocatalytic CO_2RR activity of *d*-CAT-Cu-CNT was tested in an airtight H-cell with a standard three-electrode system. An aqueous solution of 0.1 M $KHCO_3$ saturated with CO_2 was used as the electrolyte. Figure 1.3 shows the linear sweep voltammetry (LSV) curves of *d*-CAT-Cu-CNT in CO_2 saturated and Ar saturated electrolytes. A clear reduction peak at −0.9 V *versus* RHE for *d*-CAT-Cu was found in both saturated CO_2 electrolyte and Ar saturated one. According to previous reports, this reduction peak was corresponding to the reduction of Cu^{2+} to Cu^{+}. However, this reduction peak was not observed in the *d*-CAT-Cu-CNT, which could be raised from the interaction of 2D *c*-MOFs and CNT. Significantly, the current density of *d*-CAT-Cu-CNT at −1.6 V *versus* RHE is 35 mA cm^{-2}, which is larger than that of *d*-CAT-Cu without CNT doping (18 mA cm^{-2}). In addition, the current density of *d*-CAT-Cu and *d*-CAT-Cu-CNT in CO_2 saturated electrolyte were both higher than that in Ar saturated electrolyte, which further testified that CO_2 is participant in the electrocatalytic reaction.

Next, the electrolysis experiments of *d*-CAT-Cu-CNT were carried out at different potentials from −1.1 to −1.5 V *versus* RHE. As shown in Fig. 1.4, the Faradaic efficiency (FE) of H_2 was lower than 20% at all potentials, which showed that most of the electrons are used to turn CO_2 into other value-added products. Under the same condition, the FE of CO is lower than 6% at all potentials. Meanwhile, the Faradaic efficiency of C_2H_4 reached 23% at −1.5 V *versus* RHE. More importantly, FE of CH_4 achieved its maximum of 63% at −1.4 V *versus* RHE with a partial current density of 25 mA cm^{-2}, which is a considerably high selectivity in CO_2RR. The total FE of gaseous product is closed to 100% and no liquid phase product was determined.

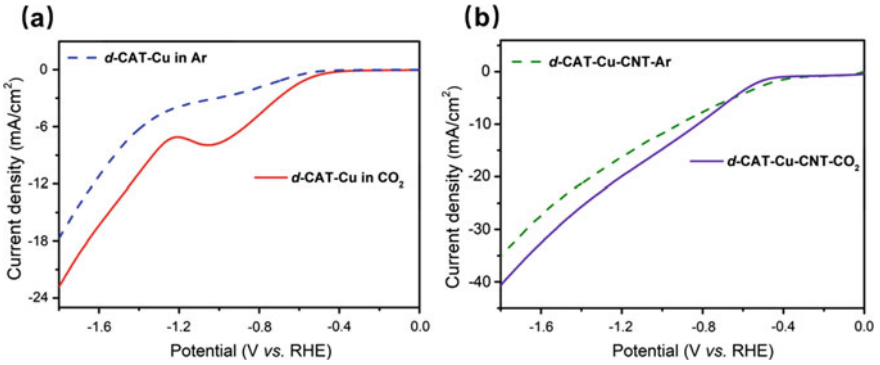

Fig. 1.3 **a** LSV curves of *d*-CAT-Cu in CO_2 and Ar saturated electrolyte. **b** LSV curves of *d*-CAT-Cu-CNT in CO_2 and Ar saturated electrolyte

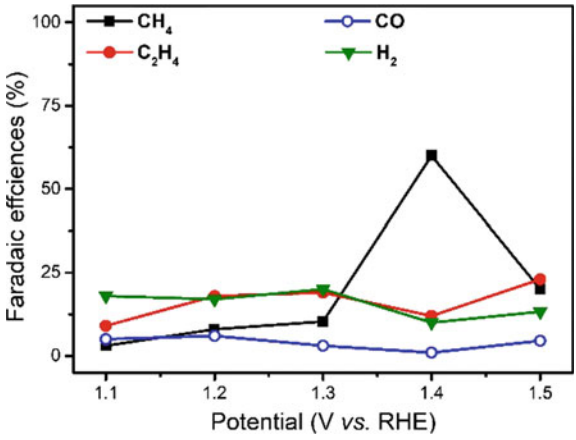

Fig. 1.4 Potential dependent CO_2RR performance of *d*-CAT-Cu-CNT

1.4 Conclusions and Perspective

In summary, a defect engineering strategy has been developed for 2D *c*-MOFs to realize their functionalization. A *d*-CAT-Cu has been synthesized and their electrocatalytic CO_2RR has been investigated. After doping with CNT, the *d*-CAT-Cu can produce methane in a FE of 63% at a current density of 25 mA cm^{-2}. This work opens a new avenue in the development of 2D *c*-MOFs.

Acknowledgements The financial support from the National Natural Science Foundation of China (nos. 81601549, 61933002). Beijing Institute of Technology Research Fund Program for Young Scholars is acknowledged. The authors acknowledge the Analysis and Testing Center of BIT for technical support.

References

Abdi J et al (2017) Synthesis of metal-organic framework hybrid nanocomposites based on GO and CNT with high adsorption capacity for dye removal. Chem Eng J 326:1145–1158

Cheetham T et al (2016) Defects and disorder in metal organic frameworks. Dalton Trans 45(10):4113–4126

Day RW, et al. (2019) Single crystals of electrically conductive two-dimensional metal–organic frameworks: structural and electrical transport properties. ACS Cent Sci 5(12):1959–1964

Dissegna S et al (2018) Defective metal-organic frameworks. Adv Mater 30(37):1704501

Fang Z et al (2015) Defect-engineered metal-organic frameworks. Angew Chem Int Ed 54(25):7234–7254

Hmadeh M et al (2012) New porous crystals of extended metal-catecholates. Chem Mater 24(18):3511–3513

Kayal S, Chakraborty A (2022) Evaluation of defect induced surface heterogeneity in metal-organic framework materials with alkali dopants employing adsorption isotherm modelling. J Indian Chem Soc 99(6):100493

Kibria MG et al (2019) Electrochemical CO_2 reduction into chemical feedstocks: from mechanistic electrocatalysis models to system design. Adv Mater 31(31):1807166

Liu Y et al (2021) The synthesis of hexaazatrinaphthylene-based 2D conjugated copper metal-organic framework for highly selective and stable electroreduction of CO_2 to methane. Angew Chem Int Ed 60(30):16409–16415

Park J et al (2018) Synthetic routes for a 2D semiconductive copper hexahydroxybenzene metal-organic framework. J Am Chem Soc 140(44):14533–14537

Peterson Gregory W et al (2017) Optimizing toxic chemical removal through defect-induced UiO-66-NH_2 metal-organic framework. Chem Eur J 23(63):15913–15916

Wang YM, Woll C (2018) Chemical reactions at isolated single-sites inside metal-organic frameworks. Catal Letters 148(8):2201–2222

Wang L et al (2019) Surface strategies for catalytic CO_2 reduction: from two-dimensional materials to nanoclusters to single atoms. Chem Soc Rev 48(21):5310–5349

Wang Z et al (2020) Defect Creation in surface-mounted metal-organic framework thin films. ACS Appl Mater Interfaces 12(2):2655–2661

Wang M, Dong R, Feng X (2021) Two-dimensional conjugated metal–organic frameworks (2D c-MOFs): chemistry and function for MOFtronics. Chem Soc Rev 50(4):2764–2793

Wu J et al (2017) CO_2 reduction: from the electrochemical to photochemical approach. Adv Sci 4(11):1700194

Yang L et al (2018) Two-dimensional metal-organic layers on carbon nanotubes to overcome conductivity constraint in electrocatalysis. ACS Appl Mater Interfaces 10(42):36290–36296

Yi J et al (2020) Highly selective CO_2 electroreduction to CH_4 by in situ generated Cu_2O single-type sites on a conductive MOF: stabilizing key intermediates with hydrogen bonding. Angew Chem Int Ed 59(52):23641–23648

Zeng L et al (2021) Multiple cuprous centers supported on a titanium-based metal-organic framework catalyze CO_2 hydrogenation to ethylene. ACS Catal 11(18):11696–11705

Zhong H et al (2022) Two-Dimensional conjugated metal-organic frameworks for electrocatalysis: opportunities and challenges. ACS Nano 16(2):1759–1780

Chapter 2
Feasibility Study on the Utilization of Underground Facilities for the Disposal of Chemical Agents

Ho-Kab Choi, Tae-Won Shin, and Sung-Il Kim

Abstract In this study, a disposal method was developed, and the effects of using underground facilities for CBR hazard toxics, especially chemical agents, were investigated. Chemical agent disposal is a sensitive, time-consuming process, and facility protection is essential during military threats. For this purpose, the operation of underground facilities to protect chemical agents from internal and external threats is considered effective. Hence, in this study, the operation of ground and underground chemical agent storage facilities was simulated using CFD Tool. The results revealed that structures above the ground exhibited a ~3–5 times larger risk distance of chemical agent contamination than that exhibited by underground structures, depending on the location of exposure. The simulation results further revealed that it is safer to store and manage chemical agents intended for future disposal in underground facilities than in ground facilities. This paper proposes a complementary direction for the design criteria of underground storage facilities for the storage of chemical agents intended for disposal. Furthermore, this study suggests technical and three-dimensional protection systems, such as warning, detection, and decontamination systems, for the effective protection of underground storage facilities from internal and external threats.

Keywords Chemical weapon · Chemical agents disposal · Underground facility

H.-K. Choi · T.-W. Shin (✉)
Department of Protection and Safety Engineering, Seoul National University of Science and Technology, Seoul, Korea
e-mail: stw49884@gmail.com

S.-I. Kim
Defense Institute of Seoul Tech, Seoul National University of Science and Technology, Seoul, Korea

G. Huang (ed.), *Proceedings of 2022 7th International Conference on Environmental Engineering and Sustainable Development (CEESD 2022)*, Environmental Science and Engineering, https://doi.org/10.1007/978-3-031-28193-8_2

2.1 Introduction

If battlefield environments, such as the Korean Peninsula, change rapidly and eventually escalate into a crisis, suppressing chemical warfare will emerge as a critical issue at the international community level. The international community will make various efforts to resolve this problem. Accordingly, the goal of these efforts is peaceful suppression of hostile countries to hold chemical warfare.

This effort was led by the Organization for the Prohibition of Chemical Weapons (OPCW), the implementing agency of the Chemical Weapons Convention (CWC), which became effective on April 28, 1997 (OPCW 2021). This organization was involved because it is estimated that hostile countries have various types of chemical agents amounting to approximately 2500–5000 tons without joining the CWC (MND 2020) and are operating many research, production, and storage facilities.

The peaceful prevention of hostile countries from possessing and using chemical warfare by the OPCW will become possible only after the war in the Korean Peninsula ends. Chemical weapons managed in the Korean Peninsula are the targets. The final step in the peaceful removal of hostile countries' chemical warfare ability is to destroy chemical weapons. It takes a long time to destroy chemical weapons possessed by hostile countries and to repurpose facilities related to chemical weapons. In particular, chemical bombs and chemical agents collected from a wide range of areas require safe long-term management until they are destroyed. This effort requires separate storage facilities; however, research on this topic remains insufficient.

In this study, we first investigated chemical agents and chemicals. Items that needed structural and technical improvement during storage and management were then determined by checking the processes of storage, management, and disposal of chemical weapons in countries that have had chemical weapons in the past. The ability of underground facilities to be used for the storage and management of chemical agents was verified using CFD Tool. Plans to utilize underground facilities in hostile countries are suggested for the technical and systematic storage and management of chemical agents in hostile countries until the OPCW peacefully and completely destroys the chemical warfare ability of hostile countries. In addition, this study proposes conditions and protection systems for the storage and demilitarization of chemical agents using underground magazines, which are currently in the developmental stage.

2.2 Understanding Chemical Agents

2.2.1 Definition and Characteristics of Chemical Agents

The CWC defines chemical weapons as all toxic chemicals and their precursors, munitions, delivery systems, and related equipment. Furthermore, toxic chemical agents are classified by their physiological actions on the human body and are thus

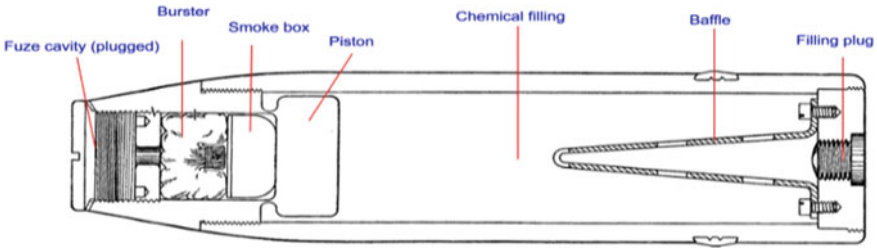

Fig. 2.1 Structure of a chemical bomb (Chemical weapons 2021)

classified as choking, blister, blood, nerve, and riot-control chemical agents (Young 2004).

One example of the large-scale deployment of chemical weapons occurred took place when German troops sprayed 150 tons of chlorine gas against the British–French Allied Forces to break through the stagnant front at the Battle of Ypres in Belgium (April 1915, World War I). During World War I, more than 200 chemical attacks caused more than 1.34 million casualties. After World War I ended, many countries competed to develop and stockpile chemical weapons.

Chemical bombs are representative forms of chemical weapons. They typically consist of various components, including toxic chemical agents and gunpowder, as shown in Fig. 2.1. Chemical bombs are produced and stored in various forms such as shells, bombs, and missile warheads, depending on the delivery system. When stored for a long time, there is a high risk of leakage of toxic chemical agents from storage facilities owing to corrosion of the shell and an increased danger of explosion.

2.3 Storage and Management of Chemical Agents

There are no separate structures or forms related to the chemical agent storage facilities. Most countries that have chemical weapons or had them in the past applied hazard classes and storage standards for ammunition and explosives using magazines.

According to the classification criteria for dangerous goods of the United Nations, chemical weapons belong to "class 6 toxic and infectious substances." Moreover, according to the detailed classification criteria for explosives, chemical weapons belong to class 6.1, and there is no need for internal distances and distances between magazines (Korea 2019). Furthermore, chemical weapons must be stored in earth-covered magazines and the floor must be painted with sodium silicate (Na_2SiO_3) to prevent it from absorbing chemical agents. The safe distance is determined by chemical toxicity, release quantity, release rate, topography, and weather conditions and is calculated using a chemical risk prediction and damage assessment method (Korea 2019).

2.4 Destruction Status of Chemical Weapons

The destruction of chemical weapons began in the late 1960s, following the US initiative. Until the 1980s, chemical weapons were destroyed by burying chemical agents on land or dumping them into the sea. Since then, international public opinion on environmental pollution has increased, and the US Congress has prohibited chemical agent disposal methods that cause environmental pollution. Thus, research on technologies that safely destroy chemical weapons has begun in earnest (Destruction of Chemical Weapons 2022).

Some countries have reported that they have chemical weapons even after continuous disposal efforts and are in the process of destroying them. Before destroying chemical weapons, some countries stored and managed them in storage facilities above the ground. The operation and management status of these chemical weapons storage facilities were examined to investigate the preconditions of these storage facilities for the stable storage and management of chemical weapons programs collected from hostile countries.

The chemical weapon storage facilities of the US were mainly constructed as earth-covered magazines (Department of the Army Pamphlet 2011), which separately store chemical agents according to their type. Similar to the US, Russia stockpiled chemical agents in various ammunitions and bulk containers and stored them in earth-covered magazines in the Ural mountain region. In particular, they separately stored the explosive components of chemical bombs, such as charges and fuses, except for complex ammunitions (Chemical Weapons 2022).

Countries that stockpiled chemical weapons stored chemical agents that were not weaponized in bulk containers for safe management during a long period of storage, and separately stored chemical bombs by separating explosive components, such as gunpowder and fuses. The separation of explosive components from chemical bombs is a process of demilitarization during the chemical agent disposal procedure. However, some countries need to improve their safety management systems, including the identification, warning, and decontamination of leaks and degenerated chemical bombs, because the chemical bombs in storage facilities contain degenerated substances or have leaks. Furthermore, most of the chemical weapon storage facilities are earth-covered in forests or open areas, and it is possible to take measures or prevent simple leaks, but they are highly vulnerable to military acts from the outside.

Therefore, in the event of war or in the presence of external attack threats in the Korean Peninsula, it is necessary to verify the type of storage facilities that will be effective for long-term operation until the chemical agents are disposed of. Toward this end, evaluations of damage caused by external attacks (air bombs) using the HPAC, a US CBR risk prediction and evaluation model, were carried out for ground and underground chemical weapons storage facilities.

2.5 Risk Assessment Based on Chemical Weapon Storage Facilities

Numerous CFD tools has been applied to analyze the effects of and determine the damage inflicted by weapons of mass destruction. Those can predict damage according to the movement path and diffusion of hazardous substances in the event of nuclear and CBR attacks or leaks. Furthermore, the CVFD tool can predict the damage in the event of nuclear accidents and attacks on chemical weapon production and storage facilities by conventional weapons.

To analyze the effective mode of long-term operation of the storage facilities until the chemical agents are destroyed, the storage facilities were classified into two types, underground and ground structures, as shown in Table 2.1, and the specifications were input. Among these chemical agents, nerve chemical agents, which are presumed to be abundant in hostile countries, were targeted.

Figure 2.2 shows simulation results depicting the striking of the inner parts of underground and ground structures using 2000 lbs fission bombs that targeted a facility in which 1200 tons of nerve (GB) chemical agents were stored.

A strike to the inner parts of the underground and ground structures using a 2000 lbs fission bomb was simulated. The results revealed that the contamination damage risk distance of an underground structure in which the probability of casualties in the contaminated area was ≥50% was approximately 19.3 km, as shown in Fig. 2.2.

Table 2.1 Specifications for attacks of chemical agent storage facilities

Classification		Construction type (Storage facilities)	
		Underground	Ground
Calculation	Target	Confinement: internal storage. Agent: GB, 1200 tons Factory type: storage (chemical weapon storage facilities) Container: sup. tank/vert (vertical tank with support) Arrangement: vertical stack (storage boxes stacked in a hexahedron)	
	Weapon	Warhead: 2000 lbs class blast/flag (2000 lbs fission bomb) Location: inside target (inside the target), near (near the target)	

※ Weather/terrain conditions: wind direction (270°, west wind), wind speed (14 km/h), temperature (15 °C), and humidity (60%). Terrain conditions: mountain range, region: Yeongju, Gyeongsangbuk-do.

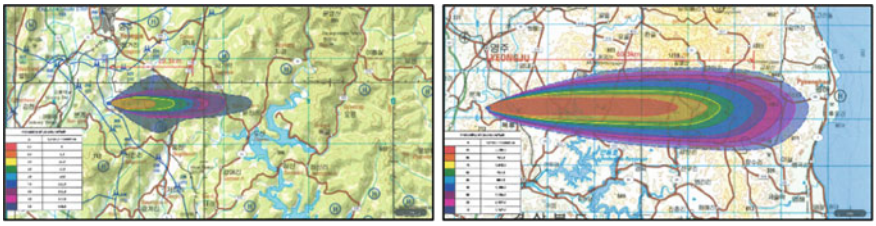

Fig. 2.2 Results of a simulation of a strike to the inner parts of underground structures (left)/a ground structure (right) using a 2000 lbs fission bomb

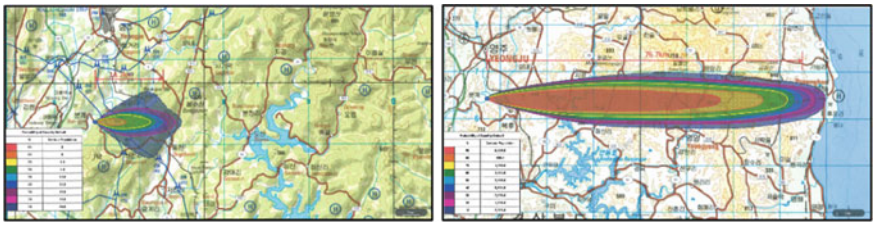

Fig. 2.3 Results of a simulation of a strike near an underground structure (left)/a ground structure (right) based on the use of a 2000 lbs fission bomb

Furthermore, the contamination damage risk distance of a ground structure in which the probability of casualties in the contaminated area was ≥50% was approximately 69.3 km, as shown in Fig. 2.2. Figure 2.3 shows the simulation results of a strike near underground and ground structures following the use of a 2000 lbs fission bomb that targeted a facility that stored 1200 tons of nerve (GB) chemical agents.

A strike near the underground and ground structures using a 2000 lbs fission bomb was simulated. The results revealed that the contamination damage risk distance of the underground structure in which the probability of casualties in the contaminated area was ≥50% was approximately 14.7 km, as shown in Fig. 2.3. Furthermore, the contamination damage risk distance of a ground structure in which the probability of casualties in the contaminated area was ≥50% was approximately 76.7 km, as shown in Fig. 2.3.

For the simulation of a strike to the inner parts of and near underground and ground structures using a 2000 lbs bomb subject to the same conditions, the results are shown in Table 2.2.

In summary, by determining the risk distance based on the contamination damage that can cause a 50% or higher probability of casualties in the area contaminated with nerve (GB) chemical agents when the inner parts of the structure are exposed, it was found that the risk distance of the ground structure is three times higher than that of the underground structure; moreover, when the parts near the structure are exposed, the risk distance of the ground structure is five times higher. This finding suggests that underground chemical agent storage facilities would be safer and easier to protect against external attacks than ground structures.

Table 2.2 Result of striking inside and near underground and ground structures

Classification	Contamination damage risk distance (50% or higher probability of casualty in the contaminated area)	
	Underground	Ground
Inside target	19.3 km	69.3 km
Near	14.7 km	76.7 km

2.6 Utilization of Underground Facilities for the Disposal of Chemical Agents

Ammunition storage facilities (among all types of military facilities) have recently been developed as underground facilities because they are safer than ground facilities (Shin 2011). Ammunition storage facilities that are built underground can safely protect explosives from accidental explosions, natural disasters, or external attacks inside storage facilities, and minimize damage. Moreover, they can reduce the required area, vigilance measures, and the maintenance and repair of ammunition storage facilities.

In addition, because the terrain of the Korean Peninsula is mostly mountainous, topographical conditions are excellent for underground storage facilities. If there are mountains and valleys opposite the entrance to the storage facilities, they can reduce the effects of storms and debris, and the spread of contamination by chemical agents.

2.7 Preconditions for Underground Facilities for Storing Chemical Agents

Chemical agent storage facilities that are built above ground, as shown in Fig. 2.4, can be highly vulnerable to external attacks. Moreover, in the event of leakages of chemical agents, the contaminated areas may be large, depending on the weather conditions. Considering the testimony from Thomas A. Schwartz, the former commander of the ROK-US combined forces that "there are more than 11,000 underground fortresses in the enemy state" (Schwartz 2001), there will be no restrictions on the operation of chemical storage facilities because various underground facilities in the hostile country can be selectively used.

Owing to the chemical warfare abilities of hostile countries and many fortified underground facilities in the region, it is highly effective to utilize various forms of existing underground facilities in mountainous areas for chemical agent storage. The preconditions of underground facilities for storing chemical agents are as follows.

First, as chemical weapons are substances classified as explosives (danger grade 6), space is required for the bulk containers, C-UXO, and ACW in the storage compartment to minimize the explosion risk. Second, C-UXO and ACW require separate spaces for demilitarization activities to separate explosive components,

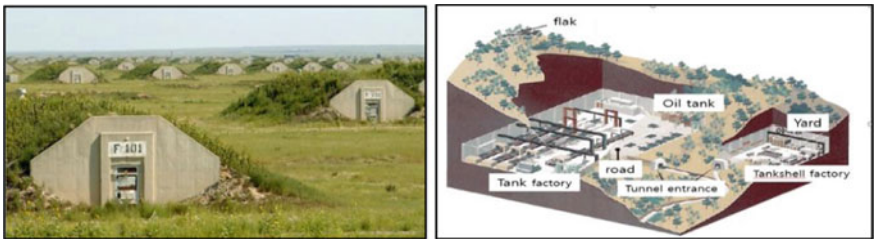

Fig. 2.4 Pueblo chemical depot and NK Kanggye UGF (assumed) (U.S. Army CMA Homepage 2022; Small World 2022). (*Source* U.S. Army CMA Homepage, Pueblo Chemical Depot [left] & Small World, https://doris.tistory.com/36 [right])

such as fuses and boosters, to shorten the time required for and ensure safety during disposal. Third, because bulk containers, C-UXO, and ACW are mainly stored in storage compartments among the components of underground magazines, a minimum compartment width is required for storing bulk containers and the operation of the supply equipment. The widths and heights of the paths must accommodate the passage of the entering vehicles and supply equipment. Fourth, spaces and safety systems must be separated to operate the chemical weapon disposal technology and related equipment. Fifth, detoxification systems must be installed along paths in connection with firefighting systems to prepare for fire accidents. Sixth, because detoxification is limited if the agents leak into the storage compartment and are absorbed by the floor, sodium silicate (Na2SiO3) must be applied to the floor to prevent this.

2.8 Protection System for Chemical Agent Underground Storage Facilities

Three-dimensional systems that protect chemical agent storage facilities against external attacks or terrorist threats must be guaranteed because the facilities operate for a long period before the chemical agents are destroyed completely.

First, physical vigilance measures must be enforced in preparation for terrorist and hostile country attacks against chemical agent storage facilities. Second, a pollution damage prediction model that applies Korean weather, topography, and alarm systems, including remotely controllable chemical agent detection systems, must be established to prevent the leakage of chemical agents. The aim of these systems is to serve as danger alerts and minimize damage by applying real-time weather and topographic conditions and by judging the location of chemical contamination sources, diffusion directions, diffusion ranges, and types of chemical agents. Third, CBR protective forces must be prepared to detect, identify, and detoxify chemical agents. A detoxification system must be established to identify the contaminated area; measure the contamination range; and detox contaminated personnel, facilities, and

areas in the event of a chemical agent leakage due to external attacks or intentional action.

2.9 Conclusions

The reliable and stable operation of chemical agent storage facilities until chemical agents can be peacefully destroyed is a crucial task that increases trust in the international community and ensures the peace of the Korean Peninsula.

The main achievements of this study are as follows. First, simulations using CFD Tool, confirmed that underground structures are safer and more effective for the protection of chemical agent storage facilities than ground structures. This is because chemical agent storage facilities must operate in the presence of military threats from hostile countries. Second, this study identified the possibility of operating chemical agent storage facilities using underground facilities of various sizes in hostile countries. Furthermore, it suggests conditions for underground storage facilities used to store chemical agents based on considerations of the design criteria of the underground magazine storage compartment, paths, bottlenecks, and entrance barriers.

Third, this study suggests that spaces are needed to ensure alarm and detection systems and demilitarization activities of C-UXO and ACW for use when underground chemical agent storage facilities are operated. Fourth, this study also highlights the need for mechanisms for responding to external military threats, such as vigilance, alarm, and internal and external detoxification systems of chemical agent storage facilities.

However, to manage chemical agents more stably in hostile countries, research on the design concepts and criteria for underground chemical agent storage facilities and continuous technological development for the disposal of chemical agents in underground storage facilities are required. And it is necessary to study the economic effects for disposal, soil and groundwater pollution.

References

Chemical weapons, http://zarco-macross.wikidot.com/wiki:chemical-weapon, last accessed 06 Sept 2021

Chemical Weapons, https://nuke.fas.org/guide/russia/cbw/cw.htm last accessed 25 April 2022

Department of the Army Pamphlet 385–64 (2011) Ammunition and Explosives Safety Standards, Washington, DC, p. 53

Destruction of Chemical Weapons, https://en.wikipedia.org/wiki/Destruction_of_chemical_weapons, last accessed 11 April 2022

Ministry of National Defense (2019) Instruction on safety management standards for ammunition and explosives, Seoul Korea, pp. 56–480

MND (2020) 2020 Defense White Paper, Seoul Korea, p. 29

OPCW: The OPCW's mission, https://www.opcw.org/about-us, last accessed 30 Sept 2021
Schwartz TA (2001) Forward deployment with more than 4,000 underground facilities, 11,000 underground fortifications nationwide, and the world's largest submarine fleet and special forces. Korea J
Shin YS (2011) A study on an underground ammunition depot suitable for our environment. Defense Quality Manag. 81
Small World, https://doris.tistory.com/36, last accessed 27 April 2022
U.S. Army CMA Homepage, Pueblo Chemical Depot, last accessed 27 April 2022
Young JW (2004) A study on the verification and abandonment methods when hostile countries declare abandonment of chemical weapons. defense policy research report (04–09), Korea Research Institute for Strategy 12 (2004)

Chapter 3
Research Progress of the Osteogenic Activity of the Active Peptides from *Caulerpa Lentillifera*

Xiaomei Huang, Dandan Xie, Jiehua Hu, Liru Lin, Meiying Zhao, Ruijuan Zeng, and Shan Lin

Abstract *Caulerpa lentillifera* is a potential cash crop, the current promotion and cultivation in China is in the development stage. Take *Caulerpa lentillifera* as a raw material to extract the active peptides. Then, investigate the effects of active peptides on the proliferation and differentiation of osteoblasts. Simultaneously, the metabolomics strategies was used to find the different metabolites and metabolic pathways, combining with other molecular biology methods and metabolomics results, to discuss the molecular mechanism of active peptide extracts. This filed of research is to provide scientific basis for the exploitation of marine resources and the development of new anti-osteoporosis drugs.

Keywords Progress · Osteogenic activity · Peptide · *Caulerpa Lentillifera*

Xiaomei Huang and Dandan Xie contribute equally to this work.

X. Huang · D. Xie · J. Hu · L. Lin · M. Zhao · R. Zeng
Department of Marine Biology, Xiamen Ocean Vocational College, Xiamen, Fujian 361100, P.R. China

X. Huang
Shanghai Institutes of Nutrition and Health, Chinese Academy of Sciences, Shanghai 200031, P.R. China

S. Lin (✉)
Department of Orthopaedics, the First Affiliated Hospital of Xiamen University, Xiamen, Fujian 361003, P.R. China
e-mail: 2018642046@xmu.edu.cn

School of Medicine, Xiamen University, Xiamen, Fujian 361102, P.R. China

The School of Clinical Medicine, Fujian Medical University, Fuzhou, Fujian 350004, P.R. China

G. Huang (ed.), *Proceedings of 2022 7th International Conference on Environmental Engineering and Sustainable Development (CEESD 2022)*, Environmental Science and Engineering, https://doi.org/10.1007/978-3-031-28193-8_3

3.1 Introduction

Osteoporosis is a progressive degenerative disease that usually occurs with age. Its pathogenesis is very complex, from the cellular level, osteoblasts are the most important material basis for osteogenesis and bone formation, and its proliferation and differentiation defects are one of the root causes of osteoporosis. At present, many bioactive food factors as well as natural products have been shown to promote the growth of osteoblasts. Among them, some small molecule polypeptides have been shown to have the ability to promote osteoblast proliferation and differentiation. In vitro experiments have also shown that small molecule collagen polypeptides can stimulate the proliferation and differentiation of osteoblasts, and then regulate the expression of osteoblasts related to bone formation, ultimately affecting the growth process of osteoblasts.

Caulerpa lentillifera is beginning to be popularize planted in China, but it has not yet been optimized utilization. Hence, its added-value of products is relatively low. The application and development of *Caulerpa lentillifera* as a cash crop, will provide a scientific basis for expanding the development of marine active peptide resources and new anti-osteoporosis drugs. The extraction of active peptides from *Caulerpa lentillifera*, as well as the research on the activity of osteogenesis are rarely reported in the literature at home and abroad.

3.2 Progress of the Treatment of Osteoporosis

Osteoporosis is a progressive degenerative bone disease that usually occurs with age (Payal et al. 2017). It is characterized by decreased bone mineral density and quality, destruction of bone microstructures, and increased bone fragility caused by a variety of factors that predispose to fractures (Sozen et al. 2017). Osteocellular cells are the smallest units that make up bones, and osteoblasts are precursors of bone cells, and their reproduction and differentiation are of great significance to the growth of bones (Fu et al. 2019). The pathogenesis of osteoporosis is very complex, from the cellular level, osteoblasts are the most important material basis for osteogenesis and bone formation, and their proliferation and differentiation defects are one of the root causes of osteoporosis. Therefore, the key to treating osteoporosis lies in how to promote the proliferation and differentiation of osteoblasts. At present, traditional estrogen replacement therapy can promote the proliferation and differentiation of osteoblasts, which has a good early effect on osteoporosis. However, its long-term safety has been widely questioned. In the search for alternatives to estrogen, many bioactive food factors (calcium, vitamin D3, collagen, etc. (Eaton-Evans 1994)) as well as natural products (icariin (Huang et al. 2018) and kaempferol (Kim et al. 2016)) have been shown to promote the growth of osteoblasts. Type I collagen, which is widely distributed in connective tissues such as ligaments and cartilage, plays an important role in the reproduction and differentiation of osteoblasts. However, collagen

has a special triple helix structure (Villa et al. 2016) and a large molecular weight (Sneha et al. 2016), which is often detrimental to the digestion and absorption of organisms. Conversely, some small molecule polypeptides (such as casein derivative active peptides (Reddi et al. 2018) and whey protein-derived peptides (Pandey et al. 2018)) have been shown to have the ability to promote osteoblast proliferation and differentiation. In vitro experiments have also shown that small molecule collagen polypeptides can stimulate the proliferation and differentiation of osteoblasts, and regulate the expression of osteoblasts-related genes related to bone formation, ultimately affecting the growth process of osteoblasts (Daneault et al. 2015). Therefore, peptides can promote the proliferation and differentiation of osteoblasts more than collagen.

A polypeptide is an active substance that is between amino acids and proteins, with amino acid numbers of 10–100. In recent years, its physiological functions have received more and more attention. The polypeptide, its structure is simpler than protein, it is easy to absorb with hypoallergenic and other advantages, it is widely used in clinical practice and can provide nutrition for the organism. At present, there are two main types of peptide products: one is a polypeptide drug or a polypeptide reagent, and the other is a health food containing a functional factor active polypeptide or an ordinary food containing an active peptide. With the rapid development of modern science, technology and equipment, the production cost of active peptides has dropped significantly, and active peptide foods and drugs have entered the golden stage. Studies have shown that the active peptide obtained by hydrolysis has a certain effect on the proliferation and differentiation of osteoblasts, and also has a certain prevention and control effect on improving osteoporosis.

3.3 Research Progress of *Caulerpa Lentillifera*

Caulerpa lentillifera is an edible seaweed grown in tropical waters and is named sea grape because of its appearance like a bunch of crystal clear green grapes (Nguyen et al. 2011). The texture of sea grapes is quite similar to salmon roe, but it is fresh and fragrant, and there is no fishy smell of fish eggs, so it is known as the green caviar in the plant, which is the perfect match of sushi, and it is very popular on the Japanese table. Sea grapes belong to the fern family of green algae, mainly distributed in Okinawa, Indonesia, Vietnam and other Asian countries (Bhesh et al. 2015). It is rich in a variety of nutrients needed by the human body, including amino acids, unsaturated fatty acids, minerals, and is also rich in macro or trace elements such as P, Ca, Mg, Cu, and Se (Paul et al. 2014). Studies have shown that 80% of *Caulerpa lentillifera* are composed of seaweed polysaccharides, collagen and dietary fiber. Among them, the protein content is significantly higher than that of terrestrial vegetables (about 10.4–14.7%), and the amino acids are relatively complete. It has a higher content of polyunsaturated fatty acids (about 16.7%) (Matanjun et al. 2009) and dietary fiber (about 8%), while its total fat content is lower (1.6–3.7%) (Tong et al. 2022), making it a class of marine cash crops with certain health functions.

At present, there are few domestic studies on *Caulerpa lentillifera.* There are some research on the extracts of *Caulerpa lentillifera.* Sharma, et al. found that the extracts of *Caulerpa lentillifera* could improve insulin resistance and regulate glucose metabolism in mice through the PI3K/AKT signaling pathway, suggesting that *Caulerpa lentillifera* extracts might be used for diabetes prevention and control (Bhesh et al. 2015). Other studies have shown that the extracts of *Caulerpa lentillifera* were effective in inhibiting cell death, significantly improved insulin secretion and expression of fat cell glucose transporters as well as the and glucose uptake (Bhesh and Dong 2014). Japanese scholar Maeda, et al. used water as an extractant to extract *Caulerpa lentillifera* polysaccharides, and found that the extracted polysaccharides could increase the expression of genes encoding cytokines through the p38 MAPK and NF-κB signaling pathways, thereby enhancing the phagocytic activity of macrophages (Maeda et al. 2012). The NF-κB mentioned in the above-mentioned study plays an indispensable role in normal physiological processes such as the immune system, skeletal system, and epithelial tissue by regulating cell reproduction, differentiation, and proliferation (Wullaert et al. 2011). NF-κB plays an important regulatory role in the skeletal system, and its important influence on the differentiation and maturation of osteoblasts and osteoclasts and their functional activities (Boyce et al. 2010), making the NF-κB signaling pathway a new research target for the treatment of diseases with abnormal bone mass growth or reduction (Chang et al. 2011).

The relatively high protein content and complete amino acid range of *Caulerpa lentillifera* have been preliminarily confirmed to have important biological activities. Do the peptide actives contained in *Caulerpa lentillifera* have high osteogenesis activity? Is there a therapeutic effect on osteoporosis? Unfortunately, there are still few reports at home and abroad on the active peptide of *Caulerpa lentillifera*, and the research on the extraction process of its active peptide is basically in the blank, and there are no reports on the osteogenesis activity of the *Caulerpa lentillifera* active peptide. Therefore, the systematic study of the extraction, isolation, purification of the active peptides of *Caulerpa lentillifera* and their biological effects on osteoblasts has become an urgent scientific and technological topic to be solved.

3.4 Metabolomics Technology Combined with Multi-technology Used to Evaluate the Cellular Biological Effect of Active Peptides

There are many ways to evaluate the cellular biological effects of biologically active substances. As a high-throughput research tool, metabolomics can be used to detect endogenous small molecules in the products of biochemical reactions, to illustrate the connections between different pathways operating in a living cell (Thomas et al. 2011). Therefore, metabolomics is often used to reflect and evaluate differences in biochemical indicators between healthy or pathological organisms.

In addition, cytometomics can provide a direction for drug development or intervention (Wang et al. 2012). Cell metabolomics can be used to qualitatively and quantitatively describe the final response of biological systems to genetic factors or changes in the external environment by detecting final metabolites regulated within the cell (Miroslava et al. 2010). At present, the metabolomics of cells has been widely used in toxicology, efficacy evaluation, cell culture monitoring, new drug research, biopharmaceutical production, food omics and other fields. In addition, in vitro cell metabolomics has many advantages such as easy operation, high reproducibility, low cost, and easy tracking of results. In recent years, advances in the study of cellular metabolomics for evaluating the biological effects of active substances have been widely recognized. Omics technology was used to detect the metabolism of osteoblasts co-cultured with active peptides of *Caulerpa lentillifera*, and combined with molecular biology techniques, it was analyzed from the aspects of gene and protein expression regulation to further verify the metabolomics results. At the same time, combined with the proliferation, differentiation and other phenotypic information of osteoblasts, multi-technology combination to evaluate the osteogenetic activity of *Caulerpa lentillifera* active peptides. It will be useful to reveal the molecular mechanism of the biological effect of the active peptide on bone cells of the *Caulerpa lentillifera.*

3.5 The Extraction of *Caulerpa Lentillifera* Active Peptides Can Promote the Development of Osteoporosis Drugs

With the increasingly serious phenomenon of population aging in modern society, osteoporosis and its complications have become one of the main diseases that lead to the decline and death of people's quality of life, and are more and more highly valued by people. At present, the treatment of osteoporosis is still an urgent problem to be solved in the clinic. The basic pathogenesis of osteoporosis is that the coupling of bone formation and bone resorption in the process of bone metabolism is unbalanced, resulting in an imbalance in the metabolism of calcium and phosphorus in the body, a decrease in osteogenesis capacity and an increase in osteoclast activity, an acceleration of bone resorption, and a gradual decrease in bone density. Therefore, it is of great significance to promote osteoblast proliferation and differentiation, improve osteoblast function and regulate bone reconstruction.

China has a long coastline, coastal islands are dotted with coastlines, and marine resources are abundant. As a common type of seaweed, *Caulerpa lentillifera* is one of the most important component of marine resources, some of its components have special biological activities, there are broad application prospects, and it is imperative to fully carry out the research of *Caulerpa lentillifera.* Due to the high value of *Caulerpa lentillifera* in nutrition, it is widely promoted in Qingdao, Shenzhen and other cities in China. A small number of areas in Fujian province have emerged small-scale of aquaculture of *Caulerpa lentillifera*, but they have not been optimized

utilization, the added-value is relatively low. In particular, the extraction and utilization of active ingredients in *Caulerpa lentillifera* are still rarely studied, the extraction process and application of *Caulerpa lentillifera* active peptides are even rarer in the literature. If the extraction process of the active peptide of *Caulerpa lentillifera* can be optimized most reasonably, and the properties of its active peptide extract can be studied and exploited, it is conducive to sustainable environmental development and will also bring immeasurable economic and social value.

Classify the *Caulerpa lentillifera* active peptide to obtain different levels of active peptide molecules with higher purity. Then, taking osteoblasts as the research object, the proliferation and differentiation of osteoblasts under the culture of *Caulerpa lentillifera* active peptide extracts were analyzed. The influence mechanism of *Caulerpa lentillifera* active peptide on the metabolic pathway of osteoblasts was explored by combining metabolomics strategies, combined with molecular biology techniques, and multiple technologies such as gene and protein expression regulation. Focusing on the main circulation pathways that are closely related to the local regulation of osteoblasts, such as the Wnt signaling pathway, the bone morphogenesis protein signaling pathway (BMP), and the mitogen-activated protein kinase (MAPK) signaling pathway, and using this as the starting point to explore the mechanism of action of *Caulerpa lentillifera* active peptides on osteoblasts, it will provide a scientific basis for the development and utilization of marine algae resources and the development of new anti-osteoporosis drugs.

3.6 Prospection

Caulerpa lentillifera is beginning to promote planted in China, but it has not yet been resource utilized, and the added-value of products is relatively low. The extraction and utilization of its active ingredients will broaden the channels for the application and development of this cash crop. The extraction of active peptides of *Caulerpa lentillifera* has not been reported in the literature at home and abroad.

The evaluation of *Caulerpa lentillifera* active peptide on osteogenetic activity by metabolomics strategies combined with multiple molecular biological methods was not reported. Research on *Caulerpa lentillifera* active peptide will provide a scientific basis for expanding the development of marine peptide resources and the development of new anti-osteoporosis drugs.

Acknowledgements This work was supported by Program of EnShi TuJia & Miao Autonomous Prefecture Bureau of Scientific & Technological Affairs (Y959K21021), Fujian educational and scientific research program for young and middle-aged teachers (JAT191320), Xiamen Ocean Vocational College Research Projects for High-level Talents (NO. 140008) and Collaborative Innovation Center Project (XTZX-ZHYY-1910).

References

Bhesh RS, Dong YR (2014) Anti-diabetic effects of *Caulerpa lentillifera*: stimulation of insulin secretion in pancreatic β-cells and enhancement of glucose uptake in adipocytes. Asian Pac J Trop Biomed 7:575–580

Bhesh RS, Hyun JK, Dong YR (2015) *Caulerpa lentillifera* extract ameliorates insulin resistance and regulates glucose metabolism in C57BL/KsJ-db/db mice via PI3K/AKT signaling pathway in myocytes. J Transl Med 13:62

Boyce BF, Yao Z, Xing L (2010) Functions of nuclear factor Kappa B in bone 1192(1):367

Chang J, Wang Z, Tang E (2011) Inhibition of osteoblastic bone formation by nuclear factor-κB. Nat Med 15(6):682–689

Daneault A, Véronique Coxam, Wittrant Y (2015) Biological effect of hydrolyzed collagen on bone metabolism. CritAl Rev Food Sci & Nutr 57(9):1922–1937

Eaton-Evans J (1994) Osteoporosis and the role of diet. Br J Biomed Sci 51(4):358

Fu Y, Sun G, Ouyang Y (2019) The effect of combined use of lithium chloride and icariin on proliferation and differentiation of osteoblasts. Chin J Osteoporos 25(9):1221–1225

Huang ZF, Cheng C, Wang J (2018) Icariin regulates the osteoblast differentiation and cell proliferation of MC3T3-E1 cells through microRNA-153 by targeting Runt-related transcription factor 2. Exp Ther Med 15:5159–5166

Kim IR, Kim SE, Baek HS (2016) The role of kaempferol-induced autophagy on differentiation and mineralization of osteoblastic MC3T3-E1 cells. BMC Complement Altern Med 16(1):333

Maeda R, Ida T, Ihara H (2012) Immunostimulatory activity of polysaccharides isolated from *Caulerpa lentillifera* on macrophage cells. Biosci Biotechnol Biochem 76(3):501–505

Matanjun P, Mohamed S, Mustapha NM (2009) Nutrient content of tropical edible seaweeds, *Eucheuma cottonii, Caulerpa lentillifera* and *Sargassum polycystum*. J Appl Phycol 21(1):75–80

Miroslava CC, David AB, Adrian SC (2010) Cell culture metabolomics: applications and future directions. Drug Discov Today 15(15–16):610–621

Nguyen VT, Ueng JP, Tsai GJ (2011) Proximate Composition, Total Phenolic Content, and Antioxidant Activity of Seagrape (*Caulerpa lentillifera*). J Food Sci 76(7):950–958

Pandey M, Kapila R, Kapila S (2018) Osteoanabolic activity of whey-derived anti-oxidative (MHIRL and YVEEL) and angiotensin-converting enzyme inhibitory (YLLF, ALPMHIR, IPA and WLAHK) bioactive peptides. Peptides 99:1–7

Paul NA, Neveux N, Magnusson M (2014) Comparative production and nutritional value of "sea grapes" — the tropical green seaweeds *Caulerpa lentillifera* and *C. racemosa*. J Appl Phycol 26(4):1833–1844

Payal G, Jehan J, Peter VG (2017) Age-related changes in bone marrow mesenchymal stromal cells: a potential impact on osteoporosis and osteoarthritis development. Cell Transplant 26(9):1520–1529

Reddi S, Shanmugam VP, Tanedjeu KS (2018) Effect of buffalo casein-derived novel bioactive peptides on osteoblast differentiation. Eur J Nutr 57(2):593–605

Sneha BS, Jin- J, Zhe P (2016) Orally available collagen tripeptide: enzymatic stability, intestinal permeability, and absorption of Gly-Pro-Hyp and Pro-Hyp. J Agric Food Chem 64(38):7127–7133

Sozen T, Ozisik L, Calik BN (2017) An overview and management of osteoporosis. Eur J Rheumatol 4(1):46–56

Thomas JW, Martin GL, Ramachandran SV (2011) Metabolite profiles and the risk of developing diabetes. Nat Med 17(4):448–453

Tong Y, Ma H, Hu T (2022) Research progress in the components and functional characteristics of *Caulerpa lentillifera*. Sci Technol Food Industry 43(7):400–406

Villa M, Wang L, Huang J (2016) Improving the permeability of lyophilized collagen–hydroxyapatite scaffolds for cell-based bone regeneration with a gelatin porogen. J Biomed Mater Res B Appl Biomater 104(8):1580–1590

Wang X, Zhang A, Han Y (2012) Urine metabolomics analysis for biomarker discovery and detection of jaundice syndrome in patients with liver disease. Mol Cell Proteomics 11(8):370–380

Wullaert A, Bonnet MC, Pasparakis M (2011) NF-κB in the regulation of epithelial homeostasis and inflammation. Cell Res 21(1):146–158

Chapter 4
Research Progress of Additives in Compound Feeds for Marine Ornamental Fish and Its Sustainable Development

Meiying Zhao, Linchun Li, Chunxiang Ai, and Xiaomei Huang

Abstract Marine ornamental fish are the most promising ornamental fish in the world. More and more individuals and families are feeding marine ornamental fish, which greatly promoted the development of the marine ornamental fish industry. The successful promotion of marine ornamental fish urgently requires the development of compound feeds to maintain the health and vibrant body color of marine ornamental fish. In this paper, typical additives in compound feed for marine ornamental fish were summarized, simultaneously, the sustainable development directions of the future development of the compound feed for marine ornamental fish were proposed.

Keywords Progress · Additives · Marine · Ornamental fish · Compound feeds

4.1 Introduction

Marine ornamental fish mainly come from the coral reef waters in the Indian Ocean and the Pacific Ocean. They are often rich in body patterns, gorgeous in body color, strange in body shapes, and are often good at hiding. Marine ornamental fish always have a primitive, quaint and mysterious natural beauty. Marine ornamental fish is the most promising ornamental fish in the world, representing the development direction of the ornamental fish field. There are more than 30 families of marine ornamental

Meiying Zhao, Linchun Li and Chunxiang Ai These authors contribute equally to this work.

M. Zhao · L. Li · X. Huang (✉)
Department of Marine Biology, Xiamen Ocean Vocational College, Xiamen, Fujian 361100, P.R. China
e-mail: huangxiaomei@xmoc.edu.cn

C. Ai
College of Ocean and Earth Science, Xiamen University, Xiamen, Fujian 361102, P.R. China

X. Huang
Shanghai Institutes of Nutrition and Health, Chinese Academy of Sciences, Shanghai 200031, P.R. China

G. Huang (ed.), *Proceedings of 2022 7th International Conference on Environmental Engineering and Sustainable Development (CEESD 2022)*, Environmental Science and Engineering, https://doi.org/10.1007/978-3-031-28193-8_4

fishes, the finch seabream, butterfly family, echinococcus family, coarse-skinned seabream family are the most common species. With the development of society and the improvement of people's living standards, more and more individuals and families breed marine ornamental fish, which greatly promotes the development of the marine ornamental fish industry. The successful promotion of marine ornamental fish urgently requires the development of compound feeds to maintain the health and vibrant body color of marine ornamental fish. However, at present, there are few high-efficiency compound feed for marine ornamental fish. Most of the feed for marine ornamental fish are the mixture of pigment and other compound feed for freshwater ornamental fish or marine fish. Simple component of the feed makes it difficult for the marine ornamental fish to maintain the health and the gorgeous body color. Therefore, the development of compound feed for marine ornamental fish is imperative.

4.2 Analysis of Feeding Conditions of Marine Ornamental Fish

The nutritional characteristics of marine ornamental fish are different from those of edible fish. One one hand, it focuses on health and brilliance, one the other hand, the nutrition of marine ornamental fish feed is similar to that of edible marine fish feed, which requires nutrients such as protein, fat, carbohydrates, vitamins and minerals. If one or more of these nutrients are missing, or the supply of nutrients is unbalanced, the corresponding nutritional deficiency symptoms, and even serious diseases, will appear on marine ornamental fish. To date, there has been a shortage of research on the nutritional needs of marine ornamental fish. Many kinds of feed for marine ornamental fish refers to the nutritional requirements of commercial fish. However, the breeding goal of ornamental fish is different from that of commercial fish, which does not focus on the pursuit of high growth rate, but pays more attention to ornamentality. The feeding conditions of ornamental fish are also different from the breeding environment of commercial fish. The ornamental fish live in transparent aquariums with relatively narrow spaces, which often face more stresses and are easily disturbed by breeders. The nutritional requirements of marine ornamental fish are insufficient, the nutritional standards of commercial fish are not applicable directly, the preparation of marine ornamental fish feed lacks theoretical guidance, and the relative industry market is uneven, hence, it is urgent to carry out in-depth research on the nutritional needs of marine ornamental fish.

4.3 Progress in the Development of Ornamental Fish Feed Additives

The colorful body color of ornamental fish is its main ornamental value and economic value. The body color of ornamental fish is the result of the combined action of carotenoids, melanin and guanine, among which, the role of carotenoids is particularly important, the main components include carotene glycol, astaxanthin, progesterone and zeaxanthin (Cui et al. 2012). However, the fish itself can not synthesize carotenoids, which would only be obtained from feed. In the ornamental fish feed, the appropriate amount of colorant can make the color of the fish more colorful and improve the ornamental value of fish. The color-enhancing effect of astaxanthin on *Pseudochromisfridmani* increased with the increase of concentration and supplementation time when the mass concentration of astaxanthin was above 25 mg/kg (Jiang et al. 2019), the addition of 100 mg/kg astaxanthin to the feed can improve the body color of the golden mandarin (Li et al. 2013), and the addition of 5000–8000 mg/kg astaxanthin can significantly improve the coloring effect of high-blood parrotfish (Li et al. 2008). Different species of ornamental fish have different utilization and color rendering effects for different kinds of pigments. Studies have shown that the redfin sailfish can convert most of the β-carotene in feed into astaxanthin for storage in the body. The content of other nutrients in the feed also affects the use and deposition of pigments, for example, when vitamin A is insufficient, some carotenoids can be converted to vitamin A, resulting in reduced coloring effect (Shi 2001).

At present, the use of colorants is mainly divided into two categories: natural colorants and chemical synthetic colorants. Due to the high price of synthetic pigments, colorants of natural origin are more widely used. Studies have shown that spirulina, haprose red coccolica, chlorella, rose petals, calendula petals, paprika powder, as well as shrimp and crab shell powder all have good color-enhancing effects (Cheng et al. 2015; Ezhil et al. 2008; Gouveia et al. 2003; Wang et al. 2016;). In addition to the pigment component, the addition of male hormones to the feed can also promote the male to show marital color, the maleization of the female fish would increase the ornamental value (Liu 2008).

Stress refers to the non-specific physiological response of an animal to external stimuli or challenges. When fish are stimulated by stress factors, physiological changes will be caused in a short period of time, such as increased capillary permeability, body color changes. When the stress intensity exceeds the limit of animal tolerance, it will cause body damage, severe and even death, that is, the so-called stress syndrome. At present, there are mainly three kinds of stresses during the breeding process of marine ornamental fish. First, nutritional stress, that is, the stress response caused by excess nutrition or lack of nutrition; The second is managerial stress, which mainly refers to the stress caused by transportation, water exchange, human interference or excessive feeding density and unreasonable collocation of polyculture varieties. The third is the stress caused by water environmental stress, such as excessive changes in water temperature, high ammonia nitrogen concentration and low

dissolved oxygen degree. Therefore, while strengthening the management of marine ornamental fish, strengthening anti-stress nutrition should be also payed attention to.

Additives with anti-stress effects can be divided into the following four categories: First, vitamin additives, including vitamin C, vitamin E, inositol and niacin. Studies have shown that when the amount of vitamin C added in the feed was 500 mg/kg, the non-specific immunity of the juveniles of the colorful angelfish could be significantly improved (Liao et al. 2012a). When the addition amounts of vitamin C was 1000 mg/kg and 2000 mg/kg, the anti-stress ability of peacock fish could be significantly improved (Lim et al. 2002). Increasing the amount of vitamin E, inositol and niacin could effectively alleviate ammonia nitrogen stress, transport stress and high temperature stress in aquatic animals (Shi et al. 2015). Second, prebiotics and probiotic additives. It has been reported that when 500 mg/kg of yeast polysaccharides were added to the feed, the serum replacement complement activity, lysozyme activity and leukocyte phagocytosis activity of colorful angelfish juveniles were significantly improved (Liao et al. 2012b). Third, plant extract additives. The addition of compound preparations such as β-dextran, rhubarb, skullcap and andrographis to the feed could significantly improve the anti-stress ability of blood parrots (Wu et al. 2016). Fourth, some trace element additives, such as yeast selenium and chromium picolinate, would be with anti-stress effects (Wang et al. 2011).

4.4 Conclusions

There are mainly three sustainable development directions for the research and development of feed for marine ornamental fish.

Above all, high-quality natural raw materials based on marine organisms could be selected as the feed for marine ornamental fish. Simultaneously, puffed pellet feed that is suitable for the growth and performance of marine ornamental fish should be produced according to the floating or sinking needs of various types of ornamental fish. The puffed feed developed should be with high stability in water which is not easy to dissolve and to expand, so as to avoid excessive pollution caused by the release of nutrients into the water. The particle size of the developed feed should be considered to meet the needs of puffed feed suitable for its caliber from fry to adult fish, small fish to large fish. At the same time, the granularity of puffed feed should be suitable to be installed in the automatic feeder for regular rotational feeding.

Furthermore, it is recommended to study the impact of several pigments on the health and body color of marine ornamental fish. Based on this, feed formula for efficient marine ornamental fish could be designed and screened out, according to the characteristics of feed raw materials, marine ornamental fish nutritional demand research data, digestion physiology and feeding habits. At the same time, the feed processing technology should be optimized and a series of high-efficiency marine ornamental fish compound feed could be produced. Feeding tests would be necessary, including the indicators of lureness, body color change of marine ornamental fish, body size index, and health status (such as liver and intestine health). The test results

could be used to optimize and improve the formulas and processing techniques for the feed, in order to produce high-efficiency compound feed for marine ornamental fish. The establishment of operating practices for the production of efficient compound feed for marine ornamental fish is also important.

Last but not least, the formula of the compound feed for marine ornamental fish is the key technology. The relevant research data of seawater fish species in the same genus can be referred to. However, due to the difference in the physiological and ecological characteristics of marine ornamental fish, as well as the lack of nutritional demand parameters of marine ornamental fish, the formula of the compound feed is hard. To solve this key technology, comparative nutritional methods should be used to analyze the nutritional requirements of seawater fish of the same family and the same diet, in order to provide more accurate nutritional requirements parameters. Only in this way, can the quality of compound feed be guaranteed.

Acknowledgements This work was supported by Program of EnShi TuJia & Miao Autonomous Prefecture Bureau of Scientific & Technological Affairs (Y959K21021), Fujian educational and scientific research program for young and middle-aged teachers (JAT191308), Xiamen Ocean Vocational College Research Projects for High-level Talents (NO. 140008) and Collaborative Innovation Center Project (XTZX-ZHYY-1910).

References

Cheng Y, Chen S, Li J (2015) Effects of combinated dietary pigments on body color of red *Carassius auratus*. Freshwater Fisheries 45(5):94–99

Cui P, Jiang Z, Cui K (2012) Effects of carotenoids on fish function and factors affecting fish coloring. Tianjin Fisheries 1:4–9

Ezhil J, Jeyanthi C, Narayanan M (2008) Effect of formulated pigmented feed on colour changes and growth of red swordtail *Xiphophorus helleri*. Turk J Fish Aquat Sci 8(1):99–101

Gouveia L, Rema P, Pereira O (2003) Colouring ornamental fish (*Cyprinus carpio* and *Carassius auratus*) with microalgal biomass. Aquac Nutr 9(2):123–129

Jiang J, Nuez-Ortin W, Angell A (2019) Enhancing the colouration of the marine ornamental fish *Pseudochromis fridmani* using natural and synthetic sources of astaxan. Algal Res 42:101596

Li X, Wang X, Mu X (2008) Effects of astaxanthin on the color of blood parrot. J Anhui Agric Sci 36:8606–8607

Li X, Li X, Zheng S (2013) Effect of astaxanthin on the body color of golden mammon. Feed Res 11:74–49

Liao C, Shao L, Wang X (2012a) Influence of dietary vitamin C on non-specific immunity of larval and juvenile *Symphysodon aequifasciatus*. Prog Fishery Sci 33(3):54–59

Liao C, Shao L, Wang X (2012b) Influence of dietary yeast immune polysaccharide on non-specific immunity of larvae and juveniles *Symphysodon aequifasciatus*. Ecol Sci 31(4):446–451

Lim L, Dhert P, Chew W (2002) Enhancement of stress resistance of the guppy Poecilia reticulate through feeding with vitamin C supplement. J World Aquaculture Soc 33:32–40

Liu M (2008) Mechanism of action of methyltestosterone on fish endocrine and its application in aquaculture. J Beijing Fisheries 5:26–29

Shi Q (2001) Effect of vitamin A and carotenoids on animal immune response. Veterinary drugs and feed additives 6:21–24

Shi Z, Zhang Y, Gao Q (2015) Dietary Vitamin E level affects the response of juvenile *Epinehelus moara* to ammonia nitrogen stress. Chin J Anim Nutr 27(5):1596–1604
Wang J, Liu W, Lu K (2011) Effects of chromium picolinate on serum biochemical parameters of heat-stressed carp *Carassius Auratus Gibelio*. Freshwater Fisheries 41(2):51–56
Wang L, Chen Z, Leng X (2016) Effect of *Haematococcus pluvialis* on growth, body color and antioxidation capacity of discus fish *Symphysodon haraldi*. Freshwater Fisheries 46(6):92–97
Wu H, Jiang J, Zhang Z (2016) Effect of a compound immune enhancer on enzyme activity and disease resistance of turbot and blood parrotfish. Jiangxi Fish Sci Technol 137(1):21–23

Chapter 5
Review of the Effects of Microaeration on Methanogens in the Anaerobic Digestion Systems

Ziqi Fan

Abstract Anaerobic digestion (AD) systems are widely used in the municipal sludge treatment and bioengineering industries. However, bioreactors were unstable due to limited biogas generation and stagnant methanogen activity. Microaeration, which involves infusing a trace quantity of oxygen into anaerobic digestors, is an effective technique for increasing the stability of AD systems and faciliting methanogens. This research examines the impact of microaeration on methanogens in AD systems and provides a comprehensive overview of the enzymatic mechanisms that occur in micro-aerated AD systems. In addition to its benefits, the future challenges and potential of microaeration will be evaluated, such as the issues of energy consumption for oxygen dosage and the coordination of methanogens and syntrophs in micro-aerated AD systems.

Keywords Methanogen · Methanogenesis · Microaeration · Methyl-coenzyme M reductases · Syntroph

5.1 Introduction

5.1.1 Anaerobic Digestion and Microaeration

Anaerobic digestion is a promising green economy technology as an alternative energy source. AD is the process of microorganisms decomposing organic matter without oxygen, concurring with biogas and microbial biomass production (Chen et al. 2008). AD processes are constituted by four stages (hydrolysis, acidogenesis, acetogenesis, and methanogenesis). Bioreactors based on AD processes have been widely deployed in manufacturing and wastewater treatment plants. Throughout these four stages, methanogenesis would be substantial for evaluating the efficiency

Z. Fan (✉)
School of Life Sciences, University of Warwick, Coventry CV4 7AL, UK
e-mail: Samfan@163.com

G. Huang (ed.), *Proceedings of 2022 7th International Conference on Environmental Engineering and Sustainable Development (CEESD 2022)*, Environmental Science and Engineering, https://doi.org/10.1007/978-3-031-28193-8_5

of AD in terms of methane production, while the digestate can be made into bedding for livestock or fertilizers (Chen et al. 2016; Speece 1983). However, previous industrial applications revealed the limitations of conventional AD systems in the instability of digesters, such as low yield of biogas (Kumar Khanal et al. 2021), insufficient use of feedstocks (Zamri et al. 2021), and impedance of methanogens (Liew et al. 2022). Hence, the conventional AD system no longer copes with demand, and a better-modified bioreactor facilitated by AD processes is urgently needed to maintain the stability of the reactors.

Microaeration is an approach with limited oxygen (0.1–1.0 mg/L) pumped into the anaerobic bioreactor (Nguyen and Khanal 2018). Although there is a risk of explosion when methane is mixed with oxygen in the range of explosive limit (4.4–17% methane, 19.95% oxygen), a trace amount of oxygen, based on past studies, has no dangerous effects on production (Chen et al. 2020). By compiling microaeration and AD systems, better hydrogen sulfide removal rates, higher biogas yield, and more effective hydrolysis efficiency can be obtained by AD reactors (Nguyen and Khanal 2018; Zeb et al. 2022). Micro-aerated digesters may avoid shock loads by promoting volatile fatty acid (VFA) oxidation and can decompose VFA content from 9.84 g COD/L to 3.21 g COD/L (Nguyen et al. 2019).

5.1.2 Correlation Between Methanogen and Methanogenesis Under the Microaeration

Micro-aerated AD systems can promote the efficiency of methanogenesis, but how do three different types of methanogenesis interact with methanogens? Hydrogenotrophic methanogenesis can convert carbon dioxide, hydrogen or formate into methane by methanogens under micro-aerobic conditions. Cultivated methanogens were from the orders *Methanobacteriales*, *Methanococcales*, *Methanomicrobiales*, *Methanocellales*, and *Methanopyrales* (Wintsche et al. 2018).

Acetoclastic methanogenesis is one of the methanogenesis processes that convert acetate to methane and carbon dioxide under the cultivation of methanogens. It has been reported that nearly 70% of the methane in nature was generated by acetoclastic methanogenesis (Fievez et al. 1999). Take *Methanosarcina* as an example, micro-aerated AD systems can facilitate the growth of *Methanosarcina* and diminish the loss of acetic acid (Zhu et al. 2022). Furthermore, a high abundance of oxytolerate Methanosarcina maintains methane production efficiency at a 12.5 ml/L reactor under a daily air load (Fu et al. 2016). Compost-enriched microbial communities within micro-aerated AD systems can be used to cultivate acetoclastic methanogens, resulting in an increase in methane production of 44.78% and 28.28% for Methanosaeta thermophila and Methanosarcina acetivorans, respectively (Hua et al. 2022).

Methylotrophic methanogenesis mainly adopts methylated substances, which are non-competitive substrates. Examples include methylated amines and dimethylsulfide (DMS) (Guo et al. 2021; Schorn et al. 2022). Other evidence could be the detection of DNA molecular weight by gel electrophoresis of acetoclastic methanogens within the Methanosaeta genus from the micro-aerobic reactors (Rodríguez et al. 2012). Besides, one of the methanogens, Methermicoccus shengliensis, can use methoxylated aromatic compounds in methylotrophic methanogenesis under the facilitation of microaeration (Tyagi et al. 2021).

5.1.3 Research Objective

Previous studies also revealed the substantial effect of microaeration in enhancing the methanogens in micro-aerated AD systems (Chen et al. 2016). It has been discovered that the abundance of acetoclastic methanogens would be much higher under the microaeration circumstances (5–10 mg O_2/L per reactor/cycle) while there was inhibition of methanogens in aerobic conditions (Yu et al. 2020). However, few papers discussed methanogenic enzymatic pathways in micro-aerated AD systems and depicted the consequences for methanogens under this circumstance. Furthermore, there was a discrepancy in the roles of micro-aerated AD systems throughout methylotrophic methanogenesis, which will be discussed in depth in this review.

The purpose of this review was to encapsulate the effect of microaeration on methanogens critically. Furthermore, the relationship between micro-aerated AD processes and methylotrophic methanogenesis was critically reviewed. The limitations and future perspectives of micro-aerated AD systems were also highlighted in this study (Fig. 5.1).

5.2 Materials and Methods

The effectiveness of methanogens under the micro-aerated AD systems has been evaluated by searching keywords from relevant scientific journals via the Web of Science and PubMed. ‘Anaerobic digestion’ and ‘Microaeration’ have been selected for browsing. Irrelevant phrases, such as mg/L, have been removed from keywords to retain the accuracy of results. (Tyagi et al. 2021; Kanehisa and Goto 2000) keywords have been selected from Web of Science and PubMed for further assessment, respectively. Keywords have been expressed by adopting VOSViewer (Kanehisa and Goto 2000).

To explore the enzymatic pathways of methylotrophic methanogenesis facilitated by micro-aerated AD systems, KEGG pathway diagrams (M00680) have been reorganized to identify the essential functional genes throughout methanogenesis. The likely consequences to the methanogens within the micro-aerated AD systems,

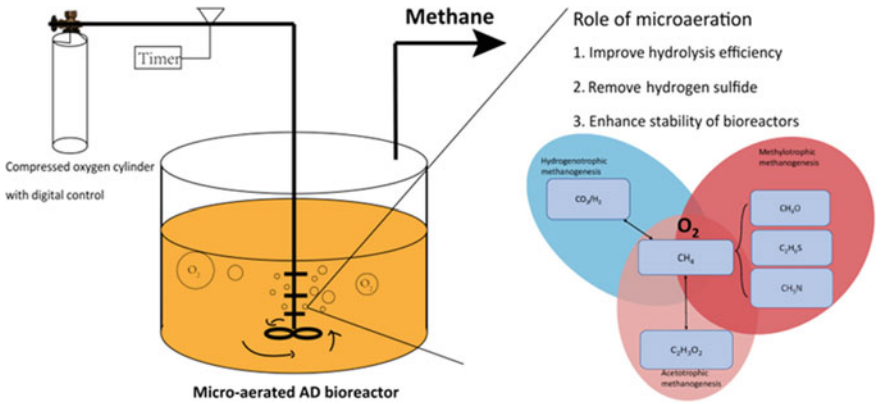

Fig. 5.1 The driven mechanisms of methanogens in micro-aerated AD systems. Microaeration systems have been controlled by the automatic analogy coupled with valves of an oxygen gas cylinder and a timer. The Vann diagram at the right bottom illustrates the cross-section of three types of methanogenesis: Hydrogenotrophic methanogenesis (blue), methylotrophic methanogenesis (red) and acetoclastic methanogenesis (amber)

thus better appreciating the variations of methanogens under the micro-aerated AD systems (Perianes-Rodriguez et al. 2016).

5.3 Results and Discussion

Microaeration systems would be beneficial for extracellular hydrolase coupled with methanogens. As Fig. 5.2 shows, corn straw, specific methanogenic activity (SMA), and food waste have simultaneously appeared with microaeration, reflecting that micro-aerated AD systems can eliminate more organic solid waste by promoting hydrolysis efficiency. A study in both the Web of Science and PubMed collections pointed out that 4 h pretreatment under microaeration can reach the highest methane yield and produce more extracellular hydrolytic enzymes (cellulase, lipase, and protease) (Ruan et al. 2019). Zhou et al. also reported the maximum concentrations of protease, alpha-glucosidase, and ATP on Day 1 would be 2–3 times higher in micro-aerated AD systems than those in conventional AD systems with the assistance of facultative bacteria and methanogens (Zhou et al. 2019).

Tetrahydromethanopterin S-methyltransferase plays a role in methyl transfer between the cofactors tetrahydromethanopterin and coenzyme M (CoM) and connects the Wood-Ljungdahl pathways (WLPs) and Methyl-coenzyme M reductases (MCRs) (Wang et al. 2021a). The recent discovery of *Candidatus Methanomixophus* offers new insights that the MTR operon also monitored the ratio of total methanogen population (TMP, Fig. 5.2a) and organic loading rate (OLR, Fig. 5.2b)

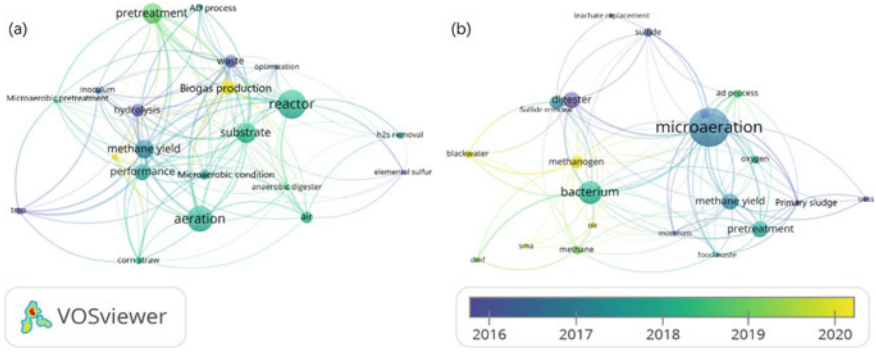

Fig. 5.2 A schematic diagram of key words derived from search outcome from **a** Web of Science and **b** PubMed (Perianes-Rodriguez et al. 2016)

by controlling the yield of methyl compounds, as methyl compounds can be converted to methane by MCRs.

MCRs are rate-limiting enzymes in micro-aerated AD systems. Correlation between MCRs and methanogens has been described in Eq. (5.1) based on the KEGG pathway, where CoBSH represents coenzyme B, and CoBS-SCoM denotes heterodisulfide (Perianes-Rodriguez et al. 2016; Wongnate et al. 2016). MCRs have three subunits (MCR A, MCR B and MCR G) and a unique cofactor known as F430 (Harirchi et al. 2022). MCRs can be classified into three categories (types I, II, and III). MCR Type I mainly comprised contigs from *Methanobacteriales*, whereas MCR type II was derived from *Methanobacteriales* and *Methanococcales*, and MCR type III from *Methanococcales* (Wagner et al. 2017). Methylotrophic methanogenesis utilizes carbon dioxide to produce methane. In contrast, hydrogenotrophic methanogenesis facilitates the species richness of archaeal methanogens that can reduce CO_2 with H_2 to generate CH_4 under the MCR enzyme via WLPs (Fig. 5.3). Under the microaeration circumstance, hydrogen would be less preferential so that methylotrophic methanogenesis would be the dominant procedure for generating methane and associated with methanogens.

$$\text{Methyl} - \text{S} - \text{COM} + CoBSH \rightarrow CH_4 + COBS - SCoM \Delta G^0 = -30kJ/mol \tag{5.1}$$

Although methanogen enzymatic pathways have been thoroughly examined, micro-aerated settings have certain limits. One of the issues is maintaining the status of microaeration with energy conservation. Microaeration systems with pumps and stirring systems rely heavily on power systems, raising operational costs and making it challenging to achieve carbon neutrality. Moreover, sustaining the methanogens requires stable temperature and persistent nutrient feeding, and the costs of accidental death of methanogens would be tremendous.

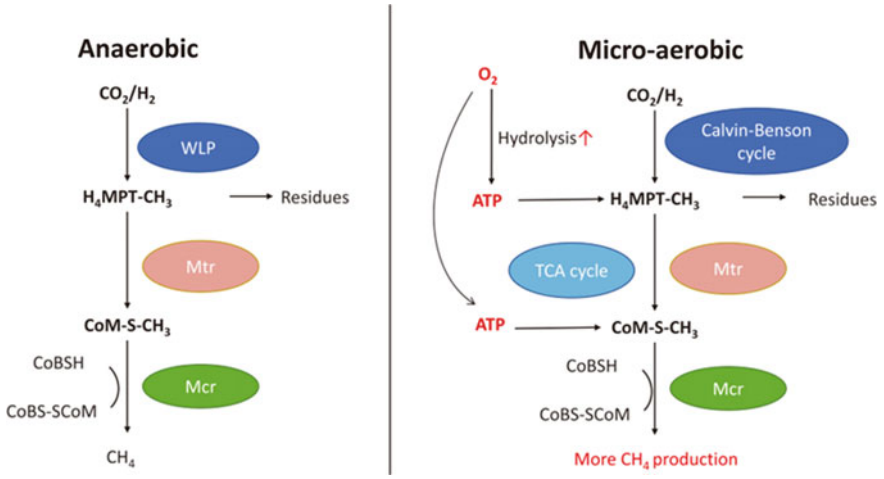

Fig. 5.3 The comparison of enzymatic pathways for methanogens under anaerobic and micro-aerobic environments. Adapted from Kanehisa and Goto (2000)

In contrast, problems with energy costs can be mitigated by introducing syntrophs into the micro-aerated AD systems, as the cooperation of syntrophs and methanogens can potentially improve methane generation efficiency in micro-aerated AD systems. According to the latest studies, *Methanosaeta spp.* is closely related to *Syntrophomonas* and *Syntrophobacter* in soils and anaerobic digesters. Micro-aerated AD systems could be inhabited by methanogens and syntrophic bacteria (Rodríguez et al. 2012). One example of a syntrophic bacteria is *S. fumaroxidans*, which can break down VFAs in a microaerobic environment (Wagner et al. 2017).

5.4 Conclusion

To summarize, micro-aerated AD systems positively affect the diversity of methanogens. Meanwhile, methylotrophic methanogenesis contributes the most regarding the enzymatic processes. Notwithstanding the high energy costs for sustaining the microaeration and diversity of methanogen energy and the risk of explosions when excessive oxygen enters the systems, micro-aerated AD systems still have a promising effect associated with methanogens.

References

Chen Y, Cheng JJ, Creamer KS (2008) Inhibition of anaerobic digestion process: A review. Biores Technol 99:4044–4064

Chen S, Cheng H, Wyckoff KN, He Q (2016) Linkages of Firmicutes and Bacteroidetes populations to methanogenic process performance. J Ind Microbiol Biotechnol 43:771–781

Chen Q, Wu W, Qi D, Ding Y, Zhao Z (2020) Review on microaeration-based anaerobic digestion: State of the art, challenges, and prospectives. Sci Total Environ 710:136388

Fievez V, Piattoni F, Mbanzamihigo L, Demeyer D (1999) Reductive acetogenesis in the hindgut and attempts to its induction in the rumen—A review. J Appl Anim Res 16:1–22

Fu S, Wang F, Shi X, Guo R (2016) Impacts of microaeration on the anaerobic digestion of corn straw and the microbial community structure. Chem Eng J 287:523–528

Guo B, Yu N, Weissbrodt DG, Liu Y (2021) Effects of micro-aeration on microbial niches and antimicrobial resistances in blackwater anaerobic digesters. Water Research **196**: 117035

Harirchi S, Wainaina S, Sar T, Nojoumi SA, Parchami M, Parchami M, Varjani S, Khanal SK, Wong J, Awasthi MK, Taherzadeh MJ (2022) Microbiological insights into anaerobic digestion for biogas, hydrogen or volatile fatty acids (VFAs): a review. Bioengineered 13:6521–6557

Hua B, Cai Y, Cui Z, Wang X (2022) Bioaugmentation with methanogens cultured in a micro-aerobic microbial community for overloaded anaerobic digestion recovery. Anaerobe 76:102603

Kanehisa M, Goto S (2000) KEGG: kyoto encyclopedia of genes and genomes. Nucleic Acids Res 28:27–30

Kumar Khanal S, Lü F, Wong JWC, Wu D, Oechsner H (2021) Anaerobic digestion beyond biogas. Bioresour Technol **337**: 125378

Liew CS, Yunus NM, Chidi BS, Lam MK, Goh PS, Mohamad M, Sin JC, Lam SM, Lim JW, Lam SS (2022) A review on recent disposal of hazardous sewage sludge via anaerobic digestion and novel composting. J Hazard Mater 423:126995

Nguyen D, Khanal SK (2018) A little breath of fresh air into an anaerobic system: How microaeration facilitates anaerobic digestion process. Biotechnol Adv 36:1971–1983

Nguyen D, Wu Z, Shrestha S, Lee P-H, Raskin L, Khanal SK (2019) Intermittent micro-aeration: New strategy to control volatile fatty acid accumulation in high organic loading anaerobic digestion. Water Res 166:115080

Perianes-Rodriguez A, Waltman L, van Eck NJ (2016) Constructing bibliometric networks: A comparison between full and fractional counting. J Informet 10:1178–1195

Rodríguez E, Lopes A, Fdz-Polanco M, Stams AJ, García Encina PA (2012) Molecular analysis of the biomass of a fluidized bed reactor treating synthetic vinasse at anaerobic and micro-aerobic conditions. Appl Microbiol Biotechnol **93**: 2181–2191

Ruan D, Zhou Z, Pang H, Yao J, Chen G, Qiu Z (2019) Enhancing methane production of anaerobic sludge digestion by microaeration: Enzyme activity stimulation, semi-continuous reactor validation and microbial community analysis. Biores Technol 289:121643

Schorn S, Ahmerkamp S, Bullock E, Weber M, Lott C, Liebeke M, Lavik G, Kuypers MMM, Graf JS, Milucka J (2022) Diverse methylotrophic methanogenic archaea cause high methane emissions from seagrass meadows. Proc Natl Acad Sci 119:e2106628119

Speece RE (1983) Anaerobic biotechnology for industrial wastewater treatment. Environ Sci & Technol **17**: 416A-427A

Tyagi VK, Bhatia A, Kubota K, Rajpal A, Ahmed B, Khan AA, Kazmi AA, Kumar M (2021) Microbial community dynamics in anaerobic digesters treating organic fraction of municipal solid waste. Environ Technol Innov 21:101303

Wagner T, Wegner CE, Kahnt J, Ermler U, Shima S (2017) Phylogenetic and structural comparisons of the three types of methyl coenzyme m reductase from methanococcales and methanobacteriales. J Bacteriol **199**

Wang T, Zhu G, Kuang B, Jia J, Liu C, Cai G, Li C (2021b) Novel insights into the anaerobic digestion of propionate via Syntrophobacter fumaroxidans and Geobacter sulfurreducens: Process and mechanism. Water Res 200:117270

Wang Y, Wegener G, Williams TA, Xie R, Hou J, Tian C, Zhang Y, Wang F, Xiao X (2021a) A methylotrophic origin of methanogenesis and early divergence of anaerobic multicarbon alkane metabolism. Sci Adv **7**: eabj1453

Wintsche B, Jehmlich N, Popp D, Harms H, Kleinsteuber S (2018) Metabolic adaptation of methanogens in anaerobic digesters upon trace element limitation. Front Microbiol **9**

Wongnate T, Sliwa D, Ginovska B, Smith D, Wolf MW, Lehnert N, Raugei S, Ragsdale SW (2016) The radical mechanism of biological methane synthesis by methyl-coenzyme M reductase. Science 352:953–958

Yu N, Guo B, Zhang Y, Zhang L, Zhou Y, Liu Y (2020) Different micro-aeration rates facilitate production of different end-products from source-diverted blackwater. Water Res 177:115783

Zamri MFMA, Hasmady S, Akhiar A, Ideris F, Shamsuddin AH, Mofijur M, Fattah IMR, Mahlia TMI (2021) A comprehensive review on anaerobic digestion of organic fraction of municipal solid waste. Renew Sustain Energy Rev 137:110637

Zeb I, Yousaf S, Ali M, Yasmeen A, Khan AZ, Tariq JA, Zhao Q, Abbasi AM, Ahmad R, Khalil TM, Yaqoob A, Bilal M (2022) In-situ microaeration of anaerobic digester treating buffalo manure for enhanced biogas yield. Renewable Energy 181:843–850

Zhou Z, Ming Q, An Y, Ruan D, Chen G, Wei H, Wang M, Wu Z (2019) Performance and microbial community analysis of anaerobic sludge digestion enhanced by in-situ microaeration. J Water Process Eng 42:102171

Zhu L, Li Y, Liu C, Li G (2022) Intermittent microaeration technology to enhance the carbon source release of particulate organic matter in domestic sewage. Water 14:1876

Chapter 6
Scale and Seasonal-Dependent Impacts of Land-Use Types on River Water Quality of Multiple Watersheds in Southern China

Dayang Sun, Jianfeng Li, Wei Jun, Huabin Li, Sheng Sheng, and Fenfei Chen

Abstract Knowledge of how land-use types influence riverine water quality is fundamental for watershed pollution mitigation and city land planning. Based on seasonal water quality data from 82 monitoring sections in 20 watersheds in Jinjiang, we reveal scale and seasonal-dependent impacts of land-use types on river water quality in the multi-watershed perspective, using kriging and redundancy analysis (RDA). Results from kriging analysis demonstrate that sections of the urban district areas have the worst water quality, and the rivers generally have better water quality in winter. RDA results suggest that the degree of interpretation and significance of correlations generally increase as the scale enlarges. Urban construction lands and farmlands show obvious seasonal and scale-dependent effects regarding their influence on stream water quality. Urban construction lands are the primary sources of pollution in summer, mainly influencing COD concentrations through surface runoff pollutions in riparian buffer zone scales, while influencing NH_3-N concentrations through sewage pollutions in the watershed scale. Farmlands in the watersheds show a positive influence on river water quality, while farmlands distributed within 100 m and 200 m buffer zone in winter show negative influences. Projects for runoff pollution reduction, sewage treatment capacity enhancement in urban areas, and sewage collection system improvement in rural areas are urgently needed for mitigation of water quality.

Keywords Water quality · Multi-watershed · Land-use

6.1 Introduction

Water quality of streams can be influenced by both natural factors (i.e., topography, rainfall, temperature, plant and soil types, etc.) and human activities (i.e., damming, agriculture activities, urbanization, etc.) in watersheds (Khatri and Tyagi 2015; Park

D. Sun (✉) · J. Li · W. Jun · H. Li · S. Sheng · F. Chen
Power China Huadong Engineering Corporation Limited, Hangzhou 311122, China
e-mail: sun_dy@hdec.com; dylan_1991@163.com

G. Huang (ed.), *Proceedings of 2022 7th International Conference on Environmental Engineering and Sustainable Development (CEESD 2022)*, Environmental Science and Engineering, https://doi.org/10.1007/978-3-031-28193-8_6

and Lee 2020; Hooper and Hubbart 2016). Land-use changes within the watersheds have been paid much attention in the last few decades due to its substantial influence on water quality of streams (Hooper and Hubbart 2016). Land-use changes in watersheds can influence stream water quality by altering physical, biochemical and ecological stream characteristics, including stream geomorphology, sediment regime, water temperature, nutrient/pollutant concentrations, aquatic habitat, and ecological biodiversity (Wertz and Shank 2019; Giri and Qiu 2016; Johnson et al. 1997; Su et al. 2016). Understanding how land-use types influence riverine water quality is fundamental for watershed pollution mitigation and city land planning.

Previous studies suggest that impervious surfaces in urban areas relates to water quality degradation (Gyawali et al. 2013; Pratt and Chang 2012; Sliva and Williams 2001), while farmlands can be important sources of non-point pollution to streams (Wertz and Shank 2019; Pratt and Chang 2012; Sliva and Williams 2001; Huang et al. 2016; Gonzales-Inca et al. 2015). Forests, on the other hand, are often found to effect positively on water quality of streams (Oliveira et al. 2016; Singh and Mishra 2014). However, how these land-use types influence riverine water quality in different scales and different seasons are still under debates, considering different results from studies with different regional background (Pratt and Chang 2012; Sliva and Williams 2001). Moreover, current studies mainly focused on single watersheds. How land-use types in a city influence riverine water qualities in a multi-watershed scale is still not clear. To investigate the scale and seasonal-dependent impacts of land-use types on river water quality in the multi-watershed perspective can provide key information for city land planning and watershed pollution mitigation projects.

Jinjiang has undergone rapid urbanization and economic developments in the last few decades and has endured serious deterioration of stream water quality. Here we collected seasonal water quality data from 82 sections in 20 watersheds in Jinjiang and investigated scale and seasonal-dependent impacts of land-use types on river water quality in the multi-watershed perspective, using kriging and redundancy analysis (RDA). Hopefully, this study can provide useful suggestions for better pollution control strategies for watersheds in Jinjiang and other similar cities.

6.2 Materials and Methods

Jinjiang located in the southeastern China (118°24′56″–118°41′10″ E, 24°30′44″–24°54′21″ N). There are 20 main watersheds in Jinjiang, most of which are seagoing streams (Fig. 6.1). The topography of Jinjiang mainly consisting of plains and hills, with the elevation ranging from 0 to 469 m (Fig. 6.1). Jinjiang has a subtropical monsoon climate. The average temperatures in Jinjiang range from 17 to 24 °C and the average precipitation is ~1147 mm.

The data of monthly water quality indicators (COD, NH_3-N and TP) from 82 monitoring section of 20 watersheds in 2018–2019 were provided by Quanzhou Municipal Ecology and Environment Bureau. The average concentrations of COD, NH_3-N and TP in June, July and August were calculated to represent the summer

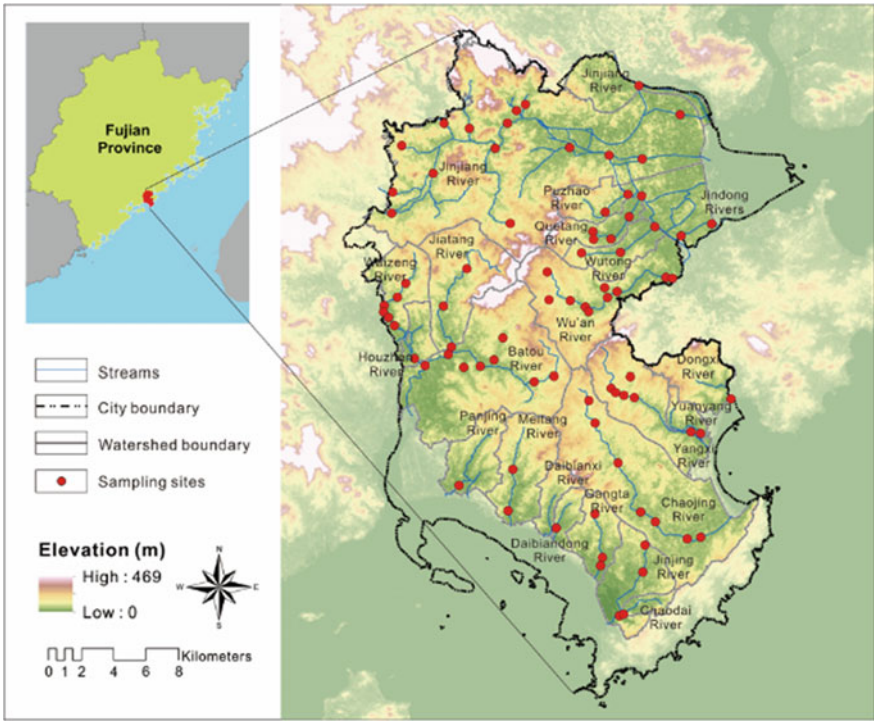

Fig. 6.1 Topography and sampling sites in 20 watersheds in Jinjiang

water quality, while those of November, December and January were calculated to indicate the winter water quality.

The land-use types of Jinjiang were provided by Quanzhou Land and Resources Bureau. The percentage of land-use types in riparian buffer zone scales (100 m, 200 m, and 500 m) were calculated using buffer tools in ArcGIS. The effect of different land-use types on riverine water quality in different scales and different seasons were further estimated using redundancy analysis (RDA) in Canoco for Windows.

6.3 Results and Discussion

6.3.1 Distributions of COD, NH_3-N and TP

In the spatial perspective, the urban centre is the area with worst stream water quality. In summer, three water quality indicators have similar distributions, with their highest values in the upper streams of Puzhao River, Quetang River and Wutong River. The

distribution of the worst water quality sites highly coincides with the location of urban centre. In these areas, concentrations of NH_3-N, TP and COD are higher than 25 mg/L, 2.5 mg/L and 120 mg/L, respectively, which is lower than the V-class standard (i.e. NH_3-N < 2.0 mg/L, TP < 0.4 mg/L, COD < 40 mg/L). In winter, the highest concentrations of NH_3-N and TP occur in the upper reaches of Quetang River and Yangxi River, while the highest concentrations of COD the upper reaches of Quetang River, Wutong River and the middle reach of Jiatang River. The urban centre is still one of the areas that have worst water quality.

In the seasonal perspective, the stream water quality in winter is generally better than that in summer. The average concentration of COD in winter (59.4 mg/L) is 28.2% lower than that in summer (82.7 mg/L). Considering the influence of seawater may reduce COD concentrations in summer months, the actual difference may be even higher. The average concentration of TP in winter (0.84 mg/L) is 11.3% lower than that in summer (0.95 mg/L). The seasonal difference of NH_3-N concentrations is unobvious.

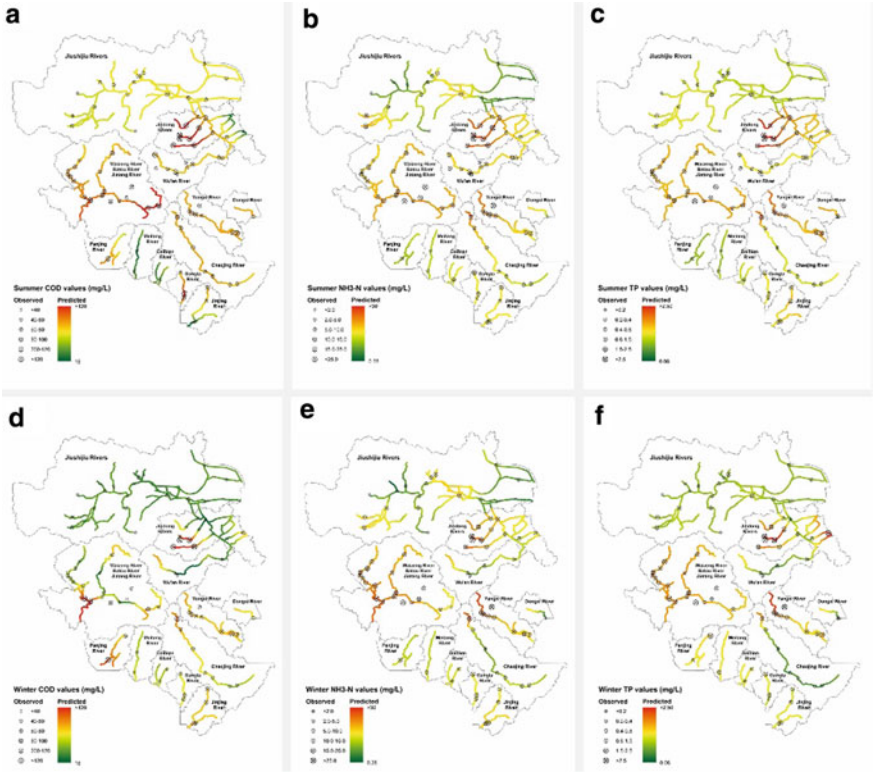

Fig. 6.2 Influence of land-use types on water quality Fig. 6.2. Distributions of observed and predicted water quality indicators in Jinjiang. **a**: summer COD; **b**: summer NH_3-N; **c**: summer TP; **d**: winter COD; **e**: winter NH_3-N; **f**: winter TP indicators

6.3.2 *Influence of Land-Use Types on Water Quality Indicators*

RDA results in summer. RDA results that indicate influence of land-use types on concentrations of COD, NH_3-N and TP in riparian buffer zone scales in summer are shown in Fig. 3a. The degree of interpretation of land-use types in riparian buffer zones to concentrations of COD, NH_3-N and TP reaches 47.6%. Garden lands in all riparian buffer zones correlate positively to TP concentrations. Garden lands in 100 m riparian and transportation lands in all riparian buffer zones correlate positively to NH_3-N concentrations. Urban construction lands in all riparian buffer zones and woodland in 100 and 200 m riparian correlate positively to COD concentrations. Other land-use types are not or negatively correlated with water quality indicators. Most interestingly, farmlands and grasslands in all riparian buffer zones negatively correlate to COD concentrations, while rural construction lands negatively correlate to TP concentrations.

RDA results that indicate influence of land-use types on concentrations of COD, NH_3-N and TP in the watershed scale in summer are shown in Fig. 3b. The degree of interpretation of land-use types in watersheds to water quality reaches 79.4%. Urban construction lands and transportation lands in the watersheds correlate positively to all three indicators. Farmlands and industry lands in watersheds correlate negatively to all three indicators. Rural construction lands correlate negatively to TP concentrations, while unused lands (including bare land, salt marsh and other unused land types) and grasslands correlate negatively to COD concentrations.

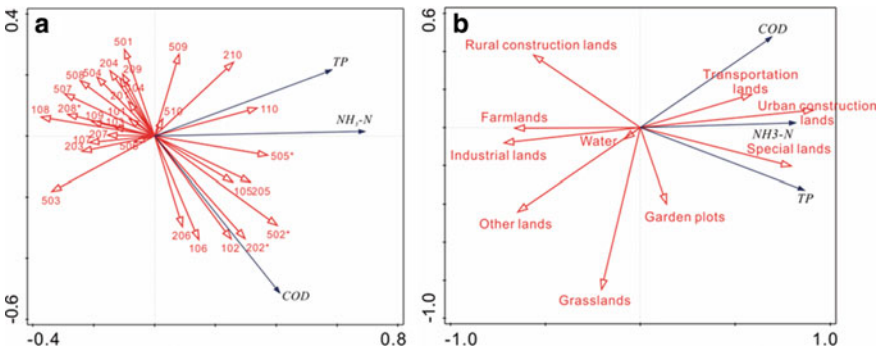

Fig. 6.3 RDA results of influences of land-use types on concentrations of COD, NH_3-N and TP in summer at buffer scales (**a**) and at watershed scales (**b**). In Fig. 3a, the first digits of numbers represent the widths of riparian buffer zones: 1–100 m, 2–200 m, 5–500 m. The second and third digits represent land-use types: 01-grasslands, 02-urban construction lands, 03-rural construction lands, 04-farmlands, 05-trasportation lands, 06-woodlands, 07-other lands (bare land, salt marsh and other unused land types), 08-water, 09-special lands (military lands, consulate lands, prison lands, religion activity lands), 10-garden lands. Stars after the land-use types represent that the influences of these land-use types on water quality indicators are significant ($p < 0.05$)

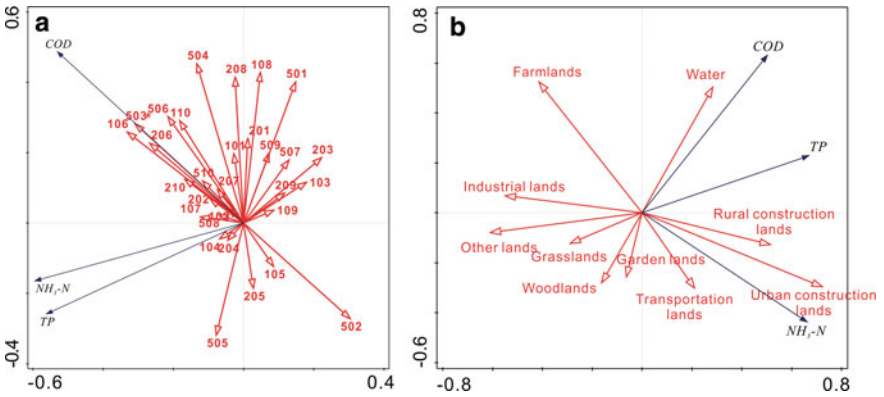

Fig. 6.4 RDA results of influences of land-use types on concentrations of COD, NH_3-N and TP in winter at buffer scales (**a**) and at watershed scales (**b**). The numbers in Fig. 4a have same meanings as those in Fig. 3a

RDA results in winter. RDA results that indicate influence of land-use types on concentrations of COD, NH_3-N and TP in riparian buffer zone scales in winter are shown in Fig. 4a. The degree of interpretation of land-use types in riparian buffer zones to water quality reaches 46.4%. The land-use types that correlate positively to COD concentrations including garden lands and woodlands in all riparian buffer zones, rural construction lands in 500 m riparian, and urban construction lands in 100 and 200 m riparian. Farmlands in 100 and 200 m riparian show positive correlation to NH_3-N and TP concentrations. The influences of other land-use types on concentrations of COD, NH_3-N and TP in riparian buffer zone scales in winter are unobvious or insignificant.

RDA results that indicate influence of land-use types on concentrations of COD, NH_3-N and TP in the watershed scale in winter are shown in Fig. 4b. The degree of interpretation of land-use types in watersheds to concentrations of COD, NH_3-N and TP reaches 62.4%. Urban construction lands and transportation lands in the watershed correlate positively to NH_3-N concentrations. Rural construction lands correlate positively to NH_3-N and TP. Farmlands correlate negatively to NH_3-N concentrations; other lands and grasslands correlate negatively to TP concentrations; woodlands and garden lands correlate negatively to COD concentrations.

6.3.3 Scale and Seasonal-Dependent Effects

RDA results show that the degree of interpretation of influences of land-use types on concentrations of COD, NH_3-N and TP in the watershed scale is remarkably higher than that in riparian buffer zone scales. In riparian buffer zone scales, the significance of influences of land-use types on concentrations of COD, NH_3-N and TP generally

increases as the buffer widths increase. This result is inconsistent with the studies on a single stream or watershed, where land-use types near the river usually have a greater influence on the water quality. This indicate that, in a multi-watershed scale, the scale effect of influence of land-use types on riverine water quality will also be enlarged.

Urban construction lands, transportation lands and rural construction lands show highly negative influence on stream water quality, which is in consistence with former studies (Zhang et al. 2009). The influence of urban construction lands on water quality show obvious scale-dependent effects. In riparian buffer zone scales, urban construction lands mainly influence COD concentrations, while in the watershed scale, urban construction lands mainly influence NH_3-N concentrations. COD concentrations and NH_3-N are often related to sewed contamination. COD concentrations are also highly related to runoff pollution. This suggests that urban construction lands influence water quality through surface runoff pollutions in riparian buffer zone scales, while through sewage contamination in the watershed scale.

The farmlands also show scale-dependent effects on riverine water quality. In the watershed scale, farmlands have positive influence on stream water quality, in both summer and winter. However, farmlands within 100 m and 200 m riparian buffers show negative influence on stream water quality in winter, as indicated by the positive correlation between farmlands and TP concentrations. Positive influence of farmlands on water quality are rarely reported in watersheds in foreign countries, probably because the foreign watersheds are usually dominated by farmlands, which become the primary source of contamination. In Jinjiang, however, the urban construction lands are the primary source of contamination in the watersheds, especially in summer when the runoff pollution increases due to the elevated rainfall. The farmlands in watershed can probably mitigate runoff pollution and thus have positive influence on stream water quality. Similar phenomenon has also been reported in Chinese cities such as Wujiang (Zhang et al. 2009). In winter, the runoff pollution from urban construction lands decreases as the rainfall reduces. The farmlands near the streams become a primary source of contamination instead.

In seasonal perspective, the riverine water quality in winter is generally better than that in summer. Two main reasons main explain the seasonal variations in the stream water quality. Firstly, streams in Jinjiang are mostly in eutrophication status. The algae blooms in summer may cause anaerobic conditions in streams, which is often followed by elevated concentration of COD (Hu et al. 2001; Gu 2012). Secondly, the increased sewage and runoff pollution may also cause deteriorated water quality.

RDA results demonstrate that the degree of interpretation of land-use types to water quality in a watershed scale is significantly higher to that in riparian buffer zone scales, indicating more intense influence of land-use types on water quality in summer. In summer, urban construction lands are the most significant factor that control stream water quality. On one hand, the productions of domestic and industrial sewage are significantly higher in summer than those in winter. This may reflect the insufficient capacity of urban sewage treatment in summer. On the other hand, the surface runoff pollutions are higher in summer, due to the elevated rainfall. In winter, both sewage and runoff pollution reduced. The urban construction lands therefore

no longer influence the stream water quality significantly. The farmlands and rural construction lands within buffer zones became the primary sources of contamination, probably reflecting that the wastewater collection systems are still not completed in rural areas.

6.4 Conclusions

This study investigated the influences of land-use types on water quality indicators from a multi-watershed perspective and revealed scale and seasonal-independent effects of influence of land-use types on stream water quality. The main conclusions of this study are as follows.

- In the spatial perspective, the urban centre is the area with worst stream water quality, while in seasonal perspective, the stream water quality in winter is generally better than that in summer.
- In the multi-watershed perspective, the degree of interpretation and significance of correlations generally increase as the scale enlarges. Urban construction lands and farmlands show obvious scale-dependent effects in regarding to their influence on stream water quality. Urban construction lands mainly influence COD concentrations through surface runoff pollutions in riparian buffer zone scales, while influence NH_3-N concentrations through sewage contamination in the watershed scale. Farmlands show positive influence to water quality in the watershed scale, while have negative influence on water quality within 100 m and 200 m buffer zone in winter.
- The degree of interpretation and significance of correlations in summer generally higher than those in winter. Urban construction lands are the primary sources of pollution in summer, while rural construction lands and farmlands are the primary sources of pollution in winter.

References

Giri S, Qiu Z (2016) Understanding the relationship of land uses and water quality in twenty first century: A review. J Environ Manage 173:41–48

Gonzales-Inca A, Kalela R, Kirkkala T, Lepisto A (2015) Multiscale landscape pattern affecting on stream water quality in agricultural watershed. SW Finland Water Res Manage 29:1669–1682

Gu PP (2012) Distribution, fluxes, production and transformation of CH_4 and N_2O in representative. Rivers and Estuaries Qingdao: Ocean University of China, pp 22–28 (in Chinese)

Gyawali S, Techato K, Yuangyai C Musikavong C (2013) Assessment of relationship between land uses of riparian zone and water quality of river for sustainable development of river basin, A case study of U-Tapao river basin, Thailand. Procedia Environ Sci **17**: 291–297

Hooper L, Hubbart A (2016) A rapid physical habitat assessment of wadable streams for mixed-land-use watersheds. Hydrology 4:37

Hu X, Gao X, Wang S, He B, Shen M, Chen Z, Xu S (2001) Water pollution in small and medium-sized rivers from suburbs of Shanghai in summer. Res Environ Yangtze Basin **5**: 258–265 (in Chinese)

Huang Z, Han L, Zeng L, Xiao W, Tian Y (2016) Effects of land use patterns on stream water quality: A case study of a small-scale watershed in the three Gorges reservoir area. China Environ Sci Pollut Res 23:3943–3955

Johnson B, Richards C, Host E, Arthur JW (1997) Landscape influences on water chemistry in Midwestern stream ecosystems. Freshw Biol 37:193–208

Khatri N, Tyagi S (2015) Influences of natural and anthropogenic factors on surface and groundwater quality in rural and urban areas Frontier of Life. Science 8:23–39

de Oliveira M, Maillard P, de Andrade Pinto J (2016) Modelling the effect of land use/land cover on nitrogen, phosphorous and dissolved oxygen loads in the Velhas River using the concept of exclusive contribution area. Environ Monitor Assess **188**: 333

Park S, Lee S (2020) Spatial varying and scale-dependent relationships of land-use types with stream water quality. Int J Environ Res Public Health 17:1673

Pratt B, Chang H (2012) Effects of land cover, topography, and built structure on seasonal water quality at multiple spatial scales. J Hazard Mater **209**: 48–58

Singh S, Mishra A (2014) Spatiotemporal analysis of the effects of forest covers on stream water quality in Western Ghats of peninsular India. J Hydrol 519:214–224

Sliva L, Williams D (2001) Buffer zone versus whole catchment approaches to studying land use impact on river water quality. Water Res 35:3462–3472

Su C, Ahern F, Chang Y (2016) Why should we pay attention to "inconsistent" land uses? A viewpoint on water quality. Landscape Ecol Engineer 12:247–254

Wertz T, Shank M (2019) Land use from water quality: Development of a water quality index across Pennsylvania streams. Ecosphere 10:e02947

Zhang Y, Chen S, Peng L (2009) Relationships between land use pattern and surface water quality in the plain river network area: A case study of Wujiang in Jiangsu Province Resources. Science 31:2150–2156 (in Chinese)

Chapter 7
Investigation on Resource Utilization of Saline Sludge to Roadbed Material

Huang Senjun, Zhang Bo, Sun Xiaoqing, Zhang Shuai, Wei Xiaodong, Wang Xuebing, and Wei Jun

Abstract The resource utilization of sediment can fully tap the potential application value of sediment and provide new materials which is instrumental in save resources. In this study, resource utilization of saline sludge from Binhai Port in Yancheng City to roadbed material was investigated and a complete technical route was proposed. The roadbed material strength of 3% (lime): 3% (Portland cement): 94% (sample) with curing agent could achieve 3.69–4.05 MPa and meet the strength requirements of road subbase, which were higher than that of roadbed material strength of 5% (Portland cement): 95% (sample) without curing agent. The leached salinity of roadbed material was less than 1.04 PSU according to PSS-78, which was about 1/10 of the original sludge. A protection measure was proposed to lead salt water to drainage ditch and prevent leached salinity into farmland. The results of this study can provide valuable reference for resource utilization of sludge, especially for saline sludge.

Keywords Saline sludge · Resource utilization · Roadbed material · Leached saltwater control

7.1 Introduction

As an important part of water body, sediment is the mixture of clay, sand, organic matter and minerals deposited at the river bed under the action of water transmission and after long-term physical, chemical and biological interaction (Sun et al. 2018). Therefore, the sediment is rich in a large amount of nutrients. At the same time, it is the

H. Senjun · Z. Bo · S. Xiaoqing · W. Xuebing · W. Jun (✉)
Power China Huadong Engineering Corporation Limited, Hangzhou 311122, China
e-mail: careerhsj@163.com

Z. Shuai · W. Xiaodong
Zhejiang Shengli Technology Holding Corporation Limited, Hangzhou 330009, China

H. Senjun
Huadong Eco-Environmental Engineering Research Institute of Zhejiang Province, Hangzhou 311122, China

G. Huang (ed.), *Proceedings of 2022 7th International Conference on Environmental Engineering and Sustainable Development (CEESD 2022)*, Environmental Science and Engineering, https://doi.org/10.1007/978-3-031-28193-8_7

reservoir of a variety of pollutants (Singh et al. 1997). The pollutants accumulated by it can be used as a secondary pollution source to directly or indirectly poison benthos or overlying aquatic organisms (Kara et al. 2017; Sin et al. 2001), and enter the food chain and affect human health through biological enrichment and other processes. Therefore, dredging engineering plays an important role in eliminating endogenous pollution. Due to the large amount of sediment with high moisture content and complex composition produced in the process of sediment dredging, it will bring serious secondary pollution to the ecological environment (Huang et al. 2021; Qureshi et al. 2021). As a result, it is very necessary to make resource utilization of the dredged sediment.

The traditional sediment landfill method is easy to cause secondary environmental pollution and is not conducive to the resource utilization. The resource utilization of sediment can fully tap the potential application value of sediment and provide new materials, which mainly includes two directions, including land use and building use. Land use refers to the application of dredged sediment to farmland, forest land, grassland, wetland, municipal greening, seedling substrate and seriously disturbed land restoration and reconstruction. For example, the dredged sediment were applied to improve dune sand in Oman (Juan José et al. 2020), strawberry cultivation from marine (Zhao et al. 2022). The construction utilization is mainly through the modification of sediment, which is used for brick making, carbonized ceramsite, road subgrade and so on. For example, the dredged sediment were used to produce porous lightweight aggregate (ceramsite) from lake (Amar et al. 2021), supplementary cementitious material (Frar et al. 2014), fired brick from Tangier and Larache port (Mezencevova et al. 2013) and Savannah Harbor (Chen et al. 2021), synthesize zeolite for removing Cd(II).

In this study, it is investigated that the dredged sediment from coastal port is tried to prepare subgrade materials, which not only can reduce the impact of saline sludge stacking on the environment, but also obtaining considerable economic benefits.

7.2 Sample Collection and Analysis

7.2.1 Study Area

The project is located between the Haidi Road and the Dongxing Road near the Binhai Harbor with area of 1.07 km^2 and stacked volume of 6.54 million square. The sludge produced by the excavation and dredged for the port's construction has been stored in a semi dry state, as shown in Fig. 7.1. Unfortunately, farmland is distributed around the site and threatened by saltwater seepage during the rainy season. Therefore, it is necessarily to conduct a research on resource utilization of saline sludge to roadbed material, which could provide shelter belts for farmland.

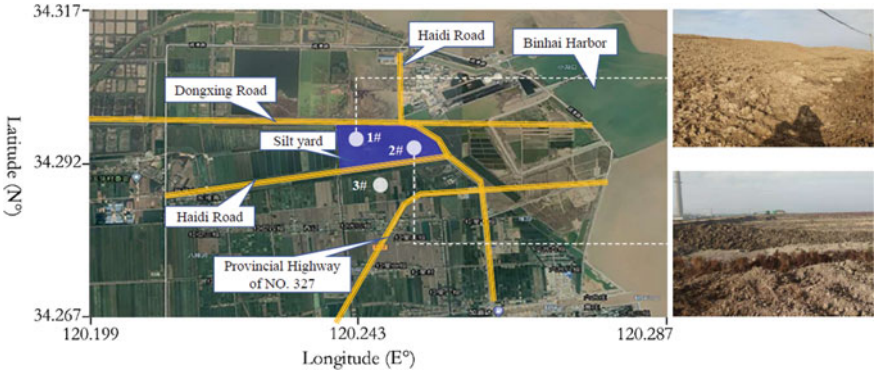

Fig. 7.1 The study area

7.2.2 Sample Collection

In order to understand the sediment characteristics, three samples were collected as shown in Fig. 7.1, among which two samples (1# and 2#) were collected at surface and with depth of 1 m, respectively; one sample (3#) was collected from the farmland with depth of 0.5 m.

7.2.3 Sample Analysis

For preparation of subgrade materials, two key indicators of mass moisture content and total salt content (TSC) were analyzed (Tab. 7.1). The mass moisture content was tested according to National Environmental Protection Standards of the People's Republic of China called "Soil-Determination of Dry Matter and Water Content-Gravimetric Method (HJ 613-2011)". The TSC was tested according to the Forestry Industry Standard of the People's Republic of China called "Analysis Methods of Water Soluble Salts of Forest Soil (LY/T 1251-1999)".

(1) The mass moisture content.

The mass moisture content (MMC) could be calculated by Eq. 1.

Table 7.1 The MMC and TSC of the collected samples

Number of samples	Depth (m)	Mass moisture content (%)	Total salt content (g/kg)
1#	0.0	10.5	10.2
	1.0	31.8	12.1
2#	0.0	15.5	11.5
	1.0	21.7	11.4
3#	0.5	34.2	0.66

$$\omega_{H_2O}=\frac{m_{w2}-m_{w3}}{m_{w3}-m_{w1}}\times 100 \tag{7.1}$$

where ω_{H_2O} is the mass moisture content (%); m_{w1} is the container mass (g); m_{w2} is the total mass of container and fresh soil (g); m_{w3} is total mass of container and dry soil (g).

(2) Test method of the total salt content.

The total salt content could be calculated by Eq. 2.

$$S=\frac{m_{s2}-m_{s1}}{m_s}\times 1000 \tag{7.2}$$

where m_s is the dry soil mass equivalent to 50 ml of leaching solution (g); m_{s1} is the mass of glass evaporating vessel (g); m_{s2} the total mass of salt and glass evaporating vessel (g).

After long-term natural drying, the surface sludge is drier than that with depth of 1.0 m. The mass moisture content are between 10.5–31.8%, which doesn't have to go through dehydration. The total salt content are between 10.2 g/kg and 12.1 g/kg, which are up to 17–20 times the salinity of farmland and causes serious environmental threat.

7.3 Roadbed Material Preparation

7.3.1 Sample Handling

The fresh sludge sample with particle size less than 5 mm was collected by dry sieving and dried by infrared drying oven until the mass moisture content lower than 12%. Afterwards, five sludge samples with different mass moisture content were obtained by add water, of which the mass moisture content was 14%, 16%, 18%, 20% and 22%, respectively. The relationship between mass moisture content (ω_{H_2O}) and dry density (ρ_{dry}) could be obtained (Fig. 7.2), from which the optimum moisture content was 17% and the maximum dry density is 1.8 g/cm^2.

7.3.2 Roadbed Material Preparation

The sludge sample was aired until the mass moisture content lower than the optimum moisture content, which was mixed with quicklime powder (3% of the sample mass) evenly and seal and stew for 72 h. Afterwards, the sludge sample was mixed with self-developed curing agent and Portland cement to make roadbed material. There were four experimental schemes, as shown in Table 7.2. For every scheme, six subsamples

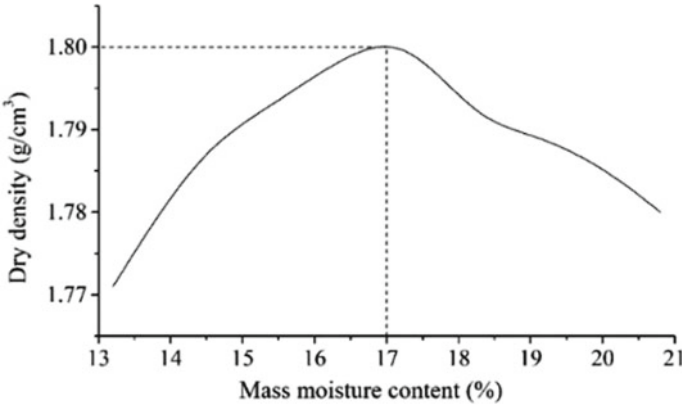

Fig. 7.2 The relationship between MMC and dry density

were made with mass moisture content of about 17%, which were sealed and cured at temperature of 25 °C for 6 days, soaked in water for 24 h on the 7th day, and then tested for 7 d unconfined strength, as shown in Fig. 7.3.

Table 7.2 Experimental schemes of sample mixed with additive

Schemes	Material proportioning	Curing agent content	Mould size
1	5% (Portland cement): 95% (sample)	0.02% (about 110 ml/t)	Φ50mm* 50 mm
2		0.03% (about 167 ml/t)	
3	3% (lime): 3% (Portland cement): 94% (sample)	0.02% (about 110 ml/t)	
4		0.03% (about 167 ml/t)	

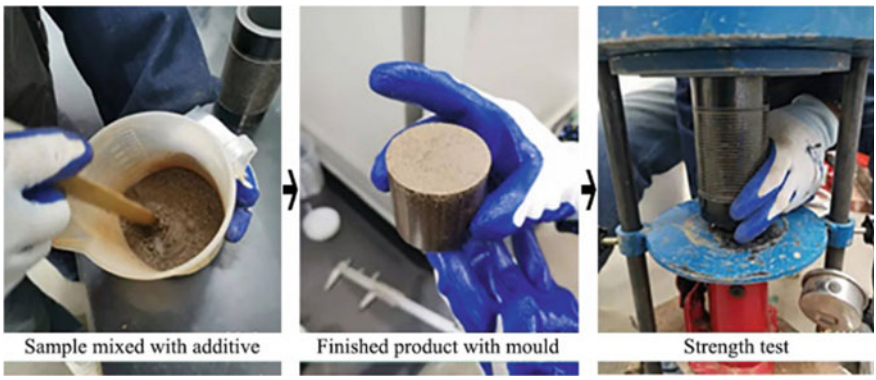

Fig. 7.3 The produce of sample preparation and testing

7.3.3 Roadbed Material Strength Test

Therefore, the experimental results of roadbed material could be achieved according to "Test Methods of Soils for Highway Engineering (JTG3430-2020)", as shown in Table 7.3. The average water absorption for schemes 1–4 were between 1.52–1.88%, which were all lower than 2% and meet the compaction standard. The 7 d unconfined strength could be 2.46–2.62 MPa for scheme 1 and scheme 2, which were 3.69–4.05 MPa for scheme 3 and scheme 4. Compared with scheme 1 and scheme 2, the strength of scheme 3 and scheme 4 were higher benefiting from the curing agent addition. The strength of roadbed material is appropriate to road subbase, which can replace the conventional materials.

7.4 Salinity Control Measures

It is necessary to consider the situation of salinity leaching when the roadbed materials are applied to actual project. Therefore, a test was conducted to evaluate the salinity leaching concentration according to the National standards of the people's Republic of China called "The Specification for Marine Monitoring-Part 4: Seawater Analysis".

Table 7.3 The water absorption and strength of subsamples

Schemes	Curing agent content	Detection index	Subsamples						Average
			①	②	③	④	⑤	⑥	
1	0.02%	Water absorption (%)	2.19	1.51	1.88	1.91	1.91	1.87	1.88
		Strength (MPa)	2.44	2.46	2.58	2.36	2.46	2.46	2.46
2	0.03%	Water absorption (%)	1.77	1.67	1.63	1.74	1.51	1.58	1.65
		Strength (MPa)	2.82	2.87	2.62	2.46	2.46	2.47	2.62
3	0.02%	Water absorption (%)	1.51	1.68	1.57	1.64	1.71	1.56	1.61
		Strength (MPa)	3.77	3.69	3.71	3.70	3.66	3.62	3.69
4	0.03%	Water absorption (%)	1.43	1.53	1.52	1.57	1.43	1.62	1.52
		Strength (MPa)	4.19	3.95	4.02	3.90	4.38	3.87	4.05

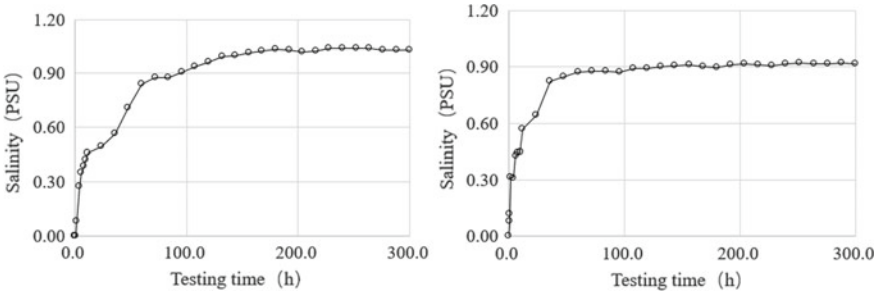

Fig. 7.4 The practical salinity value of two roadbed material samples according to PSS-78

7.4.1 Salinity Leaching Test

Firstly, the roadbed material was put into a beaker with volume of 2 L with ultra-pure water according to the ration of 1 kg produce to 2 L ultra-pure water. The salinity was determined by Portable Multi Parameter Measuring Instrument (WTW Multi 3630, Germany), as shown in Fig. 7.4. The salinity value was converted from conductivity according to PSS-78 (Practical Salinity Standard 1978). The salinity for two roadbed material samples were less than 1.04 PSU and 0.92 PSU. Though the roadbed material preparation process has reduce the salt ion release effectively, the leached salinity were slightly higher than that of farmland (0.66 g/kg).

7.4.2 Salinity Protection Measure

In view of this, a salinity protection measures was proposed to protect the farmland (Fig. 7.5). It need to set anti-seepage geo-membrane under the subgrade material and slopes on both sides of the road. The salinity water would be lead to the drainage ditch and collected. Besides, salt tolerant vegetation would be planted on slopes on both sides of the road for using leached saltwater.

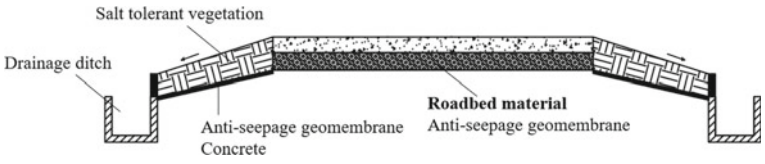

Fig. 7.5 A road structure for prevent leached saltwater

7.5 Conclusion

In the present study, a complete technical route that the saline sludge was used to preparation roadbed material has been proposed based on laboratory test. From the previous investigation, the following conclusions can be concluded.

The total salt content of saline sludge are between 10.2 g/kg and 12.1 g/kg, which are up to 17–20 times the salinity of farmland and causes serious environmental threat. The optimum moisture content and the maximum dry density of the saline sludge were 17% and 1.8 g/cm^2, respectively.

The average water absorption for schemes 1–4 were all lower than 2% and meet the compaction standard. The 7 d unconfined strength of roadbed material could be 2.46–2.62 MPa for 5% (Portland cement): 95% (sample) without curing agent, which were 3.69–4.05 MPa for 3% (lime): 3% (Portland cement): 94% (sample) with curing agent.

The leached salinity of roadbed material can be reduced to 0.92–1.04 PSU, which was slightly higher than that of farmland. Therefore, a protection measure was necessary to prevent the leached salinity into farmland.

Above all, resource utilization of saline sludge to roadbed material is feasible, which still needs further study if the roadbed material will be used to actual project.

Acknowledgements This study is supported by Research on ecological infrastructure planning and design based on EOD model (KY2021-HS-02-15) from Power China Huadong Engineering Corporation Limited.

References

Amar M, Benzerzour M, Kleib J et al (2021) From dredged sediment to supplementary cementitious material: characterization, treatment, and reuse. Int J Sedim Res 36(1):92–109

Chen J, Huang R, He OY et al. (2021) Utilization of dredged river sediments to synthesize zeolite for Cd(II) removal from wastewater. J Clean Prod **320**

Frar I, Allal LB, Ammari M et al (2014) Utilization of dredged port sediments as raw material in production of fired brick. J Mater Environ Sci 5(2):390–399

Huang SJ, Wei J, Ning SL et al. (2021) Comprehensive pollution analysis of contaminated sediment in an urban river, China. In: 5th International conference on water pollution control engineering, IOP conference series: Earth and environmental science **691** 1–7

Juan José MN, Pilar L, Dámaris NG et al. (2020) Potential of dredged bioremediated marine sediment for strawberry cultivation. Sci Rep **16**

Kara GT, Kara M, Bayram A et al. (2017) Assessment of seasonal and spatial variations of physic-ochemical parameters and trace elements along a heavily polluted effluent-dominated stream. Environ Monit Assess **189**

Mezencevova A, Yeboah NN, Burns SE et al (2013) Utilization of Savannah Harbor river sediment as the primary raw material in production of fired brick. J Environ Manage 113:128–136

Qureshi MU, Alsaidi M, Aziz M et al (2021) Use of reservoir sediments to improve engineering properties of Dune sand in Oman. Appl Sci 11:1–13

Sin SN, Chua H, Lo W et al (2001) Assessment of heavy metal cations in sediments of Shing Mun river. Hong Kong Environ Int 26(5–6):297–301

Singh M, Ansari AA, Müller G et al (1997) Heavy metals in freshly deposited sediments of the Gomati River (a tributary of the Ganga River): effects of human activities. Environ Geol 29:246–252

Sun ZL, Jiao JG, Huang SJ et al (2018) Effects of suspended sediment on salinity measurements. IEEE J Oceanic Eng 43(1):56–65

Zhao LN, Hu M, Muslim H et al. (2022) Co-utilization of lake sediment and blue-green algae for porous lightweight aggregate (ceramsite) production. Chemosphere **287**

Part II
Environmental Management for Sustainable Development

Chapter 8
The Exploration on the Path of Improving the Performance of Regional Environmental Policy in the Development of Regional Integration in China Based on the Perspective of Policy Network

Jinwen Chen

Abstract Environmental governance based on regional integration is guided by regional environmental public goals, coordinating pluralistic governance subjects, and solving the contradiction between regional holistic governance and decentralized governance. The Chinese regional environmental policy is aimed at promoting the optimal allocation of regional resources, solving regional problems, coordinating interregional relations and realizing the sustainable development of environmental governance. This paper analyzes the factors that affect the performance improvement of regional environmental policy from three dimensions: Policy target system, policy implementation process and policy implementation effect, and probes into the path of improving regional environmental policy performance. There are the paths of constructing a more perfect regional environmental policy objective system, promoting the overall management of regional environmental policy implementation process, strengthening the construction of regional environmental policy performance evaluation system basing on the perspective of policy network.

Keywords Regional integration · Regional environmental policy · Policy performance

8.1 Introduction

In recent years, although the local government has continuously adjusted and transformed the industrial structure, the ecological and environmental problems such as air pollution that seriously endanger human health still exist within a certain range. The report of the 19th National Congress pointed out: "China's regional development

J. Chen (✉)
Business School, University of Shaoxing, Shaoxing, China
e-mail: chen417jinwen@usx.edu.cn

G. Huang (ed.), *Proceedings of 2022 7th International Conference on Environmental Engineering and Sustainable Development (CEESD 2022)*, Environmental Science and Engineering, https://doi.org/10.1007/978-3-031-28193-8_8

coordination has been strengthened in the past five years. Based on the consciousness and initiative of implementing the green development concept, the ecological civilization construction has achieved remarkable results (Jinping 2017a)". With the advancement of the regional integration process, the uncoordinated and inadequate contradictions between the continuous development of local economic society and people's demand for green ecological environment have become increasingly prominent. So, "we still need to unswervingly implement the concept of innovation, coordination, green, openness, and sharing, implement regional coordinated development strategies, and establish a more effective regional coordination and development mechanism (Jinping 2017b)".

With the advancing of the society there exists the risk and risk contagion in each social domain including the environmental policy system. When numerous environmental policy have been made in Chinese local government in the past years, traditional and local legal and institutional arrangements for Chinese environmental policy making have not lived up to the solving the environmental problems fully. Scholar Yu Keping proposed the modern national governance system is an organic, coordinated, dynamic and holistic institutional operating system (Keping 2014). Therefore, regional environmental governance is an important content and priority area for regional integration development. How to improve regional environmental policy performance is important challenges and challenges that need to be solved.

8.2 The Regional Environmental Policy and Policy Risk

8.2.1 The Regional Environmental Policy Connotation

In the conceptual category of economics, the region is usually understood as the spatial carrier of human economic activity (Yamei 2013a). It is an infinitely inseparable economic and social complex created by human economic activities with specific regional components (Biding 1989). With the in-depth development of China's regional integration, the economic and social development in the region has become increasingly close. In particular, ecological and environmental problems such as air pollution in the region present the complexity and risk of cross-border public affairs. Environmental governance based on regional integration is a complex system engineering. Its essence is to reach the regional environmental governance public goals across administrative management boundaries, coordinate the functions of multiple governance entities and behavioral standards, and resolve the contradiction between environmental overall governance and decentralized governance within the region.

Regional environmental policy aims to promote the spatial allocation of regional resources, narrow regional gaps and solve regional problems in regional integration development. The local government formulates policies for regional differences

and regional issues within the region in order to coordinating inter-regional relations, improving the regional environmental policy system and acquiring sustainable development of environmental governance. Faced with the rapid growth of regional environmental governance pressure, we should optimize the regional environmental governance path based on the overall governance perspective, with a view to further improving the performance of regional environmental governance policies.

8.2.2 The Regional Environmental Policy Risk

Along with the development of the society and the technology, the various regional environmental policy risks are increasing environmental governance. Usually, the complicated organizations and relations of the policy system will use the integrative operational mode for promoting the systemic efficiency. Although that will help the regional environmental policy system advance the ability of withstanding the risk, the risk contagion will nearly cannot be avoided as the benefit conflict among the interest groups in the system. It will have the result of the impact of the risk pervasion.

The regional environmental policy risk contagion show itself as the characteristic of the snowball. The risk will transfer from the place without surveillance to the supervised place, or shift between the different places, which named the risk contagion in the regional environmental policy system and cross-domain policy system. The place firstly gives birth to the policy risk will be called the "contagious source". And the place infected by the contagious source will be called the "infected area". The crisis of the policy risk will be soon extended into the whole system by the impression of the contagious source's chain-reacting. The policy risk contagion will lead to the systemic environmental governance risk and increase the instability of the whole environmental governance system which will cause the environmental governance crisis. So the risk contagion will threaten the environmental governance systemic safety heavily and damage the benefits of the public and the society in environmental governance. To control the policy risk contagion effectively is the most important content in the environmental governance risk managing.

8.3 Case in Point: The Regional Environmental Policy in Chinese Yangtze River Delta Region

8.3.1 The Gradual Progress and Implementation of Air Pollution Governance Policy in Yangtze River Delta Region

The Yangtze River Delta region is a region that actively plays a leading role in carrying out the strategic planning of green regional environmental governance in order to

promoting the modernization of regional governance system and governance ability. The outline of Regional Integration Development Plan of the Yangtze River Delta in 2019 puts forward that the integration development of the Yangtze River Delta should closely revolve around "integration" and "high quality" in order to promoting the integrated construction of key areas such as Ecological Environment.

At present, the Yangtze River Delta region has made a positive exploration on the path of air pollution linkage control by using a good consultation mechanism of ecological environment protection, which has promoted the integration of regional environmental management. In order to further improve the performance of linkage governance of air pollution, provinces and cities in the Yangtze River Delta region have issued a series of related policies (Fig. 8.1).The goal and orientation, implementation path and development direction of air pollution linkage governance in the Yangtze River Delta region have been gradually clarified. It has completed the regional air pollution control system top-level design basically. To a certain extent, it promotes the integration of regional environmental governance in the Yangtze River Delta, promotes the deep cooperation of urban agglomeration in ecological environment linkage governance, and makes a beneficial exploration for the improvement of regional environmental governance policy performance.

8.3.2 Factors Affecting the Performance of Regional Environmental Policy Implementation: Based on the Perspective of Policy Risk Management

With the development of regional environmental governance integration, regional environmental policies are becoming more and more important. Although local governments have been making unremitting efforts to achieve regional balance and sustainable development, they have achieved certain environmental governance results and accumulated useful experience. However, there are still some problems in the process of formulating and implementing the current regional environmental policy basing on the perspective of policy risk management.

8.3.2.1 The Target System of Regional Environmental Policy Needs to be Further Improved

The construction of the target system of regional environmental policy is not perfect, which affects the effect of policy implementation to some extent. Firstly, there is a lack of systematic regional environmental policy goals. The regional environmental policy system needs multi-level policy objectives that can be linked to each other, so that policy synergies can be formed in different stages of policy evolution. Secondly, the principles of regional environmental policy objectives are relatively simple. The regional environmental policy objectives are mainly based on

time	content	main target
2008	《Cooperation Agreement on Environmental Protection Work in the Yangtze River Delta Region》	It was promoting the coordinated governance of environmental pollution in the Yangtze River Delta.
2013	《China's Air Pollution Prevention and Control Action Plan》	It was required to establish a coordination mechanism for air pollution prevention and control in Yangtze River Delta regions.
2014	《Detailed rules for the implementation of the Action Plan for the Prevention and Control of Air pollution in the Yangtze River Delta region》	The implementation of cooperative mechanism for air pollution prevention and control in Yangtze River Delta region have been made.
2018	《Three-Year Action Plan to Win the Blue Sky Defence 》	It was focusing on the sustainability of air pollution prevention and control actions in the Yangtze River Delta region.
2018	《Three-Year Action Plan for the Integration of the Yangtze River Delta Region (2018-2020)》	The "Action Road map" and task schedule jointly recognized and followed by the regional development of the three provinces and one city have been established in the Yangtze River Delta region.
2018	《Action Plan for Comprehensive Management of Air Pollution in the Autumn and Winter of 2018-2019 in the Yangtze River Delta Region》	It was Focusing on the Heavy-duty weather emergency response, strengthening the capacity building of regional environmental air quality forecasting center and improving the early warning grading standard system.
2019	《Outline of the Regional Integration Development Plan of the Yangtze River Delta》	It is proposed that establishing a demonstration zone for the development of ecological green integration in the Yangtze River Delta region.
2019	《Agreement on deepening the Coordination of Local Legislative work of the standing Committee of the people's Congress in the Yangtze River Delta Region》	It makes positive linking up related policies and focusing on environmental control, market opening and order and other key areas.
2019	《Agreement on deepening the Cooperative Mechanism of Supervision and Judicial work of the people's Congress in the Yangtze River Delta region》	It is focusing on the collaborating through regular exchanges, liaisons, and information sharing channels to promote the interconnection and sharing of judicial data information.
2019	《Overall plan for the Yangtze River Delta ecological and green integrated development demonstration zone》	It will promote the innovation of policies, systems and methods of high-quality development, take the lead in exploring the transformation from regional project coordination to regional integration system innovation, transform ecological advantages into economic and social development advantages, and explore an eco-friendly development model.
2020	《 Action Plan for "Three Unified" System Construction of Ecological Environment Management in Yangtze River Delta Ecological and Green Integrated Development Demonstration Zone》	The demonstration area implements the system innovation of cross-regional ecological environment management without breaking administrative subordination and administrative boundaries.

Fig. 8.1 Policy for the Governance of Air pollution in the Yangtze River Delta region from 2008 to 2020

the principles of planning and cooperation recently. However, in fact, the regional environmental policy objectives should also combine the principles of concentration, additional principles, and supporting principles to comprehensively play the role of regional environmental policy objectives under various principles. Third, the coordination of regional environmental policy objectives is insufficient. Regional

environmental policies cannot replace the policy objectives of each member region by formulating a common policy goal. Instead, they can effectively coordinate and link policies between member regions and regional environmental policy objectives through various economic, legal, and administrative means. Before the implementation of regional environmental policies, the pursuit of policy objectives in member regions is sometimes contradictory or competing. Therefore, coordinating policy objectives between member regions should be one of the tasks of regional environmental policies.

8.3.2.2 The Implementation Process of Regional Environmental Policy Needs to be Further Managed

The implementation process of regional environmental policies is the process of comprehensive policy in all aspects. At present, it is necessary to further strengthen management in policy promotion, policy instrument, policy implementation. Firstly, the comprehensive function of the multi-policy propaganda channel is weak. Within a certain scope, there are still problems such as insufficient publicity, single propaganda, and lack of hierarchical policy and content in urban and rural areas. This makes the comprehensive function of the multi-policy propaganda channel not fully apparent. Secondly, there is a lack of policy tools to support policy implementation. The policy tools of regional environmental policies mainly include various funds or loan instruments. At the beginning of the implementation of regional environmental policies, various funds related to regional environmental policies played a very important role in the implementation of policies. At present, it is mainly based on structural funds, and there are relatively few aggregate funds and solidarity funds. The structural funds are mainly mainly regional development funds, and there are fewer social funds. Thirdly, it needs the joint efforts of multi-level policy implementation needs to be strengthened. Relevant institutions and entities involved in the implementation of regional environmental policies will form a policy implementation chain, which will have an impact on policy implementation. In the process of the implementation of regional environmental policy, the traditional segmentation path depends heavily, and the joint force of policy implementation is affected by the degree of integration of social resources, which hinders the promotion of the joint force of policy implementation to a certain extent.

8.3.2.3 The Effect of Regional Environmental Policy Needs to be Further Evaluated

Policy assessment is also a very important component of the regional environmental policy system. It has a significant role in controlling policy risk transmission and achieving the desired policy effects. At present, the assessment of the implementation effect of regional environmental policies needs to be emphasized. Firstly, there is insufficient understanding of the strategic positioning of regional environmental

policy assessments. The assessment of regional environmental policies is aimed at promoting the realization of policy objectives and improving the long-term effects of environmental governance. On the other hand, it reflects the social and economic development prospects of individuals, regions and sectors that are concerned by policies. However, the current regional environmental policy assessment has insufficient understanding of the strategic significance of policy tool selection, policy influence, and policy risk control. Secondly, the comprehensive application of regional environmental policy assessment methods is weak. At present, regional environmental policies are mostly post-event evaluations, lacking the comprehensive application of pre-assessment and in-process assessment. The ex post assessment is mainly to analyze the breadth of policy influence and the use of policy resources, mainly focusing on the main factors leading to the success or failure of policy implementation and the sustainability of policies. Pre-assessment needs to pay attention to the strengths, weaknesses and development potential of the relevant member regions or departments. In-process assessments need to reflect assessment feedback directly in policy improvement. Thirdly, the results of regional environmental policy assessments are poorly applied. The implementation of regional environmental policies will help improve the environmental governance capacity of member areas and narrow the gap in governance levels in different member areas. However, the regional environmental policy assessment report is generally submitted to the competent authorities for decision-making reference, and is rarely included in the comprehensive assessment system for environmental governance of regional member regions, nor is it an important basis for promotion, reuse, evaluation, reward and punishment of leading cadres.

8.4 Policy Network: The Path to Improving the Performance of Regional Environmental Policy Implementation

Further improving the performance of regional environmental policies basing on the policy network, on the one hand, contributes to the centralized implementation of policies at member and regional levels, and promotes the modernization of regional environmental governance capabilities and levels. On the other hand, the process of promoting regional integration has also promoted cooperation as a key factor in the integration of regional environmental governance.

8.4.1 Policy Network: A New Method to Control the Transmission of Policy Risk

The policy network is based on the power, ability and trust of the policy maker, which is a diversified, open and adaptive way to manage the risk spread in the policy system (Klijn and Koppenjan 2000). Network members are rational utility, which can exchange resources and returns to the greatest extent. Therefore, if the policy network is used in Chinese regional environmental governance, the interests of all participants in the network are conducive to balance and coordination from the beginning, thus avoiding the risk transmission caused by conflicts of interest in the implementation of the regional environmental policy. First of all, the government should have a cooperative position. Second, in view of the special resources of the government and its role in representing the common interest, the government should establish a policy network. Third, the government needs to manage the operation of the policy network in an attempt to promote solutions to certain problems or realities the interactive process of projects that protect common interests.

8.4.2 Constructing Regional Environmental Policy Implementation System from the Perspective of Policy Network

8.4.2.1 Constructing a More Perfect Regional Environmental Policy Target System

The construction of a regional environmental policy system requires a relatively complete target system, operational implementation principles and clear and clear implementation targets. Among them, a relatively complete policy target system is the premise basis. This can achieve ecological aggregation, social aggregation and geographical aggregation among member regions, and promote a more coordinated and balanced development of regional environmental governance. Regional aggregation is a new goal of regional environmental policy, which aims to realize the harmony and balanced development of integrated regional environmental governance. “from a policy point of view, the objective of geographical convergence is to narrow existing gaps, avoid geographical imbalances and achieve a more balanced development through greater coherence between sectoral and regional policies with spatial implications and by encouraging cooperation between regions” (Yamei 2013b). In order to facilitate the formulation and implementation of regional environmental policy, ensure the rational allocation of policy resources, and give full play to the enthusiasm of regional member areas to participate in environmental governance, a series of basic principles should be established for the setting of regional environmental policy objectives, including planning principles, partnership principles, concentration principles, additional principles and auxiliary principles. In essence, regional

environmental policy is an important mechanism to solve regional environmental problems and coordinate regional conflicts of interest. Therefore, it is an important part of regional environmental policy to coordinate the objectives of regional environmental policy. At the same time, the coordination mechanism between regional environmental policy and other policy objectives is constructed, and the multi-level and multi-sector related policies are organically coordinated and coordinated, so as to achieve the best synergy.

8.4.2.2 Promoting the Overall Management of the Implementation Process of Regional Environmental Policy

Regional environmental policy is the sum of a series of policies to coordinate the environmental governance gap among countries, regions and member regions. Effective regional environmental policy depends on well-functioning organizational system, mechanism management and financial support. Therefore, promoting the overall management of the implementation process of regional environmental policy can further improve the performance of regional environmental policy. The regional environmental policy institutions are mainly responsible for the formulation, implementation and supervision of the policies of the regional environmental community, and are mainly responsible for the functions of regional environmental policy trend research, strategy formulation, publicity and coordination, information disclosure and implementation, and coordination to minimize the adverse effects of policies on member areas whose environmental governance capacity and level are relatively weak. The regional policy committee is mainly responsible for studying the development trend of ecological environment in various regions of environmental governance community. In order to strengthen regional and member regional intergovernmental cooperation, the regional policy committee can express its views or suggestions directly for the formulation and implementation of regional environmental policy, which can be used as a district. The establishment of regional environmental policy organization provides the guarantee of organization for the overall management of regional environmental policy implementation process. Therefore, the formulation, implementation, supervision and evaluation of regional environmental policy need comprehensive and scientific and institutionalized management in order to reflect the standardization and rationality of regional environmental policy.

8.4.2.3 Strengthening the Construction of Regional Environmental Policy Performance Evaluation System

"Policy evaluation, as a kind of political behavior to judge the efficiency, effect and value of policy, is an important part of the organic chain of policy operation (Zhenming 1998)". Performance evaluation of regional environmental policy is one of the basic requirements to improve regional environmental policy. In view of the fact that the current concept of regional environmental policy performance has not

yet been firmly established, the breadth and depth of performance management is insufficient, and the role of performance incentive and restraint is not strong, it is the only way to strengthen the performance of regional environmental policy before and after the event. The performance evaluation of regional environmental policy should be carried out in an all-round way, and the concept and method of performance should be deeply integrated into the whole process of policy implementation. Promoting third-party assessment of regional environmental policy is an important guarantee to improve the level of scientific decision-making and effective policy implementation, and it is also a realistic demand to promote the modernization of regional environmental governance system and governance ability. Third-party evaluation is also an effective supervision and supplement of government governance behavior, and plays an active role in social service supervision and prevention of environmental pollution risk transmission. At the same time, regularly publish the list of third-party evaluation institutions to promote fair competition among third-party evaluation institutions. Therefore, in order to carry out the third party assessment of regional environmental policy, we must adhere to the principles of service decision, objective justice, scientific standardization and practical effect, and make a comprehensive analysis of the feasibility, perfection, standardization and risk point of the policy.

In summary, the expansion and deepening of the process of regional integration not only makes the status and role of regional environmental policy more obvious, but also puts forward higher requirements for the performance of regional environmental policy. The reform and adjustment of regional environmental policy is the process of reconstructing regional environmental policy in order to promote the process of regional integration under the background of the increasing development of environmental globalization governance and knowledge economy in the twenty-first century. It helps to enhance the social cohesion and credibility of regional integration, and is also an important means and model of social fairness in the environmental governance system.

Fund Project

Zhejiang Soft Science Research Project “Research on Regional Air Pollution Control Policy Evaluation and Model Transformation: Taking Zhejiang Province as an Example” (No. 2017c35049).

References

Biding Cheng (1989) Regional economics. Comfort People Publishing House, Hefei, p 4

Jinping Xi (2017a) Decisive victory to build a well-off society in an all-round way to win a great victory in socialism with Chinese characteristics in the new era. People’s Publishing House, Beijing, pp 3–5

Jinping Xi (2017b) Decisive victory to build a well-off society in an all-round way to win a great victory in socialism with Chinese characteristics in the new era. People’s Publishing House, Beijing, pp 32–33

Keping Yu (2014) On the modernization of state governance. Social Sciences Academic Press, Beijing, p 3
Klijn EH, Koppenjan JFM (2000) Public management and policy network. Public Manage: An Int J Res Theory **2**(2): pp135–158
Yamei Wang (2013a) EU regional policy in the process of European integration. Sichuan University Press, Sichuan, p 27
Yamei Wang (2013b) EU regional policy in the process of European integration. Sichuan University Press, Sichuan, p 71
Zhenming Chen (1998) Policy science. China Renmin University Press, Beijing, pp 340–342

Chapter 9
A Joint Data-Physics-Knowledge Driven Strategy for Electric Heating Load Forecasting and Scheduling

Jie Zhang, Hao Shen, Ling Qi, and Yongjie Chen

Abstract In the background of double carbon, electric heating technology is the development trend of heating method, which is conducive to energy saving and emission reduction. As the heating load is random, volatile, and not easy to regulate, a fused electric heating scheduling method is proposed. First, clustering is carried out according to load characteristics, and a power prediction algorithm is designed based on historical data, load demand, and heating trends with a fused data-physics-knowledge inference model. Then, a load scheduling model is designed at the dispatching end, with economy and comfort indicators as the objective functions. In the platform, a control terminal is installed at the user end to implement the dispatching strategy. The method can be used as a reference for the design of load scheduling strategies under the heating transition period.

Keywords Electric heating loads · Load forecasting · Heating demand · Scheduling indicator sets · Load scheduling

9.1 Introduction

China is in the stage of accelerated urbanization and the demand for heating is growing fast. At present, remote areas are mainly heated by burning coal and firewood, which has the problems of high heating costs and environmental pollution. Some areas use gas heating, which has the advantages of high energy utilization, high reliability of power supply, and low environmental pollution, but requires high architectural design and has safety risks (Nan et al. 2021). As a new type of heating technology, electric heating technology can reduce heating costs compared to traditional methods, and also has the advantages of cleanliness and automation, which helps to save energy and reduce emissions, and is a development trend (Zhongqi et al. 2021).

J. Zhang (✉) · H. Shen · L. Qi · Y. Chen
Nanjing University of Posts and Telecommunications, Nanjing 210023, China
e-mail: 843124494@qq.com

G. Huang (ed.), *Proceedings of 2022 7th International Conference on Environmental Engineering and Sustainable Development (CEESD 2022)*, Environmental Science and Engineering, https://doi.org/10.1007/978-3-031-28193-8_9

When the weather is cold, electric heating loads can cause shocks when they are connected to the grid on a large scale for a short period, so there is a need to study electric heating load scheduling technology. The research focuses on load forecasting and scheduling. The literature (Qing et al. 2019) proposes an RBF neural network prediction model based on ridge regression estimation, which can effectively eliminate the input multicollinearity problem and improve the prediction accuracy; the literature (Yi et al. 2019) proposes a digital building electricity model construction method based on physical and data fusion modeling, which can achieve refined energy efficiency analysis of electricity consumption; the literature (Yi et al. 2021) studies the progress of data and knowledge research progress of joint-driven methods and put forward the prospect of application in power systems. The above are relatively representative studies that have improved the accuracy of load prediction to a certain extent by means of neural networks, artificial intelligence, model fusion, etc.

In terms of load scheduling, existing research includes regulation and control of equipment, load, electricity price, scheduling index, etc. Literature (Shuai et al. 2017) optimizes the operation of heating equipment according to user comfort and realizes collaborative optimization of distributed load; literature (Yulong et al. 2020) establishes a distributed electric heating load model and realizes regulation and control of electric heating load by using the group control method; literature (Ning 2013) studies direct control of centralized load process; literature (Zhiqiang et al. 2019) proposes a modeling method for aggregated load characteristics of multiple types of users, which improved the accuracy of solving the thermal load characteristics; literature (Zhang et al. 2021) studies the evaluation method of the benefits of electric heating loads, and proposed evaluation indexes and evaluation models from various aspects such as comfort and policies.

Most of the above studies are direct load regulation, failing to adjust the strategy according to the dynamic demand and satisfaction of the load. The article, therefore, investigates load forecasting and scheduling strategies, firstly clustering multi-modal loads, then establishing forecasting algorithms that consider load forecasts, heating demand, and trends, followed by designing scheduling indicator sets and scheduling models to complete load schedules.

9.2 Electric Heating Load Forecasting Algorithm

9.2.1 Load Forecasting Model Architecture

The scheduling of electric heating loads relies on accurate heating power prediction techniques. Most of the existing prediction techniques use data models to train a large amount of historical power data and predict short-time power, but the prediction accuracy is not high. Therefore, the article uses the K-Means algorithm to cluster heating users, and then builds a fusion prediction model based on the data model (Weizhao et al. 2020).

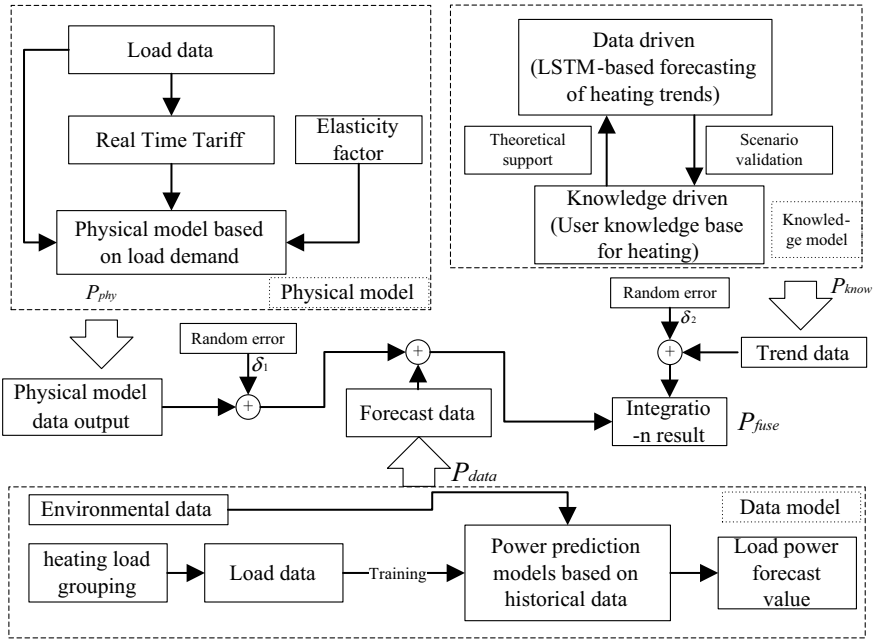

Fig. 9.1 Power forecasting based on physical data fusion

The process of the power forecasting algorithm is shown in Fig. 9.1. Firstly, a load forecasting data model based on generalized regression neural network (GRNN) and historical data of heating power is built to output power forecasting data, and is denoted as P_{data}; then a physical model based on time-of-use tariff and load demand elasticity coefficient is built to output heating demand data; then a load heating trend projection model based on knowledge inference algorithm is built to output heating trend data; finally, the data model is modified by fusing demand data and trend inference data to output short-time power forecasting data.

9.2.2 Physical Modelling in Heating Demand Forecasting

Under the influence of weather, electricity price, and other factors, there is a sudden increase and decrease in user demand for heating, and the prediction accuracy of the data model will decrease.

First, the time-sharing price calculation method on the user side is designed based on the load proportion factor. Select typical days that can reflect the user's heating condition in a certain period, and then set up the calculation formula of electricity

price according to the purchase cost C_1, transmission and distribution loss C_2, transmission and distribution price C_3, and government fund C_4, as shown in Eq. (9.1) (Yujie 2019):

$$C_{i,t} = \frac{24 \times P_{i,t}}{\sum P_{i,t}} \times (C_1 + C_2 + C_3 + C_4) \tag{9.1}$$

where $C_{i,t}$ denotes the real-time tariff of load i at moment t; $P_{i,t}$ denotes the real-time power of load i at moment t.

The price elasticity coefficient E is introduced to characterize the relationship between the load's heating demand and the real-time electricity price. According to the effect of the fluctuation of the electricity price at time t on the electricity demand at time t and time h, the price elasticity coefficient can be divided into the self-elasticity coefficient and the other elasticity coefficient, which are denoted by $E(t, t)$ and $E(t, h)$ respectively:

$$E(t,t) = \frac{Ci,t}{Pi,t=0} \times \frac{\partial Pi,t}{\partial Ci,t}, E(t,h) = \frac{Ci,h}{Pi,h=0} \times \frac{\partial Pi,h}{\partial Ci,h} \tag{9.2}$$

where $P_{i,t-0}$ represents the power at the initial moment ($t = 0$) of the i-th load.

Based on real-time electricity prices and load demand elasticity coefficients, the heating demand data of the load at moment t under the influence of electricity price fluctuations is calculated using Eq. (9.3), and is denoted as $Pphy$, which reflects the impact of real-time electricity prices on customer demand and can correct the electric heating load power forecast data output by the data model.

$$P_{phy} = P_{i,t} \times \left(1 + E(t,t) \times \frac{[C_{i,t} - C_{i,t=0}]}{C_{i,t=0}}\right) + P_{i,t} \times \sum_{\substack{h=1 \\ h \neq t}}^{24} E(t,h) \times \frac{[C_{i,h} - C_{i,h=0}]}{C_{i,h=0}} \tag{9.3}$$

9.2.3 Knowledge Modelling in Heating Demand Forecasting

Due to the influence of electricity price, temperature and other factors, the instantaneous trend change of heating power of different electric heating loads is not consistent, the knowledge inference algorithm can reason about the users' heating trend according to the change of temperature, electricity price, etc. Therefore, the article designs a heating trend inference model based on the knowledge inference

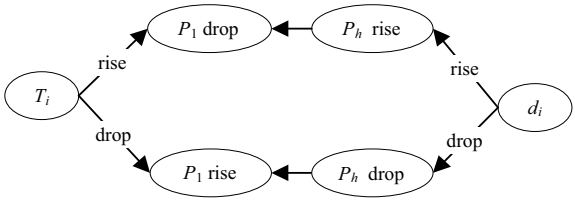

Fig. 9.2 Triadic relationship diagram

algorithm, including the knowledge inference model with and without rules (design intelligent algorithm), to obtain the users' heating trend inference data.

Knowledge Base on Changes in Heating Trends. The article constructs an incremental knowledge base for describing the links between historical data on electric heating loads, heating trends, and external environmental factors to form a knowledge system, including a rule base, a fact database, and a model algorithm base (Chunlei et al. 2010).

The rule base consists of two parts, premises and conclusions, and is represented using the concept of a triad, specifically a knowledge graph containing n entities, m relationships, and facts stored as a triad $D = \{(h, r, t)|h \in E, r \in R, t \in E\}$, each triple consists of a head entity $h \in E$, a tail entity $t \in E$ and a relationship $r \in R$ between them, where E denotes the set of entities and R the set of relationships. The article defines the following triad to construct the incremental knowledge base based on the relationship between real-time temperature T_i, load power d_i, real-time electricity price $P(h)$ and load trend $P_1(t)$, as shown in Fig. 9.2.

The factual database uses the historical data collected to store information on the process of scheduling policy and user changes, with the following formula.

$$F = \begin{bmatrix} T_1 \ \ldots \ T_n \\ C_1 \ \ldots \ C_n \\ P_1 \ \ldots \ P_n \end{bmatrix} \tag{9.4}$$

where T denotes the external temperature, C denotes the change in dynamic tariff in the dispatch strategy and P denotes the change in the customer's heating power.

The library of model algorithms includes inference algorithms, i.e. the ability to use existing knowledge from the rule base and fact database to reason about load heating trends when the electric heating load is influenced by environmental and self-inflicted factors, as well as the ability to optimize the internal parameters of the model using heuristic knowledge and experience in the inference process.

Knowledge-based Reasoning on Heating Trend. In the constructed knowledge inference model, both regular and irregular cases are included. If the knowledge base already contains relevant knowledge, the information available in the knowledge base is used to reason about the trend in heating power.

Regular inference includes the following types: (1) Consistent matching: The data to be inferred and the head entity of the knowledge are matched exactly, the content

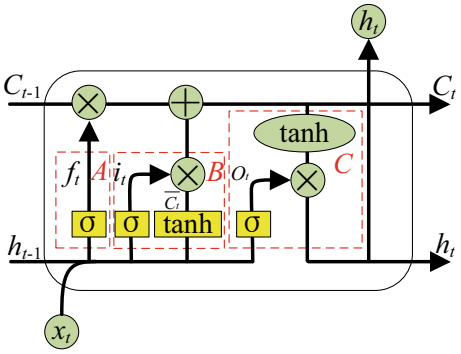

Fig. 9.3 Cell structure of LSTM

includes quarter, month, hour, temperature, and average temperature; (2) Domain value range matching: When the input quarter, month, hour, temperature, average temperature data is matched within a certain domain value range, within the set range is to be converted into the input value defined by the rule, for the more volatile data to be inferred, there are different matching objects and domain value ranges.

When consistent matching and threshold matching are not possible, a knowledge inference model based on a long and short-term memory neural network (LSTM) is used (Zhongwei et al. 2019), with the model inputs being temporal data, temperature data, and load power and the outputs being load heating trend prediction data. The LSTM model uses a cellular structure as shown in Fig. 9.3 and includes three controls, the forgetting gate, the input gate, and the output gate, corresponding to parts A, B and C in the figure. In the forgetting gate, the load information is selectively allowed to pass forward through a neural layer using a sigmoid function and a point-by-point multiplication operation. The input gate is used to determine the load information to be added inside the cell state. The output gate is box C in Fig. 9.3, where a sigmoid function is used to determine the fraction of cell states that need to be output, and then the tanh function is used to process the cell states and output the load trend results.

9.2.4 Data-Physics-Knowledge Fusion Power Prediction Algorithm

Combining the data, physical and knowledge models in Fig.n9.1, we can obtain the accurately predicted power of the electric heating load. The output of the power prediction model based on historical data is denoted as $P_{data}(t)$, which represents the power prediction data at time t. The physical model outputs the heating demand power data of users under the influence of real-time electricity price, which is denoted as $P_{phy}(t)$, and during the experimental process, there may be random errors caused by environmental conditions and unstable measuring instruments, so random errors δ_1 are added; the knowledge inference model outputs the heating trend data of users

under the influence of electricity price, time and temperature, which is denoted as $P_{know}(t)$, and random errors δ_2 are added, and Eq. (9.5) is used for fusion calculation.

$$P_{fuse}(t) = P_{data}(t) \times m/p + P'_{phy}(t) \times n/p + P'_{know}(t) \times k/p \tag{9.5}$$

In formula (9.9), $P'_{phy}(t)$ represents the sum of $P_{phy}(t)$ and δ_1; $P'_{know}(t)$ denotes the sum of $P_{know}(t)$ and δ_2; m、n、k are the ratios of $P_{data}(t)$, $P'_{phy}(t)$ and $P'_{know}(t)$, and p is the sum of the three. The scale coefficients predicted by the model are fused and used as the fused predicted power output.

9.3 The Scheduling Strategy for Electric Heating Loads

9.3.1 Electric Heating Load Dispatch Model Architecture

The designed load scheduling model includes two parts, the scheduling layer, and the user layer, as shown in Fig. 9.4.

The scheduling layer deploys a load scheduling model, which consists of three parts: Load prediction, calculation of dispatch indicator set, and optimal power allocation. First, the fusion algorithm is used to predict the heating power of the electric heating load and calculate the value of the dispatch indicator based on the

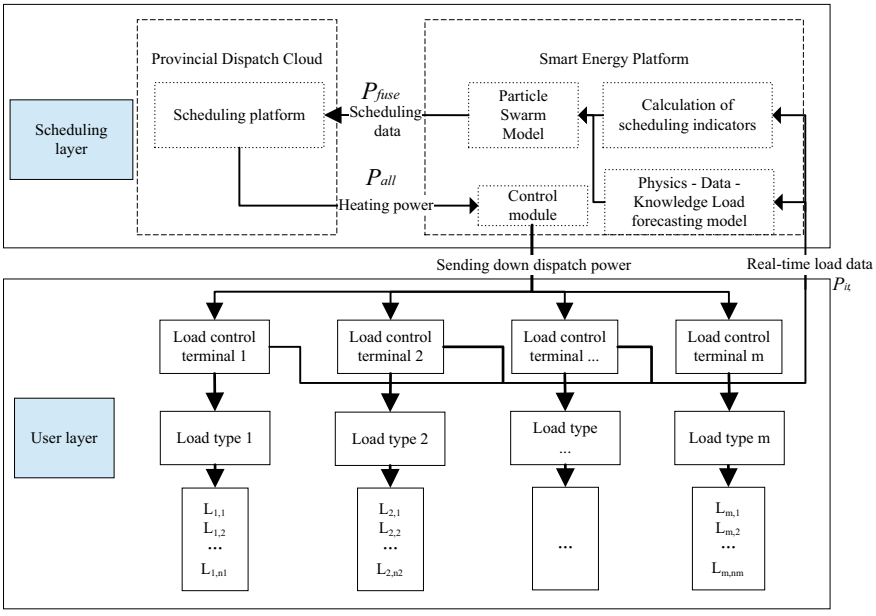

Fig. 9.4 Implementation architecture of two-layer scheduling strategy

real-time heating power fed back from the load control. Then, using the particle swarm optimization algorithm, the power prediction value is used as the initial power dispatch value, and the data of the dispatch indicator is set as the constraint. The final model outputs the power allocation result that maximizes the dispatching benefit and uploads it to the provincial dispatching cloud; the provincial dispatching cloud then issues the heating power $Pall$ according to the uploaded dispatching demand.

9.3.2 Scheduling Indicator Set

Economic Indicator. The economy indicator reflects the economic consumption of the customer in terms of heating before and after the use of the scheduling strategy. The article uses the consumption with the scheduling strategy in place and without the heating equipment participating in the scheduling to calculate it, as shown in Eq. (9.6). The smaller the value of this value, the lower the cost of heating at the current moment after the scheduling.

$$E^{cost} = \frac{[C_{i,t}P(i,t) + C_{i,t}L_{fit}]\Delta t}{[C_{i,t}P_{fit} + C_{i,t}L_{fit}]\Delta t} \tag{9.6}$$

where E^{cost} is the electricity economy indicator; $C_{i,t}$ is the real-time electricity price for load i at moments t; $P(i,t)$ is the load consumed by the heating equipment at moment t; $Pfit$ and is the operating power of heating and other equipment under non-participating dispatch, respectively; Δt is 60 min.

Comfort Indicator. Electricity comfort is the average percentage error between the dispatched power and the power consumed by the equipment in normal operation after the dispatch strategy has been implemented. Electricity comfort can be expressed as Eq. (9.7).

$$E^{fit} = \frac{P(i,t) - P_{fit}}{P_{fit}} \tag{9.7}$$

where $Pfit$ is the power consumption of the heating equipment running all the time, $P(i,t)$ is the dispatching power, E^{fit} is less than 0, and the smaller it is the less the dispatching power is sent down to meet the heating demand and the lower the comfort level of the user.

Scheduling Strategy Implementation. The article designs a particle swarm algorithm-based load optimization scheduling model. In the implementation of the load scheduling strategy, the load control terminal at the user layer sends the real-time heating power of the user to the scheduling layer, and the load scheduling model at the scheduling layer predicts the short-time heating power using a data-physics-knowledge inference model. The particle swarm algorithm in the scheduling model then takes the short-time heating power as the initial scheduling value and uses the

set of scheduling indicators as the model constraint to output a power scheduling value that meets the objective function.

Taking into account the economic and comfort requirements of users with heating, the objective function used in the scheduling model is as follows, where F is the output of the objective function, and the larger the value, the better the scheduling effect.

$$F = 1/E^{cost} + E^{fit} \tag{9.8}$$

When implementing the scheduling strategy, the constraints of the particle swarm algorithm include the following three: (1) Economical index requirements, the economical index reflects the consumption ratio after optimization and before optimization, the index range needs to be 0.5–1.5 to guarantee the economic benefits of the scheduling layer and the user layer in an integrated manner. (2) Fairness indicator requirements. The fairness indicator is used to avoid the situation where the heating is turned off for too long when the heating demand is high, and the value should be in the range of 0–1.

$$\begin{aligned} &0.5 \leq E^{fit} \leq 1.5 \\ &C = Ci, t + \Delta Ci, t \end{aligned} \tag{9.9}$$

where, $\Delta Ci, t$ is the amount of tariff adjustment, when the comfort level is less than 1, reduce the heating tariff, otherwise increase the tariff appropriately, so that the comfort index is maintained at around 1.

9.4 Algorithm Simulation

To verify the dispatching strategy proposed in the article, a customer load in a region of Northern Europe was selected for testing, where the energy meter is used as a load control terminal to collect data such as voltage, current, power and ambient temperature, and can issue control commands to the circuit breaker for the throwing and cutting control of controllable loads.

9.4.1 Load Forecasting Experiment

The article called the K-means algorithm package of the SK-learn library to classify the loads into four categories. Then for each class of load, a prediction algorithm was used for power prediction. As shown in Fig. 9.5, the load raw data curve form "-" and the data model prediction results are shown in the figure in the curve form "."; the physical model corrects the data and the correction results are in the form of the curve "-."; the data is then corrected with the knowledge-based inference of the load

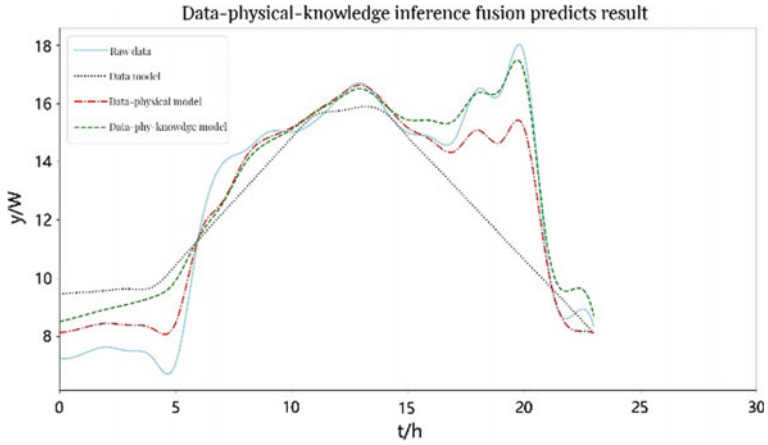

Fig. 9.5 Load forecast results of the next day

Table 9.1 Comparison of prediction standard deviation

Methods	Prediction standard deviation
Traditional forecasting method	4.948
Data-Physics Fusion	0.859
Data-Physics-Knowledge Inference	0.867

heating trend data in the form of the curve "–". The predicted standard deviations are shown in Table 9.1.

Combined with the graphical analysis, the fusion forecasting algorithm is more accurate. In addition, the prediction accuracy of the modified knowledge inference model is not significantly different from the physical model correction, but the knowledge inference model is more accurate for the inference of the heating trend of the load, and better reflects the change of the load trend between 17:00 and 21:00.

9.4.2 Scheduling Strategy Model Solver

The particle swarm algorithm is used to solve the scheduling model, and the solution results are shown in Fig. 9.6, where the red and blue curves are the heating power data before and after optimization respectively. It can be seen that after using the scheduling strategy, the load power fluctuation situation is reduced and the power mutation is less, which is conducive to the stable operation of the grid.

In addition, according to the set of scheduling indicators designed in the article, the implementation of the strategy was analyzed. Taking the 7th h as an example, the

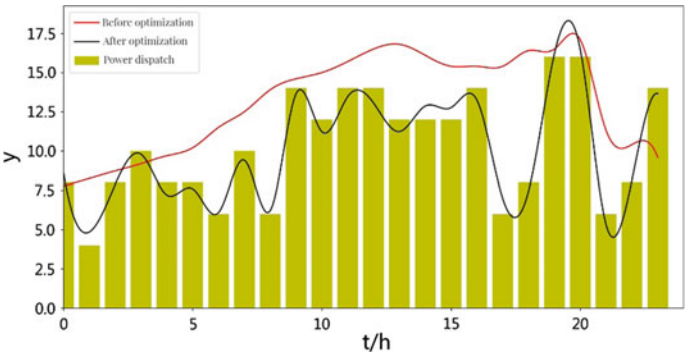

Fig. 9.6 Scheduling strategy model solving

user's power before scheduling was 4.67 kWh with a consumption of 5.51 RMB, and after scheduling was 3.035 kWh with consumption of 1.902 RMB, the value of the user's economic indicator was 0.345, indicating that the user's heating consumption expenditure situation had decreased; the comfort indicator was 0.65, indicating that the scheduling strategy was effective in ensuring The final calculated W value is 3.549, which is greater than 1, indicating that the scheduling strategy is effective. Compared with traditional methods, the dispatching strategy proposed in the article can reduce consumption to a greater extent and meet the requirements of economy and comfort while ensuring user satisfaction.

9.5 Conclusion

To address the existing scheduling challenges of electric heating loads, the paper innovatively proposes a joint data-physics-knowledge inference model-driven electric heating load scheduling strategy, which improves the accuracy of load power prediction by jointly modifying the power prediction results of traditional load prediction algorithms through physical models and knowledge inference models. In addition, the paper proposes an optimal scheduling strategy based on the particle swarm algorithm by fusing power prediction data and index set data and implements the optimal scheduling of electric heating loads in combination with load control terminals. The results show that the algorithm can output more accurate load power prediction information, and the two-tier scheduling strategy can meet the requirements of the scheduling indexes and obtain better scheduling results.

The load prediction algorithm and the scheduling strategy designed in the paper can provide more accurate power prediction data and scheduling data for grid dispatching companies and load aggregators and provide loads with more comfortable and less expensive heating methods.

Funding This research was funded by Jiangsu Postgraduate Practice Innovation Program (SJCX21_0304): Research on double-level scheduling of electric heating loads and information security protection strategies.

References

Chunlei H, Feng W, Jianjun W (2010) Intelligent online hydropower dispatching based on knowledge reasoning[J]. Automat Electric Power Syst **34**(21): 50–54, 115

Nan Z, Bowen L, Huan L, Gang L, Rucong W, Quan H, Philbert M, Shan L, Yuguang Z, Riaz A, Mohammed IZA, Crispin P, Renjie D (2021) The potential co-benefits for health, economy and climate by substi-tuting raw coal with waste cooking oil as a winter heating fuel in rural households of northern China[J]. Environ Res **194**

Ning L (2013) Design considerations of a centralized load controller using thermostatically controlled appli-ances for continuous regulation reserves[J]. IEEE Trans Smart Grid 4(2):914–921

Qing X, Chao Z, Shuangshuang Z, Jian L, Dan G, Yongchun Z (2019) Research on short-term power load forecasting method based on machine learning [J]. Electric Measure Instrument 56(23):70–75

Shuai F, Kunqi J, Bingqing G, Limin J, Zhihua W, Guangyu H (2017) Collaborative optimal operation strategy for decentralized electric heating loads[J]. Automat Electric Power Systems 41(19):20–29

Weizhao X, Huan T, Min C (2020) Research on evaluation model of three-phase electric energy meter based on K-means++ algorithm[J]. Electric Measure Instrument **57**(17): 142–146

Yi T, Xiao H, Chaohai Z (2019) Power consumption modeling method of digital buildings based on physical-statistical model [J]. Distribut Utilizat **36**(10): 16–21, 29

Yi T, Rui G, Jianfeng D, Chenyi Z, Chaoming Z, Jie D (2021) Subsequent commutation failure prediction of HVDC by integrating physical-driven and model-driven methods[J]. Electric Power Construct **42**(05): 69–80

Yujie Z (2019) Reaearch on electric heating load adjust ability evaluation and cluster control strategy[D]. Northeast Electric Power University

Yulong Y, Tong W, Leiyang Z, Jinsong L, Yue H, Ruitong L (2020) Distributed electric heating load group modeling and standby optimization[J]. Electric Measure Instrument 57(02):81–87

Zhang Z, An J, Zhou X, Sun P, Rong C (2021) Wei Ling. Research on comprehensive benefit evaluation of electric heating based on AHP and TOPSIS method[J/OL]. Electrical Measure Instrument **1–7**: 12–27

Zhiqiang W, Shan W, Xinyue Z, Wenxia L, Qi G, Qifang C (2019) Load characteristics modeling of regional electric heating system considering difference of users response behaviors[J]. Automat Electric Power Systems 43(07):67–73

Zhongqi Z, Xiqiang C, Kaining S, Mao F, Jinsong Y (2021) Economic analysis of time shifting electric heating load under time-of-use pricing policy[J]. Shan-dong Electric Power **48**(03): 6–10

Zhongwei Z, Lei C, Xiliang C, Dalei K, Tianting S (2019) Survey of knowledge reasoning based on neural network[J]. Comput Eng Appl **55**(12): 8–19, 36

Chapter 10
Internet Use and Pro-environment Behavior: A Mediating Effect Analysis Based on Class Identity

Xuedong Liang and Jinghong Sun

Abstract In modern society, environmental problems are increasingly serious, the public can obtain environmental information through different channels and take measures accordingly, the Internet has become a significant source for everyone to take in environmental information. Based on the 2013 database of China General Social Survey, a theoretical model was established to empirically analyze the impact path of Internet use on pro-environment behavior with class identity as the mediating variables. The results show that Internet use plays an important role in pro-environment behavior, and it also indirectly affects pro-environment behavior through class identity.

Keywords Internet use · Class identity · Pro-environment behavior · The mediation effect

10.1 Introduction

Nowadays, urbanization and industrialization are accelerating, and the ecological environment is facing unprecedented challenge. Environmental issues affect people's health and life, and all of these environmental problems mainly rooted in human activities, it also suggests that the environmental problems existing at present can be improved if people can take some positive actions. In today's society, the Internet has become the trend of The Times, enabling the dissemination of all kinds of information to be more extensive. By virtue of its own "information source" function, the Internet can present the increasingly severe environmental pollution problem to the public, so that people gradually attach importance into the relationship between Internet use and pro-environment behavior. At present, scholars have conducted certain studies

X. Liang · J. Sun (✉)
Business School, Sichuan University, Chengdu 610000, Sichuan, China
e-mail: 2020225020090@stu.scu.edu.cn

X. Liang
Sichuan Haina Rendong Science and TechnologyCo.Ltd, Mianyang, China

G. Huang (ed.), *Proceedings of 2022 7th International Conference on Environmental Engineering and Sustainable Development (CEESD 2022)*, Environmental Science and Engineering, https://doi.org/10.1007/978-3-031-28193-8_10

on the relationship between the two. Lu Chuntian and Quan Xiaojuan concluded that the use of traditional media can strengthen people's trust in central and local governments, while the use of new media is on the contrary (Lu and Quan 2015). Adams et al. found that the use of new media such as the Internet is conducive to increasing people's cognition and understanding of environmental problems and risks (Adams and Gynnild 2013). Tang Feng et al. found that Internet use would reduce people's evaluation of satisfaction with government environmental governance (Tang et al. 2021). In view of previous studies, we believe that Internet use plays a crucial role in pro-environment behavior, and the study of the relationship between the two plays an important role in cultivating people to form a green and healthy lifestyle.

Summing up the previous research, scholars have obtained rich research results, but there are certain deficiencies. The current research mainly tests the linear correlation between research objects and pro-environment behaviors, in many cases, there may be mediating variables among variables. Lin Bing et al. found that environmental identity has an effect on environmental behavior (Lin and Liu 2014). Wang Xiaonan found that socioeconomic status is of vital importance for environmental behavior (Wang and Liu 2017). Therefore, based on CGSS2013 data and considering class identity as a mediator, this study constructed a model, which is conducive to explain how Internet use influence pro-environmental behavior.

10.2 Theoretical Basis and Research Hypothesis

10.2.1 Direct Mechanism

Since the reform and opening up, China's economy has grown rapidly. At the same time, environmental problems have become increasingly serious. In the era of digital economy, the continuous development of the Internet has promoted the progress of information and communication technology, people often get information through the Internet in their daily life, and a lot of information about the environment spread online can arouse people's emotional resonance and crisis awareness, and then form a positive pro-environment behavior. In order to keep the ratings, the network media will be more like report some negative news which can easily attract attention to the people who generally want to be able to in the shortest possible time to obtain the largest amount of information, thus producing a series of actions (Peng et al. 2019). People can through the use of the Internet to check some news on climate change, this is a kind of effective method to get environmental knowledge, which can let the public awareness that environment is closely related to their own interests. Based on the above discussion, Internet use is likely essential for promoting pro-environmental behavior among the public. The following hypotheses are proposed in this paper.

H1: Internet use has a direct and significant positive effect on pro-environmental behavior.

10.2.2 Indirect Mechanism

With the rapid increase of China's economy, social strata are becoming increasingly differentiated. At present, scholars have conducted extensive studies on the influencing factors of class identity. As a media communication tool, the Internet has a great impact on citizens' class identity, which profoundly affects users' psychological state and their feelings about the actual environment around them. Zhou Baohua found that the use of the Internet and mobile phones have an impact on social members' class identity (Zhou 2010). Different classes of people can have the information, and have their own opinion in platform (Wang and Wu 2014), the use of different types of media will make users form different culture class cognition, at the same time, some low objective class status user can express views on the Internet, get a lot of browsing, finally get information dissemination ability, and form new identities in the virtual space. In general, Internet use plays an important role in shaping personal class identity. Therefore, the following hypotheses are as follows in this paper.

H2: Internet use has a direct and significant positive effect on class identity.

The subjects of pro-environment behavior are people in different living environments, but the uneven distribution of resources promotes the emergence of social classes. In line with Maslow's hierarchy of needs theory, people's needs can be divided into multiple levels, including physiology, safety, self-realization, etc. When the lowest level of material needs are realized, the higher level of spiritual and cultural needs will have an incentive effect on individuals and guide human activities. Some scholars conducted analysis at the national level and found that people in developed countries pay more attention to environmental issues (Inglehart 1995). According to the concept of relative deprivation, people of lower class have a strong need for survival, and usually only pursue the guarantee of their own life, and they have a greater tolerance for environmental conditions. On the other hand, the upper class is more likely to experience comfortable living conditions, so they are more concerned about environmental issues. Different social strata lead to different demands, thus affecting pro-environment behaviors. Therefore, the following hypotheses are as follows in this paper.

H3: Class identity has a direct and significant positive effect on pro-environment behavior.

In the theory of innovation and diffusion, the upper class will use media adoption as a status symbol. According to Zhou Baohua's research, the use of new media is not only a kind of cultural capital, but also reflects the ability of economic capital. Therefore, the use of the Internet can reshape class (Zhou 2010). Compared with people at the bottom, people in the middle and upper classes are more sensitive to the environment and have higher requirements for living quality, so they are more likely to realize the importance of environmental issues. Through the use of the Internet, all strata will form a correct understanding of environmental risks, and increase the attention and understanding of environmental conditions. Through the use of the Internet, class identity can be improved, and then change their own needs

for the environment, and implement a series of pro-environment behaviors. Through the review of existing literature, it is found that Few articles take class identity as a mediating variable to discuss its mediating effect in the influence of Internet use on pro-environment behavior. Therefore, the following hypotheses are proposed in this paper.

H4: Class identity performs a mediating role between Internet use and pro-environment behavior.

10.3 Data, Variables and Models

10.3.1 Data Sources

The data in this paper are from the 2013 Database of China General Social Survey jointly conducted by Renmin University of China and Hong Kong University of Science and Technology. Jin Hengjiang etc. based on this database research the impact of media use on individual environmental behavior (Jin et al. 2013), Peng Yuan spring based on the database research analyzes the residents' health impact on environmental behavior (Peng and Qu 2010). And this paper studied the mediating factors of the correlation between Internet use and pro-environmental behavior on the basis of this database.

10.3.2 Variable

Dependent variable: pro-environment behavior. CGSS 2013 questionnaire measures pro-environmental behavior with 10 questions, the answer items are "never," "occasionally," and "often," which are assigned 1, 2, and 3.

Independent variable: Internet use. CGSS 2013 questionnaire measures this variable with 1 question, the answer items are "never", "rarely", "sometimes", "often" and "very often", and the five items are assigned 1, 2, 3, 4 and 5.

Intermediary variable: class identification. CGSS 2013 questionnaire measures class identity through one question, 10 points represent the top layer and 1 point represent the bottom layer.

Control variables. In this study, some demographic variables were added as control variables for statistical analysis, such as gender, age, total income and education level.

10.3.3 Model to Establish

This study refers to the unitary parallel multiple mediation model established by Liu and Ling (2009), and takes Internet use as the independent variable, class identity as the intermediary variable, and pro-environment behavior as the dependent variable to establish a parallel multiple mediation model. The regression equation is as follows:

$$PEB = a_0 + a_1 IU + a_2 Z_i + \varepsilon_1 \tag{10.1}$$

$$CI = b_0 + b_1 IU + b_2 Z_i + \varepsilon_2 \tag{10.2}$$

$$Y = c_0 + c_1 IU + c_2 CI + c_3 Zi + \varepsilon_3 \tag{10.3}$$

and a_1 is the total effect of IU on PEB, c_1 is the direct effect of IU on PEB, b_1c_2 is the mediating effect of CI on PEB, Z_i is a series of control variables, ε_1, ε_2 and ε_3 are random error terms, a_0, b_0 and c_0 are constants.

10.4 Empirical Results

10.4.1 Descriptive Statistics of Variables

See Table 1.

10.4.2 Common Method Deviation Test

Since the data source in this study is relatively single and self-statement is the only answer method, the relationship between variables is more susceptible to the influence of common method variance. To test common method deviation, this paper adopts Hamann's single factor test method. The output results get three factors with characteristic roots greater than 1. The first common factor can explain 35.324% of the total variance, which conforms to the requirement that the maximum variance extracted is less than 50% of the critical value of the total explanatory variance. Therefore, there is no serious common method deviation and the data can be analyzed statistically.

10.4.3 Correlation Analysis

According to the results of Table 10.2, There is a positive correlation between Internet use, class identity and pro-environment behavior. Internet use is positively correlated with pro-environment behavior ($R = 0.325$, $P < 0.01$). Internet use is positively correlation with class identity ($R = 0.173$, $P < 0.01$). Class identity is positively correlation with pro-environment behavior ($R = 0.166$, $P < 0.01$). Through the analysis, the correlation between variables is basically compliant with the hypothesis of this study.

Table 10.1 Descriptive statistics of variables

Variable	Variable definition	Maximum	Minimum	Average	Variance
IU	Frequency of Internet use	5.0	1.0	2.253	2.515
Age	The age of the residents surveyed	4	1	3.01	1.224
GI	The total income of the households surveyed	16.11809566	0.0953101798	9.334559087	14.645
Gender	The sex of the residents surveyed	2	1	1.5	0.25
EL	The education level of the residents surveyed	14	1	4.92	9.355
CI	The social class to which the residents surveyed identified themselves	10	1	4.32	2.813
PEB	The frequency of pro-environment behaviors of the surveyed residents	3	1	1.518	0.112

Table 10.2 Correlation analysis

	Age	GI	Gender	EL	IU	CI	PEB
Age	1						
GI	−0.055**	1					
Gender	−0.022*	−0.159**	1				
EL	−0.436**	0.187**	−0.119**	1			
IU	−0.631**	0.164**	−0.057**	0.645**	1		
CI	−0.077**	0.078**	0.030**	0.204**	0.173**	1	
PEB	−0.145**	0.135**	−0.01	0.405**	0.325**	0.166**	1

Note **,* respectively represents significant at the 1% and 5% levels

10.4.4 Regression Analysis

Multiple regression analysis of Internet use on pro-environment behavior. Model 3 is the regression model of the control variables of pro-environment behavior, and Model 4 is the regression model of pro-environment behavior with the addition of independent variables of Internet use. As can be seen from Table 10.4, in Model 4, Internet use has a significant positive impact on individual pro-environment behavior ($\beta = 0.037$, $P < 0.01$). The maximum VIF of each variable in the regression equation is 2.331, far less than 10, showing that there is no multicollinearity. Therefore, assume H1 is verified.

The mediating role of class identity in the relationship between Internet use and pro-environment behavior. Taking class identity as a dependent variable, Model 1.1 in Table 10.3 is the regression model of controlling variables on class identity, and Model 1.2 is the regression model of class identity with the addition of independent variables Internet use. As can be seen that Internet use has a marked positive impact on class identity ($\beta = 0.111$, $P < 0.01$). The maximum VIF of each variable in the regression equation is 2.331, far less than 10, indicating that there is no multicollinearity. Therefore, assume that H2 is verified. In Table 10.4, Model 5 is a regression model of individual pro-environment behavior with class identity as an independent variable. It can be shown that class identity has a significant positive influence on individual pro-environment behavior ($\beta = 0.016$, $P < 0.01$). The maximum VIF of each variable in the regression equation is 1.340, far less than 10, indicating that there is no multicollinearity. Therefore, hypothesis H3 is verified. Model 6 is the regression model of the pro-environment behavior after the addition of the mediating variable class identity on the basis of Model 4. It can be seen that the influence of Internet use on the pro-environment behavior ($\beta = 0.035$, $P < 0.01$) is lower than that of Model 4, but it still shows a significant positive effect. Class identity still had a significant positive influence on individual pro-environment behavior ($\beta = 0.015$, $P < 0.01$). The maximum VIF of each variable in the regression equation is 2.342, far less than 10, indicating that there is no multicollinearity. Therefore, hypothesis H4 is verified.

10.4.5 Robustness Test

Finally, bootstrap method was used to test robustness, and the Process program of SPSS software was used to further verify the mediating effect of class identity on the link between Internet use and pro-environment behavior. Table 10.5 indicates that the direct effect of independent variable Internet use on pro-environment behavior is 0.0345, accounting for 93.75% of the total effect. The indirect effect of the independent variable Internet use on the dependent variable pro-environment behavior through the intermediary variable class identity is 0.0016, accounting for 4.35% of the total effect, and the 95% confidence interval is [0.0011, 0.0023] (excluding zero),

Table 10.3 Regression test of Internet use and class identity

	Model 1.1	Model 1.2
Age	0.027	0.096**
GI	0.022**	0.019**
Gender	0.212**	0.214**
EL	0.115**	0.089**
IU		0.111*
R2	0.047	0.052
Adjusted R2	0.047	0.051
ΔR2		0.004
F	138.774	122.695
VIF (MAX)	1.294	2.331

Table 10.4 Regression test of pro-environment behavior

	Model 3	Model 4	Model 5	Model 6
Age	0.012**	0.035**	0.012**	0.034**
GI	0.006**	0.005**	0.006**	0.005**
Gender	0.034**	0.035**	0.031**	0.032**
EL	0.046**	0.037**	0.044**	0.036**
IU		0.037**		0.035**
CI			0.016*	0.015**
R2	0.171	0.184	0.177	0.189
Adjusted R2	0.171	0.184	0.177	0.189
ΔR2				
F	579.597	506.845	484.242	436.499
VIF (MAX)	1.294	2.331	1.34	2.342

Note VIF stands for variance inflation factor; *: $P < 0.05$, **: $P < 0.01$

indicating that class identity acts as the mediator in the relationship between Internet use and pro-environment behavior. This further supports hypothesis H4.

10.5 Conclusions

This study reveals the mechanism of the influence of Internet use on pro-environment behavior, and the introduction of class identity into the framework can help improve and promote the level of pro-environment behavior of individuals. It concluded that Internet use has a significant positive influence on individuals' pro-environment

Table 10.5 Mediating effects of Bootstrap test

The total effect of Internet use on pro-environment behaviour						
	Effect	S.E.	*t*	*p*	LLCI	ULCI
Intern use	0.0368	0.0027	13.3823	0	0.0314	0.0422
The direct effects of Internet use on pro-environment behaviour						
	Effect	S.E.	*t*	*p*	LLCI	ULCI
Intern use	0.0345	0.0027	12.5571	0	0.0291	0.0399
The indirect effects of Internet use on pro-environment behaviour						
	Effect	Boot SE		Boot LLCI	Boot ULCI	
Class identity	0.0016	0.0003		0.0011	0.0022	

behavior and class identity performs the function of an intermediary between Internet use behavior and environment.

Environmental pollution is a difficult problem that the whole society is facing. The whole people should participate in environmental protection. The practical implications of this study are as follows. First, the government has a duty-bound responsibility in environmental protection. The Internet is an important platform for people to express their opinions and obtain information. The government should make a prompt response and timely release environmental information through the Internet to ensure people's right to know about environmental conditions. Second, in the process of formulating and implementing environmental protection policies, government should consider the different needs of various social strata from various aspects and angles. For the citizens of higher social class, we should focus on cultivating people's awareness of environmental protection and environmental responsibility, and for individuals in low social class to enhance their class identity, appropriate material rewards and spiritual incentives can be given.

The research in this paper also has some limitations. First of all, this research data from China's largest and most comprehensive social investigation, but different countries have different cultural background, the way and purpose of Internet use has certain difference, the influence of the environmental behavior of kiss is also different, future research can expand the scope of sample. Second, we only found multiple mediating effects of class identity, and future research can further explore whether there are other mediating variables between Internet and pro-environment behavior.

Funding Resources

This paper was supported by the Fund (71871151).

References

Adams PC, Gynnild A (2013) Environmental messages in online media: The role of place. Environ Commun: A J Nature Culture 7(1):113–130

Inglehart, R (1995) Public support for environmental protection: objective problems and subjective values in 43 societies. PS: Polit Sci Politics 28(1):57

Jin H J, Yu L H, Zhang G L. The influence of media use on individual environmental protection behavior – Empirical research based on CGSS 2013 data. J Res (02):46–55+148

Lin B, Liu LB (2014) Environmental identity: a new perspective of foreign environmental sociology research. J Jilin Normal Univ (Humanities & Social Science Editionn), 42(05):77–82

Liu SS, Ling WQ (2009) Multiple mediation models and their applications. J Psychol Sci 32(02):433-435+407

Lu CT, Quan XJ. (2015) Media Use and Trust in Government: Based on the Analysis of CGSS2010 Data. Chinese J Journal Commun 37(05):66–80

Peng DY, Li YC, Li CQ (2019) The influence of internet use on environmental attitude and literacy. Finance Economics 08:97–109

Peng YC, Qu SY. Impact of residents' health status on environmental behavior: an analysis based on CGSS2013. J Nanjing Tech Univ (Social Science Edition), 19(04):41-51+115

Tang F, Liu XL, Li B, Du XW (2021) Government's environmental image, Internet use and public satisfaction with environmental Governance[J]. China Popul Resour Environ 31(7):107–115

Wang XN, Liu L (2017) Multilevel analysis of public environmental behaviour intention-based on 2013CSS dataset. J Jishou Univer (Social Sciences), 38(1):80–90

Wang W B, Wu H L (2014) Internet use and its impact on social identity: an empirical analysis based on CGSS2010 data[J]. Jianghai Acad J (05):92–100

Zhou BH (2010) New media use and subjective class identification: theoretical interpretation and empirical test. J Res 2:29–40

Chapter 11
How Does Intergovernmental Environmental Cooperation Affect Regional Environmental Pollution Control?

Huixu Li, Xianwen Wang, and Lanjian Liu

Abstract Collaboration is already widely used to solve regional pollution problems, but the effectiveness of cooperation and its impact on environmental pollution need to be more fully accounted for. This paper establishes a environmental impact analysis framework of intergovernmental environmental cooperation, we explores the influence of intergovernmental environmental cooperation on environmental pollution and its action path by using fact-based intercity agreements data from the Yangtze River Delta region in China. We find that increasing the level of intergovernmental environmental cooperation can significantly reduce pollution emissions. The optimization of industrial structure, green technological innovation, and fiscal expenditure on environmental protection all play a mediating role in this process. This study contributes to the understanding of the environmental impact of intergovernmental cooperation and its process of action. Additionally, these results have both theoretical and practical implications for providing more ideas for reducing pollution emissions.

Keywords Intergovernmental cooperation · Environmental pollution · Mediated effect

11.1 Introduction

In recent decades, due to globalization and regionalization, the cooperation among public administrations is needed to achieve holistic governance (Youm and Feiock 2019). However, when it comes to environmental issues, the impact of cooperation has not been fully argued. Thus, it is crucial to explore the relationship and mechanism between cooperation and environmental impacts for managers to make

H. Li (✉) · L. Liu
Chang'an University, Xi'an, Shaanxi 710064, China
e-mail: Lihuixu11@163.com

X. Wang
Dalian University of Technology, Dalian, Liaoning 116024, China

G. Huang (ed.), *Proceedings of 2022 7th International Conference on Environmental Engineering and Sustainable Development (CEESD 2022)*, Environmental Science and Engineering, https://doi.org/10.1007/978-3-031-28193-8_11

rational choices. Research has begun to consider the environmental results of cooperative behavior (Yeung et al. 2021), but limited by the objective quantification of the level of cooperation, there is a lack of "fact" based environmental cooperation performance evaluation, and the mechanisms by which collaboration affects the environment remain largely unanswered.

Noting these gaps, this study constructs a theoretical framework for the environmental impact of intergovernmental cooperation, and establishes a model of cooperation degree by using various environmental arrangements from the Yangtze River Delta (YRD) city cluster in China to explore the impact of interlocal cooperation on pollution and the operating mechanism.

11.2 Hypotheses

11.2.1 Intergovernmental Environmental Cooperation

Public-Public collaborative activity is often established by entering into an informal or formal agreement (Yi et al. 2018). However, the agreements have different legal effect, which will affect the cooperative performance. Therefore, we believe that, under the premise of considering the effectiveness, the higher the level of cooperation, the more likely the local governments will be to translate their contractual environmental governance responsibilities into practical actions. Accordingly, we propose Hypothesis 1.

> Hypothesis 1: Improving the level of intergovernmental cooperation is conducive to improving the environmental pollution situation.

11.2.2 Influence Path

Industrial structure optimization. Optimization of industrial structure can effectively reduce pollution (Oosterhaven and Broersma 2007). The binding nature of environmental agreements forces local governments to accelerate the elimination of outdated production capacity, to reduce the share of secondary industries. Thus, we anticipate,

> Hypothesis 2a: Intergovernmental cooperation will control pollution emissions by optimizing industrial structure.

Green technology innovation. Under the constraint of cooperation, local governments may encourage enterprises to carry out green technology innovation to reduce environmental pollution. Thus, we anticipate,

Hypothesis 2b: intergovernmental cooperation will control pollution emissions through green technology innovation.

Financial expenditure on environmental protection. Environmental protection spending by the government has a positive effect on controlling pollution (Tang et al. 2014). The agreements can increase the incentive for local governments to increase investment in environmental protection. Accordingly, Hypothesis 2c is proposed.

Hypothesis 2c: Intergovernmental cooperation help to reduce pollution emissions by increasing fiscal spending on environmental protection.

11.3 Variables and Models

11.3.1 Variables

The level of intergovernmental environmental cooperation. Based on previous studies we believe that the effectiveness of the cooperation stems from the credibility of the contract signer and the legal validity of the contract form (Du et al. 2021).

In terms of the administrative level of the cooperation subject, the scoring table is constructed as shown in Table 11.1.

Regarding the forms of cooperation, we classify the environmental collective action in YRD urban agglomeration into eight categories, and, based on their legal effect, we build a scoring table, as shown in Table 11.2.

After collecting the agreements, we calculate as follows:

$$\mathrm{COS}_i = \sum_{j=1}^{n} \alpha \cdot \beta \cdot r_{i,j} \tag{11.1}$$

In Eq. (11.1), COS_i is the level of environmental cooperation of city i, α and β are the score coefficients of the contracted subject and the form of agreement, respectively. r is the score of city i participation in the environmental collaboration event J (r is 1 or 0), and n is the total number of all environmental cooperation events in the city cluster.

Table 11.1 Scoring table of administrative levels of government subjects

	Prefecture-level cities	District	Township
Prefecture-level cities	3		
District	3	2	
Township	2	2	1

Table 11.2 Intergovernmental agreement form rating scale

Informal agreements	Score	Formal agreements	Score
Investigation	1	Declaration	3
Forum	1.5	Memorandum	4
Meeting	2	Plan (Planning, guidance)	5
		Framework Agreement	6
		Cooperation Agreement	7

Environmental pollution. We use per capita sulfur dioxide emissions as the proxy variable of environmental pollution (ENP) (Wang and Zhou 2021).

Mediation variables. We use the proportion of tertiary industry output in GDP to represent the optimization of industrial structure (IND). The number of green patent applications per 10,000 people represents progress in green technology (TEC). The proportion of environmental expenditure to public finance expenditure per capita represents the government's investment in environmental protection (FIN).

Control variables. We use the population per square meter (POD), the proportion of foreign direct investment in GDP (FOR), per capita GDP (ECO) and the proportion of urban population in total population (URB) to control the differences in population size, opening up, economic development and urbanization among cities.

11.3.2 Models

The mediating effect model is constructed as following:

$$\ln\mathrm{ENP}_{i,t} = \alpha_0 + \alpha_1 \ln\mathrm{COS}_{i,t} + \alpha_2 \ln\mathrm{CV}_{i,t} + u_i + \lambda_i + \varepsilon_{i,t} \tag{11.2}$$

$$\ln\mathrm{M}_{i,t} = \beta_0 + \beta_1 \ln\mathrm{COS}_{i,t} + \beta_2 \ln\mathrm{CV}_{i,t} + u_i + \lambda_i + \varepsilon_{i,t} \tag{11.3}$$

$$\ln\mathrm{ENP}_{i,t} = \gamma_0 + \gamma_1 \ln\mathrm{COS}_{i,t} + \gamma_2 \ln\mathrm{M}_{i,t} + \gamma_3 \ln\mathrm{CV}_{i,t} + u_i + \lambda_i + \varepsilon_{i,t} \tag{11.4}$$

In the equation, $\ln\mathrm{ENP}_{i,t}$ represents environmental pollution; $\ln\mathrm{COS}_{i,t}$ is level of intergovernmental environmental cooperation, $\ln\mathrm{CV}_{i,t}$ is control variables and $\ln\mathrm{M}_{i,t}$ denotes the intermediate variables, all variables are in logarithmic form.

11.3.3 Data Source

This research uses three main sources of agreements data: First, we collected intergovernmental agreements from *China Digital Newspaper*, as the *Digital Newspaper database* uses Chinese as the primary language, we used *qianding* (signing), *kaocha* (inspection), *jiaoliu* (exchange), *gongjian* (co-construction), *ronghe* (integration), *hezuo* (cooperation), *xiezuo* (collaboration), *shengtai* (ecology), *huanjing* (environment), *shuiwuran* (water pollution), *kongqi* (air), *xieyi* (agreement), *huiyi* (conference), *luntan* (forum), and *diaoyan* (investigation) as keywords. All keywords were manually screened after full-text retrieval. Second, we collect agreements from government websites and eco-environmental bureaus in cities. Third, using the yearbook data to supplement the information. Finally, we obtained 383 intergovernmental environmental agreements from 2010 to 2019 for 27 cities in YRD city cluster through the three specified ways.

The data of green technology patents are obtained from the *China Patent Publication Notice System of the State Intellectual Property Office*, and the remainder of the data on intermediary variables, environmental pollution, and control variables are obtained from the *China Urban Statistical Yearbook*, *China Urban and Rural Construction Statistical Yearbook*, as well as the statistical yearbooks of each city.

11.4 Empirical Results

11.4.1 Basic Regression

Table 11.3 reports the results of cooperation on environmental pollution. Model 2 shows the results with the inclusion of control variables. As expected, the effect of intergovernmental cooperation on environmental pollution is significant in both Model 1 and Model 2, indicating that increasing the level of cooperation among local governments can effectively reduce pollution.

11.4.2 Mediating Effect Model

The result in Table 11.4 indicates the influence paths of cooperation on environmental pollution.

In Table 11.4, the column (1)–(3) show the estimated results of the level of intergovernmental environmental cooperation on industrial structure, green technology, and fiscal expenditure on environmental protection, respectively. The column (4) reports the direct effect of the level of interlocal environmental cooperation on pollution.

Table 11.3 Impacts of intergovernmental cooperation on environmental pollution

	Model 1			Model 2		
	Coef.	st.err	T-value	Coef.	st.err	T-value
lnCOS	−0.294***	0.061	−4.77	−0.246***	0.051	−4.80
lnPOD				−3.239***	1.142	−2.84
lnURB				−6.515***	0.820	−7.94
lnFOR				0.363***	0.136	2.67
lnECO				3.755***	0.640	5.86
Cons_	5.000***	0.201	24.85	−17.496**	7.473	−2.34
R^2	0.099			0.400		

Notes $^{***}p < 0.01$, $^{**}p < 0.05$, $^{*}p < 0.1$

Table 11.4 Mediating effects of intergovernmental cooperation on environmental pollution

	(1)	(2)	(3)	(4)
	lnIND	lnTEC	lnFIN	lnENP
lnCOS		0.060**	0.063**	−0.155***
lnIND				−2.288***
lnTEC0				−0.612***
lnFIN				−0.326***
Cons_	5.759***	−4.178	1.892	−7.746
Control variables	Yes	Yes	Yes	Yes
R^2	0.559	0.757	0.167	0.625

Notes $^{***}p < 0.01$, $^{**}p < 0.05$, $^{*}p < 0.1$

The results indicate there are three impact paths of cooperation on environmental pollution: industrial structure optimization, green technological progress, and public financial support. The overall impact of intergovernmental environmental cooperation level on environmental pollution is 0.246%, and the direct effect is 0.16%.

11.5 Conclusions

Improving the level of intergovernmental cooperation helps to curb pollution. According to the two-stage theory of intergovernmental cooperation, on the one hand, we can build more environmental cooperation links by improving the willingness of local governments to participate in cooperation. On the other hand, the establishment of more formal cooperation mechanisms among local governments can also improve the governance level of participating agents and can curb environmental pollution. In

addition, the inter-municipal environmental cooperation curb environmental pollution by optimizing industrial structure and gradually closing down outdated production facilities. Cooperation among local governments promotes the improvement of the level of green technology, thereby reducing pollutant emissions. Additionally, cooperation encourages local governments to increase public expenditure on environmental protection to control environmental pollution.

References

Du H, Guo Y, Lin Z, Qiu Y, Xiao X (2021) Effects of the joint prevention and control of atmospheric pollution policy on air pollutants-a quantitative analysis of Chinese policy texts. J Environ Manag 300:113721

Oosterhaven J, Broersma L (2007) Sector structure and cluster economies: a decomposition of regional labour productivity. Reg Stud 41(5):639–659

Tang E, Liu F, Zhang J, Yu J (2014) A model to analyze the environmental policy of resource reallocation and pollution control based on firms' heterogeneity. Resour Policy 39:88–91

Wang X, Zhou D (2021) Spatial agglomeration and driving factors of environmental pollution: a spatial analysis. J Clean Prod 279:123839

Yeung DW, Zhang Y, Bai H, Islam SM (2021) Collaborative environmental management for transboundary air pollution problems: a differential levies game. J Ind Manag Optim 17(2):517–531

Yi H, Suo L, Shen R, Zhang J, Ramaswami A, Feiock RC (2018) Regional governance and institutional collective action for environmental sustainability. Public Adm Rev 78(4):556–566

Youm J, Feiock RC (2019) Interlocal collaboration and local climate protection. Local Gov Stud 45(6):777–802

Chapter 12
Research on Optimal Scheduling Model of Direct Supply Electric Vehicle Charging Station of Distributed Photovoltaic Power Station

Linjing Yan, Nan Wang, and Xiangming Kong

Abstract Distributed photovoltaic power generation is an effective way to use renewable energy, direct electric vehicle charging not only alleviates the pressure of the State Grid under the current situation of the popularization of new energy vehicles, but also avoids the energy loss caused by transit, so it has become a real-time energy production and marketing mode. According to the characteristics and laws of distributed photovoltaic power generation, this paper studies the optimal scheduling of direct supply electric vehicles. On the premise of ensuring normal operation, according to the actual operation situation, taking the operation cost of electric vehicle charging station as the objective function, the optimal scheduling mathematical model of electric vehicle charging station directly supplied by distributed photovoltaic power station is established. Combined with the idea of integration, the method and steps of using genetic algorithm to solve real-time adjustment scheduling are designed, the problem of real-time distribution scheme of electric vehicle charging station directly supplied by distributed photovoltaic power station is reasonably solved. This algorithm is simple and easy to implement, and has good scalability. It is suitable for rapid migration and has strong practicability. It provides theoretical basis and technical support for the operation of distributed photovoltaic charging stations in cities.

Keywords Scheduling model · Distributed photovoltaic power station · Genetic algorithm

L. Yan · N. Wang · X. Kong (✉)
Beijing Polytechnic, Beijing 100176, China
e-mail: 101582@bpi.edu.cn

L. Yan
e-mail: 101457@bpi.edu.cn

N. Wang
e-mail: 101177@bpi.edu.cn

G. Huang (ed.), *Proceedings of 2022 7th International Conference on Environmental Engineering and Sustainable Development (CEESD 2022)*, Environmental Science and Engineering, https://doi.org/10.1007/978-3-031-28193-8_12

12.1 Introduction

With the rapid development of electric vehicles in China, especially in Beijing, Shanghai and other big cities, the number of electric vehicles has increased significantly, exposing new contradictions in the process of energy conservation and emission reduction. On the one hand, the power generation mode dominated by coal power conflicts with the goal of "zero pollution" of electric vehicles. On the other hand, the sharp rise in power consumption has also brought great pressure to the State Grid. The development, allocation and utilization of renewable energy has become an effective way to solve the current contradiction (Li et al. 2009; Wei 2010; Locment et al. 2010).

According to the regional centralized characteristics of electric vehicle charging stations, the development of distributed photovoltaic power stations as the charging source of electric vehicles is a practical, clean and environment-friendly measure. At present, many countries and regions have carried out demonstration projects related to distributed photovoltaic power generation. Distributed photovoltaic power generation is also being promoted in rural areas of China to subsidize households and push to the power grid (Xiangning et al. 2013). Although the distributed photovoltaic power generation technology has been relatively mature, in the urban environment, the capacity configuration and optimal scheduling of distributed photovoltaic power stations directly charging electric vehicles still need to be further studied. In order to realize the instant charging at the peak of power generation and reduce the circulating power of energy storage; Reasonable distribution of peak power consumption, good user protection and analysis of periodic data to optimize the dispatching of charging sources and reduce the load peak valley difference.

12.2 Operation Management and Strategy of Distributed Photovoltaic Charging Station

In short, the distributed photovoltaic charging station takes the energy obtained from photovoltaic power generation as the charging source of electric vehicles. However, due to the volatility and intermittency of photovoltaic power generation, it also needs to be equipped with an energy storage system with a certain capacity. Therefore, compared with conventional charging stations, distributed photovoltaic charging stations need to be equipped with photovoltaic power generation system, energy storage system, AC distribution network and required AC converters and converters. Its operation principle can be summarized as the following three charging methods or their combination: photovoltaic power generation is directly used for electric vehicle charging; The energy of photovoltaic power generation is stored in the energy storage system and then used for electric vehicle charging; The state grid directly charges electric vehicles.

In terms of operation strategy, first of all, ensure sufficient supply; Secondly, ensure the stability of distribution network, that is, avoid excessive peak valley difference of load; Finally, the economic benefit of the charging station is optimized. Taking one day as a time cycle, according to the mobilization and demobilization time of N vehicles, the system allocates the charging source and charging time according to the photovoltaic power generation and step price.

12.3 Analysis of Distributed Photovoltaic DC Output Power

Beijing is located in the middle latitudes of the northern hemisphere, with four distinct seasons and obvious regularity of solar intensity. The monthly total radiation generally presents a parabolic trend. From January, the monthly total radiation begins to increase, and increases the fastest from March to May. May and June are the highest values of the whole year, and begin to decline after June. Since July is the rainy season, the monthly total radiation decreases rapidly, followed by September to November, and December is the lowest value of the whole year. The monthly radiation data of a certain area in Beijing in a certain year are shown in Table 12.1 (kcal/cm^2), and the scatter diagram is shown in Fig. 12.1.

According to the research, the DC output power of photovoltaic power generation is directly proportional to the amount of solar radiation, but has nothing to do with the ambient temperature and other conditions.

Similarly, combined with the specific location of a distributed photovoltaic power station and the solar radiation under different meteorological conditions, the binary function with date and meteorological conditions as independent variables and solar radiation as dependent variables can be fitted to obtain the DC output power function.

12.4 Optimal Dispatching Model and Solution of Distributed Photovoltaic Power Station

12.4.1 Objective Function

According to the actual operation, on the premise of ensuring that the optimal dispatching scheme is not changed, this paper takes the electricity charge of distributed photovoltaic power generation as the benchmark, and the charging cost comes from the power purchase of the power grid, that is, the lowest power purchase cost of the power grid is the objective function.

The charging station purchases electricity from the power grid using the time of use price, and divides 24 h into three sections according to the peak and valley characteristics of the load, as shown in Table 12.2 (Xinyi et al. 2014).

Table 12.1 Monthly radiation data of a district in Beijing

January	February	March	April	May	June	July	August	September	October	November	December
6.4	7.8	11.6	12.9	15.7	15.5	12.8	12.2	11.3	9.0	6.1	5.6

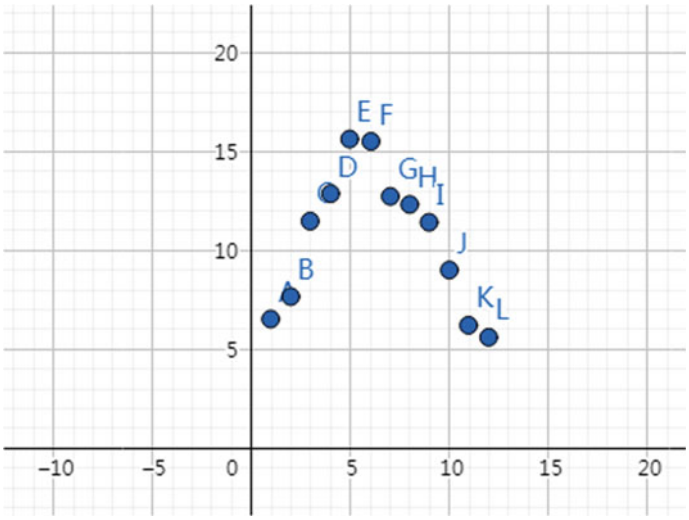

Fig. 12.1 Scatter diagram of monthly radiation in an area of Beijing

Table 12.2 Time of use tariff for power purchase of power grid

Time interval	Electricity price I (yuan/kWh)
Peak period (8:00–12:00, 17:00–21:00)	0.869 (I_1)
Peacetime period (12:00–17:00, 21:00–0:00)	0.365 (I_2)
Valley period (12:00–8:00)	0.687 (I_3)

According to the electricity price of the above periods, according to the power demand, the power purchase cost of the power grid is

$$C = I_1 \cdot q_1 + I_2 \cdot q_2 + I_3 \cdot q_3 \tag{12.1}$$

where q_1, q_2, q_3 is the electricity consumption in each period.

In the actual operation process, the charging scheme needs to be optimized in real time according to photovoltaic power generation and automobile power consumption.

Since the DC output power of photovoltaic power generation is directly proportional to the amount of solar radiation, the prediction function of daily DC output power can be obtained by fitting and analyzing the historical data in combination with meteorological information $p(t)$, then the power generation is predicted in $t_1 \sim t_2$ time period

$$E = \int_{t_1}^{t_2} p(t)dt \tag{12.2}$$

If $t_1 \sim t_2$ time period is set, the power storage consumption is D and the power demand of the vehicle is W, it can be divided into the following situations:

If $E + D \geq W$, continue to increase energy storage and power purchase fee $C = 0$;

If $E + D < W$, the power grid power purchase cost will be incurred,

$$C = \sum_{i=1}^{3} a \Delta t_i I_i \tag{12.3}$$

Among them, a is the output power of the power grid, Δt_i is the charging time in the i th time period, and I_i is the electricity price in the i th time period.

Therefore, the objective function is:

$$\min C = \sum_{i=1}^{3} a \Delta t_i I_i \tag{12.4}$$

Constraints:

$$W - E - D \geq \sum_{i=1}^{3} a \Delta t_i \tag{12.5}$$

12.4.2 Solution Method

Collect the charging demand information of all vehicles when the k-th vehicle enters the site. The charging power distribution results of each vehicle are expressed in -1, $+1$ and 00 respectively, which can be distributed according to the time period of segmented pricing, as shown in Table 12.3.

Combined with the coding design of genetic algorithm, assuming that the charging mode is not changed every half an hour, Then the charging distribution results can be divided into half an hour according to the time period of segmented pricing. For example, the charging power distribution result of the k-th vehicle can be designed as follows: $\underbrace{00 + 1 + 1 - 1 \ldots 00}_{96\,\text{bits}}$, every two of them are one cell, if the distribution result is photovoltaic charging, it will display $+1$; if the distribution result is grid

Table 12.3 Charging distribution scheme

Vehicle	Peak period 18:00–12:00			Peacetime period 1 12:00–17:00			Peak period 2 17:00–21:00			Peacetime period 2 21:00–24:00			Valley period 0:00–8:00		
	−1	+1	00	−1	+1	00	−1	+1	00	−1	+1	00	−1	+1	00
1															
⋮															
k															

charging, it will display −1; if not charging, it will display 00. The first 16 bits are a unit, followed by 20 bits, 16 bits, 12 bits and 32 bits. Then the charging allocation scheme of k vehicles generates a matrix of k rows and 48 columns.

- Step 1: construct chromosome and generate initial population

According to the charging distribution scheme, the subject adopts decimal system for chromosome coding, and the representation of chromosome adopts matrix form:

$$X_{k\times 48} = \begin{pmatrix} x_{11} & x_{12} & \cdots & x_{1,48} \\ x_{21} & x_{22} & \cdots & x_{2,48} \\ \vdots & \vdots & \ddots & \vdots \\ x_{k1} & x_{k2} & \cdots & x_{k,48} \end{pmatrix} \tag{12.6}$$

Each element in the matrix is based on the charging distribution scheme every half an hour from 8:00 a.m. to 8:00 the next day, the row vector represents the charging allocation scheme of each vehicle, after determining the element values in the matrix, the general charging distribution scheme for the k-th vehicle is determined.

We use the following rules to generate the initial population: ① The parking time period of each vehicle shall be divided according to the time period specified by the chromosome. If it is less than half an hour, it shall be automatically assigned as power grid charging, with a value of −1 and no charging time period of 00; ② Calculate the sum of $m_1 = \sum_{j=1}^{48}\sum_{i=1}^{k}\left|x_{ij}\right|$ after the initial assignment and the number of unassigned time periods m_2, Calculate the total power generation of distributed photovoltaic power generation in the current parking period, and convert it into the total charging time according to the power (converted into the number of charging time periods n in half an hour); ③ According to an order in the matrix, the values of the elements in the matrix are determined one by one, and a chromosome is generated. The method is to randomly assign −1 or +1 to the unassigned element, At this time, $\sum_{j=1}^{48}\sum_{i=1}^{k}\left|x_{ij}\right| - m_1 = m_2$ is satisfied, And extract the number of time periods n_1 assigned with value +1, And meet $n_1 \le n$; ④ Cycle according to the above method until the number of initial population is reached. To ensure population diversity, we can also generate several chromosomes in line order (changing the position of the starting line by line or interlaced exchange). Several chromosomes are also produced in the order of columns, the initial population is generated when a number of chromosomes are produced in diagonal order in both directions and the number of the initial population is reached.

- Step 2: determine the fitness function

Because the fitness function requires the maximum, the fitness function is determined as $C_l = \frac{1}{C(k)}$.Where $C(k)$ is the objective function, and the maximum value of fitness function is the optimal scheme.

- Step 3: natural selection

The selection is made according to the proportion of adaptive values, and the elite retention strategy is adopted:L chromosomes in each generation population are arranged in descending order according to the fitness value C_l ($l = 1, 2, \ldots, L$), and the first 10 chromosomes are selected directly into the next generation population. $L - 10$ chromosomes are generated by the chromosome roulette of the previous generation population. In this way, the best ones can survive to the next generation. It can also avoid the huge difference of selection opportunities caused by different fitness values between individuals, maintain the diversity of individuals in the next generation population, and effectively improve the convergence speed of the algorithm.

- Step 4: chromosome cross recombination

Select individuals according to probability p_c for multi-point crossing, in this paper, the crossover rate is set as $p_c = 0.4$, Since the element exchange of $x_{i1} \sim x_{i8}(i = 1, 2, \ldots k)$, $x_{i,9} \sim x_{i,18}(i = 1, 2, \ldots k)$, $x_{i,19} \sim x_{i,26}(i = 1, 2, \ldots k)$, $x_{i,27} \sim x_{i,32}(i = 1, 2, \ldots k)$ and $x_{i,33} \sim x_{i,48}(i = 1, 2, \ldots k)$ in the distribution scheme does not affect the fitness value, the method of crossing between different sections is designed. After proper adjustment, the fitness function value of each chromosome of the new generation is calculated, and the fitness function value of the mother is compared, and the one with the larger function value of the two chromosomes is selected to enter the next generation.

- Step 5: variation

The new population created by the crossing, special mutation strategies should also be adopted to mutate the chromosome with the mutation rate $p_m = 0.02$, the specific operation process is as follows:

Find an element from the element assigned with -1 by generating a random number, and mutate the element into $+1$, verify the constraint conditions. The number of mutations should not exceed 10.

- Step 6: judge the conditions for stopping evolution

In the algorithm design, the reasonable design of each parameter is an important factor for success. Crossover rate and mutation rate according to the design in this paper, we set for 200 largest evolution algebra, operation is as follows: if the iterative algebra is 200, then stop the evolution, select the best chromosome as a charging scheme, or for 50 generations equals the best fitness function value of the chromosome is terminated, output the optimal chromosome as the charging scheme.

12.5 Conclusion

This paper analyzes the generation characteristics and laws of distributed photovoltaic power stations, taking the lowest operation cost of electric vehicle charging station as the objective function, the optimal dispatching mathematical model of

direct supply electric vehicle charging station of distributed photovoltaic power station is established. In solving the model, the integration idea is combined with genetic algorithm, and a real-time optimal scheduling algorithm is designed to reasonably solve the real-time scheduling problem of direct supply electric vehicle charging station of distributed photovoltaic power station. In practical application, the parameters and data involved in this algorithm are easy to extract, the programming steps are universal and simple, can realize rapid migration, and has strong practicability.

References

Li X, Lopes LAC, Williamson SS (2009) On the suitability of plug-in hybrid electric vehicle (PHEV) charging infrastructures based on wind and solar energy. In: IEEE power & energy society general meeting, PES'09, pp 1–8

Locment F, Sechilariu M, Forgez C (2010) Electric vehicle charging system with PV grid-connected configuration. In: 2010 IEEE vehicle power and propulsion conference (VPPC), pp 1–6

Wei F (2010) Electric car charging station configured with 10 kW photovoltaic power generation system. Electr Eng 10:94–96

Xiangning X, Zheng C, Nian L (2013) Integrated mode and key issues of renewable energy sources and electric vehicles' charging and discharging facilities in microgrid. Trans China Electrotechn Soc 28(2):1–14

Xinyi Lu, Nian L, Zheng C, Jianhua Z, Xiangning X (2014) Multi-objective optimal scheduling for PV-assisted charging station of electric vehicles. Trans China Electrotechn Soc 29(8):46–56

Chapter 13
Low Carbon Economy Optimal Dispatching Strategy for a Power System Based on GCN Classification

Changjun Li, Xin Yin, Hongjun Zhao, Xiujun Li, Hao Shen, and Ling Qi

Abstract In the context of the "dual carbon" goal, the optimization strategy based on carbon transaction costs is considered in power system operation. Firstly, the equipment modeling is carried out and different generators are classified according to their carbon emissions based on the graph convolutional network. Then, an exponential efficiency economic function of carbon transaction cost is established. Thus, a comprehensive economical optimization strategy is constructed. Finally, various scenarios are simulated to show the low carbon dispatching effectiveness.

Keywords Carbon trading · Graph convolutional networks · Exponential efficiency economic functions · Economic optimization

13.1 Introduction

The research about the optimization of electrical and thermal coordination in power systems focuses on economic dispatch. Wang et al. (2020) takes into account the electro-thermal coupling characteristics into the IES to establish a complete DR mechanism, which greatly improves the economics of system operation. Fanga et al. (2019) considers temperature losses in the system and uses the heat storage properties of DHN to establish an optimal scheduling model, which greatly improves its economy compared to the traditional scheduling model. Fulu and Zhou (2019) proposes a model for electricity-gas-heat integrated energy systems that participate in multiple markets while considering market benefits and operating costs, and the results show that the maximization of comprehensive benefits can be achieved through system coordination. Liu et al. (2020) takes into account the delayed nature of the heating system as well as the complex optimization problems into its electric

C. Li · X. Yin · H. Zhao · X. Li
State Grid Xinjiang Electric Power Co. Ltd., Urumqi 830002, China

H. Shen (✉) · L. Qi
Nanjing University of Posts and Telecommunications, Nanjing 210023, China
e-mail: 1129744104@qq.com

G. Huang (ed.), *Proceedings of 2022 7th International Conference on Environmental Engineering and Sustainable Development (CEESD 2022)*, Environmental Science and Engineering, https://doi.org/10.1007/978-3-031-28193-8_13

heat dispatch model and proposes to operate the electric boiler in combination with the heat storage tank to greatly reduce its operating costs.

Among the many measures to reduce carbon emissions, carbon trading is one of the more effective (Xiang et al. 2021). Wang and Wang (2019) establishes a model of the electricity-heat-natural gas coupling system, taking the stepped carbon trading mechanism into account in the economic dispatch model to reduce a small number of carbon emissions. Zhang (2020) uses the dispatchable value of multiple loads of electricity, heat, and gas, and considers the carbon trading mechanism with integrated energy service. The carbon scheduling model has greatly improved the low-carbon nature of the system. Cui (2021) by modeling P2G operations and carbon trading mechanisms, carbon trading costs are taken into account in the objective function, which not only optimizes economic costs but also reduces carbon emissions.

In summary, most of the current studies on carbon trading mechanisms have failed to consider the reward and punishment mechanism, and there are certain shortcomings. To this end, this paper proposes a stepped carbon trading mechanism with reward and penalty coefficients based on graph convolution network classification. The rationality of the optimization strategy is verified by comparing different typical scenarios.

13.2 Optimization Model of Electric-Gas-Heat Equipment

13.2.1 Basic Structure of Electric-Gas-Heat Equipment

The structure of the electric-gas-heat equipment system in the power system is presented. The system is made up of energy generator sets (including wind generator sets and photovoltaic generator sets), carbon capture devices, power-to-gas devices (P2G), gas turbines, electric heating boilers, heat storage tanks, and various energy loads (electricity load, heat load, and air load). Among them, wind turbines and photovoltaic units are linked to the grid to provide electrical energy to the electricity load, and the waste heat generated in the power generation of the gas turbine could be used to meet the heat load demand. At the same time, the system is linked to the external natural gas network and power grid, and the natural gas energy and electric energy can be achieved from the outside and supplied to the gas and electricity loads.

A carbon capture device (CCS) is to capture and collect CO_2 produced by the operation of various large power plants so as not to be directly discharged into the atmosphere. Carbon capture technology has greatly improved the utilization efficiency of carbon dioxide and contributed to a low-carbon environment to a certain extent. Combine carbon capture device with P2G equipment and supply CO_2 captured

by CCS as raw material to P2G device. P2G plants use their carbon capture capabilities to improve the economics of storing CO_2 while also increasing the use of waste wind and light.

1. The model of the gas turbine

The system distributes electrical energy to the electricity load, P2G device, and carbon capture device. The carbon capture device captures the CO_2 emitted by the gas turbine and part of the gas load to provide carbon raw materials for the P2G device. Electrolysis inside the P2G device produces hydrogen and CO_2 methanation, and Re-flow the produced methane into the natural gas pipeline. The gas turbine converts gas energy into electrical energy and heat energy. The complete combustion of natural gas to generate thermal power is formulated as follows.

$$G_t^{GT} = \frac{\rho_G L_G}{\Delta t} V_t^{GT} \tag{13.1}$$

where t is the period time, G_t^{GT} is the total thermal power that the gas turbine use the natural gas at the moment t, ρ_G is the density of natural gas, L_G is the low calorific value of natural gas, V_t^{GT} is the natural gas consumption volume in the period t, Δt is the step.

Then the total thermal power of the gas turbine is expressed as:

$$\eta_t^{GT} G_t^{GT} = \frac{\eta_t^{GT} \rho_G L_G}{\Delta t} V_t^{GT} = \eta_t^{DGT} P_t^{GT} + H_t^{GT} \tag{13.2}$$

where η_t^{GT} is the total thermal efficiency of the gas turbine, P_t^{GT} is the power generated by the gas turbine in the period t, η_t^{DGT} is the thermoelectric conversion efficiency of the gas turbine, H_t^{GT} is the heating power of the gas turbine.

There is a coupling relationship between the power generation power and the heating power of the gas turbine. The physical models are given below.

$$H_t^{GT} = \lambda_t^{GT} P_t^{GT} \tag{13.3}$$

$$P_t^{GT} = \frac{\eta_t^{GT} G_t^{GT}}{\eta_t^{DGT} + \lambda_t^{GT}} = \frac{\eta_t^{GT} \rho_G L_G}{\Delta t (\eta_t^{DGT} + \lambda_t^{GT})} V_t^{GT} \tag{13.4}$$

where H_t^{GT}, λ_t^{GT}, and P_t^{GT} are the heating power, the electric-heat ratio, and the power generation of the gas turbine in the period t, respectively.

In addition, there is an electric heating boiler in the system to convert electrical energy into thermal energy. Meanwhile, the heat storage tank and the battery have the functions of thermal energy and electric energy storage.

2. The model of the P2G device

P2G devices consume electrical power to re-convert CO_2 into methane, which is supplied to the natural gas grid or gas storage tanks for use. If the natural gas output

power G_t^{P2G} of the P2G and the natural gas volume V_t^{P2G} in the period t satisfy a certain proportional relationship, the electric power P_t^{P2G} of the P2G device is expressed as:

$$P_t^{P2G} = \alpha_t^{P2G} G_t^{P2G} \tag{13.5}$$

where α_t^{P2G} is the conversion factor of P2G in the period t.

13.2.2 Classification of Generator Sets Based on GCN Networks

The carbon dioxide emission data is a kind of time series data, which is continuously generated with the change in time. The data at the next moment is influenced to some extent by the data at the last moment. Long short-term memory neural networks and one-dimensional temporal convolutional neural networks in deep learning are both typical methods for characterizing temporal dependencies for sequence data.

Inspired by the visual graph method proposed by Lucas et al., this study transforms time series data into a non-Euclidean graph structure to capture the structural features of time series data. This method of transforming time series data into graph structure through the visual graph method to complete downstream tasks has achieved ideal results on a variety of datasets. The specific method is that it draws a set of time series data as a histogram in chronological order, if the connection (line of sight) between the column vertices of any two pairs of time data (t_a, y_a) and (t_b, y_b) will not be affected by any time data (t_c, y_c) between them. If the column is occluded, it is considered that there is a connection between the two-time points (green line), otherwise, it is regarded as not connected (red line), which is described by the formula as:

$$y_c < y_b + (y_a - y_b)\frac{t_b - t_c}{t_b - t_a} \tag{13.6}$$

The time points are regarded as the nodes of the graph, and the connection relationship between the time points is regarded as the edge. No matter what direction the graph is scaled and translated, the connection relationship between the nodes will not be changed.

This method needs to traverse all time points and establish a complete edge relationship after pairwise comparison. The time required to build a graph will increase exponentially with the number of time nodes. It is very time-consuming to convert the data structure using the traditional visual method. Therefore, this study limited the comparison per point to 15 days, focusing on the short-term effects of the data. In this way, the time when each point in the graph establishes the neighbor relationship will be consistent.

The carbon emissions of generator sets are divided into 7 intervals, denoted by $A_i (i = 0, 1, 2)$. Combine the load data P, oxygen content data SP_{O^2}, air humidity RH, and wind speed v_w that affect the carbon emission of the generator set into a time node signal X:

$$X = [P, SP_{O^2}, RH, v_w], X \in R^{n \times 4} \tag{13.7}$$

The node signal X is fed into the neural network as an input feature. This neural network model consists of three Chebyshev convolution layers and each of which collects the information of K-order neighbor nodes for convolution calculation. The obtained convolution result is nonlinearly transformed by the activation function as the input feature of the next convolution layer, and the same calculation process is repeated. The activation function of the first two layers of the network is a linear rectifier unit function, which is shown as follows.

$$\text{ReLu}(n) = \max(0, n) \tag{13.8}$$

In case 1, output is 0 (input is less than 0); In case 2, output is equal to the input value and the derivative is 1 (input is greater than or equal to 0). Such a calculation only needs to judge the positive or negative of the input and does not require complex mathematical calculations, so the convergence speed is faster than other activation functions. The activation function of the last layer of the network is Softmax, and the expression is:

$$\text{Softmax}(n) = \frac{1}{1 + e^{-z}} \tag{13.9}$$

It maps the input between (0, 1) and can be used to represent probability. However, when the output is close to 0 or 1, its derivative is close to 0, which is highly likely to experience a gradient disappearance.

The final output of the network is a node embedding matrix composed of the embedding vectors of all nodes in the graph network. The label category corresponding to the maximum value in the embedding vector of each node is the category classification result of each node. According to the evaluation indicators and evaluation methods commonly used in classification tasks, the classification results are obtained, and applied to carbon trading below.

13.2.3 Exponential Energy Efficiency Economic Function

Carbon trading means that companies put their excess carbon credits on the market for purchase by those who are short of carbon credits, thereby reducing carbon emissions and protecting the ecological environment. The basic principle is as follows: the government or regulatory authorities, aiming to reduce energy consumption,

first allocate carbon emission shares to carbon emission enterprise, and the initial carbon emission quotas are generally distributed free of charge. Production enterprises formulate corresponding production plans according to the initial quota and have the power to emit a certain amount of carbon pollutants into the atmosphere within the validity period of the carbon emission quota. For carbon emission entities with high energy consumption, if the carbon pollutants discharged in the production process exceed the allocation quota, corresponding carbon emission quotas must be purchased in the carbon trading market to make up for the difference in carbon emissions, otherwise, the excess emissions will be the number of carbon pollutants pays fines. For carbon emission entities with low energy consumption, if there are remaining carbon emission quotas, they can be placed on the market for sale to obtain corresponding benefits.

Unlike traditional carbon emission policy, the carbon trading mechanism can reduce carbon emissions and significantly improve energy efficiency through economic means, at the same time, it can reduce business costs.

The carbon emission difference compared with the quota of the *i*-th generator unit is shown as follows:

$$D_{CO_2,i} = Q_i^{pre} - Q_i^f \tag{13.10}$$

where $D_{CO_2,i}$ is the carbon emission difference of the *i*-th generator unit; Q_i^{pre} is the predicted carbon emission value of the *i*-th generator unit; Q_i^f is the carbon emission quota of the *i*-th generating unit.

The expression of carbon transaction cost is as follows:

$$C_{CO_2,i} = \begin{cases} \tau e^{|D_{CO_2,i}|}\left|D_{CO_2,i}\right| + k_1 a_1, D_{CO_2,i} \le -P \\ \tau e^{|D_{CO_2,i}|}|D_{CO_2,i}| + k_2 a_2, -P < D_{CO_2,i} \le 0 \\ -\tau e^{|D_{CO_2,i}|}\left|D_{CO_2,i}\right| + k_3 a_3, 0 < D_{CO_2,i} < P \\ -\tau e^{|D_{CO_2,i}|}\left|D_{CO_2,i}\right| + k_4 a_4, D_{CO_2,i} \ge P \end{cases} \tag{13.11}$$

where $C_{CO_2,i}$ is the carbon transaction cost of the *i*-th generator unit; Q_i^f τ is the transaction price of carbon emission; k_1, k_2, k_3 and k_4 are the carbon emission reward and punishment functions of different types of generating units respectively; a_1, a_2, a_3 and a_4 are the carbon emission bonuses and penalties for different types of generator sets.

13.3 Low-Carbon Economy Optimal Dispatch Strategy

13.3.1 Optimization Model

The objective function is:

$$\min F = C_{de} + C_{gas} + C_{CO_2,i} \tag{13.12}$$

Among them, the energy storage device cost is:

$$C_{de} = \beta_e \sum_{t=1}^{T} \left(P_t^{ch} + P_t^{dis}\right) \tag{13.13}$$

where β_e is the electricity efficiency; P_t^{ch} and P_t^{dis} are the charging and discharging power of the energy storage device in the period t.

The gas cost is:

$$C_{gas} = \beta_g \sum_{t=1}^{T} \left(f_t^{GT} + f_t^{GB} - f_t^{P2G}\right) \tag{13.14}$$

where β_g is the basic gas price; f_t^{GT} and f_t^{GB} are the gas consumption rates of the gas turbine and gas boiler in the period t, respectively; f_t^{P2G} are the methane volume generated by the P2G equipment in the period t.

13.3.2 Restrictions

13.3.2.1 Electric and Thermal Power Balance Constraints

$$P_t^{buy} - P_t^{sell} + P_t^{GT} + P_t^{dis} = P_t^{L} + P_t^{ch} - P_t^{pv} - P_t^{wt} + P_t^{P2G} + P_t^{CCS} \tag{13.15}$$

$$H_t^{GT} + H_t^{GB} = H_t^{L} \tag{13.16}$$

where P_t^L and H_t^L are the electricity and heat loads at the moment t; P_t^{pv} and P_t^{wt} are the photovoltaic output and the fan output power at the moment t; $H^{GB,\min}$ and $H^{GB,\max}$ are the lower and upper limits of the gas turbine output.

13.3.2.2 Energy Storage System Constraints

Gas Storage Device Constraints

The gas energy stored in the storage tank in the period $t + 1$ is limited by the gas energy stored in the storage tank in the period t and the gas storage or output power of the storage tank in the period t.

Thermal Storage Device Constraints

The heating power of the electric heating boiler at the moment t is limited by the electric heat conversion efficiency of the electric heating boiler in the period t and the power consumption.

The heat loss of the thermal storage tank is related to the stored heat, but its heat loss rate is very small in the case of good insulation, and its thermal energy in the period $t + 1$ is limited by its thermal energy lost in the period t and the heat absorption power or heat release power in the period t.

Storage Device Constraints

The battery has electrical losses in the process of charging and discharging and storing electrical energy, and its dynamic characteristics of charging and discharging can be expressed as:

$$\begin{cases} P^{P2G,\min} \le P_t^{P2G} \le P^{P2G,\max} \\ P^{CCS,\min} \le P_t^{CCS} \le P^{CCS,\max} \\ Q_t^N \ge 0 \end{cases} \tag{13.17}$$

where $P^{P2G,\min}$ and $P^{P2G,\max}$ are the lower and upper limits of the power consumption of the P2G equipment, respectively; $P^{CCS,\min}$ and $P^{CCS,\max}$ are the lower and upper limits of the power consumption of the carbon capture system operation, respectively.

CHP Unit Electric Heating Output Constraints

The electric output of the CHP unit must be between its upper and lower limits, and the thermal output of the CHP unit must also be between its upper and lower limits.

Gas Turbine Thermal Output Constraint

$$H^{GT,\min} \le H_t^{GT} \le H^{GT,\max} \tag{13.18}$$

where $H^{GT,\max}$, $H^{GT,\min}$ are the upper and lower limits of the thermal output of the gas turbine.

13.4 Simulation

13.4.1 Example Description

In summary, this paper takes a new power system as an example to verify the effectiveness of the constructed model. In terms of market electricity price parameters, the electric energy interaction between the power system and the upper-level power grid is settled according to the real-time electricity price (Anand and Ramasubbu

2018). In terms of equipment parameters of the new electric power system, the gas low calorific value of the CHP unit and the gas boiler is taken as 9.7, and other equipment parameters can be known from Table 13.1. In addition, according to carbon market transactions, the benchmark value method is used to pre-allocate free carbon emission quotas for the power system. The carbon emission sources within the power system are gas-fired boilers and CHP units. 0.425, the actual carbon emission coefficient is 0.528 for gas-fired boilers and CHP units, the basic carbon price is 0.25 ¥/kg, and the basic gas price is 2.7 ¥/kg. The model can be handled by CPLEX solver through MATLAB software very well.

13.4.2 Scheduling Results and Electrical Heat Supply and Demand Balance Analysis

The optimal daily scheduling scheme is obtained by solving the model.

13.4.2.1 Electric and Thermal Power Balance Analysis

In the process of comprehensive energy dispatching, it is necessary that power constraints and thermal constraints must be satisfied. After optimal dispatching, the schematic diagrams of the electric-thermal power balance of the model constructed are shown in Figs. 13.1 and 13.2. From Fig. 13.1, it can be concluded that due to

Table 13.1 Basic parameters of gas turbine

The device name	The parameter name	The parameter value
CHP units	Installed capacity/kW	1000
	Thermogenesis efficiency	0.8
	Thermoelectric ratio	0.3
Gas boilers	Thermogenesis efficiency	9.3
Energy storage systems	Upper charge power cap/kW	180
	Upper discharge power cap/kW	180
	Charge from start to end/kWh	280
	Efficiency	0.98
	SOC range	0.1–0.9
P2G device	Conversion efficiency	0.55
	CO_2 feedstock ratio	1.06
	P2G capacity/kW	600
Carbon capture device	Carbon capture efficiency	0.5
	Carbon capture capacity/kW	400

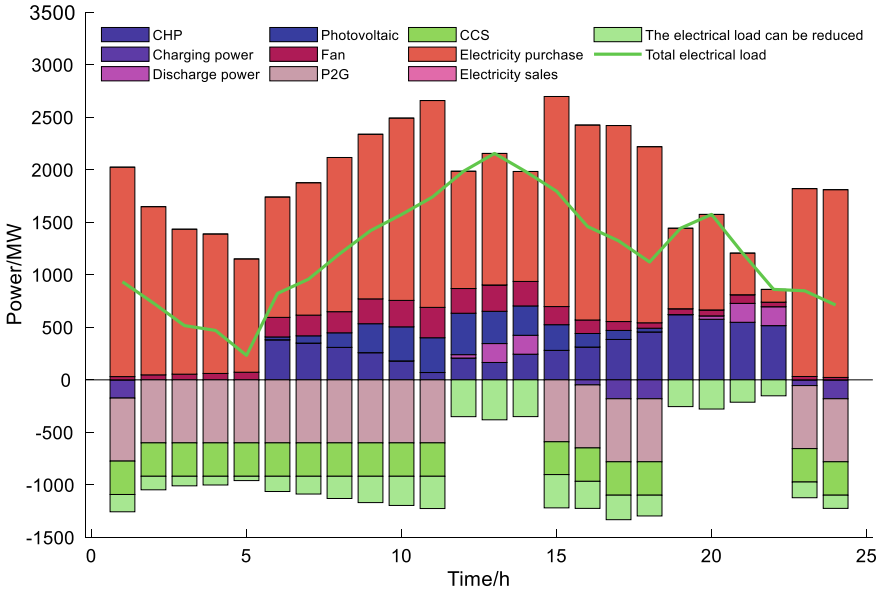

Fig. 13.1 Electric power balance diagram

the low level of output of renewable energy sources, the power system must buy much power from the external grid to realize the power load balance. In terms of thermal load balance, the internal thermal load of the system is mainly satisfied by the thermal power of the gas boiler and CHP unit, and most of time is supplied by the CHP unit. If the thermal power of CHP unit is not enough, the gas boiler needs to be started to compensate, but the opposite is not necessary. Residual heat load demand. Overall, both electrical power and thermal power can achieve power balance.

13.4.2.2 Analysis of Operation Strategy of Carbon Capture Units and P2G Plants

The power system aggregates carbon capture and P2G devices, which can capture and absorb CO_2, and synthesize the CH4 gas required for the operation of gas turbines and gas boilers, thereby realizing the recycling of by-products and improving the operating economy. The curves of the operating strategies of the P2G unit and the carbon capture unit with the real-time electricity price can be seen in Fig. 13.3. Both P2G energy consumption and carbon capture energy consumption are closely related to real-time electricity prices. The energy consumption and carbon capture energy consumption are both at a high level, for example, in 1–6 h, the P2G energy consumption is maintained at around 600 MW, while the carbon capture energy consumption is maintained at around 300 MW. At 7–10 h and 15–16 h, the energy

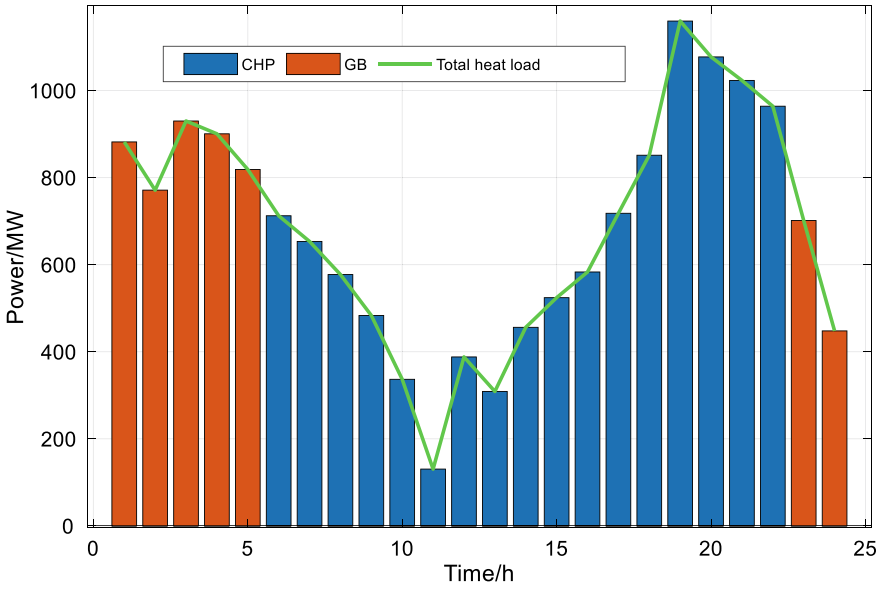

Fig. 13.2 Thermal power balance diagram

consumption of P2G and carbon capture decreased to a certain extent, while at 11–14 h and 19–22 h, the energy consumption of P2G and carbon capture was zero. This is mainly because when the real-time electricity price is high, the power system can obtain high profits by participating in electricity market transactions. Therefore, in the system, most of the power generation of the aggregation units is used to directly access the Internet to participate in electricity market transactions, and there is almost no remaining electricity. When the P2G system and the carbon capture system are energized, the energy consumption of these two systems is close to zero; When the electricity price is at a low level, the income of the power system participating in the electricity market transaction is low, while the income of participating in the carbon market transaction is high. Therefore, the P2G and carbon capture systems operate at the highest power and absorb the maximum amount of energy. Excess CO_2 is used to reduce CO_2 emissions, and to sell excess carbon emission rights to obtain high income in the carbon trading market, so when electricity prices are low, the power consumption of P2G and carbon capture systems reaches the highest value. In the rest of the period, the system's revenue in the electricity market and carbon trading market is almost the same, so the corresponding energy consumption of P2G and carbon capture is lower than when the electricity price is a much lower level because part of the output power is also used to participate in electricity market transactions.

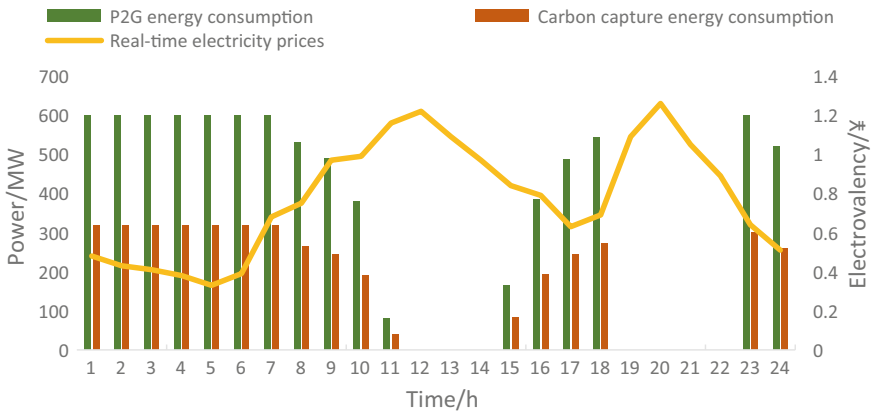

Fig. 13.3 Energy consumption curve of P2G device and carbon capture device

13.4.3 Analysis of the Economy and Environmental Friendliness of the System

To reflect the effectiveness of considering carbon trading on the economics and consumption reduction of the power system, the following comparison scenarios are also set up:

- S1: Consider carbon capture systems, but participating in carbon market transactions is not considered;
- S2: A carbon capture system is not considered, but participation in the carbon trading market is considered;
- S3: Consider carbon capture systems and consider participating in carbon market transactions.

Under the three scenarios, the optimization results of carbon emissions, carbon transaction costs, and total operating costs of the power system are shown in Table 13.2. It can be seen that considering the carbon capture system and considering the system's participation in carbon market trading can greatly reduce the total operating cost of the system. Comparing S1 and S2, when the carbon capture system is not considered to participate in the carbon market transaction, due to the lack of CO_2 treatment and absorption, the power system needs to achieve a large amount of carbon emission rights from the carbon market. Market transaction costs have increased significantly, resulting in a significant increase in total operating costs compared to scenarios that do not participate in carbon market transactions. Therefore, if a new type of power system is considered to participate in carbon market transactions, it should ensure that there are sufficient CO_2 treatment methods to reduce the carbon emissions within the system, thereby increasing the benefits of the carbon market.

Comparing S1 and S3, it can be seen that considering carbon market trading and not considering carbon market trading, the overall carbon emissions of the power

Table 13.2 Comprehensive energy system optimization results under different scenarios

Comparison items	S1	S2	S3
Total operating cost/¥	19453.72	20953.15	17445.56
Total carbon footprint/kg	17263.26	20361.12	15264.12
The total output of carbon-containing units/kW	15531.23	11982.83	13587.16
Carbon market trading proceeds/¥	0	−2108.34	−676.148

system can be reduced through the stimulation of carbon prices, and carbon emissions are reduced by about 11.58%. Therefore, the carbon market trading mechanism has a better influence on energy saving.

The operating power of gas turbines varies in different scenarios. In S2, the operating power of gas-fired units is generally low, because the carbon capture system could not be considered. This is mainly because if the output of gas-fired units is too high, the corresponding carbon emissions are also high, and the total carbon market transaction cost of the system will be will increase significantly, which cannot reflect the economy of the scheduling strategy. In contrast, the operating power of gas turbines in S1 and S3 is much lower. In S1, since carbon market transactions are not considered, the carbon emissions of gas turbines have no significant impact on the total cost. Therefore, the power emissions of gas turbines in scenario 1 are the highest of the three scenarios.

13.5 Conclusion

In summary, a low-carbon economy optimization dispatching strategy is proposed for a power system based on graph convolution network classification. The carbon transaction cost is taken into account in the operating cost, and a hybrid integer linear programming model (MILP) is established. The efficient solution of the model is realized by CPLEX solver by MATLAB software. Through the analysis of the total operating cost, total carbon emissions and benefits of the system in different scenarios, the carbon market trading mechanism opposes a more obvious influence on energy saving, which greatly reduces the total operating cost while also reducing carbon emissions and maintaining the ecological environment.

In the future, we will continue our research on the optimization of low carbon economy dispatch in the power system in the context of “double carbon”, the real-time carbon trading price, the behavioral characteristics of demand-side users and the characteristics of different load devices, in order to further improve the economy and low carbon of the power system and make a contribution to the beautification of the ecological environment.

Acknowledgements We gratefully acknowledge the support of the project of the State Grid Xinjiang Electric Power Co., Ltd. (No. SGXJ0000TKJS2200255).

References

Cui D, Ge W, Zhao W (2021) Economic low-carbon clean dispatching of power system containing P2G considering the comprehensive influence of multi-price factor. J Electr Eng Technol

Eladla AA, ElDesouky AA (2019) Optimal economic dispatch for multi heat-electric energy source power system. Electr Power Energy Syst, 21–35

Fanga Y, Zhaoa S, Wang N (2019) Power system stochastic optimal dispatch considering thermal and electrical coordination. Electr Power Energy Syst, 772–780

Liu B, Li J, Zhang S (2020) Economic dispatch of combined heat and power energy systems using electric boiler to accommodate wind power. IEEE Access 8:41288–41297

Wang Y, Wang Y, Huang Y (2019) Operation optimization of regional integrated energy system based on the modeling of electricity-thermal-natural gas network. Appl Energy, 1–27

Wang Y, Ma Y, Song F, Ma Y (2020) Economic and efficient multi-objective operation optimization of integrated energy system considering electro-thermal demand response. Energy, 1–19

Xiang Y, Wu G, Shen X, Ma Y, Gou J, Xu W, Liu J (2021) Low-carbon economic dispatch of electricity-gas systems. Energy, 226, 120267

Xu F, Zhou R, Cao J (2019) Coordinated and optimized scheduling of electricity-heat-gas in virtual power plants in various markets. Proceed CSU-EPSA 31(9):35–42

Zhang K, Xu N, Ling Y, Zhou B, Song Y (2020) Economic dispatch analysis of comprehensive energy system considering carbon trading. In: IOP conference series: earth and environmental science, p 546

Chapter 14
Research and Practice on High Impact Pollution Control of Urban Lakes—A Case Study of Yanjia Lake in Wuhan

Shufang He, Qin Zhu, Zhuo Huang, and Baojie Jia

Abstract Non-point source pollution which has not been effectively controlled is an important reason for the continuous deterioration of urban lake water quality, because of its unique high impact, burstiness and intermittency, it is difficult to use the traditional sewage treatment technology for centralized control and treatment, which has become one of the key issues in lake treatment. Domestic and foreign studies show that decentralized ecological treatment is an effective measure to control non-point source pollution. Combined Sewer Overflows (CSOs) is the most important pollution source of Yanjia Lake, which is a typical urban lake with high impact pollution. The practice of pollution control in Yanjia Lake shows that the combined process of magnetic microfiltration and constructed wetland can shorten the recovery time of water quality after rain, and can effectively control the high impact pollution of Urban Lakes.

Keywords High impact pollution control · Urban lakes · Yanjia lake

14.1 The Introduction

Since the 1980s, the focus of water pollution prevention and control is rain pollution diversion and waste sewage collection and treatment, urban lake point source pollution has been effectively controlled, which has alleviated urban lake pollution to a certain extent. However, the point source pollution controlling has not prevented the urban lakes pollution fundamentally. The non-point source pollution has become an important reason for the continuous deterioration of urban lakes water quality. Compared with point source pollution, urban surface runoff and Combined Sewer

S. He (✉) · Z. Huang · B. Jia
Changjiang River Scientific Research Institute, Wuhan 430010, China
e-mail: abby-21@163.com

Q. Zhu
Changjiang Design Group Co. Ltd, Wuhan 430010, China

G. Huang (ed.), *Proceedings of 2022 7th International Conference on Environmental Engineering and Sustainable Development (CEESD 2022)*, Environmental Science and Engineering, https://doi.org/10.1007/978-3-031-28193-8_14

Overflows (CSOs) caused by rainfall are difficult to use traditional sewage treatment technology for centralized control and treatment because of their unique high impact, burstiness and intermittency. As a result, urban rivers and lakes are seriously polluted, and the trend of returning to black and odor in the rainy season is obvious. The control of high impact pollution in urban lakes has become one of the most important problems in lake improvement.

14.2 Research Status at Home and Abroad

The research on urban non-point source pollution started earlier in foreign countries, Germany began to carry out the initial rainwater purification technology research from the beginning of the last century (Deming and Wei 2008). The most typical measures are to build a large number of rainwater tanks to intercept and divert the initial rain, deal with the CSOs, and take decentralized ecological measures to reduce and purify sewage at the source (Horie et al. 2005). In 1964, the United States has begun a series of studies to control CSOs pollution during rainy days, and relevant studies showed that the interception of 11 mm initial rainwater could reduce the overflow pollution load by 65% in the rainy season and 90% in the whole year (Wu et al. 2003). In 1994, the United States proposed to effectively combine CSOs pollution control with rainstorm runoff control, and try to take some green measures of storm management to control overflow pollution, such as biological retention system (Xue et al. 2008). Japanese scholars believe that adding rainwater storage facilities and infiltration facilities, using the surplus storage space of large-scale rainwater trunk pipes to store rainwater, and improving and placing filters to separate sand particles, can effectively alleviate CSOs pollution (Furukawa 2022).

In China, the research on urban runoff pollution control started relatively late, and there were few studies on the control of CSOs pollution (Liang et al. 2002). Lizhu et al. (2009) designed a multi-layer percolation medium system for surface runoff pollution in Beijing, which has a good removal effect on nitrogen and phosphorus pollutants. Honglin et al. (2015) analyzed reduction of urban runoff pollutants by soil in the process of infiltration in Xi'an. Field test results show that the concentration of ammonia nitrogen decreases after the surface runoff is retained in the soil. Ying et al. (2012) designed a sewage interception device for road rainwater outlet—sewage interception hanging basket, which is helpful to improve the pollution of rainwater runoff. Lan et al. (2001) collected and purified the stormwater runoff collected from urban roofs through green Spaces or artificial soil layers, or penetrated underground, and reduce the water pollution caused by rainwater runoff. In conclusion, there have been some researches and practices in the treatment for initial rainwater in China, but low-cost and efficient solutions are also lacking to cope with the high impact pollution, which is sudden, large volume, and have heavy pollution. The traditional technology still has various limiting factors such as high cost, low utilization rate and difficult to popularize. Therefore, it's difficult to meet the requirements of lake improvement.

14.3 High Impact Pollution Control Practice in Yan Jia Lake

14.3.1 Lake Overview

Yanjia Lake is located in the old City of Yangluo, Xinzhou District, Wuhan City, at the junction of Wuhu River system and Zhangdu Lake system. With a water area of 0.2 km^2 and a catchment area of 4.68 km^2. At present, the water quality of Yan Jia Lake fluctuates between bad V and V, and the water quality deteriorates obviously after rain.

As a typical urban adjusting and storing Lake, YanJia Lake undertake regulation and drainage function in the old city during the rainy season. The contradiction between discharging pollution and draining is prominent. The old city used a closed confluence pipe network system, which basically realizes the pollution interception in the dry season. In the rainy season, the old city is prone to waterlogging. In order to reduce the risk of waterlogging, the interception well was opened to drain water, which brought a large amount of rain and sewage mixed flow, causing a high impact pollution on Yan Jia Lake, and the water quality deteriorated significantly after the rain. The CSOs pollution of Yan Jia Lake is serious during the rainy season.

14.3.2 Pollution Characteristics

At present, dry season pollution interception and round-the-lake pollution interception have been basically implemented in Yan Jia Lake, CSOs is the main pollution source. Theoretically, the pollutants in CSOs are the superposition of pollutants in municipal sewage, pipe sediment and stormwater runoff. Therefore, the pollutant content of CSOs can be greater than that of storm runoff in the same period (Yun 2009).

CSOs water quality processes are monitored at 15-min intervals during typical rainfall. Figures 14.1 and 14.2 show that the CSOs pollution of Yanjia Lake shows similar change rules under different rainfall intensities.

(1) The concentration of pollutants increases rapidly in a short period of time, reaches the highest point, and then slowly reduce to reach stability, the maximum content far exceeds the content of pollutants in urban sewage.
(2) The initial scouring efficiency of COD, BOD and SS is high. and the effluent pollutant concentration was high in the first 60 min.
(3) The initial effect of short history and high intensity rainfall is more obvious, which is consistent with the characteristics of high impact pollution
(4) The concentrations of ammonia nitrogen and TP in CSOs were significantly higher than those in storm runoff due to the presence of base flow in the dry season.

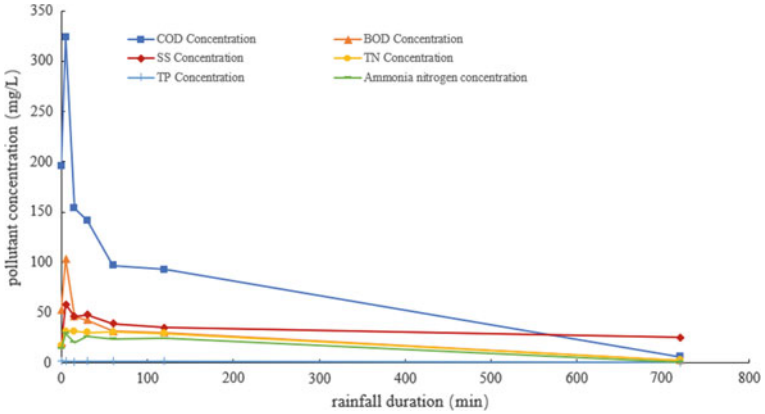

Fig. 14.1 Water quality process of CSOs under rainstorm

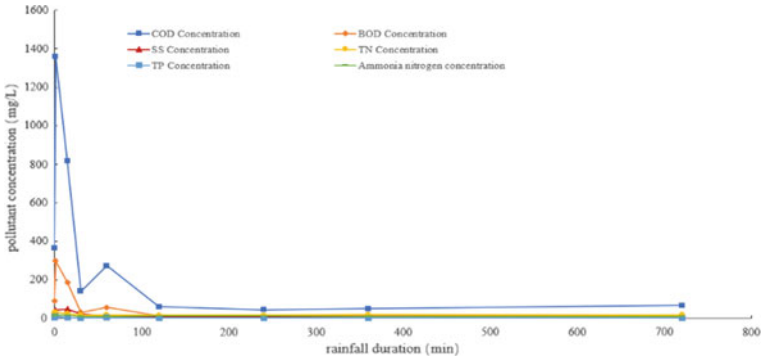

Fig. 14.2 Water quality process of CSOs under moderate rain

14.3.3 Pollution Control Scheme

Based on the whole process control method, CSOs can be controlled by means of source reduction, process purification and terminal storage treatment. Among them, the source reduction is mainly aimed at the collection and treatment system of the pipe network to carry out the work, while the process purification requires a series of purification measures to be set along the runoff. Both methods should not be used alone for reasons such as large investment, long time consuming and late effect of land receipts. The terminal treatment can mainly include storage ponds, integrated treatment equipment, multistage ecological treatment system and other engineering measures.

Considering that it is difficult to complete the source treatment projects in the short term, the control of CSOs pollution should be carried out simultaneously with source control and terminal storage treatment.

14.3.3.1 Renovation of Source Pipe Network

Hydraulic calculation was carried out on the confluence pipe in the old city, and the flow was checked according to the 2-year recurrence interval of the rainstorm. The drainage pipes that meet the 2-year recurrence interval of the storm shall be retained and used as storm water pipes. If the pipe diameter meets discharge requirements of sewage, whose pipes that do not meet the stormwater drainage requirements for the 2-year recurrence interval of storms will be used as sewage pipes. The storm water pipes were rebuilt according to the 3-year recurrence interval of storms. For the separate sewage system, we shall reform the rain and sewage mixing wrong contact point, and repair the defective pipe.

After the pipe network renovation and the diversion of rain and sewage water, the drainage of Xinao Sluice will be transformed from rain and sewage mixed flow to rainwater, which will greatly reduce the impact of CSOs pollution and alleviate the water pollution of Yan Jia Lake.

14.3.3.2 Terminal Storage Treatment

Before the renovation of pipe network and the diversion of rain and pollution are completed, the CSOs pollution should be stored and treated in situ to ensure the water quality of Yan Jia Lake after rain. Due to unique hydrological and water quality characteristics such as burstiness, random and strong impact of urban CSOs pollution, it is necessary to select the treatment technology which can run randomly and intermittently and has strong resistance to the impact load of water quantity and quality.

According to the analysis of water quality, the initial overflow contains a large amount of suspended matter, and the content of particulate pollutants is high. Considering the land use situation, treatment effect and operation and maintenance requirements, magnetic microfiltration water purification equipment is recommended for this project, see Table 14.1 for specific comparison. Magnetic particle water purification equipment can quickly reduce the concentration of suspended matter, and has obvious advantages in land occupation, construction cycle, direct operation cost, efficiency and automation degree.

(1) The comparison and selection of advanced biochemical treatment technology

The removal effect of ammonia nitrogen by physical and chemical process is not good, the selection of advanced biochemical treatment process should focus on the removal effect of ammonia nitrogenand the available treatment technology include breakpoint chloranation, ion exchange, electrochemical, constructed wetland and EHBR membrane technology. Through the comparison and selection of the above five ammonia nitrogen removal technology, it is recommended to use constructed wetland for nitrogen removal, and the comparison and selection is shown in Table 14.2.

Table 14.1 Comparison and selection of physicochemical treatment technology

Treatment technology	Overspeed integration processing equipment	Gas flotation method	Magnetic microfiltration	High efficiency settling tank
Advantages	Fast speed, Small footprint, Low operating cost, Intermittent operation	Small footprint, the removal of light impurities is particularly good	Impact resistant load, High efficiency, small footprint, Low operating cost	Impact resistant load, Fast speed, More conducive to reconstruction and expansion
Disadvantages	The treatment effect on ammonia nitrogen and total phosphorus is general	For some high density and relatively large volume, the removal effect is low, and the power consumption is large	Magnetic powder should be added regularly, the treatment effect of ammonia nitrogen is not good	Prone to mud, Low degree of automation, High O&M requirements, Low efficiency, Large footprint
Construction time	<15 days	<15 days	<10 days	>30 days
Construction cost	High	Low	Low	High
Built form	Integrated equipment	Integrated equipment	Integrated equipment	Reinforced concrete

After sufficient comparison, the project adopts the combined technology of magnetic microfiltration and constructed wetland to treat the rain sewage overflow and discharge it. After removing a large amount of particulate pollutants by magnetic microfiltration technology, the effluent is discharged into the vertical flow constructed wetland for biochemical treatment and finally discharged into Yan Jia Lake. It can greatly reduce the pollutants entering the lake before renovation of source pipe network, and stabilize the lake water quality in flood season.

In conclusion, the high-impact pollution control technology route of Yan Jia Lake is shown in Fig. 14.3. Before rainwater and sewage diversion, terminal storage treatment for rainwater and sewage overflow, was carried out by regulating storage pond + magnetic microfiltration + vertical flow constructed wetland. After the diversion of rainwater and sewage, the initial rainwater is discharged to the sewage treatment plant.

Table 14.2 Comparison and selection of nitrogen removal technology

Technology	Breakpoint chloranation	Ion exchange	Electrochemical	Constructed wetland	EHBR membrane technology
Advantages	Fast speed, High efficiency, stable treatment effect	High efficiency, stable treatment effect, Simple process	Efficient and safe, Fast speed, no secondary pollution, good removal effect	Technical maturity, Good removal effect, strong resistance to impact load, Environment friendly	Can be installed directly in water, Good removal effect and low running cost
Disadvantages	High ecological risk	Practical engineering application cases are few	Expensive to build, and the running cost is high	Regular harvesting is required	Intermittent operation requires one week buffer time
Floor space	Small	Medium	Small	Medium	Large
Construction cost	Low	Medium	Very high	Medium	High
Operating costs	Medium	Medium	High	Low	Low
Comparison analysis	High ecological risk, not recommended	There are few practical cases, not recommended	High investment cost, not recommended	Mature and stable process, good effect, no ecological risk, recommended	It cannot meet the requirements of intermittent operation

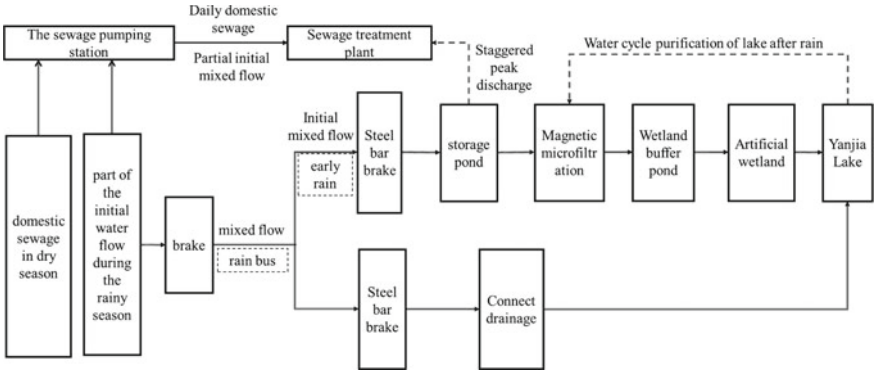

Fig. 14.3 High impact pollution control technology roadmap of Yanjia lake

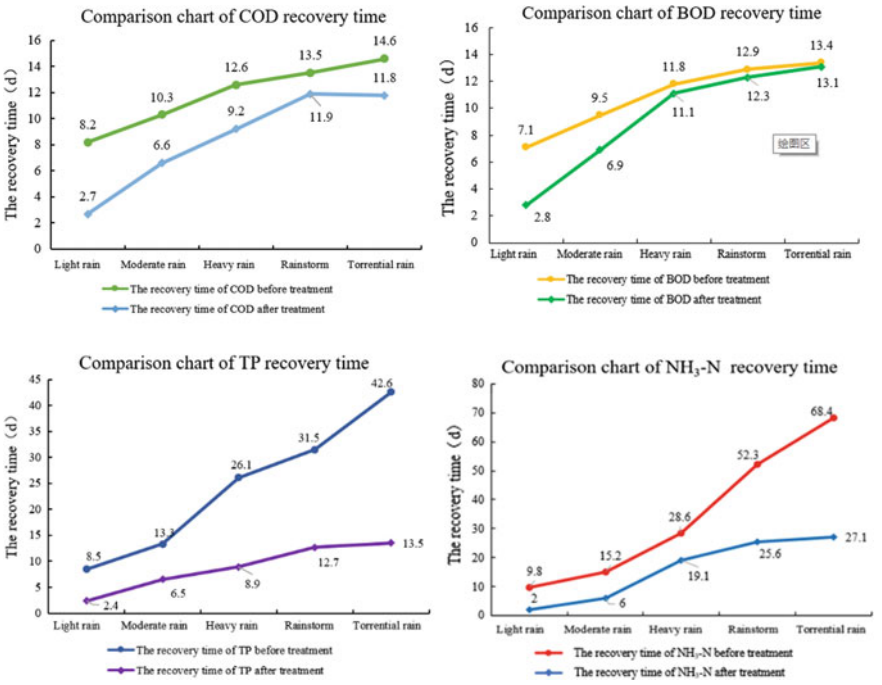

Fig. 14.4 Comparison of water quality recovery time under different rainfall levels before and after treatment

14.3.4 Control Effect Prediction

According to the load of pollutants in the lake under different grades of rainfall, combined with the reduction amount of each project measure, the time needed for lake water quality recovery under different grades of rainfall is predicted.

See Fig. 14.4 for the comparison of recovery cycles of various pollutants before and after treatment. It can be seen from the figure that, with the same rainfall level, the implementation of this project will greatly shorten the recovery cycle of water quality, especially the reduction of TP and ammonia nitrogen recovery cycles, which is conducive to the stable water quality standard of Yanjia Lake.

14.4 Conclusions and Suggestions

1. The treatment practice of Yan Jia Lake shows that the end storage treatment can can effectively control the CSOs pollution, greatly reduce the impact of pollution load, shorten the recovery period of water quality after rain, and prevent

repeated black and odor after rain. It is an effective way to control the high-impact pollution.
2. After sufficient process demonstration, the combined process of "magnetic microfiltration + constructed wetland" can quickly remove particulate pollutants, deal with urban CSOs pollution with large flow and high concentration, meet the needs of interstitial operation, and effectively deal with urban high-impact pollution.
3. On the basis of the existing pipe network transformation and terminal storage treatment, the sponge transformation should be promoted as soon as possible to reduce urban high-impact pollution load, so as to truly realize the whole process pollution control and ensure the long-term stability of the water quality of Yanjia Lake.

Fund Program

The project supported by the National Key Research and Development Program of China (Project No. 2022YFE0117000)and the Key research project of water conservancy in Hubei Province(Project No. HBSLKY202336).

References

Braune MJ, Wood A (1999) Best management practices applied to urban runoff quantity and quality contr01. Water Sci Technol 39(12):117–121

Deming J, Wei J (2008) Study on Water quality of urban stormwater runoff at home and abroad. Geophys Geochem Explor (4)

Furukawa K (2002) Activated sludge treatment of wet weather wastewater in Osaka City. Japan: GESAP

Honglin Y, Ying W, Chunde X (2015) Abatement effect of soil on pollutants in urban stormwater runoff. Bull Soil Water Conserv 35(3):112–116

Horie N, Kabata M, Sano H (2005) Japanese project spirit 21: development and testing of CSO treatment technologies and instrumentation systems. Japan: EWRI

Lan O, Wu C, Huizhen W (2001) Study on horizontal flow infiltration purification of urban roof rainwater green space. Urban Environ Urban Ecol 14(6):24–26

Liang Z, Jinbang C, Yan C (2002) Cause analysis and maintenance countermeasures of urban slow flow water pollution. Adv Water Sci 13(3):384–388

Lizhu H, Shaoyuan F, Yueyuan D (2009) Purification of nitrogen and phosphorus pollutants from urban stormwater runoff by multilayer percolating media system. J Environ Sci 29(5):960–967

Wu C, Yan L, Junqi L (2003) Water quality and pollution control of urban rainwater at home and abroad. Water Supply Drain 29(10):38–42

Xue Y, Wu C, Junqi L (2008) Control and management of overflow pollution in confluence system pipeline at home and abroad. China Water Wastewater 24(16):7–11

Ying C, Jianqiang Z, Xiaoling Z, Bo H, Hequn M (2012) Experimental study on hanging basket of road rainwater inlet in Xi'an City. J Saf Environ 12(5):69–72

Yun H (2009) Study on water pollution and control of artificial water surface in urban river. Xi'an University of Architecture and Technology

Part III
Energy, Water and Environment

Chapter 15
A Fuzzy Bi-level Optimization Method for Urban Ecosystem Management—A Case Study of Xiamen, China

L. C. Fang, S. G. Wang, P. P. Gao, and Z. H. Ma

Abstract A fuzzy bi-level programming (FBP) model is established for managing urban ecosystem under uncertainty. FBP cannot only handle the parameter uncertainty in the objective function, but also weigh the pursuit and conflict between different decision makers. FBP is then applied to the ecosystem management of Xiamen City, in which the system benefit, ecosystem service values and carbon emissions under different scenarios are considered. Results indicate that (i) the schemes with high system benefit face greater default risks; (ii) carbon sequestration and oxygen release are the main functions of the local ecological services; (iii) bi-level model exhibits more eco-friendly than the single-level model, but the system benefit is slightly reduced.

Keywords Fuzzy · Bi-level · System benefit · Ecosystem · Uncertainty

15.1 Introduction

Urban ecosystem is a complex system that includes the economy, ecology, society, environment and other fields. There exist a large number of uncertainties. Firstly, the economic and environmental elements in the ecosystem are themselves uncertain, and these factors influence each other, making the uncertainty more prominent. Secondly, when people calculate the value of ecological services, many uncertainties of ecological parameters and material prices exist, which makes the calculation results deviate with the reality. The fuzzy programming method for the uncertainty problem can be used. Fuzzy possibilistic programming mainly uses the fuzzy parameters to represent the fuzzy variables, which can effectively handle the fuzzy parameters without accurate values in the system model, and reflect the influence of the uncertainty of the parameters in the objective function on the system benefit. Pal

L. C. Fang · S. G. Wang (✉) · P. P. Gao · Z. H. Ma
School of Environmental Science and Engineering, Xiamen University of Technology, Xiamen 361024, China
e-mail: wsg@sdu.edu.cn

G. Huang (ed.), *Proceedings of 2022 7th International Conference on Environmental Engineering and Sustainable Development (CEESD 2022)*, Environmental Science and Engineering, https://doi.org/10.1007/978-3-031-28193-8_15

et al. (2011) solved land allocation problem for the optimal production of agricultural crops using fuzzy goal programming, and vaguely described the utilization of total arable land and the realization of the desired level of seasonal crop production. Nevertheless, system often have different decision layers and decision goals. Bi-level programming can weigh the pursuit of various interest layers from an overall perspective. Gong et al. (2022) used bi-level programming to provide optimization solutions for China's long-term energy system planning, helping decision-makers to optimize multi-regional energy systems in a low-carbon manner.

Unfortunately, few people currently combine fuzzy programming and bi-level programming to urban ecosystem. This research establishes a fuzzy bi-level programming (FBP) for ecosystem in Xiamen, China, which can rationally allocate land resources and coordinate economic and ecological development.

15.2 Methodology

Decision-makers are often disturbed by various uncertainties that can affect the accuracy of the system results in the planning process. The fuzzy possibilistic programming (FP) method can effectively address the impact of such uncertainty. It can be expressed as (Simic 2015):

$$\text{Max } \widetilde{f} = \sum_{j=1}^{k} \widetilde{c}_j x_j \tag{15.1}$$

where "~" represents the fuzzy mathematical symbol, and the $\widetilde{c}_j$ represents the fuzzy parameter (Zhou 2015). It is described as $\widetilde{c}_j = (c^c, \omega)$, where c^c is the center point and ω is the spread distance. According to the fuzzy membership function, objective function can also be translated into:

$$\text{Max } \widetilde{f} = \sum_{j=1}^{k} \widetilde{c}_j x_j \tag{15.2}$$

By introducing the minimum necessity measure level of the variable, the fuzzy possibilistic programming (FP) model can be formulated (Fang 2022):

$$\text{Max } \widetilde{f} = \sum_{j=1}^{k} c_j^c x_j - \sum_{j=1}^{k} \lambda w_j x_j \tag{15.3}$$

where λ represents the necessity level, which reflects the attitude of the decision makers towards the uncertainty avoidance of the objective function (Zeng et al. 2016).

Bi-level programming (BP) is a systematic optimization method with two-layer hierarchical structure, which can effectively solve the multiple interest conflict problem. It can be defined as follows (Lv et al. 2021):

$$\underset{x_1}{\text{Max}}\ f_1(x_1, x_2) \tag{15.4-a}$$

$$\underset{x_2}{\text{Max}}\ f_2(x_1, x_2) \tag{15.4-b}$$

$$\sum_{j=1}^{n} a_{ij}x_j \le b_i,\ i = 1, 2, \ldots, k \tag{15.4-c}$$

We calculate that the upper model solution is $\left(x_1^U, x_2^U, f_1^U\right)$ and the lower model solution is $\left(x_2^L, x_2^L, f_2^L\right)$. x_1 has a change range of x_1^U and its maximum tolerance value is r. The membership function of the decision variable x_1 can be expressed as (Hu et al. 2022):

$$\mu_{x_1}(x_1) = \begin{cases} \frac{x_1 - \left(x_1^U - r\right)}{r},\ if\ x_1^U - r < x_1 \le x_1^U \\ \frac{\left(x_1^U + r\right) - x_1}{r},\ if\ x_1^U < x_1 \le x_1^U + r \end{cases} \tag{15.5}$$

The most preferred result is x_1^U, and the preference would continuously increase in the interval of $\left[x_1^U - r, x_1\right]$ and would continuously decrease in the interval of $\left[x_1^U, x_1^U + r\right]$. The membership function of upper target function can then be stated as (Ma et al. 2020):

$$\mu_{f_1}(f_1(x)) = \begin{cases} 1,\ when\ f_1(x) > f_1^U \\ \frac{f_1(x) - f_1^L}{f_1^U - f_1^L},\ when\ f_1^L \le f_1(x) \le f_1^U \\ 0, when\ f_1(x) < f_1^L \end{cases} \tag{15.6}$$

At the same time, the membership function of the lower model is $\mu_{f_2}(f_2(x))$. The optimal solution of the whole model is transformed into solving the overall satisfactory degree of the upper and lower level (Yu et al. 2020):

$$\text{Max}\ \alpha \tag{15.7-a}$$

subject to:

$$\mu_{x_1}(x_1) \ge \alpha I \tag{15.7-b}$$

$$\mu_{f_1}[f_1(x)] \ge \alpha \tag{15.7-c}$$

$$\mu_{f_2}[f_2(x)] \ge \alpha \tag{15.7-d}$$

$$\sum_{j=1}^{n} a_{ij} x_j \leq b_i \tag{15.7-e}$$

where α is the overall satisfactory degree and $\alpha \in [0, 1]$. I is the unit vector.

15.3 Case Study

In recent years, Xiamen City has witnessed rapid increase of population and continuous expansion of built-up areas, leading to the continuous extrusion of ecological land and the destruction of a large number of woodlands and wetlands. Therefore, it is urgent to achieve a reasonable ecosystem optimization model to realize economically-efficient and ecologically harmonious development.

Upper level (maximize the system benefit):

$$\text{Max } f = PRO + ESV \tag{15.8-1}$$

Lower level (maximize the ecosystem service values):

$$\text{Max } f = ESV \tag{15.8-2}$$

$$PRO = L \times \sum_{j=1}^{3} \sum_{t=1}^{1} PI_{j,t} \times \widetilde{IEB}_{j,t} \tag{15.8-3a}$$

$$\begin{aligned} ESV = L \times \Bigg\{ & \sum_{c=1}^{4} \sum_{t=1}^{1} PE_{c,t} \times \widetilde{CRE}_{c,t} + \sum_{c=1}^{4} \sum_{t=1}^{1} PE_{c,t} \times CAC_{c,t} \times \left(\widetilde{CT}_t + 0.73 \times \widetilde{OP}_t \right) \\ & + \sum_{c=1}^{4} \sum_{t=1}^{1} PE_{c,t} \times CAS_{c,t} \times \widetilde{CSR}_t + \sum_{c=1}^{4} \sum_{t=1}^{1} PE_{c,t} \times CCE_{c,t} \times SRE_t \times \widetilde{RC}_t \\ & + \sum_{c=1}^{4} \sum_{t=1}^{1} PE_{c,t} \times CWE_{c,t} \times \widetilde{CST}_t + \sum_{c=1}^{4} \sum_{t=1}^{1} PE_{c,t} \times SEE_{c,t} \times \widetilde{CES}_t \\ & + \sum_{c=1}^{4} \sum_{t=1}^{1} PE_{c,t} \times \widetilde{ETV}_{c,t} \Bigg\} \end{aligned} \tag{15.8-3b}$$

Constraints include total area, forestry and grass coverage, water resources, carbon emission, sewage purification, solid waste discharging, COD discharging, population and area scale constraint.

$$\begin{cases} \sum_{c=1}^{4} PE_{c,t} + \sum_{j=1}^{3} PI_{j,t} \le S_t \\ \left(\sum_{c=1}^{4} PE_{c,t} \times VAE_{c,t} + \sum_{j=1}^{3} PI_{j,t} \times VAI_{j,t} \right) / S_t \ge PFG_t \\ \sum_{j=1}^{3} PI_{j,t} \times WCI_{j,t} + \sum_{c=1}^{4} PE_{c,t} \times QEW_{c,t} \le AW_t \\ \sum_{j=1}^{3} PI_{j,t} \times CEI_{j,t} - \sum_{c=1}^{4} PE_{c,t} \times CAC_{c,t} \le ACE_t \\ \sum_{j=1}^{3} PI_{j,t} \times SDI_{j,t} - \sum_{c=1}^{4} PE_{c,t} \times CWE_{c,t} \le AWD_t \\ \sum_{j=1}^{3} PI_{j,t} \times SWI_{j,t} - \sum_{c=1}^{4} PE_{c,t} \times SWE_{c,t} \le ASW_t \\ \sum_{j=1}^{3} PI_{j,t} \times CPI_{j,t} - \sum_{c=1}^{4} PE_{c,t} \times CAE_{c,t} \le ACD_t \\ \sum_{j=1}^{3} PI_{j,t} \times UP_{j,t} \ge TP_t \\ MINE_{c,t} \le PE_{c,t} \le MAXE_{c,t},\ MINI_{j,t} \le PI_{j,t} \le MAXI_{j,t} \end{cases} \tag{15.8-4}$$

where c = type of ecological land; j = type of non-ecological land; t = time periods; L = period years; $PE_{c,t}$ = ecological land area; $PI_{j,t}$ = non-ecological land area; $IEB_{j,t}$ = economic benefit; $CRE_{c,t}$ = climate regulation value; $CAC_{c,t}$ = CO_2 absorption capacity; CT_t = carbon tax; OP_t = oxygen price; $CAS_{c,t}$ = SO_2 absorption capacity; CSR_t = SO_2 removal cost; $CCE_{c,t}$ = water conservation capacity; SRE_t = surface runoff coefficient; $CWE_{c,t}$ = sewage purification capacity; CST_t = sewage treatment cost; $SEE_{c,t}$ = soil conservation quantity; CES_t = soil transportation cost; $ETV_{c,t}$ = leisure and recreation value; S_t = total land area; $VAE_{c,t}$ = green rate of ecological land; $VAI_{j,t}$, = green rate of non-ecological land; PFG_t = total green rate; $WCI_{j,t}$ = water consumption; $QEW_{c,t}$ = ecological water demand; AW_t = total water resources; $CEI_{j,t}$ = carbon emissions; ACE_t = allowable carbon emissions; $SDI_{j,t}$ = sewage discharge; AWD_t = allowable sewage discharge; $SWI_{j,t}$ = solid waste emissions; $SWE_{c,t}$ = solid waste purification capacity; ASW_t = allowable solid waste emissions; $CPI_{j,t}$ = COD discharge; $CAE_{c,t}$ = COD purification capacity; ACD_t = allowable COD discharge; $UP_{j,t}$ = population capacity; TP_t = total population; $MINE_{c,t}$ = minimum ecological land area; $MAXE_{c,t}$ = maximum ecological land area; $MINI_{j,t}$ = minimum non-ecological land area; $MAXI_{j,t}$ = maximum non-ecological land area.

15.4 Result and Discussion

Figure 15.1 presents the results of system benefit and overall satisfactory degree under different necessity levels (λ). Results indicate that the system benefit would decrease with increasing necessity level. The higher the necessity level, the less the uncertainty in the objective function, and the less the system benefit, indicating the conservative attitude of the decision makers towards the expected goal. On the contrary, the lower the necessity level, the more the system benefit, indicating that the decision makers are optimistic about the expected goal, but the greater the risk of default faced. Therefore, policy makers should weigh the system benefit against the risk of default. The results show that overall satisfactory degree would increase with the increasing necessity level. When λ increases from 0.6 to 1.0, the overall satisfaction would increase from 0.501 to 0.571. The high necessity level leads to the reduced uncertainty of the objective function, the final decision result is closer to the pursuit of the respective decision level.

Figure 15.2 presents the results of different types of ecosystem service value, including carbon fixation and oxygen release (CO), climate regulation (CR), air purification (AP), water conservation (WC), sewage purification (SP), soil conservation (SC) and leisure and recreation (LR), respectively. CO and CR occupy the main position, accounting for [34.7, 35.0] % and [24.5, 25.7] % of the total ecosystem service value respectively, indicating that urban ecosystems play an important role in promoting the carbon cycle and reducing greenhouse gases. In addition, the total ecosystem service value would reduce from 19.33×10^9 RMB¥ ($\lambda = 0.6$) to 17.76×10^9 RMB¥ ($\lambda = 1.0$). It shows that the ecosystem service value would decrease as necessity level increases, but the risk of default faced would decrease, indicating the conservative attitude of decision makers.

Figure 15.3 presents the results of planning area and carbon emissions when λ equals 0.8. FR, GL, WL, WT, AL, CR and MI refer to forest, grassland, wetland, water, agricultural land, commercial and residential land, and mining and industry land, respectively. The bi-level model would plan more ecological land and less non-ecological land than single level model, mainly because the single level model only pursues the maximum economic benefit and ignores the ecological value. Bi-level

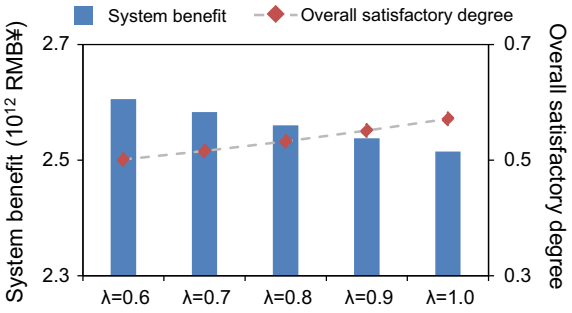

Fig. 15.1 The results of system benefit and overall satisfactory degrees

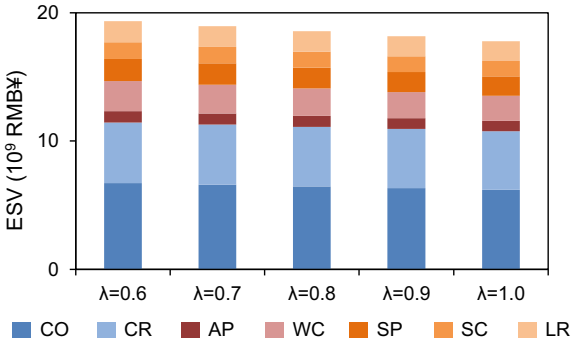

Fig. 15.2 The results of different types of ecosystem service value

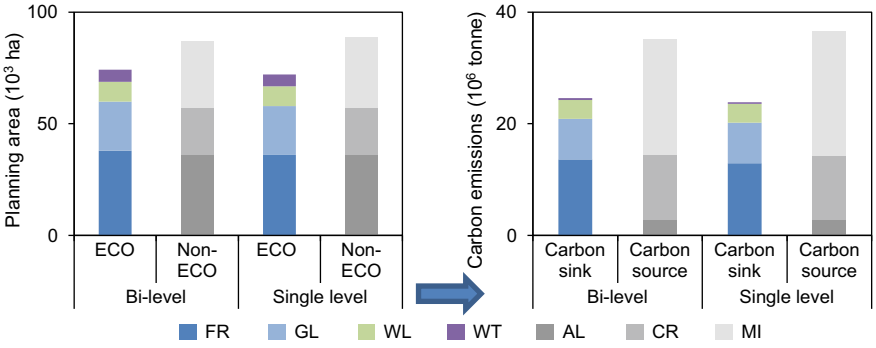

Fig. 15.3 The results of planning area and carbon emissions ($\lambda = 0.8$)

weighs the relationship between economic development and ecological protection, enabling the upper and lower layers to achieve the most satisfactory decision results. In addition, the bi-level model would have less carbon emissions than the single level model, mainly because the industrial and mining land is the main carbon source. The bi-level model reduces the planning of industrial and mining land, and the construction and protection of ecological land increase the carbon sink amount.

15.5 Conclusions

In this research, a fuzzy bi-level programming (FBP) is established for ecosystem management of Xiamen City. By solving the model, the patterns of land allocation, system benefit, ecosystem service value and carbon emission under different scenarios are obtained. Furthermore, the effects of uncertainty factors on urban ecosystems are analyzed, and trade-offs between different stakeholders are addressed

and quantified. Some findings can be obtained as follows: (i) schemes with high system benefit face the higher the risk of default, so decision makers should balance the relationship between system benefit and default risk when seeking the optimal scheme; (ii) carbon sequestration and oxygen release are the main functions of the local ecological services, which is mainly due to the high forest and grass coverage rate in Xiamen, and local decision makers should limit the blind expansion of the built-up areas and protect the ecological land; (iii) the bi-level model is more eco-friendly than single level, but the system benefit are reduced slightly, and the decision makers need to balance the relationship between ecological environment protection and economic development.

Acknowledgements This research was supported by the Start-up Project for Advanced Talent of Xiamen University of Technology in the First Half of 2022 (YKJ22011R) and the Educational and Scientific Research Project for Young and Middle-aged Teachers in Fujian Province (JAT210347).

References

Fang BW (2022) Minimizing a linear objective function under a max-overlap function fuzzy relational equation constraint. Fuzzy Sets Syst 447:1–21

Gong JW, Li YP, Lv J, Huang GH, Suo C, Gao PP (2022) Development of an integrated bi-level model for China's multi-regional energy system planning under uncertainty. Appl Energy 308:118299

Hu ZN, Wang L, Qin JD, Lev B, Gan L (2022) Optimization of facility location and size problem based on bi-level multi-objective programming. Comput Oper Res 145:105860

Lv J, Li YP, Huang GH, Nie S, Gong JW, Ma Y, Li Y (2021) Synergetic management of energy-water nexus system under uncertainty: an interval bi-level joint-probabilistic programming method. J Clean Prod 292:125942

Ma Y, Li YP, Huang GH (2020) A bi-level chance-constrained programming method for quantifying the effectiveness of water-trading to water-food-ecology nexus in Amu Darya River basin of Central Asia. Environ Res 183:109229

Pal BB, Banerjee D, Sen S (2011) The use of chance constrained fuzzy goal programming for long-range land allocation planning in agricultural system. Control Comput Inf Syst 140:174–186

Simic V (2015) Fuzzy risk explicit interval linear programming model for end-of-life vehicle recycling planning in the EU. Waste Manage 35:265–282

Yu L, Li QW, Jin SW, Chen C, Li YP, Fan YR, Zuo QT (2020) Coupling the two-level programming and copula for optimizing energy-water nexus system management-A case study of Henan Province. J Hydrol 586:124832

Zeng XT, Huang GH, Yang XL, Wang X, Fu H, Li YP, Li Z (2016) A developed fuzzy-stochastic optimization for coordinating human activity and eco-environmental protection in a regional wetland ecosystem under uncertainties. Ecol Eng 97:207–230

Zhou M (2015) An interval fuzzy chance-constrained programming model for sustainable urban land-use planning and land use policy analysis. Land Use Policy 42:479–491

Chapter 16
Energy Consumption of Cities from a Consumption-Based Perspective: A Case Study of Fujian

X. P. Chen, J. Liu, and P. P. Gao

Abstract The high rate of urbanization leads to a surge in social demand for energy. The structure of final consumption is closely related to the amount of energy consumption. In this study, the input-output method is employed to analyze the structure of final consumption and its energy consumption in nine cities of Fujian Province. The main findings are summarized as follows: (i) Xiamen (2353 persons/km^2) and Putian (690 persons/km^2) are both high population density and consumer-oriented cities, while the others are producer-oriented. (ii) The final consumption structure of cities is dominated by fixed capital formation and urban residents' consumption, followed by government consumption and rural residents' consumption, ranked last by fixed capital formation. (iii) Fuzhou and Quanzhou have the highest total consumption-based consumption. (iv) All cities belong to the type of producer-oriented energy consumption more than consumer-oriented energy consumption, and the top three are Xiamen, Fuzhou and Quanzhou.

Keywords Consumption-based accounting · Energy consumption · City · Input–output model

16.1 Introduction

Along with the rise of urbanization and economic development, energy demand becomes increasingly urgent. One of the most important features of urbanization is population change, and population change is most frequently reflected between cities. Therefore, it is necessary to study the energy consumption of cities within a single province. As far as the geographical scale is concerned, previous studies

X. P. Chen · J. Liu (✉) · P. P. Gao
School of Environmental Science and Engineering, Xiamen University of Technology, Xiamen 361024, China
e-mail: 2017000027@xmut.edu.cn

G. Huang (ed.), *Proceedings of 2022 7th International Conference on Environmental Engineering and Sustainable Development (CEESD 2022)*, Environmental Science and Engineering, https://doi.org/10.1007/978-3-031-28193-8_16

have concentrated on global (Wu and Chen 2017), national (Zhang 2020), and individual provinces (Dong et al. 2020). However, few studies have examined the energy consumption of cities.

Nowadays, using input–output method (IOM) to study energy consumption has become a widely used method (Duan and Chen 2017). Input–output analysis, also known as 'industrial linkage' analysis. Based on the input–output table, it is widely used in the study of various aspects of environmental economic system, it can reflect the relationship between various departments of the economic system (Kim et al. 2021). Fan et al. (2020) used the input–output method to study the impact of consumption activities of residents with different income levels on China's energy and water consumption from the perspective of consumers. Yongwei (2020) applies the time-input output method to reflect the diffusion process of intersectoral effects of energy consumption.

When calculating the greenhouse gas emissions, two aspects need to be given consideration, one is based on production accounting (PBA) and the other is based on consumption accounting (CBA) (Liu et al. 2018). Therefore, the producer-oriented and consumer-oriented of energy consumption are introduced. In Zheng's study, PBA, as a producer, which counts carbon emissions, generates from domestic production in production process, in which includes exports (Zheng et al. 2021). According to Zhong's study, CBA acquires the total carbon emissions for the final goods, which comprises imports, of which the duty of carbon emissions is attributed to the consumer (Zhong 2021). Although PBA has its advantages, it does not take the final destination and final consumer of goods and services into consideration.

The purpose of this study is to explore the final consumption structure and the energy consumption caused by the final consumption structure in nine cities of Fujian Province. The model can analyze the energy demand of each specific city and find out the causes of energy consumption in each city.

16.2 Methodology and Data

16.2.1 Methodology

To evaluate consumption-based energy consumption at the city level, First, the energy intensity of each city is calculated first:

$$\partial_i = \frac{e_i}{X_i} \tag{16.1}$$

where e_i is the energy consumed by the i city, X_i represents the total output of city i. ∂_i indicates the intensity of energy consumption in the i city.

Secondly, this study adopts the Leontief equation to calculate CBA caused by the final demand of each city. According to Mi's study on the relationship of "local

production emissions + import emissions (domestic and foreign) = CBA" and "local production emissions + export emissions (domestic and foreign) = PBA" (Mi et al. 2019), the calculation of consumer-oriented energy is the local energy consumption plus the E_i^{IM}, and the calculation of consumer-oriented energy is the local energy consumption plus the E_i^{EX}:

$$E_i^{RC} = \partial^{\text{diag}}(I - A)^{-1} Y_{\text{i}}^{RC} \tag{16.2}$$

$$E_i^{UC} = \partial^{\text{diag}}(I - A)^{-1} Y_i^{UC} \tag{16.3}$$

$$E_i^{GC} = \partial^{\text{diag}}(I - A)^{-1} Y_i^{GC} \tag{16.4}$$

$$E_i^{FC} = \partial^{\text{diag}}(I - A)^{-1} Y_i^{FC} \tag{16.5}$$

$$E_i^{IC} = \partial^{\text{diag}}(I - A)^{-1} Y_i^{IC} \tag{16.6}$$

$$E_i^{IM} = \partial^{\text{diag}}(I - A)^{-1} Y_i^{IM} \tag{16.7}$$

$$E_i^{EX} = \partial^{\text{diag}}(I - A)^{-1} Y_i^{EX} \tag{16.8}$$

where ∂^{diag} represents the diagonal matrix of energy consumption intensity. $(I-A)^{-1}$ is the Leontief matrix, I is a $n \times n$ identity matrix; A is the direct requirement matrix of input–output table in i city. $Y_{\text{i}}^{RC}, Y_i^{UC}, Y_i^{GC}, Y_i^{FC}, Y_i^{IC}, Y_i^{IM}, Y_i^{EX}$ are the diagonal matrix of urban residents' consumption, rural residents' consumption, government consumption, fixed capital formation, inventory change, import and export of city i, respectively. Correspondingly, E_i^{RC}, E_i^{UC}, E_i^{GC}, E_i^{FC}, E_i^{IC}, E_i^{IM}, E_i^{EX} refer to the energy consumption caused by urban residents' consumption, rural residents' consumption, government consumption, fixed capital formation, inventory change, import and export of city i.

16.2.2 Data Sources

The input–output table of 9 cities is derived from the statistics bureau of each city in Fujian Province. For example, the 2017 input–output table of Fuzhou is obtained from the Fuzhou statistics bureau. Energy consumption is obtained from the 2018 Fujian Statistical Yearbook. The population and land area of each city are obtained from the 2018 Statistical Yearbook of each city.

16.3 Result and Discuss

16.3.1 Consumption-Based Economic Structure Analysis for 9 Cities in Fujian Province

For the purpose of a comprehensive analysis of the consumption structure for 9 cities in Fujian Province, it is carried out from three parts: (i) population density (ii) composition of final consumption (iii) GDP and import/export analysis. Figure 16.1 shows the socio-economic analysis for nine cities in Fujian Province in 2017. In terms of population density, Xiamen ranked first (2353 persons/km^2), followed by Putian (690 persons/km^2) and Quanzhou (673 persons/km^2). Xiamen not only has a small geographical area, but also has a population in-migration rate of 56.4% in 2017 relative to 2016, which leads to a higher population density than others. Putian is ranked second because it covers an area of only 4.2 × 103 km^2, but has a population of 2.9 million as Sanming. Quanzhou ranks third due to having the largest population compared to others.

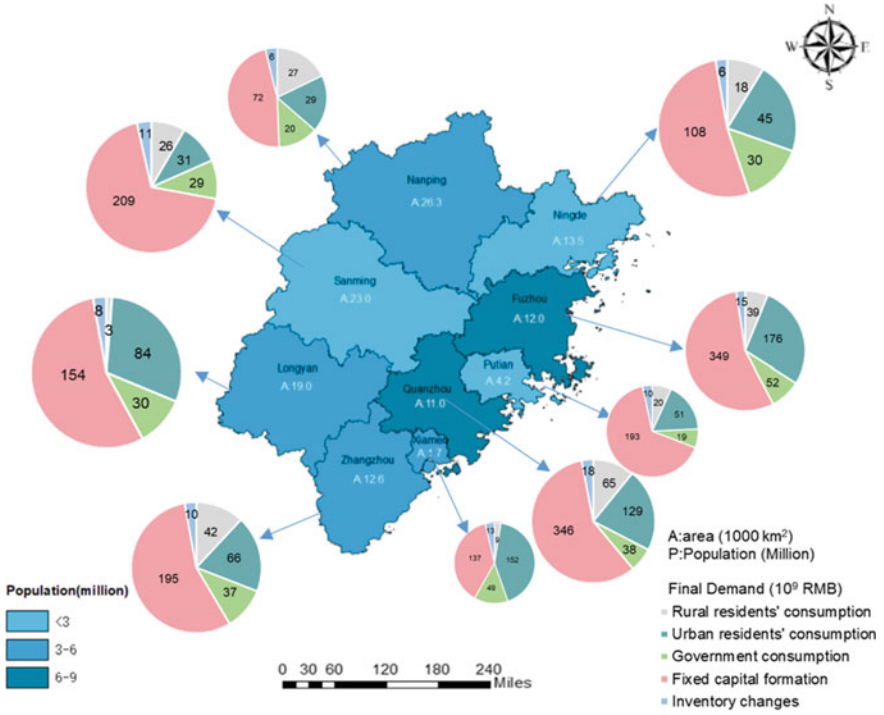

Fig. 16.1 Socio-economic analysis for nine cities in Fujian province in 2017

In terms of final consumption, it is divided into rural residents' consumption, urban residents' consumption, government consumption, fixed capital formation and inventory change, respectively. Except for Xiamen, the final consumption share of other cities is: fixed capital formation > urban residents' consumption > rural residents' consumption > government consumption > inventory change or fixed capital formation > urban residents' consumption > government consumption > rural residents' consumption > inventory change. The discrepancies caused by the different urbanization proportion of each city. For Xiamen, the order of its final consumption from high to low is: urban residents' consumption > fixed capital formation > government consumption > inventory change rural residents' consumption. The reason for the phenomenon is that Xiamen not only has a highly modernized infrastructure, but also has the highest urbanization rate (89.1%) and urban per capita consumption (32,009 yuan) in the city.

In terms of GDP and import/export analysis for 9 cities in Fujian Province in 2017, it can be seen in Fig. 16.2. The top three cities with the highest GDP are Quanzhou, Fuzhou and Xiamen. When the sum of exports and local outflow is greater than that of imports and local inflow, it is called a producer -oriented city; otherwise, it is called a consumer -oriented city. Fujian Province is located on the coast, most of the cities are producer -oriented cities, except Xiamen and Putian. Compared with other cities, Xiamen and Putian are both cities with large population density and few manufacturing industries. Therefore, they are consumer -oriented cities.

In short, Xiamen and Putian are both high population density and consumer-oriented cities; while the others are producer-oriented. The final consumption structure of cities is dominated by fixed capital formation and urban residents' consumption, followed by government consumption and rural residents' consumption, ranked last by fixed capital formation.

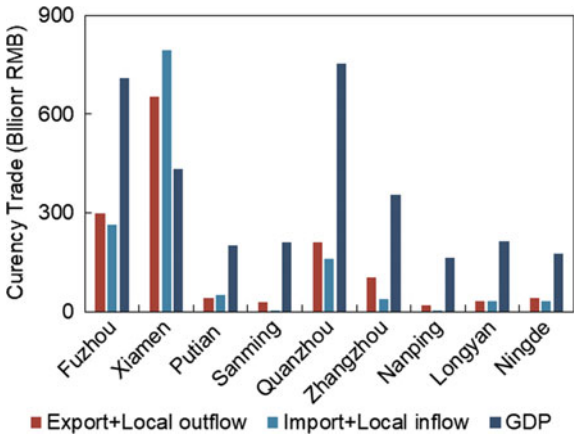

Fig. 16.2 Gross Domestic Product (GDP) and import/export analysis for 9 cities in Fujian Province in 2017

16.3.2 Consumption-Based Accounting of Energy Consumption for 9 Cities in Fujian Province

Figure 16.3 shows consumption-based energy consumption for final demand for 9 cities in Fujian in 2017. Fuzhou and Quanzhou have the highest total energy consumption, and they have similar development patterns, which place more emphasis on the development of industry (i.e. manufacturing) and construction, and agriculture has the smallest share of GDP. Since Nanping has the lowest urbanization rate (35.1%) and few industries in comparison with other cities, it consumes the least amount of energy. For energy consumption for final demand, the largest proportion of energy consumption is fixed capital formation, followed by urban residents' consumption. The energy consumption generated by capital formation is mainly used for building construction, machinery manufacturing, etc. Energy consumption by urban residents is mainly consumed for clothing, food, housing and transportation, etc.

As displayed in Fig. 16.4, the consumer-oriented energy consumption and producer-oriented energy consumption for 9 cities can be presented. The difference between consumer-oriented and producer-oriented energy consumption in Fujian Province is mainly determined by the geographical location and energy consumption intensity. All cities belong to the type of producer-oriented energy consumption more than consumer-oriented energy consumption. This is because Fujian Province is originally a major export province, with exports reaching RMB 711 billion and imports reaching RMB 447 billion in 2017. Consumer-based and producer-based energy consumption ranked in the top three are Xiamen, Fuzhou and Quanzhou. From Fig. 16.1, they are all coastal cities, which provides a geographical advantage for import and export. Moreover, they have high population density, both have

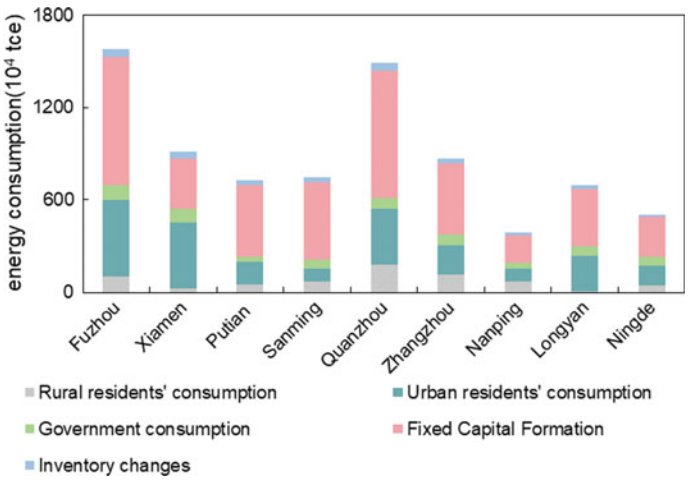

Fig. 16.3 Consumption-based energy consumption for final demand for 9 cities in Fujian in 2017

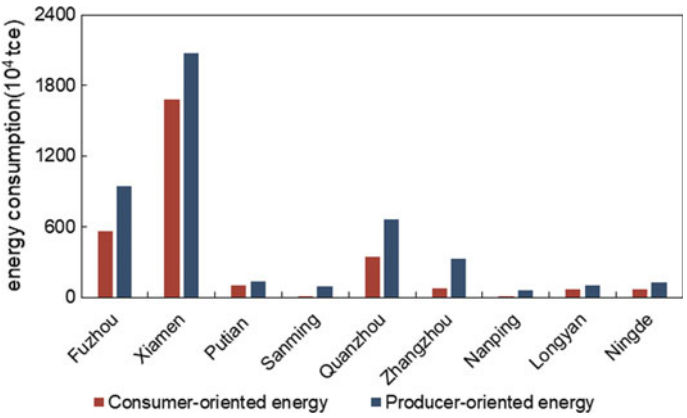

Fig. 16.4 Analysis of consumer-oriented energy consumption and producer-oriented energy consumption for 9 cities in Fujian in 2017

urbanization rates of over 50%, and the per capita living consumption expenditure of urban residents has reached 26,000 RMB.

In general, Fuzhou and Quanzhou have the highest total consumption-based consumption. For energy consumption for final demand, the largest proportion of energy consumption is fixed capital formation, followed by urban residents' consumption. All cities belong to the type of producer-oriented energy consumption more than consumer-oriented energy consumption, and the top three are Xiamen, Fuzhou and Quanzhou.

16.4 Conclusion

This study uses the input–output table of 9 cities in 2017 to calculate the final consumption structure of each city and analyze its energy consumption structure. It reveals the economic development, final consumption structure, and imports and exports of each city. Moreover, it analyzes the energy consumption caused by final consumption in each city and divides the energy consumption into producer- oriented and consumer-oriented.

Acknowledgements This work was supported by the Youth Program of Fujian Provincial Social Sciences Foundation of China (FJ2020C010).

References

Dong Y et al (2020) Aggravation of reactive nitrogen flow driven by human production and consumption in Guangzhou City China. Nat Commun 11(1):1209

Duan CC, Chen B (2017) Energy-water nexus of international energy trade of China. Appl Energy 194:725–734

Fan JL, Chen KY, Zhang X (2020) Inequality of household energy and water consumption in China: an input-output analysis. J Environ Manag, 269

Kim Y-J, Lee S-G, Trimi S (2021) Industrial linkage and spillover effects of the logistics service industry: an input–output analysis. Serv Bus 15(2):231–252

Liu L et al (2018) Environmentally-extended input-output simulation for analyzing production-based and consumption-based industrial greenhouse gas mitigation policies. Appl Energy 232:69–78

Mi Z et al (2019) Carbon emissions of cities from a consumption-based perspective. Appl Energy 235:509–518

Wu XF, Chen GQ (2017) Global primary energy use associated with production, consumption and international trade. Energy Policy 111:85–94

Yongwei C et al (2020) Using a temporal input-output approach to analyze the ripple effect of China's energy consumption. Energy, 211

Zhang Y et al (2020) The impacts of interprovincial electricity transmission on China's water crisis: mitigate or aggravate. J Clean Prod, 266

Zheng X et al (2021) Development of a factorial water policy simulation approach from production and consumption perspectives. Water Res 193:116892

Zhong W, et al (2021) Evolving household consumption-driven industrial energy consumption under urbanization: a dynamic input-output analysis. J Clean Prod, 289

Chapter 17
Analysis of Sectoral Linkages of Carbon Emissions in Fujian Province Using an Absolute Weighted Analysis

Z. M. Sun, J. Liu, and X. Li

Abstract The realization of China's low carbonization depends on the joint efforts of all provinces. As China's first ecological civilization pilot zone, Fujian should contribute to carbon emission reduction. This paper employs the absolute weighted analysis method (AWA) to calculate carbon-based backward and forward linkage in Fujian in 2017. AWA can analyze the linkages between sectors and identify the important sectors of carbon dioxide emissions. Main findings can be summarized as: (i) The weighted carbon based back link (WCBBL) and The Weighted carbon based forward link (WCBFL) of Mental and nonmetal products industry (MAN) Both are greater than 1, indicating that MAN plays a key role in both the production and demand sides of carbon dioxide emissions. (ii) The energy conversion accounts for a large proportion of demand-side carbon dioxide emissions, and carbon-based backward linkage is enhanced. Empirical analysis shows that economic-industry linkage has a significant impact on carbon-based industrial linkage. Therefore, in the context of low carbonization, promoting the development and utilization of renewable energy is the key to Fujian's carbon dioxide emissions. At the same time, we need to strengthen technological innovation, which is the key to industrial upgrading.

Keywords Absolute weighted analysis · Sectoral linkage · Carbon emission

Z. M. Sun · J. Liu (✉)
Fujian Engineering and Research Center of Rural Sewage Treatment and Water Safety, School of Environmental Science and Engineering, Xiamen University of Technology, Xiamen 361024, China
e-mail: zyljing@126.com

X. Li
School of Film Television and Communication, Xiamen University of Technology, Xiamen 361024, China

G. Huang (ed.), *Proceedings of 2022 7th International Conference on Environmental Engineering and Sustainable Development (CEESD 2022)*, Environmental Science and Engineering, https://doi.org/10.1007/978-3-031-28193-8_17

17.1 Introduction

Greenhouse gases produced by anthropogenic economic activities are widely considered to be the main reason of unusual changes in climate. In 2021, global greenhouse gas emissions reached 59 billion tons. China needs to make greater efforts to reduce carbon emissions. Fujian, as a province with low total carbon emissions and low intensity, takes Fujian as an example to study the sectoral linkage of carbon emission. As product value chains become more complex, carbon flows are more harder to track. In this context, exploring carbon linkages between industrial sectors can find important factors of CO_2 emissions in the economic sectors (Zhao et al. 2016).

sectoral linkage analysis can analyze linkages between industrial sectors (Yang and Zheng 2014). It is divided into backward linkage and forward linkage. Wen and Wang (2019) calculated carbon-based linkages across different industries in China, but did not consider industry size (Wen and Wang 2019). We use the absolute weighted analysis (AWA) of industrial linkage because Fujian has great development in industrial scale and high degree of industrial correlation, forming a complete and developed economic system (Xu et al. 2017). Our study can give evidence to help Fujian reconsider the impact of industrial linkages on carbon dioxide emissions from economic sectors.

17.2 Methodology

17.2.1 AWAM of Sectoral Linkage

The analysis of sectoral linkage is completed after adjustment of the input–output table (IOT) (Lin and Sun 2010). Set the economy to have n sectors, $\mathbf{Z}$ is a intermediate flows matrix. $\mathbf{x}$ and $\mathbf{y}$ represent the total output and final demand, respectively. $\mathbf{v}$ is a The added-value matrix.

$$x = (I - A)^{-1} y \tag{17.1}$$

$$c' Z = x' B + v = x' \tag{17.2}$$

$\mathbf{A} = \mathbf{Z}(\mathbf{X})^{-1}$ represents the technological coefficient matrix. $\mathbf{c}$ is the column vector of $n \times 1$, we can get $\mathbf{Xc} = \mathbf{x}$. $(\mathbf{I}\text{-}\mathbf{A})^{-1}$ is the input matrix of the full demand coefficient, which represents the inverse of the Leontief matrix, denoted by $\mathbf{L}$ (Leontief 1936). $\mathbf{B} = (\mathbf{X})^{-1}\mathbf{Z}$ represents the distribution coefficient matrix. $(\mathbf{I}\text{-}\mathbf{B})^{-1}$ is the the integral supply coefficient matrix, which represents the inverse matrix of Ghosh matrix, denoted by $\mathbf{G}$ (Augustinovics 1970).

We calculate weighted backward linking (WBL) by the weight of the final demand. Weighted forward linking (WFL) is calculated by the weight of the added value. The

computational expressions of WBL and WFL are expressed as:

$$WBL = \frac{YL'c}{c'x/n} \tag{17.3}$$

$$WFL = \frac{VGc}{c'x/n} \tag{17.4}$$

Therefore, if the WBL of an industry is greater than 1, it means that the demand-pulling effect of this industry is bigger than the average impact of all sectors. If the WFL of an industry is bigger than 1, it represents that the supply-pull effect of that industry is bigger than the average effect of all industries.

Direct carbon intensity is the total carbon dioxide emitted per unit of output. The direct carbon intensities of n economic sectors are defined by the matrix CI. The weighted carbon based back link (WCBBL) and The Weighted carbon based forward link (WCBFL) are shown below:

$$eefd = Y' \cdot L' \cdot CI \tag{17.5}$$

$$eeva = V \cdot G \cdot CI \tag{17.6}$$

$$WCBBL = \frac{EEFD \cdot L' \cdot c}{c' \cdot EEFD \cdot L' \cdot c/n} \tag{17.7}$$

$$WCBFL = \frac{EEVA \cdot G \cdot c}{c' \cdot EEVA \cdot G \cdot c/n} \tag{17.8}$$

A sector's WCBBL can be used to analyze the carbon dioxide emissions contained in the required inputs for all sectors to average the final net demand for that sector. The WCBFL of a sector can be used to analyze the CO_2 emissions contained in intermediate inputs from that sector to all sectors to calculate the average value added from that sector. Therefore, a sector's WCBBL bigger than 1 means that the sector will significantly promote the implied carbon dioxide emissions on the demand side. Then the WCBFL of a sector is bigger than 1, which means that the sector is an important sector of implied carbon dioxide emissions from the production side (Sun et al. 2020).

17.3 Case Study

17.3.1 Data Sources

The Fujian input–output table in this study was obtained from the National Bureau of Statistics of China, and the carbon emissions of various industries were obtained from Carbon Emission Accounts and Datasets (CEADs). We have re-divided the original sectors in the input–output table into new 17 sectors, which are: Agriculture (AGR), Mining (MIN), Petroleum processing coking and nuclear fuel processing industry (PRC), Woodworking industry (WPF), Paper and printing industry (PMP), Food and tobacco processing industry (FTP), Construction industry (CON), Accommodation catering industry (ACC), Machinery and transport equipment manufacturing industry (MTP), Mental and nonmetal products industry (MAN), Chemical products industry (CPI), Wholesale and retail transportation and warehousing industry (WRT), Material and energy conversion (MEC), Electrical industry (ELM), Textile industry (TEX), Other manufacturing industry (OMA) and Other service industry (OSE).

17.4 Results and Discussions

17.4.1 Cross Analysis

WCBBL and WCBFL calculated carbon-based backward and forward sectoral linkages. The top three WCBBL sectors and the top four WCBFL sectors in Fujian Province are defined by the 2017 calculation results (see Figs. 17.1 and 17.2).

The WCBL of MEC is significantly higher than that of other sectors. In 2017, the MEC achieved a WCBL of 11.49, which represents the CO_2 emissions required for net final demand in this sector far exceeding those of other sectors. At the same

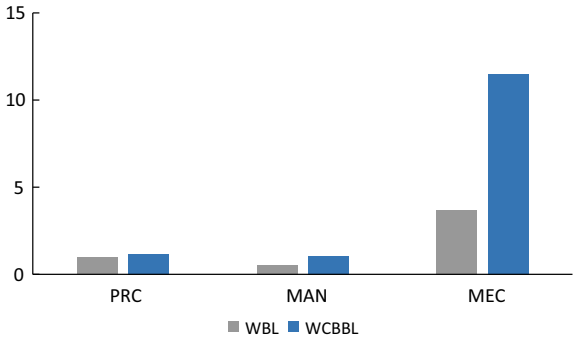

Fig. 17.1 WCBBL and WBL of the top three sectors with the highest WCBBL in 2017

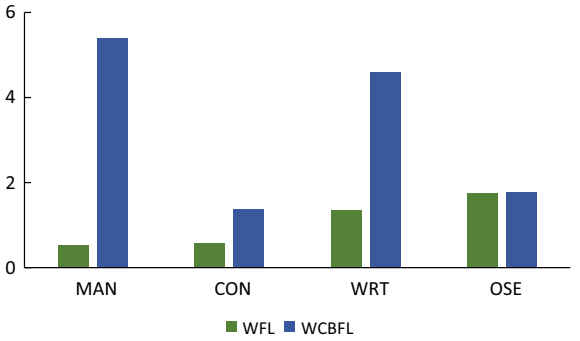

Fig. 17.2 WCBFL and WFL of the top four sectors with the highest WCBFL in 2017

time, the WCBBL of MAN and PRC is also greater than 1, which means that the CO_2 emissions of these three sectors are significantly higher than the average level in terms of demand. It can be found that resource sector have a significantly high carbon based forward link. Among these three sectors, only the WBL of MEC is greater than 1, which means that MEC has a great role in promoting the development of Fujian.

There were 4 sectors with WCBFL greater than 1, of which the WCBFL of MAN and WRT were 5.39 and 4.61, respectively, indicating that the carbon dioxide used for intermediate input in these two sectors was much higher than that of other sectors, and the WCBFL of CON and OSE was also greater than 1, these four sectors are all important emission sectors on the supply side, accounting for a large amount of carbon dioxide emissions on the supply side. It is worth noting that in 2017, only one sector of MAN in Fujian had WCBBL and WCBFL greater than 1 at the same time, which represents that the main driving factors of carbon dioxide emissions in Fujian are very different from the consumption side and the production side.

17.5 Conclusion

This paper uses AWA to analysis carbon-based sectoral linkages. WCBBL represents an important sector that reflects specific carbon dioxide emissions on the demand side, and WCBFL represents an important emitting sector on the production side.

The following conclusions are drawn by comparing the relationship between WCBBL and WCBFL and carbon dioxide emissions in various sectors. First, the development of renewable energy should continue. Strengthening the development of all kinds of renewable energy is an urgent matter to change the energy structure and reduce the carbon dioxide emission on the supply side. Secondly, improving the production structure is the top priority to develop the high efficiency and high quality of the production side. It is necessary to further deepen the production side reform. The above findings can lead to effective CO_2 reductions.

Acknowledgements This work was supported by the Youth Program of Fujian Provincial Social Sciences Foundation of China (FJ2020C010).

References

Augustinovics M (1970) Methods of international and intertemporal comparison of structure. Contrib Input-Output Anal 1:249–269

Leontief WW (1936) Quantitative input and output relations in the economic systems of the United States. Rev Econ Stat, 105–125

Lin B, Sun C (2010) Evaluating carbon dioxide emissions in international trade of China. Energy Policy 38(1):613–621

Sun CW, Chen LY, Xu YH (2020) Industrial linkage of embodied CO_2 emissions: evidence based on an absolute weighted measurement method. Resour Conserv Recycl 160:104892

Wen W, Wang Q (2019) Identification of key sectors and key provinces at the view of CO_2 reduction and economic growth in China: linkage analyses based on the MRIO model. Ecol Ind 96:1–15

Xu X, Mu M, Wang Q (2017) Recalculating CO_2 emissions from the perspective of value-added trade: an input-output analysis of China's trade data. Energy Policy 107:158–166

Yang C, Zheng Z (2014) Analysis of the theoretical Issues on the measurement of industrial linkage. Stat Res 31(12):11–19

Zhao X, Liu C, Sun C, Yang M (2016) Does stringent environmental regulation lead to a carbon haven effect? Evidence from carbon-intensive industries in China. Energy Econ 86(2):104631

Chapter 18
A Structural-Path-Analysis Input–Output Model for Carbon Emission Policy Simulation in Fujian Province

T. C. Cai, J. Liu, and X. Li

Abstract The high-speed economic development and urbanization have brought overhigh carbon emissions. In this study, a structural-path-analysis input–output model (SIOM) is formulated by combining the input output model (IOM) with structural path analysis (SPA) to simulate the effects of carbon emission reduction policies from the angles of final demand and industrial technology improvement. The main results are: (i) By the results of SPA, seven sectors are identified to investigate the effects of reducing carbon emissions under various policies. (ii) the simulation results show that ITI (industrial technology improvement policy) applied to ESW (Production and Supply sector of Electric Power, Steam, and Hot Water) and FD (final demand policy) applied to Con (Construction) have the best effect on carbon emission reduction. The research results can help the government to formulate more reasonable carbon emission policies.

Keywords Carbon emission · Input output model · Structural path analysis

18.1 Introduction

Global warming and climate change are the results of rising carbon emissions (Ali 2018). Carbon emissions are out of control, which endangers not just the world's sustainable development capacity but also the existence and progress of humanity (Wang et al. 2019).

T. C. Cai · J. Liu (✉)
Fujian Engineering and Research Center of Rural Sewage Treatment and Water Safety, School of Environmental Science and Engineering, Xiamen University of Technology, Xiamen 361024, China
e-mail: zyljing@126.com

X. Li
School of Film Television and Communication, Xiamen University of Technology, Xiamen 361024, China

G. Huang (ed.), *Proceedings of 2022 7th International Conference on Environmental Engineering and Sustainable Development (CEESD 2022)*, Environmental Science and Engineering, https://doi.org/10.1007/978-3-031-28193-8_18

Leontief proposed an input–output model (IOM), which can use the input output table to calculate physical flows among the sectors (Leontief 1936). Structural path analysis (SPA) is used to uncover the main transmission pathways and sectors in complex networks. Therefore, Many environmental studies employ SPA to gain a better understanding of environmental problems (Jia et al. 2019). However, SPA is rarely used for CO_2 research in Fujian Province.

This study investigates carbon emissions in Fujian Province, identifies key sectors, and simulates the impacts of different policies on key sectors to reduce carbon emissions. The results will provide some suggestions for policymakers.

18.2 Methodology and Data

18.2.1 Structural Path Analysis

Structural path analysis is a useful tool that measures the direct environmental transmission from the upstream sector to the downstream sector. By following the intricate production process, it also identifies the pathway with the greatest environment protection (Feng et al. 2019). The total carbon emissions flow among sectors at various production layers (PL) can be acquired by the following formula (18.1a–c):

$$C_{ji}^{1\to 0} = \varepsilon_j \mathbf{A}_{ji} d_i \tag{18.1-a}$$

$$C_{kj}^{2\to 1} = \varepsilon_k \mathbf{A}_{kj} \mathbf{A}_{j:} \mathbf{D} \tag{18.1-b}$$

$$C_{lk}^{3\to 2} = \varepsilon_l \mathbf{A}_{lk} \mathbf{A}_{k:} \mathbf{A} \mathbf{D} \tag{18.1-c}$$

where ${C_{ji}}^{1\to 0}$ denotes the CO_2 stream from PL^1 to PL^0 among sectors. ${C_{kj}}^{2\to 1}$ denotes the CO_2 stream from PL^2 to PL^1 among sectors. ${C_{lk}}^{3\to 2}$ denotes the CO_2 stream from PL^3 to PL^2 among sectors.

18.2.2 Policy Simulation

When simulating industrial technology improvement policy (ITI) on a sector, the technical coefficient of the sector should be reduced. If the final demand does not change, the total output and economic flow of various sectors will change (Zheng et al. 2021). Therefore, the direct, indirect, and total carbon emissions can be acquired through Eqs. (18.2)–(18.8):

$$a_{mn}^{\mathrm{I}} = a_{mn} \times \alpha_{mn} \tag{18.2}$$

$$\mathbf{X}^{\mathrm{I}} = [\mathbf{I} - \mathbf{A}^{\mathrm{I}}]^{-1}\mathbf{D} \tag{18.3}$$

$$\mathbf{Z}^{\mathrm{I}} = \mathbf{X}^{\mathrm{I}}\mathbf{A}^{\mathrm{I}} \tag{18.4}$$

$$DC_i^{\mathrm{I}} = \begin{cases} DC_i \times \frac{x_i^{\mathrm{I}}}{x_i} & i \neq n \\ DC_i \times \frac{x_i^{\mathrm{I}}}{x_i} \times \alpha_{mn} \times \frac{IC_{mn}}{IC_{.n}} & i = n \end{cases} \tag{18.5}$$

$$\varepsilon^{\mathrm{I}} = \mathbf{DC}^{\mathrm{I}}[\mathbf{X}^{\mathrm{I}} - \mathbf{Z}^{\mathrm{I}}]^{-1} \tag{18.6}$$

$$\mathbf{IC}^{\mathrm{I}} = \varepsilon^{\mathrm{I}}\mathbf{Z}^{\mathrm{I}} \tag{18.7}$$

$$\mathbf{TC}^{\mathrm{I}} = \mathbf{DC}^{\mathrm{I}} + \mathbf{IC}^{\mathrm{I}} \tag{18.8}$$

where α_{mn} represents the degree of technical coefficient change; $a^{\mathrm{I}}{}_{mn}$ represents the technical coefficient between m and n after applying ITI; $\mathbf{A}^{\mathrm{I}}$, $\mathbf{X}^{\mathrm{I}}$, and $\mathbf{Z}^{\mathrm{I}}$ represent the technology coefficient matrix, total output matrix, and monetary flow matrix after applying ITI; $\mathbf{DC}^{\mathrm{I}}$, $\mathbf{IC}^{\mathrm{I}}$, and $\mathbf{TC}^{\mathrm{I}}$ represent direct, indirect, total carbon emission after applying ITI.

When the final demand policy (FD) is applied to a sector, the final demand of the sector should be reduced, thus leading to changes in the total output and monetary flow of various sectors. If the technical coefficient remains unchanged, the direct carbon emissions of a sector will be reduced by the same extent as the total output (Liu et al. 2018). So the direct, indirect, and total carbon emissions can be obtained through (18.9)–(18.15):

$$\mathrm{d}_{\mathrm{n}}^{\mathrm{d}} = \mathrm{d}_{\mathrm{n}} \times \beta_{\mathrm{n}} \tag{18.9}$$

$$\mathbf{X}^{\mathrm{d}} = [\mathbf{I} - \mathbf{A}]^{-1}\mathbf{D}^{\mathrm{d}} \tag{18.10}$$

$$\mathbf{Z}^{\mathrm{d}} = \mathbf{X}^{\mathrm{d}}\mathbf{A} \tag{18.11}$$

$$DC_i^{\mathrm{d}} = DC_i \times \frac{x_i^d}{x_i} \tag{18.12}$$

$$\varepsilon^{\mathrm{d}} = \mathbf{DC}^{\mathrm{d}}[\mathbf{X}^{\mathrm{d}} - \mathbf{Z}^{\mathrm{d}}]^{-1} \tag{18.13}$$

$$\mathbf{IC}^{\mathrm{d}} = \varepsilon^{\mathrm{d}}\mathbf{Z}^{\mathrm{d}} \tag{18.14}$$

$$\mathbf{TC}^{\mathrm{d}} = \mathbf{DC}^{\mathrm{d}} + \mathbf{IC}^{\mathrm{d}} \tag{18.15}$$

18.2.3 Data Sources

In this study, the Fujian input–output table is from the National Bureau of Statistics of China, and the carbon emissions of various sectors are from carbon emission accounts and datasets (CEADs). There are 42 sectors in the original input–output table. According to the characteristics of industries, 42 sectors are merged into 21 sectors.

18.3 Result and Discussion

18.3.1 Structural Path Analysis

Figure 18.1 represents carbon emission flow in various production layers. The carbon emission flow is displayed in the graph from left to right. Since the carbon flows of NP, ESW, and MP in low PL primarily originate from themselves in high PL, it is likely that they may lower their carbon emissions by enhancing their production methods. The carbon emissions of Ser, Con, and Equ in PL^0 are much larger than the carbon emissions in high PL, denoting large carbon flows from other sectors in high PL to these sectors in PL^0. On the contrary, the carbon emissions of ESW, Tra, NP, and MP in high PL are much higher than the carbon emissions in PL^0. Therefore, seven key sectors including Ser, Con, Equ, ESW, MP, NP, and Tra are selected to simulate the impacts of the various policies.

18.3.2 Policy Simulation Analysis

S1 to S14 represent the scenarios of ITI and FD application in Ser, Con, Equ, ESW, MP, NP, and Tra respectively. The variation of the carbon emissions in different sectors under various policies is shown in Fig. 18.2. For the application of ITI, S4 (29.12×10^6 ton, 108.07×10^6 ton, and 137.20×10^6 ton, respectively) ranks at the top with the changes in carbon emissions, denoting that the application of ITI on ESW has a good performance in the carbon emission reduction effect, while S5 (11.12×10^6 ton, 19.82×10^6 ton, and 30.94×10^6 ton, respectively) has the smallest changes. From the results of FD, the application of FD on Con can maximize carbon emission reduction. This is because S9 (21.12×10^6 ton, 42.46×10^6 ton, and 63.59×10^6 ton, respectively) can largely decrease direct, indirect, and total carbon emissions. In addition, carbon emissions drop a small degree in S11 (12.12×10^6 ton, 17.85×10^6 ton, and 29.98×10^6 ton, respectively), indicating that the ITI has a better performance on ESW than the FD on it. Therefore, the applications of ITI on ESW (S4) and FD on Con (S9) have the best effect on carbon emission reduction.

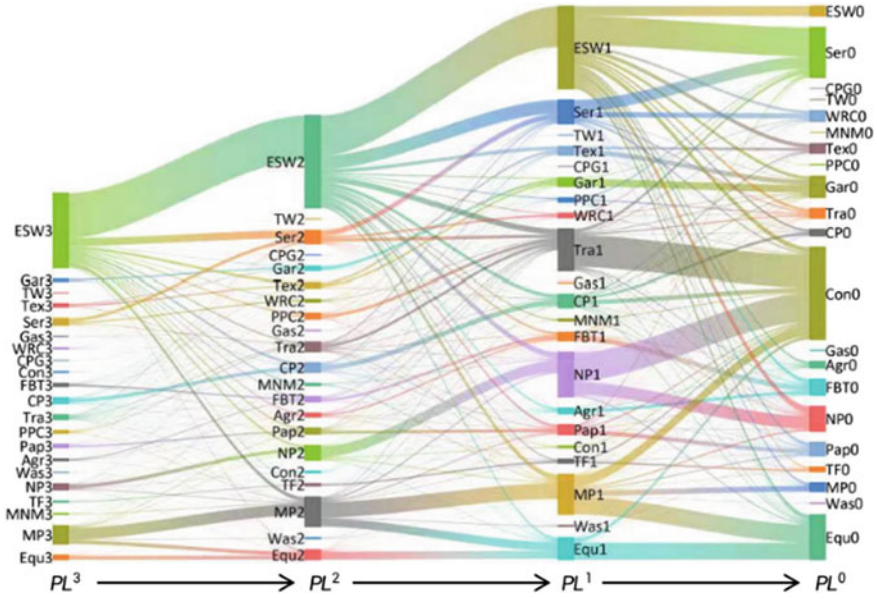

Fig. 18.1 CO_2 paths among sectors in 2017

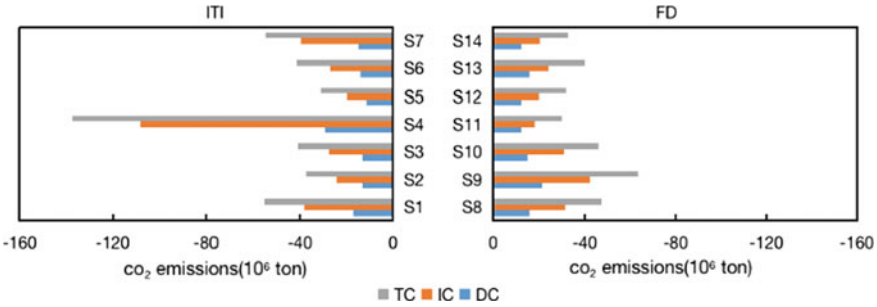

Fig. 18.2 CO_2 changes under different scenarios

18.4 Conclusion

In this study, SIOM is developed by combining input output model with structural path analysis to simulate the impacts of carbon reduction policy from the angles of final demand and industrial technology improvement. SIOM has been used in Fujian province, China. The key findings and conclusions are as follows: (i) According to the results of the SPA, seven sectors including Ser, Con, Equ, ESW, MP, NP, and Tra are identified to investigate the effects of reducing carbon emissions under various policies. (ii) From the application of ITI, S4 has the largest reduction in carbon emissions, indicating that ITI applied to ESW has the best carbon emission reduction

effect. (iii) From the results of FD, the application of FD on Con can maximize carbon emission reduction. This is because S9 can largely decrease direct, indirect, and total carbon emissions. These findings can help the government formulate more reasonable carbon emission policies.

Acknowledgements This work was supported by the Youth Program of Fujian Provincial Social Sciences Foundation of China (FJ2020C010).

References

Ali G (2018) Climate change and associated spatial heterogeneity of Pakistan: empirical evidence using multidisciplinary approach. Sci Total Environ 634:95–108

Feng CY, Qu S, Jin Y et al (2019) Uncovering urban food-energy-water nexus based on physical input-output analysis: the case of the Detroit Metropolitan Area. Appl Energy 252:9

Jia NF, Gao XY, Liu DH et al (2019) Identification and evolution of critical betweenness sectors and transactions from the view of CO_2 reduction in supply chain network. J Clean Prod 232:163–173

Leontief WW (1936) Quantitative input and output relations in the economic systems of the United States. Rev Econ Stat, 105–125

Liu L, Huang G, Baetz B et al (2018) A factorial ecologically-extended input-output model for analyzing urban GHG emissions metabolism system. J Clean Prod 200:922–933

Wang W, Zhou C, Li X (2019) Carbon reduction in a supply chain via dynamic carbon emission quotas. J Clean Prod 240:118244.1–118244.12

Zheng XG, Huang GH, Li JY et al (2021) Development of a factorial water policy simulation approach from production and consumption perspectives. Water Res 193:17

Chapter 19
Assessment of Climate and Land Use/Cover Change Impacts on Watershed: A Multi-model Ensemble Runoff Simulation Method

Z. P. Xu, Y. P. Li, and G. H. Huang

Abstract Changes in land use/cover and climate could significantly affect hydrological processes of watersheds. In this study, a multi-model ensemble runoff simulation (MERS) approach is developed, which incorporates input data simulated by the CA–Markov model and GCM into the hydrological model (SWAT). The method can not only forecast runoff processes under the influences of land use/cover change (LUCC) and climate change and obtain the possible range of future runoff, but also evaluate the main factors affecting the runoff process in the study area. Then, the method is applied to simulate runoff results under 48 different climate change and LUCC scenarios in the upper basin of Amu Darya River in Central Asia. The results indicate that: (i) the annual average runoff would decrease by 43.33–80.99 m^3/s in the future period (2025–2055); (ii) compared with LUCC, climate change is the main contributor to variations in hydrological processes, and its contribution is 83.35–99.00%; (iii) the rising temperature would lead to the reduction of the glacier area, which would further affect the runoff process.

Keywords Climate change · LUCC · SWAT model

19.1 Introduction

Climate change and land use/cover change (LUCC) are the two most important factors influencing hydrological processes (Shi et al. 2013). Climate change directly affects the hydrological cycle and runoff process of the basin, and LUCC caused by human activities also changes the underlying surface conditions and the distribution process of hydrological cycle (Yifru et al. 2021). The separate and joint effects of

Z. P. Xu · Y. P. Li (✉) · G. H. Huang
Center for Energy, Environment and Ecology Research, School of Environment, Beijing Normal University, Beijing 100875, China
e-mail: yongping.li@iseis.org

Y. P. Li · G. H. Huang
Faculty of Engineering and Applied Science, University of Regina, Regina, SK S4S 0A2, Canada

G. Huang (ed.), *Proceedings of 2022 7th International Conference on Environmental Engineering and Sustainable Development (CEESD 2022)*, Environmental Science and Engineering, https://doi.org/10.1007/978-3-031-28193-8_19

LUCC and climate variation may trigger significant changes in watershed hydrological processes (Meng et al. 2019). Therefore, it is essential to comprehend and distinguish the influences of LUCC and climate variation on runoff, which is conducive to accurately understand the main influencing factors and trend of runoff change.

Previously, some research works were carried out to explore the impacts of climate variation or LUCC on runoff. For example, Zhang et al. (2011) integrated RCMs, weather generators, and hydrological model to explore the hydrological response to climate change in Canada's Assiniboia watershed. Warburton et al. (2012) used the Agricultural Catchments Research Unit (ACRU) model to explore the influence of LUCC on hydrological responses in three different watersheds in South Africa. Luo et al. (2020) used cellular automata (CA) filter and neural network algorithm to predict LUCC scenarios, and combined the results with the SWAT model to assess the effect of urbanization and the hydrological responses. Khanal et al. (2021) used a glacier hydrological model to simulate the runoff trends of 15 alpine rivers in Asia under future climate change scenarios. Generally, previous studies mostly focused on the separate impacts of vegetation cover, human activities, climate change on runoff. Less studies comprehensively considered LUCC and climate change simulations to predict runoff processes.

Therefore, the purpose of this study is to develop a multi-model ensemble runoff simulation (MERS) approach, which takes LUCC and climate change into account. Multiple future LUCC and climate change scenarios will be simulated by CA–Markov model and GCMs, which will be used as input data for the SWAT model to forecast the runoff results in future period. Then, the influences of LUCC and climate change on runoff will be assessed. The novelty of the method include: (i) it can explore the independent and comprehensive effects of LUCC and climate change on runoff, and the contribution of the two changes to runoff change can also be calculated; (ii) through comparing runoff simulation results under extreme scenarios, the method can assess the hydrological response of specific elements; (iii) the range and trend of future runoff changes can be more accurately revealed by comparing the runoff processes under multi-scenarios.

19.2 Methodology

In this study, a multi-model ensemble runoff simulation (MERS) approach is developed to simulate runoff based on the prediction of LUCC and climate change scenarios, and to assess the impacts of the two changes. In MERS, climate and LUCC scenarios are simulated using GCMs an CA–Markov model respectively. Then, the SWAT model is established based on the basic data of the study area. Taking the simulated LUCC and climate change scenarios data as input, the runoff processes are forecasted by the hydrological model. The separate and interactive impacts of LUCC and climate variation on runoff are assessed by analyzing multi-scenarios runoff results.

The LUCC scenarios are simulated by CA–Markov model. The model can more accurately quantitatively simulate the spatial–temporal variations of land use/cover, integrating CA model and Markov model (Firozjaei et al. 2019). Based on the prescribed future change policies, LUCC scenarios under different development states can be forecasted by the CA–Markov model. GCM, an efficient tool for reproducing global climate change, has been widely used in forecasting and evaluating future climate change. Multiple GCMs are used simultaneously to simulate climate change scenarios in this study.

SWAT model is a spatially distribute model based on the physical mechanism of hydrological cycle process, which can be applied to complex and large basins (Liu et al. 2017). The model parameters and input data such as DEM, land cover and climate data are important elements in the establishment of a SWAT model. In this study, SUFI-2 algorithm is used for calibrating model parameters. NSE and R^2 are the indicators for validating model performance. LUCC and climate change scenarios are forecasted by CA–Markov model and GCMs, which are the input data for the hydrological model. Then, the SWAT model is used for forecasting the future runoff processes under multi-scenarios.

In this study, the influences of climate variation and LUCC could be evaluated and the calculation formulas are as follows:

$$\Delta Q_{L,C} = Q_{L,C} - Q_{\text{baseline}} \tag{19.1}$$

where $Q_{L,C}$ is the annual average runoff under each change scenario and Q_{baseline} is the annual average runoff in the baseline period. $\Delta Q_{L,C}$ represents the change in the average annual runoff under changing scenarios compared to the baseline period.

$$\eta_L = \frac{Q_{L,baseline} - Q_{baseline}}{\Delta Q_{L,C}} \tag{19.2}$$

$$\eta_C = \frac{Q_{baseline,C} - Q_{baseline}}{\Delta Q_{L,C}} \tag{19.3}$$

where $Q_{L,\text{baseline}}$ represents the annual average runoff under the future climate change scenarios when land use/cover data is the baseline period scenario. Similarly, $Q_{\text{baseline,C}}$ is the annual average runoff results under the future LUCC scenarios when the meteorological input data is the baseline period data. η_L represents the contribution of LUCC to runoff variation and η_C is the contribution of climate change.

19.3 Study Area and Data

The upper Amu Darya River Basin is the study area. The total length of the river is 2400 km and it is one of the main rivers in the Aral Sea Basin (Sun et al. 2019). The river originates from the plateau mountains, and mainly relies on glaciers and

snowmelt to supply the river. The climatic condition in this region is sensitive, and the impacts of LUCC on local economic development and natural hydrological processes are also worthy of attention. However, there are few hydrological and meteorological observation sites and data, and few studies focus on hydrological cycle in this area, so it is necessary to explore the hydrological processes and influencing factors.

In this study, Geographic data (i.e., DEM, land use/cover and soil) are used to construct SWAT models. The continuous daily runoff data from 1979 to 1986 are the basic data for the calibration and validation of the hydrological model. For scenarios prediction, land use/cover in 2000, 2010 and 2015 are selected to forecast different LUCC scenarios in 2030, 2040, 2050. There are four types of trends in LUCC scenarios: (i) S1 is a sustainable development policy, and land use/cover development is balanced and limited; (ii) S2 is the current development policy that would not change the trend; (iii) S3 is a rapid development policy with environmental damage; (iv) GM scenario is a glacier melting scenario, assuming that the glacier area would shrink sharply. Data for future climate change scenarios are derived from the NEX-GDDP-CIMP6 downscaled dataset, including CanESM5, CNRM-CM6-1, and IPSL-CM6A-LR models under SSP126, SSP245, SSP370, SSP585 scenarios.

19.4 Result and Discussion

Figure 19.1 shows the LUCC scenarios in 2030, 2040 and 2050 under four scenarios (i.e., S1, S2, S3 and GM) forecasted by the calibrated CA–Markov model. The results show that bare land, urban, farmland and water areas would increase under each LUCC scenario. The change of glacier area would be on a downward trend even under non-extreme scenarios. In the S3 scenario, the rapid development of the economy would result in an increase in the farmland and urban area compared to other scenarios. The glaciers would melt rapidly and the area would decrease sharply under the GM scenario. The area of bare land and water would also increase accordingly.

Table 19.1 and Fig. 19.2 respectively represent the annual average values and multi-year change processes of precipitation and temperature under different climate change scenarios from 2025 to 2055. The results reveal that, compared with the baseline period (−3.14 °C), the temperature would show an upward trend under all scenarios, with an average temperature increase of 2.13–4.40 °C. Under the general global warming trend, the temperature rise would have an impact on the hydrological processes of the basin. In detail, the average temperature increase of the CanESM5 model under the SSP585 scenario would be the largest, which is 1.26 °C. The average temperature rise of the IPSL-CM6A-LR model under SSP126 scenario would be smaller, reaching −1.01 °C. Trends in annual average rainfall would be less obvious. However, the multi-year average rainfall in each scenario would increase by 34.58–134.83 mm compared with the baseline period (612.36 mm). The average rainfall under the SSP585 scenario of the CNRM-CM6-1 model would increase the most at

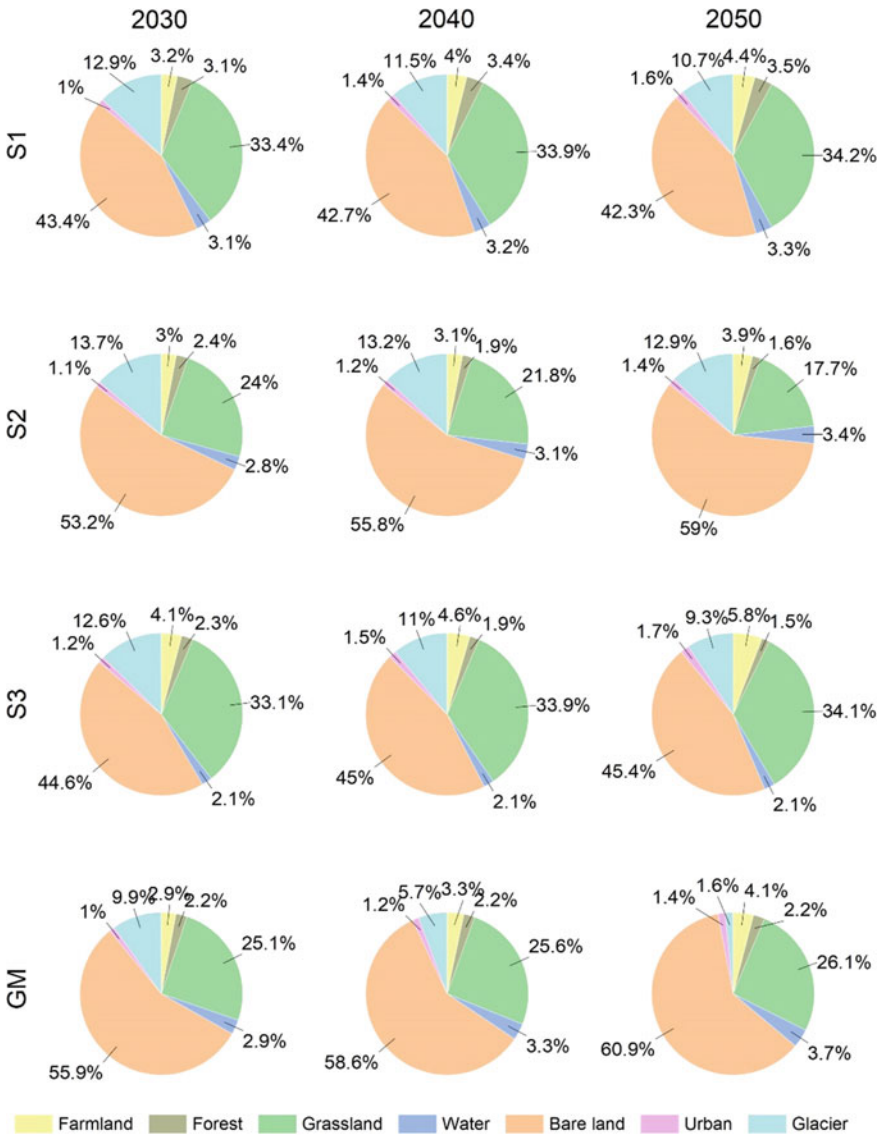

Fig. 19.1 LUCC scenarios

747.19 mm. The average rainfall for the CanESM5 model under the SSP245 scenario would have the smallest increase of 646.94 mm.

The SWAT model is constructed based on the basic data of the watershed, such as DEM, historical land use/cover and climate data, which is calibrated by the SUFI-2 algorithm. The NSE and R^2 of the simulation results respectively 0.83 and 0.87 during

Table 19.1 Average annual precipitation (P) and temperature (T) for different scenarios

Scenarios	P (mm)	T (°C)	Scenarios	P (mm)	T (°C)
Can_126	649.81	0.03	Cnr_370	731.28	−0.58
Can_245	646.94	0.53	Cnr_585	747.19	−0.15
Can_370	654.03	0.95	Ips_126	673.72	−1.01
Can_585	689.15	1.26	Ips_245	687.96	−0.77
Cnr_126	730.81	−0.72	Ips_370	728.10	−0.56
Cnr_245	703.63	−0.64	Ips_585	679.19	−0.60

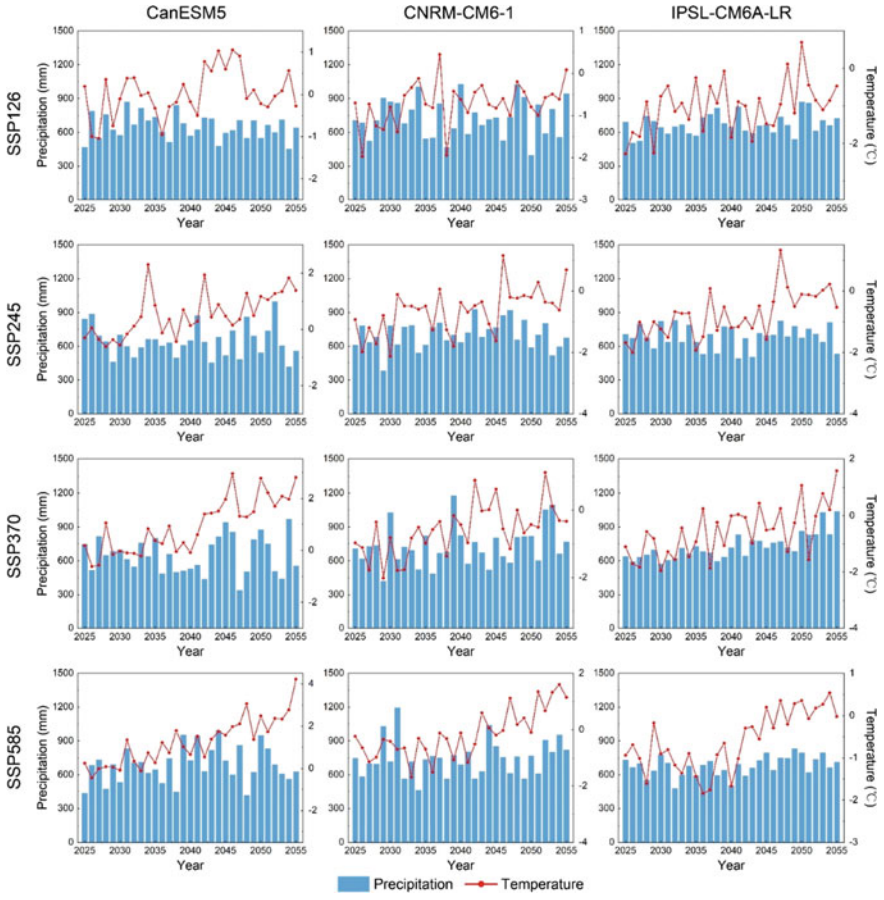

Fig. 19.2 Climate change scenarios

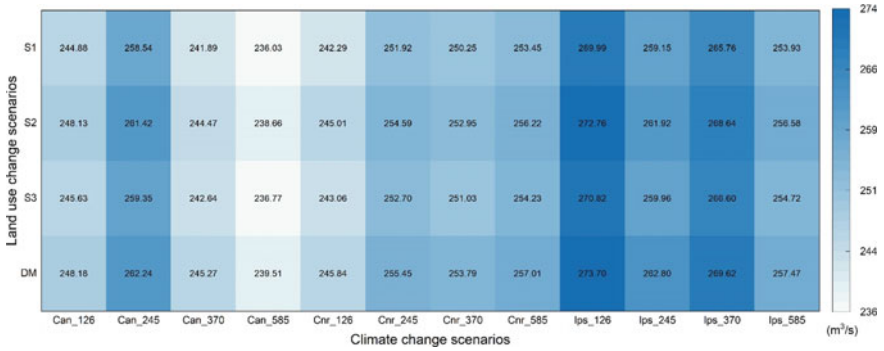

Fig. 19.3 Average annual runoff results under 48 scenarios

the verification period, indicating that the SWAT model could well simulate the hydrological processes in this area. Figure 19.3 shows the average annual runoff under 48 scenarios. In Fig. 19.4, the runoff processes under different scenarios are compared. The results show that compared with the annual average runoff of 317.03 mm in the baseline period, the future runoff would decrease by 43.33–80.99 mm. The runoff processes under the same LUCC scenarios and various climate scenarios would be significantly different, revealing that runoff processes are sensitive to climate change. Based on the results in Table 19.1, Figs. 19.1, 19.3 and 19.4, under the SSP585 scenario of the CanESM5 model, the average rainfall is basically the same as that under the SSP245 scenario of the IPSL-CM6A-LR model, but the discrepancy of average temperature would be 2.03 °C. The runoff would be larger under the scenarios of higher average temperature. Similar results could also be obtained by comparing other scenarios. The results reveal that the temperature increasing is accompanied by a decrease in runoff, which may be related to the decrease in glacier area caused by increasing temperature. Comparing the results with the same meteorological input data, the runoff results under different LUCC scenarios are similar (Fig. 19.4(iii)), indicating that LUCC has little effect on the runoff process.

Table 19.2 lists the contributions of LUCC and climate variation to runoff. The results indicate the contributions of climate variation are 83.35–99.00%, which would be much greater than the contributions of LUCC. Specifically, the contribution of climate change under the higher temperature scenario would gradually decrease. The reason for this result may be that the glacier area would decrease as the temperature increases, and the influence of the underlying surface on the runoff process would also increase. Under the GM scenario, the contribution of LUCC would be generally high, indicating that glacier area is a crucial factor affecting the hydrological cycle.

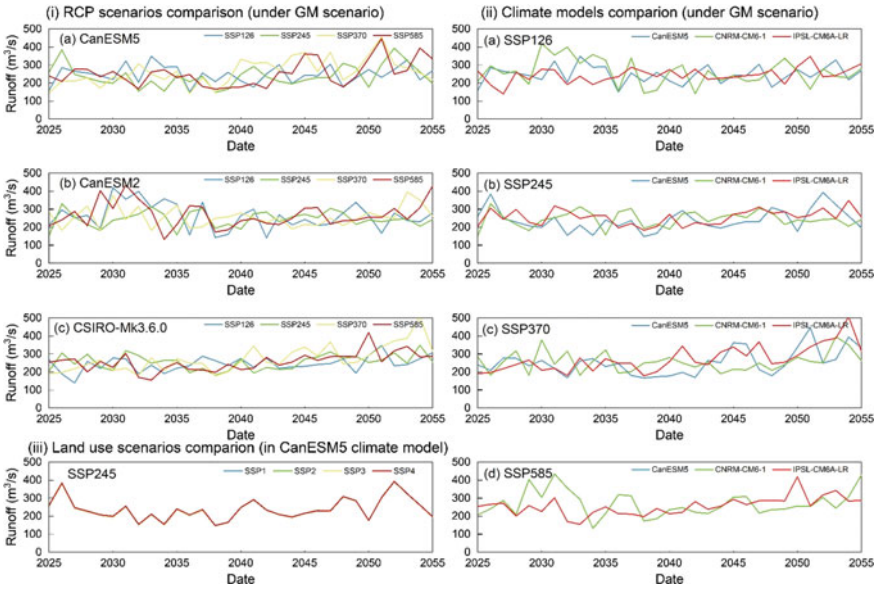

Fig. 19.4 Comparison of runoff processes under different scenarios

19.5 Conclusions

In this study, a MERS method has been developed to simulate runoff processes under multiple change scenarios. The MERS method has the advantage of revealing the individual and comprehensive effects of LUCC and climate variation on runoff. Then, the method has been used for runoff forecasting in the upper basin of Amu Darya River. Runoff processes under 48 scenarios (4 LUCC scenarios, 3 climate models under 4 SSP scenarios) are simulated. The results can reveal the influencing factors and changing trend of the runoff process.

Some major findings are: (i) the glacier area under the S1, S2, and S3 scenarios would decrease by 0.76–3.36%, and under the GM scenario, it would decrease by 8.41%; (ii) in the future period, the possible reduction range of the annual average runoff in the study area would be 43.33–80.99 m^3/s; (iii) compared with LUCC, the contributions of climate change to runoff are 83.35–99.00%, which would be a crucial influence on the runoff change in this area; (iv) the melting of glaciers due to global warming would affect the changes in runoff processes. The results could help enrich the hydrological simulation research in Amu Darya River Basin, and provide a reference for the change trend of hydrological processes.

Table 19.2 The contributions of LUCC and climate change to runoff

Scenarios		S1 (%)	S2 (%)	S3 (%)	DM (%)
Climate change	Can_126	98.11	95.97	90.80	88.87
	Can_245	96.91	93.27	86.23	83.35
	Can_370	93.82	92.74	90.11	89.13
	Can_585	99.00	97.71	94.86	93.76
	Cnr_126	98.30	98.23	94.61	93.57
	Cnr_245	91.61	90.61	88.37	87.49
	Cnr_370	98.41	96.42	92.51	91.00
	Cnr_585	98.70	97.76	95.66	94.87
	Ips_126	93.62	91.73	87.72	86.15
	Ips_245	96.66	95.13	92.04	90.79
	Ips_370	98.51	97.72	96.03	95.39
	Ips_585	97.77	96.12	92.64	91.27
LUCC	Can_126	1.89	4.03	9.20	11.13
	Can_245	3.09	6.73	13.77	16.65
	Can_370	6.18	7.26	9.89	10.87
	Can_585	1.00	2.29	5.14	6.24
	Cnr_126	1.70	1.77	5.39	6.43
	Cnr_245	8.39	9.39	11.63	12.51
	Cnr_370	1.59	3.58	7.49	9.00
	Cnr_585	1.30	2.24	4.34	5.13
	Ips_126	6.38	8.27	12.28	13.85
	Ips_245	3.34	4.87	7.96	9.21
	Ips_370	1.49	2.28	3.97	4.61
	Ips_585	2.23	3.88	7.36	8.73

Acknowledgements This research was supported by the Strategic Priority Research Program of Chinese Academy of Sciences (XDA20060302).

References

Firozjaei MK, Sedighi A, Argany M, Jelokhani-Niaraki M, Arsanjani JJ (2019) A geographical direction-based approach for capturing the local variation of urban expansion in the application of CA-Markov model. Cities 93:120–135

Khanal S, Lutz AF, Kraaijenbrink PDA, van den Hurk B, Yao T, Immerzeel WW (2021) Variable 21st century climate change response for rivers in high mountain Asia at seasonal to decadal time scales. Water Resour Res 57(5):e2020WR029266

Liu YR, Li YP, Huang GH, Zhang JL, Fan YR (2017) A Bayesian-based multilevel factorial analysis method for analyzing parameter uncertainty of hydrological model. J Hydrol 553:750–762

Luo X, Li J, Zhu S, Xu Z, Huo Z (2020) Estimating the impacts of urbanization in the next 100 years on spatial hydrological response. Water Resour Manag 34(5):1673–1692

Meng C, Zhang H, Wang Y, Wang Y, Li J, Li M (2019) Contribution analysis of the spatial-temporal changes in streamflow in a typical elevation transitional watershed of southwest china over the past six decades. Forests 10(6):495

Shi P, Ma X, Hou Y, Li Q, Zhang Z, Qu S, Chen C, Cai T, Fang X (2013) Effects of land-use and climate change on hydrological processes in the upstream of Huai river, China. Water Resour Manag 27(5):1263–1278

Sun J, Li YP, Suo C, Liu YR (2019) Impacts of irrigation efficiency on agricultural water-land nexus system management under multiple uncertainties-a case study in Amu Darya River basin, Central Asia. Agric Water Manag 216:76–88

Warburton ML, Schulze RE, Jewitt GPW (2012) Hydrological impacts of land use change in three diverse South African catchments. J Hydrol 414–415:118–135

Yifru BA, Chung I-M, Kim MG, Chang SW (2021) Assessing the effect of land/use land cover and climate change on water yield and groundwater recharge in east African rift valley using integrated model. J Hydrol Reg Stud 37:100926

Zhang H, Huang GH, Wang D, Zhang X (2011) Uncertainty assessment of climate change impacts on the hydrology of small prairie wetlands. J Hydrol 396(1):94–103

Chapter 20
An Ecological-Network Input–Output Clustering Model for Analyzing CO_2 Emission System

P. P. Wang, G. H. Huang, and Y. P. Li

Abstract Excessive carbon dioxide (CO_2) emission has been challenges to regional sustainable development. In this study, an ecological-network input–output clustering (ENIOC) model is developed to analyze CO_2 emission system. ENIOC can recognize the complex characteristics and relationships within CO_2 emission system from network and statistical perspectives. ENIOC is applied to Jiangsu. Some major findings are as follows: (i) electricity-heat supply and metal smelting industries are dominant CO_2 emission contributors (i.e., 16.4% and 12.3% of the total CO_2 emission, respectively); also, they provide plenty of carbon-intensive products for supporting construction and heavy industries; (ii) the CO_2 emission system is relatively unstable; optimize the structure of key pathways (e.g., mining → metal smelting → metal products) could mitigate CO_2 emission across the supply chain; (iii) CO_2 mitigation policy should focus on the sectors in cluster 2 (e.g., chemical, metal product and equipment industries) to reduce their dependency on carbon-intensive products from other sectors; CO_2 mitigation policy also should focus on metal smelting and electricity-heat supply industries (i.e., the sectors in cluster 3) to improve their efficiencies of energy use.

Keywords CO_2 emission · Ecological network · Multivariate statistical method

20.1 Introduction

Human health and well-being are potentially threatened by climate change (Romanello et al. 2021). The most significant contributor to climate change is known

P. P. Wang · G. H. Huang (✉) · Y. P. Li
State Key Joint Laboratory of Environmental Simulation and Pollution Control, China-Canada Center for Energy, Environment and Ecology Research, UR-BNU, School of Environment, Beijing Normal University, Beijing 100875, China
e-mail: huang@iseis.org

G. H. Huang · Y. P. Li
Faculty of Engineering and Applied Science, University of Regina, Regina, SK S4S 0A2, Canada

G. Huang (ed.), *Proceedings of 2022 7th International Conference on Environmental Engineering and Sustainable Development (CEESD 2022)*, Environmental Science and Engineering, https://doi.org/10.1007/978-3-031-28193-8_20

as carbon dioxide (CO_2) emission. Regional development has always been associated with the depletion of energy and resources, leading to huge CO_2 emission pressure (Mahlknecht et al. 2020). It is essential to mitigate CO_2 emission risks on the development of social economy and environmental sustainability; thus, more robust methods are desired to explore the complex CO_2 emission system.

Input–output analysis (IOA) is useful to trace economic flows along supply chains and express environmental responsibility (Marques et al. 2013). Ecological network analysis (ENA) is widely used to reveal the linkages of various components in a metabolism system (Liu et al. 2018). Many previous studies combined IOA and ENA to analyze the flows of various ecological factors (e.g., energy, water, CO_2 and waste) from multiple perspectives. Xu et al. (2021) proposed an energy-water-CO_2 ecological network to search the complex relationships among different sectors for water utilization, energy consumption, and CO_2 emission in the metabolic processes of the system. Tian et al. (2022) constructed an industrial waste metabolic input–output model to explore the industrial waste discharge and the relationships among different sectors. However, IOA and ENA are inadequate to further analyze potential information concealed in a series of input–output data. K-means cluster analysis (KCA) is an attractive multivariate statistical method, which can explain complex data matrices and group observations of different type (Kijewska and Bluszcz 2016). Zheng et al. (2021) developed an inter-regional heavy-metal emission cluster model to group various provinces based on the trade characteristics, and then promote the rationality of heavy-metal policy. Comert et al. (2022) proposed a Hopfield neural network based on clustering algorithms to group the large-size green vehicle routing problem, and then find the routing problem for each cluster to help CO_2 emission mitigation. However, few studies integrate IO, ENA and KCA to analyze the complicated network characteristics and relationships in CO_2 emission system.

Therefore, this study constructs an ecological-network input–output clustering (ENIOC) model to provide a new framework for analyzing CO_2 emission system. ENIOC incorporates IO, ENA and KCA into a general framework. The feasibility of ENIOC has been demonstrated in evaluating the CO_2 emission system of Jiangsu province. The novelty and contribution are as follows: (i) recognize the complicated characteristics and relationships within CO_2 emission system from trading- and ecological-network perspectives; (ii) cluster multiple sectors based on their behaviors in the CO_2 emission metabolism network, which can provide a more comprehensive evaluation of the system through network and statistical perspectives.

20.2 Methodology

An ecological-network input–output clustering (ENIOC) model is developed from monetary input–output framework. CO_2 emission flows among various sectors can be obtained through (Zhang et al. 2014):

$$\varepsilon = E[X - Z]^{-1} \tag{20.1}$$

$$IE = \varepsilon Z \tag{20.2}$$

$$T_i = IE_{ji} + E_i \tag{20.3}$$

where E represents the direct CO_2 that enter or flow out of the system; ε represents the embodied CO_2 coefficient matrix; Z represents the value flow matrix; $X = [x_{ij}]_{n\times n}$, $i = j$ and $x_{ij} = x_i$, $i \neq j$ and $x_{ij} = 0$, where X is the economic output; IE is indirect CO_2 emission matrix; T_i represents the sum of total CO_2 flow which enters sector i. Ecological network analysis (ENA) is powerful to disclose mutual relationships of sectors. In this study, multiple ENA tools are applied, including network utility analysis, network control analysis and network centrality analysis (Li et al. 2018; Xu et al. 2019).

K-means cluster analysis (KCA) is useful to identify similar clusters based on similar characteristics within the class and dissimilar characteristics among various classes (Islam et al. 2018). In this study, the indicators of emission rate index (EI), influence weight (IW) and reaction weight (RW) are also obtained through ENA (Li et al. 2018; Yang et al. 2014). The sectors are clustered through multiple indicators (i.e., IE, E, T, EI, IW and RW) to further disclose the complicated sectoral characteristics.

20.3 Study Area and Data

The proposed ENIOC model is applied to analyzing the CO_2 emission system for Jiangsu province, which is one of the most developed provinces in China. The province had a population of more than 85.0 million and the gross domestic product (GDP) of 11.6 trillion RMB in 2021. With the rapid economic growth from 2002 to 2012, the province consumed a large amount of fossil energy, which resulted in CO_2 emission increasing from 89.5 Mt in 2002 to 189.8 Mt in 2012 (Xu et al. 2017). Thus, it is essential to develop robust methods to explore the CO_2 emission system and facilitate the sustainable development. In this study, the input–output table in 2017 (from Jiangsu's Bureau of Statistics) is adopted due to this is the latest year that Jiangsu's input–output data are available. In addition, the CO_2 metabolic system is aggregated into 24 sectors, as shown in Table 20.1. Jiangsu Statistical Yearbook provides the detailed data of the regional population and GDP. China Emission Accounts and Datasets (CEADS) provides the detailed data of sectoral direct CO_2 emission.

Table 20.1 Abbreviation for sectors

Abbreviation	Sector
S1	Agriculture
S2	Mining
S3	Food processing
S4	Garments
S5	Timber processing
S6	Paper products
S7	Petroleum processing and coking
S8	Chemical
S9	Non-metallic mineral products
S10	Metal smelting and calendaring products
S11	Metal products
S12	General machinery
S13	Transportation equipment
S14	Electrical machinery
S15	Communication equipment, computers and other electronic equipment
S16	Instruments
S17	Other manufacturing
S18	Electricity and heat production and supply
S19	Gas production and supply
S20	Water production and supply
S21	Construction
S22	Transport, storage and postal services
S23	Wholesale, retail trade and catering services
S24	Other service

20.4 Result and Discussion

Figure 20.1a presents the sectoral CO_2 emission. S18, S10 and S8 accounted for 16.4%, 12.3% and 10.0% of the total CO_2 emission, respectively; they were the main emitters in Jiangsu. S18, S10 and S22 contributed most direct CO_2 emission (i.e., 62.9%, 22.3% and 6.1% of the total, respectively). S8, S10 and S15 had massive of indirect CO_2 emission (i.e., 11.5%, 10.4% and 10.3% of the total, respectively). Results indicate that electricity-heat supply, metal smelting and transportation industries directly consume many fossil fuels and lead to a large amount of CO_2 emission in the processes of production; conversely, chemical and electronic equipment industries cause lots of CO_2 emission in the processes of consumption. Figure 20.1b shows the indirect CO_2 emission transfers among various sectors. Indirect CO_2 emission induced by inter-sectoral transactions have an uneven distribution. For example,

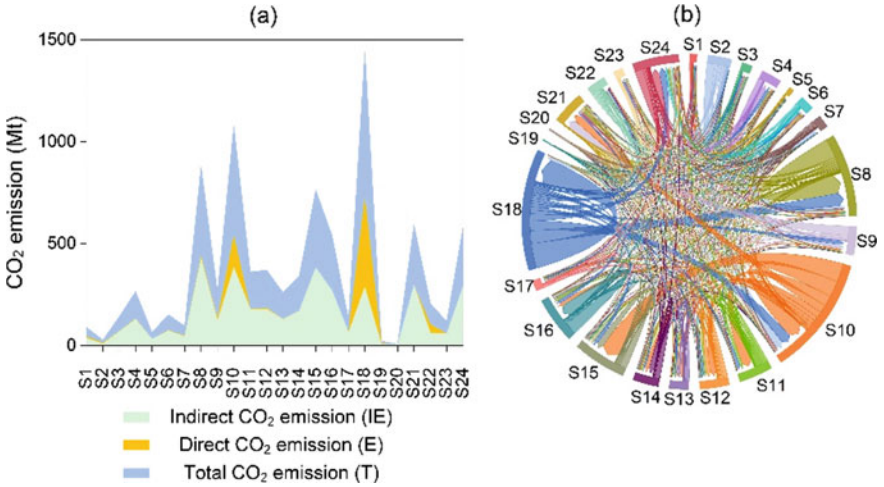

Fig. 20.1 **a** CO_2 emission and **b** indirect CO_2 emission transfers

S18's CO_2 mainly exported to S8, S10 and S24 (i.e., 291.0 Mt); S10's CO_2 mainly exported to S15, S11 and S21 (i.e., 362.0 Mt). Results reveal that electricity-heat supply and metal smelting industries provide plenty of carbon-intensive products for supporting construction and heavy industries.

Figure 20.2a presents the network utility relationships between pairwise sectors. The network mutualism index of the system was 0.74. The proportion of exploitation relationship pairs was 55.3%, followed by 27.3% of competition relationship and 17.3% of mutualism relationship. Results indicate that the CO_2 emission system is relatively unstable; there exists many unreasonable commodity transactions, which could aggravate the CO_2 emission pressure. Figure 20.2b shows the dependence of one sector on other sectors. For example, S21, S15 and S16 were highly dependent on other sectors; conversely, S2, S18 and S7 were always relied on by other sectors. This is because energy and resources related industries control raw materials; construction and equipment industries demand various kinds of intermediate inputs from other sectors.

Figure 20.3a presents the centrality of various sectors. For instance, it was significant for the centrality of transactions from S10 to S11, S12, S13, S14, S15 and S16. Results reveal that metal products industry and equipment related industries have lots of CO_2 inflows hidden in their transactions with metal smelting industry. It is important for production-side CO_2 reduction to focus on the upstream sectors (e.g., metal smelting, mining, chemical and electricity-heat industries); also, the downstream sectors (e.g., metal products, equipment and non-metallic mineral industries) need to optimize the structure of their demands. Figure 20.3b shows the centrality network of CO_2 emission transactions. Several transactions (e.g., S2 → S10, S10 → S11, S2 → S7, S18 → S10, S18 → S8 and S10 → S15) had higher centrality. Results indicate that mining → metal smelting → metal products (i.e., S2 → S10 → S11)

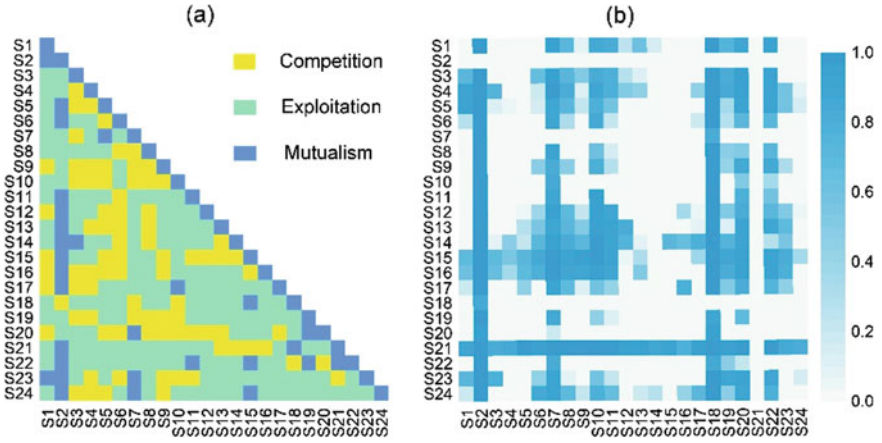

Fig. 20.2 **a** network utility relationships and **b** dependence relationships

is the most important pathway in the CO_2 emission metabolism network. Optimize the structure of key pathways could mitigate CO_2 emission across the supply chain.

Figure 20.4 shows the sectoral similarity and disparity in the four clusters (indicators: IE, E, T, EI, IW and RW). IE, E and T reveal the amount of CO_2 emission. EI indicates the CO_2 emission rate of the sectors (Li et al. 2018). IW reveals the impact of one sector on the system; RW indicates one sector's ability to respond to the system (Yang et al. 2014). Cluster 1 (i.e., G1) included S1, S3, S4, S5, S6, S9, S13, S17, S20 and S23. These sectors (e.g., agriculture, food and textile) are not carbon-intensive. Cluster 2 (i.e., G2) included S8, S11, S12, S14, S15, S16, S21 and S24. These sectors (e.g., chemical, metal product and equipment) not only produce

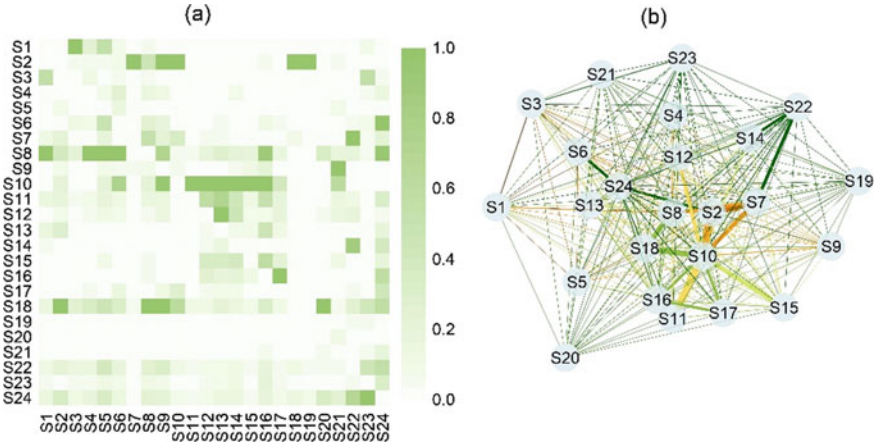

Fig. 20.3 **a** sectoral centrality and **b** centrality network of CO_2 emission transactions

lots of carbon-intensive commodities, but also require the support of many other products in the system. Cluster 3 (i.e., G3) included S10 and S18. The emission rate of the sectors (i.e., metal smelting and electricity-heat supply) is higher; also, the sectors have a great influence on the system. Cluster 4 (i.e., G4) included S2, S7, S19 and S22. These sectors (i.e., mining, petroleum, gas supply and transportation) are relatively insensitive to the system. Thus, CO_2 mitigation policy should focus on the sectors in clusters 2 and 3. The sectors in cluster 2 could upgrade technology to reduce the intermediate inputs from other sectors. The sectors in cluster 3 could develop clean energy and improve their efficiencies of energy use; meanwhile, balance the economic development and CO_2 emission reduction.

20.5 Conclusions

This study proposes an ecological-network input–output clustering (ENIOC) model to analyze CO_2 emission system. ENIOC is superior in disclosing the complicated characteristics and relationships within CO_2 emission system from network and statistical perspectives. ENIOC has been applied to Jiangsu province. Major findings are as follows: (i) electricity-heat supply and metal smelting industries are dominant CO_2 emission contributors (i.e., 16.4% and 12.3% of the total CO_2 emission, respectively); also, they provide plenty of carbon-intensive products for supporting construction and heavy industries; (ii) there exists many unreasonable commodity transactions and the CO_2 emission system is relatively unstable; construction and equipment industries are highly dependent on energy and resources related industries; (iii) according to the centrality, production-side CO_2 reduction could focus on the upstream sectors (e.g., metal smelting, mining, chemical and electricity-heat industries); demand-side CO_2 reduction could focus on the downstream sectors (e.g., metal products, equipment and non-metallic mineral industries); also, optimize the structure of key pathways (e.g., mining $\rightarrow$ metal smelting $\rightarrow$ metal products) could mitigate CO_2 emission across the supply chain; (iv) CO_2 mitigation policy should focus on the sectors in cluster 2 (e.g., chemical, metal product and equipment industries) to reduce their dependency on carbon-intensive products from other sectors; CO_2 mitigation policy also should focus on metal smelting and electricity-heat supply industries (i.e., the sectors in cluster 3) to improve their efficiencies of energy use.

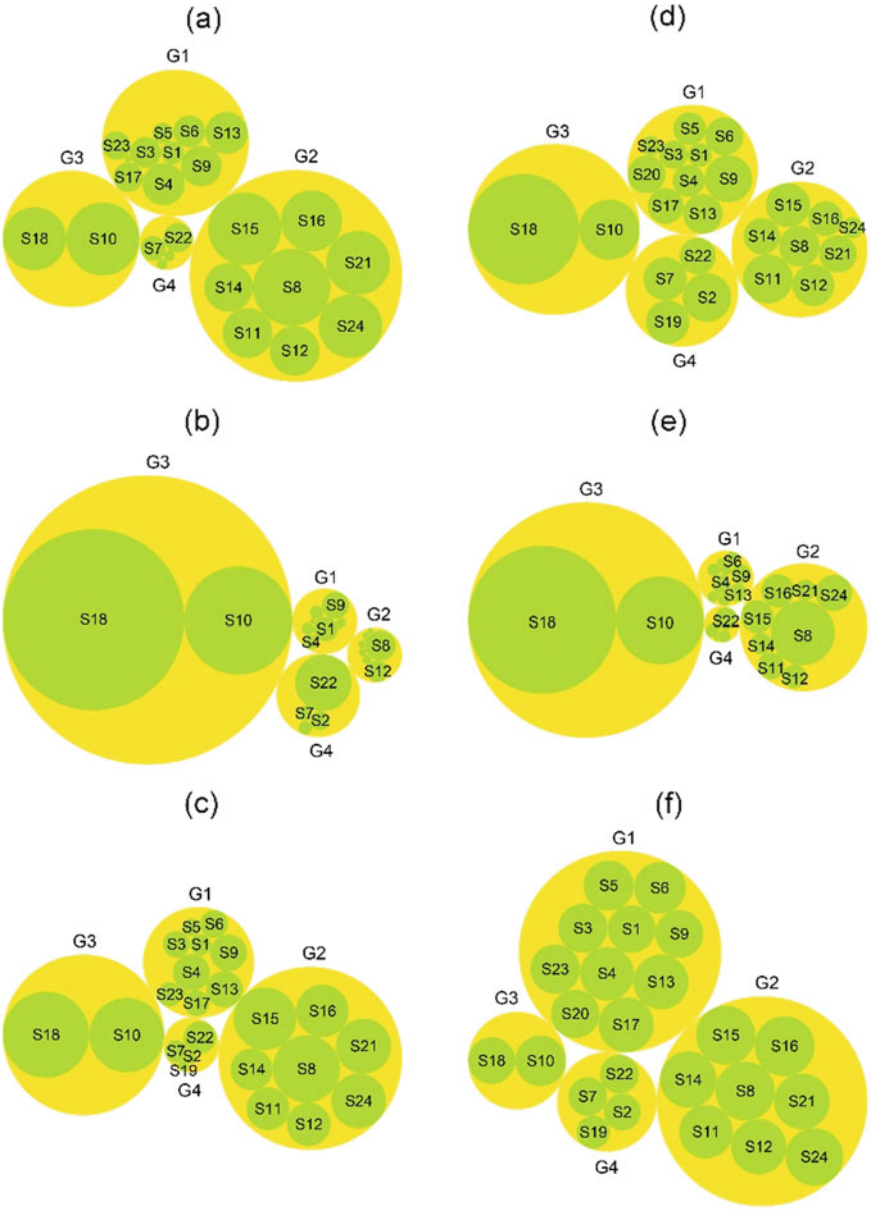

Fig. 20.4 Clustering results for sectors. *Notes* **a**–**f** are respectively the visualization of IE, E, T, EI, IW and RW (i.e., indirect, direct and total CO_2 emission, and emission rate index, influence weight and reaction weight) in the four clusters (i.e., G1-G4)

Acknowledgements This research was supported by the Strategic Priority Research Program of Chinese Academy of Sciences (XDA20060302).

References

Comert SE, Yazgan HR, Turk G (2022) Hopfield neural network based on clustering algorithms for solving green vehicle routing problem. Int J Ind Eng Comput 13(4):573–586

Islam ARMT, Shen S, Haque MA, Bodrud-Doza M, Maw KW, Habib MA (2018) Assessing groundwater quality and its sustainability in Joypurhat district of Bangladesh using GIS and multivariate statistical approaches. Environ Dev Sustain 20(5):1935–1959

Kijewska A, Bluszcz A (2016) Research of varying levels of greenhouse gas emissions in European countries using the k-means method. Atmos Pollut Res 7(5):935–944

Li JZ, Huang GH, Liu LR (2018) Ecological network analysis for urban metabolism and carbon emissions based on input-output tables: a case study of Guangdong province. Ecol Model 383:118–126

Liu LR, Huang GH, Baetz B, Huang CZ, Zhang KQ (2018) A factorial ecologically-extended input-output model for analyzing urban GHG emissions metabolism system. J Clean Prod 200:922–933

Mahlknecht J, González-Bravo R, Loge F (2020) Water-energy-food security: a Nexus perspective of the current situation in Latin America and the Caribbean. Energy 194:116824

Marques A, Rodrigues J, Domingos T (2013) International trade and the geographical separation between income and enabled carbon emissions. Ecol Econ 89:162–169

Romanello M, McGushin A, Di Napoli C, Drummond P, Hughes N, Jamart L et al (2021) The 2021 report of the Lancet Countdown on health and climate change: code red for a healthy future. Lancet 398(10311):1619–1662

Tian GL, Xia Q, Wu Z, Fu TB (2022) Ecological network analysis of industrial wastes metabolism based on input-output model for Jiangsu, China. Waste Manag 143:23–34

Xu SC, Zhang L, Liu YT, Zhang WW, He ZX, Long RY, Chen H (2017) Determination of the factors that influence increments in CO_2 emissions in Jiangsu, China using the SDA method. J Clean Prod 142:3061–3074

Xu XL, Huang GH, Liu LR, He CY (2019) A factorial environment-oriented input-output model for diagnosing urban air pollution. J Clean Prod 237:117731

Xu WH, Xie YL, Cai YP, Ji L, Wang BS, Yang ZF (2021) Environmentally-extended input-output and ecological network analysis for Energy-Water-CO_2 metabolic system in China. Sci Total Environ 758:143931

Yang ZF, Zhang Y, Li SS, Liu H, Zheng HM, Zhang JY et al (2014) Characterizing urban metabolic systems with an ecological hierarchy method, Beijing, China. Landsc Urban Plan 121:19–33

Zhang Y, Zheng HM, Fath BD, Liu H, Yang ZF, Liu GY, Su MR (2014) Ecological network analysis of an urban metabolic system based on input-output tables: model development and case study for Beijing. Sci Total Environ 468–469:642–653

Zheng BY, Huang GH, Liu LR, Zhai MY, Li Y (2021) Inter-regional cluster analysis of heavy-metal emissions. J Clean Prod 282:124439

Chapter 21
Synergetic Planning of Multi-regional Energy System Under Climate Change and Uncertainty

Y. F. Li, Y. P. Li, and G. H. Huang

Abstract Climate change and uncertainty have significant impacts on the multi-regional energy system in terms of both supply and demand. In this study, a multi-regional energy model is developed based on the interval linear programming method. The model could not only describe the complex relationship between inter-regional interaction and energy transmission in detail, but also provide optimal schemes for regulating electricity generation mix, mitigating carbon emissions, and minimizing system cost. The results show that: (i) from 2021 to 2050, the proportion of fossil fuels in energy and electricity supply will show a decreasing trend, and the regional energy and electricity structure will be optimized; (ii) under the RCP4.5 scenarios, regional carbon emissions will peak around 2040 and show a decreasing trend after the peak, with a reduction of about 1.45%; (iii) the BTH region should bear additional costs of carbon emission reduction under the RCP4.5 scenarios, the total system cost is about 1.2 times of that under the RCP8.5 scenarios.

Keywords Synergetic planning · Multi-regional energy system · Climate change

21.1 Introduction

Climate change has broad implications for energy systems (Mei et al. 2020). On the one hand, climate change alters the endowment of renewable energy (such as wind, solar and water energy) by affecting rainfall, wind speed, sunshine, temperature and other factors, thus affecting the availability of renewable energy resources (Mei et al. 2021). On the other hand, the need for energy is inextricably linked to climate change,

Y. F. Li · Y. P. Li (✉) · G. H. Huang
State Key Joint Laboratory of Environmental Simulation and Pollution Control, China-Canada Center for Energy, Environment and Ecology Research, UR-BNU, School of Environment, Beijing Normal University, Beijing 100875, China
e-mail: yongping.li@iseis.org

Y. P. Li · G. H. Huang
Faculty of Engineering and Applied Science, University of Regina, Regina, SK S4S 0A2, Canada

G. Huang (ed.), *Proceedings of 2022 7th International Conference on Environmental Engineering and Sustainable Development (CEESD 2022)*, Environmental Science and Engineering, https://doi.org/10.1007/978-3-031-28193-8_21

such as variations in temperature and precipitation (Lv et al. 2020). In addition, different carbon emission allowances under different climate change scenarios have different impacts on energy supply, processing, transformation and consumption (Lv et al. 2021). Therefore, it is urgent to develop the multi-regional energy model, which could combine the availability of renewable resources, terminal energy demand and the projections of carbon emission allowances under climate change.

Wang et al. (2014) developed a multi-regional energy optimization model taking into account regional resource endowment differences and inter-regional power transmission capacity, and proposed a multi-region power energy system expansion and generation scheme under climate change (Wang et al. 2014). Handayani et al. (2017) investigates reasonable trade-offs between carbon dioxide (CO_2) mitigation and electrification in a developing country context, taking multi-regional energy system in Indonesia as a case study (Handayani et al. 2017). Gong et al. (2022) formulated multi-regional energy model to deliver optimal structure for energy system over a long-term horizon through synergistically diminishing system cost and CO_2 emissions based on the bi-level joint-probabilistic programming method (Gong et al. 2022). However, most of the currently developed multi-regional energy models do not fully reflect the interaction and mutual aid among regions, and do not include the impact of climate change and uncertainty in the analytical framework.

Therefore, this study aims to develop a multi-regional energy model under climate change and uncertainty. Interval linear programming (ILP) will be applied to reflect the uncertain information of energy, economy, environment and other aspects under multi-climate scenarios. The novelty and contribution of the model include: (i) it could describe the complex relationship between inter-regional interaction and energy transmission in detail; (ii) optimal schemes for planning multi-regional energy system could be generated, which will provide useful information for regulating electricity generation mix, mitigating carbon emissions, and minimizing system cost.

21.2 Methodology

Interval linear programming (ILP) could directly introduce the interval numbers representing uncertain information into the general linear programming model, without considering the probabilistic partial information or fuzzy membership information of parameters (Suo et al. 2021). The general form of ILP can be expressed as follows.

$$\text{Min } f^{\pm} = C^{\pm}X^{\pm} \tag{21.1}$$

Subject to:

$$A^{\pm}X^{\pm} \leq B^{\pm} \tag{21.2}$$

$$X^{\pm} \geq 0 \tag{21.3}$$

where $X^{\pm} \in \{\Re^{\pm}\}^{n\times l}$, $C^{\pm} \in \{\Re^{\pm}\}^{l\times n}$, $A^{\pm} \in \{\Re^{\pm}\}^{m\times n}$, $B^{\pm} \in \{\Re^{\pm}\}^{m\times l}$ and $\Re^{\pm}$ Denotes the sets of uncertain numbers. According to the algorithm proposed by Huang et al. (1992), this model could be solved by an interactive two-step method (Huang et al. 1992). Firstly, the submodel corresponding to the lower bound of the objective function f^{-} (to the min-type objective) is constructed and solved. Then, on the basis of f^{-}, a submodel corresponding to the upper bound of the objective function is built and solved, so as to obtain the final solution sets $f^{\pm}_{\text{opt}} = \left[f^{-}_{\text{opt}}, f^{+}_{\text{opt}}\right]$ and $x^{\pm}_{j\,\text{opt}} = \left[x^{-}_{j\,\text{opt}}, x^{+}_{j\,\text{opt}}\right]$.

21.3 Case Study

21.3.1 Statement of Problem

The continuous increase of energy consumption and the energy structure dominated by fossil fuels have led to high carbon emissions in many countries and regions, which have had a serious impact on climate, environment, society, economy and other aspects (Jin et al. 2018). As one of the powerful engines of China's economic development, energy consumption in Beijing (BJ), Tianjin (TJ) and Hebei (HB) has also increased year by year. In 2020, the electricity consumption in the Beijing-Tianjin-Hebei (BTH) region increased by 13.88% compared with that in 2017, and the average annual growth rate was 12.20% higher than that of energy consumption. However, the current installed capacity of thermal power in the BTH region accounts for 67.60%, and the electricity generation accounts for 84.48% (Lv et al. 2018). The utilization rate of thermal power equipment is higher than that of clean energy. Under the background of climate change and uncertainty, how to further play the role of basic power security of thermal power, while rapidly improving the power generation and consumption capacity of clean energy, is an crucial problem to be solved by the multi-regional energy system.

In this study, 2021–2050 is selected as the planning period, and every five years is a period (Luo et al. 2022). The data required by the model are mainly obtained through expert consultation, field investigation and data review (Mei et al. 2021). In addition, two representative concentration pathways (RCP4.5 and RCP8.5) and three global climate models (CSIRO-Mk3.6.0, CNRM-CM5, MPI-ESM-MR) and their weighted average (AVE) are selected in this study. Thus, a total of eight climate change scenarios are generated, namely, CSIRO_RCP4.5, CSIRO_RCP8.5, CNRM_RCP4.5, CNRM_RCP8.5, MPI_RCP4.5, MPI_RCP8.5, AVE_RCP4.5 and AVE_RCP8.5.

21.3.2 Modeling Formulation

The multi-regional energy model developed in this study covers the supply of several primary energy sources (coal, oil, natural gas and various renewable energy sources), four energy processing technologies, ten electricity conversion technologies, three air pollutants and one greenhouse gas. The detailed objective functions and constraints could be expressed as follows.

$$\text{Min } f^{\pm} = \underbrace{\sum_{i=1}^{3}\sum_{k=1}^{16} BKC_{ik}^{\pm}\cdot BKL_{ik}^{\pm} + \sum_{i=1}^{3}\sum_{k=1}^{16} TKC_{ik}^{\pm}\cdot TKL_{ik}^{\pm} + \sum_{i=1}^{3}\sum_{k=1}^{16} HKC_{ik}^{\pm}\cdot HKL_{ik}^{\pm}}_{\text{Cost for primary fossil energy extraction}}$$

$$\underbrace{\begin{aligned}&+\sum_{i=1}^{3}\sum_{k=1}^{16} CBO_{ik}^{\pm}\cdot ABO_{ik}^{\pm} + \sum_{j=1}^{7}\sum_{k=1}^{16} CBW_{jk}^{\pm}\cdot ARB_{jk}^{\pm} + \sum_{i=1}^{3}\sum_{k=1}^{16} CTO_{ik}^{\pm}\cdot ATO_{ik}^{\pm}\\ &+\sum_{j=1}^{7}\sum_{k=1}^{16} CTW_{jk}^{\pm}\cdot ART_{jk}^{\pm} + \sum_{i=1}^{3}\sum_{k=1}^{16} CHO_{ik}^{\pm}\cdot AHO_{ik}^{\pm} + \sum_{j=1}^{7}\sum_{k=1}^{16} CHW_{jk}^{\pm}\cdot ARH_{jk}^{\pm}\end{aligned}}_{\text{Cost for Out - of - area energy purchase}}$$

$$\underbrace{\begin{aligned}&+\sum_{i=1}^{3}\sum_{r=2}^{3}\sum_{k=1}^{16} CBR_{irk}^{\pm}\cdot ABR_{irk}^{\pm} + \sum_{r=2}^{3}\sum_{j=1}^{7}\sum_{k=1}^{16} CBP_{jrk}^{\pm}\cdot ABP_{jrk}^{\pm} + \sum_{i=1}^{3}\sum_{k=1}^{16} CTR_{1,ik}^{\pm}\cdot ATR_{1,ik}^{\pm}\\ &+\sum_{i=1}^{3}\sum_{k=1}^{16} CTR_{3,ik}^{\pm}\cdot ATR_{3,ik}^{\pm} + \sum_{j=1}^{7}\sum_{k=1}^{16} CTP_{1,jk}^{\pm}\cdot ATP_{1,jk}^{\pm} + \sum_{j=1}^{7}\sum_{k=1}^{16} CTP_{3,jk}^{\pm}\cdot ATP_{3,jk}^{\pm}\\ &+\sum_{i=1}^{3}\sum_{r=1}^{2}\sum_{k=1}^{16} CHA_{irk}^{\pm}\cdot AHR_{irk}^{\pm} + \sum_{r=1}^{2}\sum_{j=1}^{7}\sum_{k=1}^{16} CHP_{jrk}^{\pm}\cdot AHP_{jrk}^{\pm}\end{aligned}}_{\text{Cost for regional energy purchase}}$$

$$\underbrace{\begin{aligned}&+\sum_{m=1}^{4}\sum_{k=1}^{16}\left(FCPB_{mk}^{\pm}\cdot JZB_{mk}^{\pm} + VCPB_{mk}^{\pm}\cdot APB_{mk}^{\pm}\right)\\ &+\sum_{m=1}^{4}\sum_{k=1}^{16}\left(FCPT_{mk}^{\pm}\cdot JZT_{mk}^{\pm} + VCPT_{mk}^{\pm}\cdot APT_{mk}^{\pm}\right)\\ &+\sum_{m=1}^{4}\sum_{k=1}^{16}\left(FCPH_{mk}^{\pm}\cdot JZH_{mk}^{\pm} + VCPH_{mk}^{\pm}\cdot APH_{mk}^{\pm}\right)\end{aligned}}_{\text{Cost for energy processing}}$$

$$\underbrace{\begin{array}{l}+\sum_{n=1}^{11}\sum_{k=1}^{16}\left(FCCB_{nk}^{\pm}\cdot CCB_{nk}^{\pm}+VCCB_{nk}^{\pm}\cdot ACB_{nk}^{\pm}\right)+\sum_{h=1}^{2}\sum_{k=1}^{16}VHBP_{hk}^{\pm}\cdot HCB_{hk}^{\pm}\\ +\sum_{n=1}^{11}\sum_{k=1}^{16}\left(FCCT_{nk}^{\pm}\cdot CCT_{nk}^{\pm}+VCCT_{nk}^{\pm}\cdot ACT_{nk}^{\pm}\right)+\sum_{h=1}^{2}\sum_{k=1}^{16}VHTP_{hk}^{\pm}\cdot HCT_{hk}^{\pm}\\ +\sum_{n=1}^{11}\sum_{k=1}^{16}\left(FCCH_{nk}^{\pm}\cdot CCH_{nk}^{\pm}+VCCH_{nk}^{\pm}\cdot ACH_{nk}^{\pm}\right)+\sum_{h=1}^{2}\sum_{k=1}^{16}VHHP_{hk}^{\pm}\cdot HCH_{hk}^{\pm}\end{array}}_{\text{Cost for energy conversion}}$$

$$\underbrace{\begin{array}{l}+\sum_{n=1}^{11}\sum_{k=1}^{16}\left(FKRB_{nk}^{\pm}\cdot BCB_{nk}^{\pm}+VKRB_{nk}^{\pm}\cdot CEB_{nk}^{\pm}\right)\\ +\sum_{n=1}^{11}\sum_{k=1}^{16}\left(FKRT_{nk}^{\pm}\cdot BCT_{nk}^{\pm}+VKRT_{nk}^{\pm}\cdot CET_{nk}^{\pm}\right)\\ +\sum_{n=1}^{11}\sum_{k=1}^{16}\left(FKRH_{nk}^{\pm}\cdot BCH_{nk}^{\pm}+VKRH_{nk}^{\pm}\cdot CEH_{nk}^{\pm}\right)\end{array}}_{\text{Cost for conversion technology expansion}}$$

$$\underbrace{\begin{array}{l}+\sum_{k=1}^{16}\left[CMB_{k}^{\pm}\cdot RCB_{k}^{\pm}\cdot\left(\sum_{m=1}^{4}CPB_{mk}^{\pm}\cdot APB_{mk}^{\pm}+\sum_{n=1}^{11}OCB_{nk}^{\pm}\cdot ACB_{nk}^{\pm}\right.\right.\\ \left.+\sum_{h=1}^{2}CHB_{hk}^{\pm}\cdot HCB_{hk}^{\pm}\right)+BCC_{k}^{\pm}\cdot BCL_{k}^{\pm}\cdot\left(BMC_{k}^{\pm}\cdot BZM_{k}^{\pm}+BSC_{k}^{\pm}\cdot BZS_{k}^{\pm}\right.\\ \left.\left.+BTC_{k}^{\pm}\cdot BZT_{k}^{\pm}+BJT_{k}^{\pm}\cdot BZJ_{k}^{\pm}+\sum_{j=1}^{5}BYC_{jk}^{\pm}\cdot BZY_{jk}^{\pm}+BQC_{k}^{\pm}\cdot BZQ_{k}^{\pm}\right)\right]\end{array}}_{\text{Cost for carbon and pollutant reduction}} \tag{21.4}$$

subject to:

(1) Regional resource availability constraints

Primary energy extraction:

$$BKL_{ik}^{\pm}\le MEB_{ik}^{\pm} \tag{21.5}$$

Primary energy purchase:

$$ATR_{irk}^{\pm}+AHR_{irk}^{\pm}\le BKL_{ik}^{\pm} \tag{21.6}$$

Secondary energy purchase:

$$ATP_{jrk}^{\pm} + AHP_{jrk}^{\pm} \leq MPB_{jk}^{\pm} \tag{21.7}$$

Hydroenergy:

$$ACB_{nk}^{\pm} \leq MWB_{k}^{\pm} \tag{21.8}$$

Solar energy:

$$\sum_{n=6}^{7} ACB_{nk}^{\pm} \leq MSB_{k}^{\pm} \tag{21.9}$$

Wind energy:

$$\sum_{n=8}^{9} ACB_{nk}^{\pm} \leq MFB_{k}^{\pm} \tag{21.10}$$

(2) Constraints for the availability of resources outside the region

Primary energy:

$$ABO_{ik}^{\pm} + ATO_{ik}^{\pm} + AHO_{ik}^{\pm} \leq MEO_{ik}^{\pm} \tag{21.11}$$

Secondary energy:

$$ARB_{jk}^{\pm} + ART_{jk}^{\pm} + ARH_{jk}^{\pm} \leq MPO_{jk}^{\pm} \tag{21.12}$$

(3) Constraints on the mass balance

$$\begin{aligned} &APB_{mk}^{\pm} \cdot ECP_{mk}^{\pm} + ACB_{1,k}^{\pm} \cdot ECC_{1,k}^{\pm} + ACB_{10,k}^{\pm} \cdot ECC_{10,k}^{\pm} \\ &\leq BKL_{ik}^{\pm} + \sum_{r=2}^{3} ABR_{irk}^{\pm} + ABO_{ik}^{\pm} \end{aligned} \tag{21.13}$$

(4) Constraints for the balance of supply and demand

$$\begin{aligned} &BKL_{ik}^{\pm} + \sum_{r=2}^{3} ABR_{irk}^{\pm} + ABO_{ik}^{\pm} - ATR_{1it}^{\pm} - AHR_{1it}^{\pm} - APB_{mk}^{\pm} \cdot ECP_{mk}^{\pm} \\ &- ACB_{1,k}^{\pm} \cdot ECC_{1,k}^{\pm} - ACB_{10,k}^{\pm} \cdot ECC_{10,k}^{\pm} \geq BZM_{k}^{\pm} \end{aligned} \tag{21.14}$$

(5) Constraints for power generation

$$APB_{mk}^{\pm} \le JNB_{mk}^{\pm},\ APT_{mk}^{\pm} \le JNT_{mk}^{\pm},\ APH_{mk}^{\pm} \le JNH_{mk}^{\pm} \tag{21.15}$$

$$\begin{aligned} CCB_{nk}^{\pm} &= BCZ_{n}^{\pm} + BCB_{nk}^{\pm} \cdot CEB_{nk}^{\pm} \\ CCT_{nk}^{\pm} &= TCZ_{n}^{\pm} + BCT_{nk}^{\pm} \cdot CET_{nk}^{\pm} \\ CCH_{nk}^{\pm} &= HCZ_{n}^{\pm} + BCH_{nk}^{\pm} \cdot CEH_{nk}^{\pm} \end{aligned} \tag{21.16}$$

(6) Constraints for carbon emissions and pollutant emission reduction

$$\begin{aligned} &(1 - RCB_{k}^{\pm}) \cdot \left(\sum_{m=1}^{3} CPB_{mk}^{\pm} \cdot APB_{mk}^{\pm} + \sum_{n=1}^{11} OCB_{nk}^{\pm} \cdot ACB_{nk}^{\pm} + \sum_{h=1}^{2} CHB_{hk}^{\pm} \cdot HCB_{hk}^{\pm} \right) \\ &+(1 - BCL_{k}^{\pm}) \cdot \left(\begin{array}{l} BMC_{k}^{\pm} \cdot BZM_{k}^{\pm} + BSC_{k}^{\pm} \cdot BZS_{k}^{\pm} + BTC_{k}^{\pm} \cdot BZT_{k}^{\pm} + \\ BJC_{k}^{\pm} \cdot BZJ_{k}^{\pm} + \sum_{j=1}^{5} BYC_{jk}^{\pm} \cdot BZY_{jk}^{\pm} + BQC_{k}^{\pm} \cdot BZQ_{k}^{\pm} \end{array} \right) \le BTP_{k}^{\pm} \end{aligned} \tag{21.17}$$

(7) Constraints for the 0–1 variables

$$BCB_{nk}^{\pm} = \begin{cases} 1, \text{if the capacity is expanded} \\ 0, \text{if otherwise} \end{cases} \tag{21.18}$$

$$BCT_{nk}^{\pm} = \begin{cases} 1, \text{if the capacity is expanded} \\ 0, \text{if otherwise} \end{cases} \tag{21.19}$$

$$BCH_{nk}^{\pm} = \begin{cases} 1, \text{if the capacity is expanded} \\ 0, \text{if otherwise} \end{cases} \tag{21.20}$$

21.4 Results and Discussion

Figure 21.1 shows the crude coal supply schemes of BTH region under different climate change scenarios. The results show that the energy resources supply of BTH region is mainly dominated by coal, BJ is mainly dominated by natural gas, TJ is mainly dominated by oil, and HB is mainly dominated by coal. During 2021–2050, the proportion of fossil energy supply in BTH shows a decreasing trend, while the proportion of renewable energy supply shows an increasing trend. Specifically, under the AVE_RCP4.5 scenario, the proportion of coal in BTH will decrease from 59.0 to 48.7%, the proportion of oil will decrease from 21.0 to 18.7%, the proportion of natural gas will increase from 14.9 to 16.7%, and the amount of renewable energy

resources supply will increase from 5.2 to 15.9%. The proportion of renewable energy resources supply in the AVE_RCP8.5 scenario is lower than that in RCP4.5, and the proportion of renewable energy resources supply in BTH will increase from 5.1 to 14.2%.

Figure 21.2 shows the power supply structure of BTH under diverse climate scenarios. The results display that the proportion of fossil fuel power generation and purchased electricity in the total power supply in BTH is decreasing, while the proportion of renewable electricity generation is increasing. Taking AVE scenario as an example, under RCP4.5, the proportion of non-renewable electricity generation will decrease from 65.5 to 49.5%, the proportion of outsourced electricity generation will decrease from 23.4 to 13.8%, and the proportion of renewable electricity generation will increase from 11.1 to 36.8%. Under RCP8.5, the proportion of fossil fuels

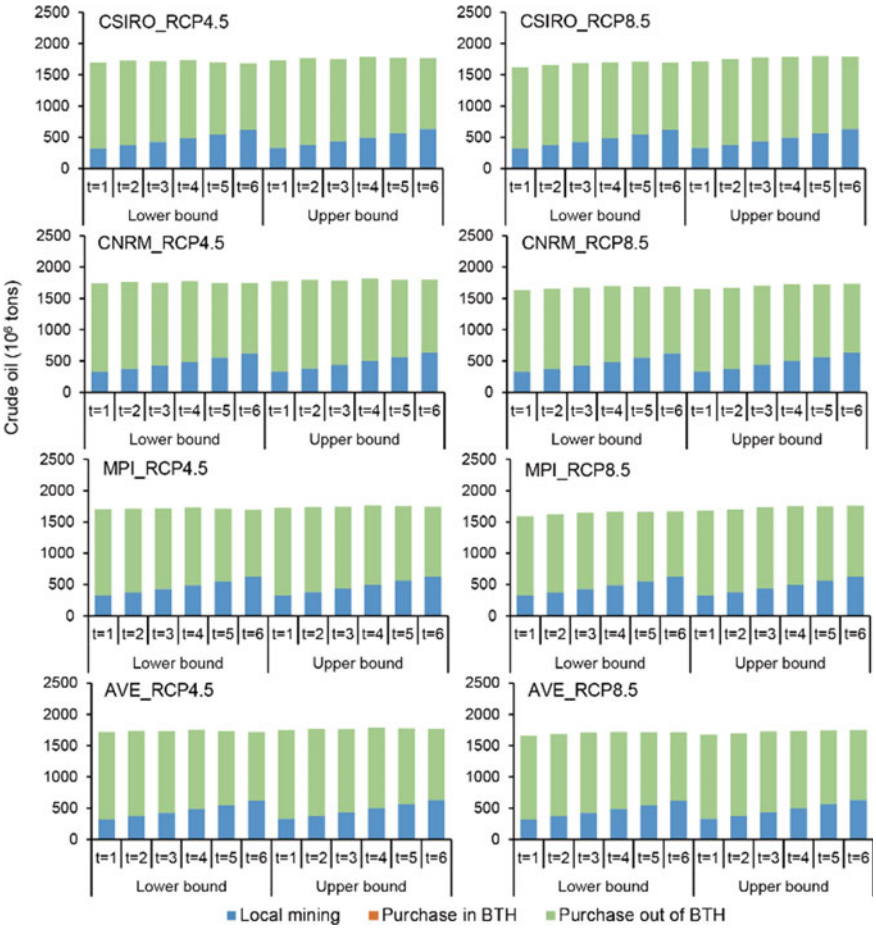

Fig. 21.1 Crude coal supply of BTH under climate change

and purchased electricity is higher than that of RCP4.5 (51.5% and 16.2% respectively in 2050), while the proportion of renewable energy generation is lower than that of RCP4.5 (32.4% in 2050). The proportion of coal-fired electricity generation in the region shows a decreasing trend, while the proportion of gas-fired electricity generation will increase first and then decrease. Taking AVE_RCP4.5 as an example, the proportion of coal-fired electricity generation will decrease from 51.1% to 36.4%, and the proportion of gas-fired electricity generation will increase from 14.5 to 15.3% (around 2030), and then decrease to 13.1%. The results show that in the next 30 years, the power supply structure of the BTH region will still be dominated by fossil fuels, but its proportion in the regional power supply will gradually decrease.

Figure 21.3 shows the carbon emissions of BTH under different scenarios. The results show that under RCP4.5, the total regional carbon emission will increase first and then decrease, reaching the peak around 2040. Under RCP8.5, the total regional

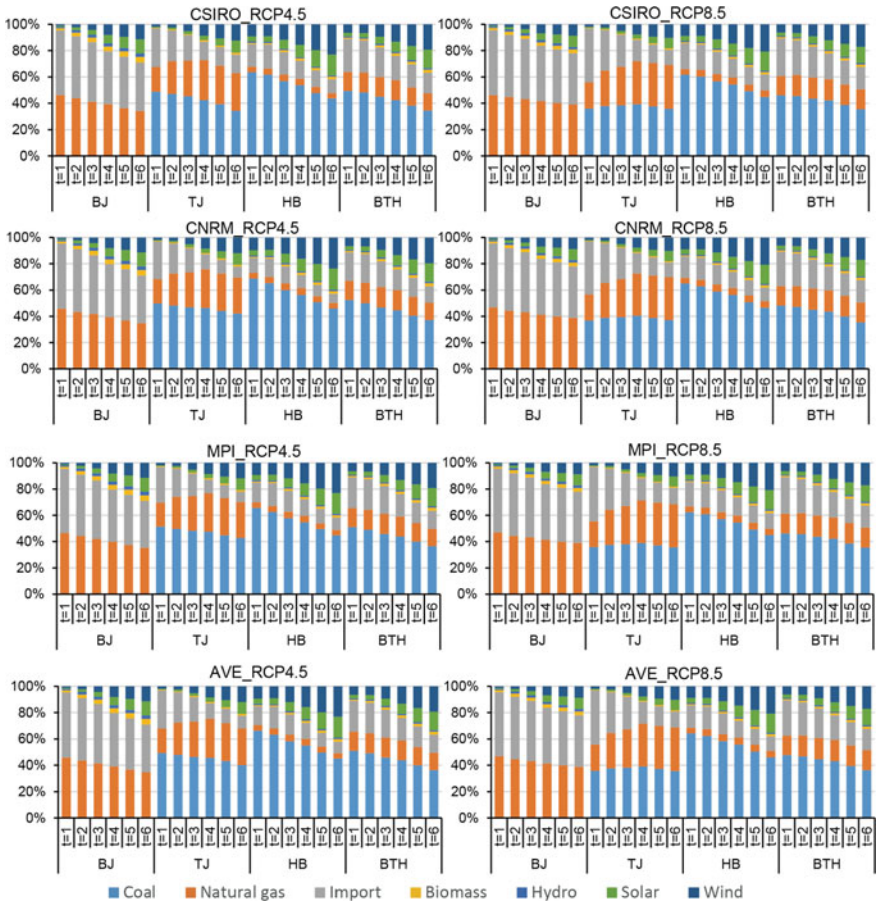

Fig. 21.2 Power supply structure of BTH under climate change

carbon emissions will show an increasing trend. Taking AVE scenario as an example, under RCP4.5, the total regional carbon emissions will increase by [234.9, 264.3] × 106 tons from 2021 to 2040, with an average increase of 8.0%. From 2041 to 2050, the total regional carbon emissions will decrease by [45.5, 50.2] × 106 tons, with an average reduction of 1.4%. Under RCP8.5, the total regional carbon emissions will increase by [785.0, 904.9] × 106 tons, with an average increase of 21.7%.

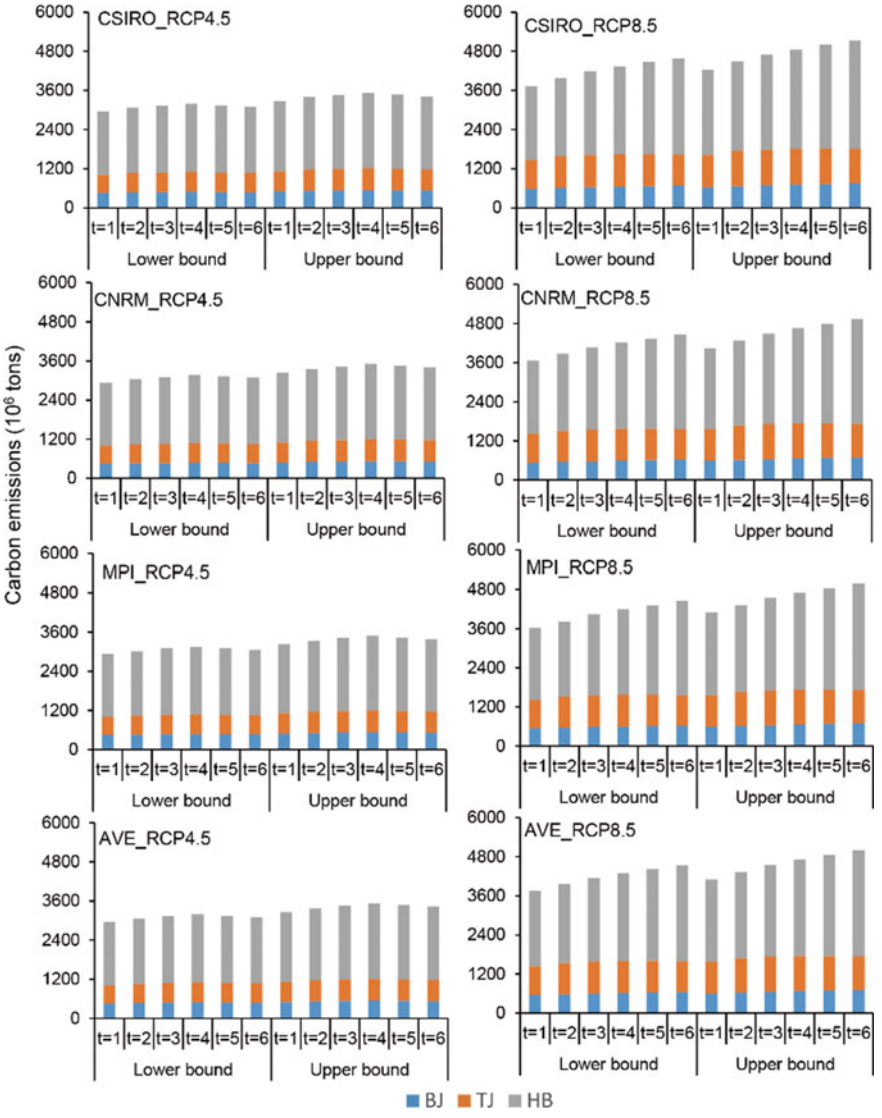

Fig. 21.3 Carbon emissions of BTH under climate change

21.5 Conclusions

This study developed a multi-regional energy model with the goal of mitigating carbon emissions and minimizing system cost, where the constraints of energy purchase within the region, energy purchase outside the region, supply and demand balance, capacity expansion, pollutant emission reduction and carbon emission reduction are considered comprehensively. It aims to provide decision support for multi-regional energy system management under climate change and uncertainty. The results showed that: (i) from 2021 to 2050, the proportion of fossil fuel in energy and electricity supply will show a decreasing trend, and the regional energy and electricity structure will be optimized; (ii) under the RCP4.5 scenarios, regional carbon emissions will peak around 2040 and show a decreasing trend after the peak, with a reduction of about 1.45%; (iii) the BTH region should bear additional carbon emission reduction costs under the RCP4.5 scenarios, the total system cost is about 1.2 times of that under the RCP8.5 scenarios.

Acknowledgements This research was supported by the Strategic Priority Research Program of Chinese Academy of Sciences (XDA20060302).

References

Gong JW, Li YP, Lv J, Huang GH, Suo C, Gao PP (2022) Development of an integrated bi-level model for China's multi-regional energy system planning under uncertainty. Appl Energy 308:118299

Handayani K, Krozer Y, Filatova T (2017) Trade-offs between electrification and climate change mitigation: an analysis of the Java-Bali power system in Indonesia. Appl Energy 208:1020–1037

Huang GH, Baetz BW, Patry GG (1992) A grey linear programming approach for municipal solid waste management planning under uncertainty. Civ Eng Syst 9:319–335

Jin SW, Li YP, Xu LP (2018) Development of an integrated model for energy systems planning and carbon dioxide mitigation under uncertainty–Tradeoffs between two-level decision makers. Environ Res 164:367–378

Luo Z, Ji L, Xie Y, Zhai L, Cai Y (2022) Water-carbon nexus relationship and interaction mechanism analysis within Beijing-Tianjin-Hebei urban agglomeration. J Environ Manag 321:115823

Lv J, Li YP, Shan BG, Jin SW, Suo C (2018) Planning energy-water nexus system under multiple uncertainties–a case study of Hebei province. Appl Energy 229:389–403

Lv J, Li YP, Huang GH, Suo C, Mei H, Li Y (2020) Quantifying the impact of water availability on China's energy system under uncertainties: a perceptive of energy-water nexus. Renew Sustain Energy Rev 134:110321

Lv J, Li YP, Huang GH, Nie S, Gong JW, Ma Y, Li Y (2021) Synergetic management of energy-water nexus system under uncertainty: an interval bi-level joint-probabilistic programming method. J Clean Prod 292:125942

Mei H, Li YP, Suo C, Ma Y, Lv J (2020) Analyzing the impact of climate change on energy-economy-carbon nexus system in China. Appl Energy 262:114568

Mei H, Li YP, Lv J, Chen XJ, Lu C, Suo C, Ma Y (2021) Development of an integrated method (MGCMs-SCA-FER) for assessing the impacts of climate change–a case study of Jing-Jin-Ji region. J Environ Inf 38:145–161

Suo C, Li YP, Mei H, Lv J, Sun J, Nie S (2021) Towards sustainability for China's energy system through developing an energy-climate-water nexus model. Renew Sustain Energy Rev, 135

Wang C, Ye M, Cai W, Chen J (2014) The value of a clear, long-term climate policy agenda: a case study of China's power sector using a multi-region optimization model. Appl Energy 125:276–288

Author Index

G. Huang (ed.), *Proceedings of 2022 7th International Conference on Environmental Engineering and Sustainable Development (CEESD 2022)*, Environmental Science and Engineering, https://doi.org/10.1007/978-3-031-28193-8